EXPERIMENTAL EVALUATION OF A PASSIVE WATER COOLED CONTAINMENT CONCEPT

by

JYH-TZONG HWANG

B.S., NATIONAL TSING HUA UNIVERSITY, HSIN-CHU, TAIWAN, ROC
(June 1981)

SUBMITTED TO THE DEPARTMENT OF
NUCLEAR ENGINEERING IN PARTIAL
FULFILLMENT OF THE
REQUIREMENTS FOR THE
DEGREE OF

DOCTOR OF PHILOSOPHY

at the

MASSACHUSETTS INSTITUTE OF TECHNOLOGY

July 1994

© Massachusetts Institute of Technology, 1994.
All rights reserved

Signature of Author: _____
Department of Nuclear Engineering
July, 1994

Certified by: _____
Neil E. Todreas
Thesis Supervisor

Certified by: _____
Michael J. Driscoll
Thesis Co-supervisor

Accepted by: _____
Allan F. Henry
Chairman, Departmental Graduate committee

MASSACHUSETTS INSTITUTE

NOV 16 1994

Science

EXPERIMENTAL EVALUATION OF A PASSIVE WATER COOLED CONTAINMENT CONCEPT

by

JYH-TZONG HWANG

Submitted to the Department of Nuclear Engineering
on July 22, 1994 in partial fulfillment of the
requirements for the Degree of Doctor of Philosophy in Nuclear Engineering

ABSTRACT

Advanced water reactors are being designed to utilize a passive containment cooling system to remove post-accident reactor sensible heat and core decay heat to the ultimate heat sink by natural convection. Such systems usually involve cooling the outside of the containment, which causes the in-containment steam to condense and thereby remove heat from the reactor system. These passive containment cooling designs differ primarily in cooling location and methods. However, the low heat transfer capability of current passive containment cooling designs has limited applications.

The objective of this thesis research was to explore a high heat removal capability passive containment cooling system: the prefilled water-air annulus – an annulus prefilled with water such that the water boils off and a smooth transition to a natural circulation air system results, that can allow a high power rating reactor design. The prefilled water-air annulus passive containment cooling concept, which is similar in some respects to the "water wall" approach explored by others, involves innovation regarding the location of the water and the means and geometry for heat transfer to circumvent the heat transfer limitations of the previous approaches.

A small scale proof-of-principle test was designed and constructed to provide data in verification of the concept. The selection of the test apparatus dimensions was based on a scaling analysis to ensure achievement of the appropriate turbulence regime and to achieve proper simulation of the heat transfer coefficient. Our results show that the heat transfer coefficient and the heat removal capability of the experiment are in good agreement with the predictions of an analytical/numerical model. The analysis also shows that the heat removal capability of a full scale version of the proposed passive water cooled containment can accommodate the decay heat production of a high power rating reactor design.

Thesis Supervisor:

Dr. Neil E. Todreas — Title: Professor of Nuclear Engineering

Thesis Co-supervisor:

Dr. Michael J. Driscoll — Title: Professor Emeritus of Nuclear Engineering

ACKNOWLEDGMENTS

I would like to express my sincere gratitude to Professor Neil E. Todreas and Professor Michael J. Driscoll for their advice and guidance throughout this study. I would like to extend my gratitude to Professor Peter Griffith for his technical advice during the course of this work. I would also like to thank the Atomic Energy Council of the Republic of China and the Electric Power Research Institute for their financial assistance.

I thank a number of current and former students for the useful technical discussions we have had through this study. These include Pavel Hejzlar and Mirela Gavrilas. I also thank Joseph Caloggero and Robert Nuttall for their assistance in the experiment setup.

This work is dedicated to my parents Liang-Chi and Yu-Ying, my wife Chen-Lin, and my son Chuan-Pang.

TABLE OF CONTENTS

LIST OF FIGURES

LIST OF TABLES

NOMENCLATURE

Symbol	Description
General English Notation	
A	cross-sectional area
BWR	boiling water reactor
C	constant
C_{sf}	Rohsenow's nucleate boiling heat transfer correlation constant
C_p	specific heat, constant pressure
D	diameter
D_e	hydraulic diameter
D_h	heated diameter
g	gravitational acceleration
H	height
h	heat transfer coefficient
h	enthalpy
K_c	form loss coefficient
K_f	friction loss coefficient
k	thermal conductivity
L	characteristic length
LOCA	loss of coolant accident
M	molecular mass
m	mass
$\dot{m}$	mass flow rate
P	pressure
PCCS	passive containment cooling system
PWR	pressurized water reactor
$\dot{Q}$	power
q"	heat flux
R	gas constant
	radius

S	surface area
SF	heat storage factor
T	temperature
TC	thermocouple
t	time
U	thermal conductance
V	velocity
W	gap width
y	mole fractions
z	axial distance

Dimensionless Numbers and Groups

$Gr_{q''} = \frac{g\beta q'' D^4}{k\nu^2}$	Grashof number
$Gr = \frac{g\beta \Delta T D^3}{\nu^2}$	Grashof number
$Nu = \frac{hD_e}{k}$	Nusselt number
$Pr = \frac{C_p \mu}{k}$	Prandtl number
$Ra = Gr \cdot Pr$	Rayleigh number
$Re = \frac{\rho V D_e}{\mu}$	Reynolds number

General Greek Symbols

β	thermal expansion coefficient
δ	wall surface roughness
∂	uncertainty
Δ	difference
	wall thickness
ε	surface emissivity
μ	dynamic viscosity
ν	kinematic viscosity

v	specific volume
π	constant, 3.14159
ρ	density
Σ	summation
σ	Stefan-Boltzman constant
	surface tension
ϕ	relative humidity

Subscripts

1	state at time 1
2	state at time 2
air	air
atm	atmosphere
B	saturated boiling
b	buoyancy
cond	condensate
	condensation heat transfer
cont	containment
conv	convection
decay	decay heat
duct	duct wall
eff	effective
FC	free convection
f	liquid phase of water
fg	liquid to vapor phase change
fg	fiberglass
g	vapor phase of water
gal	galvanized steel pipe
i	boiling incipience
in	inlet
j	node number
loss	heat loss
mix	steam-air mixture
NB	nucleate pool boiling

o	outlet
pi	inner water pool
pl	water pool
po	outer water pool
pool	water pool
PVC	PVC pipe
rad	radiative heat transfer
removal	removal power
sat	saturation
SCB	subcooled boiling
ss	stainless steel
stm	steam
total	total heat transfer
vapor	vapor contained in the air
vessel	heated vessel
w	wall
wi	duct wall inner surface
wo	heated wall outer surface
wtr	water

Superscripts

$\bar{}$	average

CHAPTER 1

INTRODUCTION

1.1 Introduction

In current nuclear power reactors, active means that require complex backup systems have been commonly adopted in the safety or emergency systems. Protection of the public and plant investment depends on the reliability of these complex systems. For the revival of the nuclear power option worldwide, many feel that stronger emphasis must be placed on assurance of safety by passive means, which rely on natural processes for reactor core cooling and decay heat removal, in addition to simplification and enhanced performance of safety systems. Thus, passive safety features have been one of the characteristics emphasized in the design of the advanced reactor systems. Containment, the last barrier to confine fission products, is also an impediment to heat transfer, which motivates consideration of design alternatives that enhance passive decay heat removal, while still maintaining containment integrity during normal and accident conditions.

Advanced water reactors are being designed to utilize a passive containment cooling system (PCCS) to remove reactor sensible heat and core decay heat to the ultimate heat sink by natural convection. These passive containment cooling concepts typically rely upon cooling on the outside of the containment to condense in-containment steam and thereby remove heat from the reactor system. These passive containment cooling designs differ primarily in cooling location and methods. However, the low heat transfer capability of current passive containment cooling designs has limited the scope of applications: all such reactors have low power output. Therefore it is desirable to design a passive containment cooling system which at the same time allows a higher power rating, and hence, improved economic competitiveness.

The objective of this thesis research is to explore the heat transfer capability of a passive water cooled containment concept – a prefilled water-air annulus passive containment cooling system. As shown in Figure 1.1, a prefilled water-air annulus is a normal air-convection annulus prefilled with water such that the water boils off and a smooth transition to a natural circulation air system results. The enhanced heat removal in

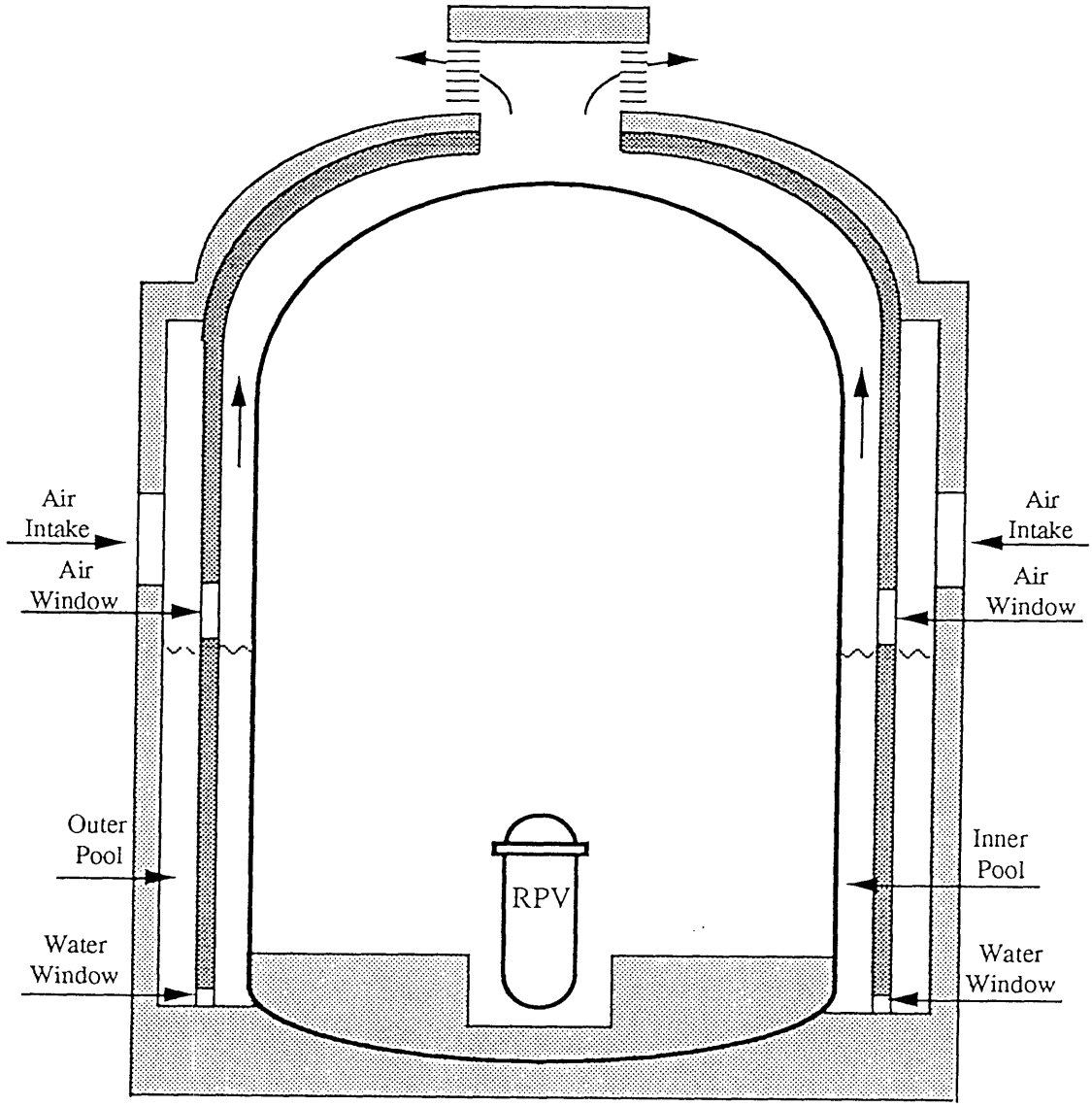

Figure 1.1 Schematic of Prefilled Water-Air Annulus Passive Containment Cooling System

the early stages following a severe accident allows a high power rating reactor design. The prefilled water-air annulus passive containment cooling concept is related to designs, previously explored by others called the "water wall" approach (discussed in Chapter 2 of this report); however the current configuration involves innovation regarding the location of the water and the means and geometry for heat transfer to circumvent the heat transfer limitations of the previous approaches. A prefilled water-air annulus, as will be demonstrated experimentally, can allow a high power rating reactor design. The goal is to accommodate a 1300 MWe pressurized water reactor design with entirely passive and long term heat removal functions.

1.2 Contribution of This Study

This thesis study focuses on the experimental evaluation of a passive water cooled containment concept – a prefilled water-air annulus design. The major contribution of this thesis study is to set up and conduct a small scale containment test – the proof-of-principle test, and provide basic data for the verification of the concept. Tests were run for both air-only and water-filled conditions; therefore, the test results can also be applied to the heat transfer performance evaluation of either an air-cooled or a water-cooled containment, as well as the hybrid design of present interest.

This research work also involves innovation regarding the location of the water and the means and geometry for heat transfer of a passive water cooled containment system which can accommodate a high power rating reactor. A computer program – PREWAS is developed, based on a simplified model, to evaluate the feasibility of the proposed passive water cooled containment. The code is validated against the small scale experiment and then used to scope out the design of a full scale containment of this type for a representative 1300 MWe (4000 MWth) pressurized water reactor.

The test results of the proof-of-principle experiment can also be used to validate other current analytical models and codes for containment analysis.

1.3 Organization of This Thesis

Chapter 2 provides a description of selected passive containment cooling designs.

These include: General Electric's isolation condenser, Hitachi's suppression chamber water wall, Toshiba's drywell water wall, and a drywell cooler for boiling water reactors; the KfK composite containment with air annulus, and Westinghouse's air annulus with water film for pressurized water reactors. Analytical or experimental demonstration of the heat transfer performance for each passive cooling design is also discussed.

Chapter 3 addresses the issues concerning details of the design of the experiment. These include: a scaling analysis for the selection of the test apparatus dimensions to achieve the desired functions of the experiment, a detailed description of the test apparatus and the instrumentation calibration, and the procedure for experimental determination of the heat transfer performance of the design.

Chapter 4 deals with the documentation and analysis of the proof-of-principle experimental results. The evaluation of the heat transfer performance for both air-only and water-filled tests is discussed. The test results are compared with predictions by a simplified analytical model – PREWAS, and other experimental results for similar test geometry. Also included in this chapter is a sensitivity analysis of the heat transfer performance to heated vessel surface emissivities , the form loss coefficients in the air path, the noncondensables in the supplied steam, and the pool temperature distribution.

Chapter 5 presents the analysis for the application of the proof-of-principle experimental results to a prototype full scale containment. The proposed containment cooling geometry and the design limits are discussed. The analysis is also based on PREWAS calculations. Both air-cooled and water-cooled containment performance are examined.

Chapter 6 begins with a summary of the thesis, and is followed by the conclusions and recommendations for future work in the area of passive water cooled containment design.

Appendix A documents a thorough data reduction and error analysis for the heat transfer performance evaluation of the experiment. Appendix B summarizes all the test data and test results. A comparison between the test results and the predictions by PREWAS is also included in Appendix B. Appendix C provides a description of the simplified model (PREWAS) for the evaluation of passive water cooled containment heat transfer performance. Finally, the calculation of the form loss coefficient in the air path is presented in Appendix D.

CHAPTER 2

ADVANCED LIGHT WATER REACTOR PASSIVE CONTAINMENT COOLING DESIGN

2.1 Introduction

Several passive containment cooling systems have been developed for advanced reactors. These passive containment cooling systems differ in cooling location and methods. General Electric has adopted use of an isolation condenser in its SBWR design [M-1]. Toshiba, Hitachi and MIT have developed various water wall configurations for SBWR containment cooling [D-1, K-2, K-5, O-2]. Westinghouse utilized an air annulus with water film cooling approach in its AP600 design [S-4]. The Karlsruhe Nuclear Research Centre (KfK) has proposed a composite containment concept that utilized an air annulus passive cooling geometry for a high power rated reactor, 1300 MWe, [E-1]. In addition, there are several other passive containment cooling designs for various advanced water cooled reactors, for example: AECL's in-containment vacuum tank for CANDU [S-3]; B&W's augmented heat capacity approach, the pebble bed, for B-600 [K-9]; UCLA's gravity assisted heat pipes for advanced light water reactors [A-1]; and various types of passive containment spray designs. Furthermore, the advanced gas or liquid metal cooled reactors, MHTGR, PIUS, and PRISM, rely only on passive systems to remove decay heat. However, the low heat transfer capability of current passive containment cooling designs has limited applications: all such reactors, except the KfK composite containment, have low power output.

This chapter provides a description of selected passive containment cooling designs. These include: General Electric's isolation condenser, Hitachi's suppression chamber water wall, Toshiba's drywell water wall, and a drywell cooler for the boiling water reactors; the KfK composite containment with air annulus, and Westinghouse's air annulus with water film for the pressurized water reactors. Analytical or experimental demonstration of the heat transfer performance for each passive cooling design is also discussed.

2.2 Passive Containment Cooling System for Boiling Water Reactors

Four kinds of passive containment cooling systems for boiling water reactors - isolation condenser, suppression chamber water wall, drywell water wall, and drywell cooler - will be described briefly in this section. The heat transfer performance of each passive containment cooling system are also discussed. Figure 2.1 shows a schematic of each of the passive containment cooling system concepts for boiling water reactors [O-2].

2.2.1 Isolation Condenser

The isolation condenser was originally designed for early boiling water reactors to prevent reactor over-pressurization and to remove decay heat during reactor isolation events, without losing coolant from the reactor pressure vessel. General Electric has extended the use of the isolation condenser technology in their SBWR, 600 MWe rated power, as a passive containment cooling system [M-1]. The isolation condenser system consists of steam supply lines from the main steam lines, heat transfer tube bundles in the isolation condenser pool, condensate return lines to the reactor pressure vessel, and noncondensables vent lines to the suppression pool, which are used to purge noncondensables in the isolation condenser tubes.

Decay heat removal is achieved passively as follows. In the reactor isolation cooling mode, decay heat steam is piped to the isolation condenser tube bundles submerged in the pool of water located above the core and outside the containment. This steam condenses inside the tubes and heats the surrounding water. The condensate water returns by gravity to the reactor vessel. Decay heat is ultimately released to the atmosphere as water boiled-off from the isolation condenser pool. In the event of a loss of coolant accident, depressurization valves vent steam from the reactor to a suppression pool positioned above the reactor pressure vessel, and the released steam is channeled by natural circulation to the tube-side heat transfer surfaces where it rapidly condenses. The condensate returns by gravity to the reactor vessel and noncondensables are passively purged to the suppression pool. Heat transfer from the tubes to the surrounding isolation condenser pool water is accomplished by natural convection. Steam produced in the pool is vented into the atmosphere. The water volume of the isolation condenser pool enables cooling for three days without operator action.

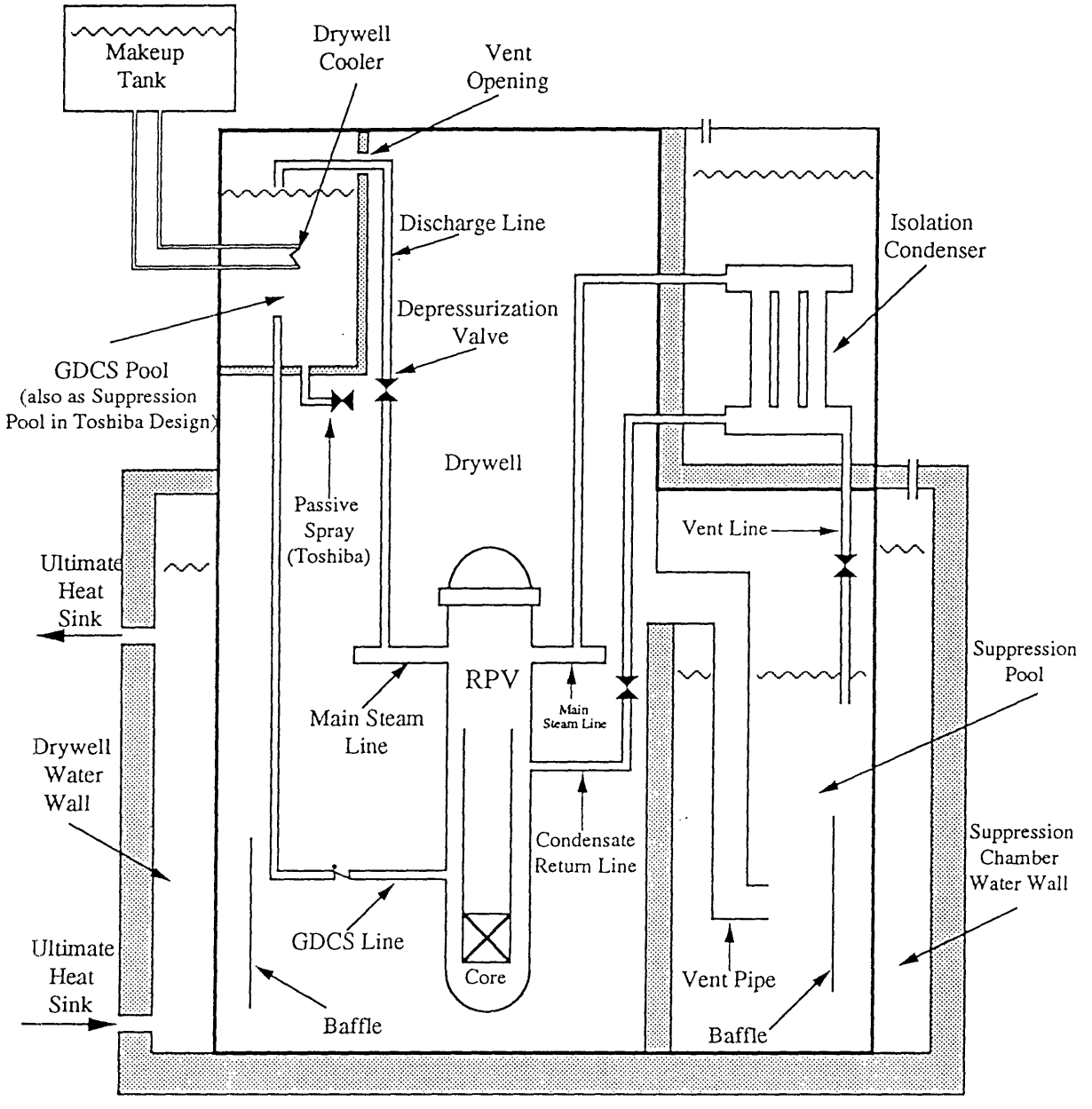

Figure 2.1 Composite Schematic of Passive Containment Cooling Designs for BWRs (Adapted from [O-2])

The heat removal capability of the isolation condenser has been demonstrated to be very effective, since it removes decay heat steam directly from the reactor pressure vessel, which is the hottest portion inside the containment. Oikawa et al. [O-2], compared the heat transfer performance of the isolation condenser, suppression chamber water wall, drywell water wall, and drywell cooler and suggested that the isolation condenser has good heat removal capability and the smallest heat transfer area among the options considered. They also evaluated the heat transfer performance of the isolation condenser over a wide range of break spectra, and confirmed its effectiveness.

2.2.2 Suppression Chamber Water Wall

The suppression chamber water wall is adopted in the Hitachi simplified BWR (HSBWR) concept [K-2, K-3]. The containment, consisting of a steel shell, is equipped with a suppression pool as the traditional boiling water reactor design, and surrounded by an outer pool (the water wall). The function of the suppression chamber water wall during a loss of coolant accident is described as follows.

Steam generated in the reactor vessel due to decay heat flows into the drywell through a break, resulting in a pressure rise in the drywell. The water level in the vent pipes is pushed down by the pressure rise in the drywell, and the steam released from the break associated with the noncondensables is vented into the suppression pool through the vent pipes. The steam is then condensed in the pool water, and the noncondensables are accumulated in the wet well. The steam condensation induces natural convection in the suppression pool and causes the pool temperature to increase. Thus the decay heat is temporarily stored in the suppression pool. The heated suppression pool is, then, cooled by the outer pool (the water wall) by natural circulation and conduction through the containment steel wall. The water in the outer pool is evaporated and the steam is released to the environment. Therefore, the temperature increase in the suppression pool is limited, which also limits the steam partial pressure increase in the wet well; hence the containment pressure is suppressed by decay heat removal through the water wall.

To evaluate the heat removal capability of the suppression chamber water wall passive containment cooling design, the thermal hydraulic behavior in the suppression pool and the outer pool have been examined experimentally and analytically by Hitachi. Their analyses show that the concerns of this design are thermal stratification and natural convective heat

transfer coefficients in the pools. The thermal stratification in the suppression pool, caused by the stagnant flow below the vent pipe outlets, separates the pool into an upper high temperature region and a lower low temperature region, and affects the effective volume and heat transfer area to the outer pool. They observed in the experiment that the thermal stratification boundary was initially located just below the vent pipe outlet, but moved downward gradually due to vertical heat conduction. To mitigate the thermal stratification effect, installation of a baffle in the suppression pool has been proposed. The effectiveness of the baffle was confirmed experimentally, and its optimal configuration was obtained by analysis with the static head-balance model. They demonstrated that the optimized baffle configuration can increase heat transfer to the outer pool 50 %.

Kataoka et al., measured the natural convective heat transfer coefficients for both downward and upward flow in the suppression pool and the water wall, and claimed that they can be expressed by $Nu = 0.13\ Ra^{1/3}$. The condensation heat transfer coefficients in the presence of noncondensables were also measured along a long wall. Their results showed that the averaged condensation heat transfer coefficients can be expressed by $h_{cond} = 0.43\ (m_a/m_s)^{-0.8}$, where m_a/m_s is the mass ratio of noncondensables and steam; and the vertical variations of the condensation heat transfer coefficients are within 10% of the averaged coefficients. They concluded that the decay heat removal capability of the suppression chamber water wall design can accommodate a 600 MWe plant.

2.2.3 Drywell Water Wall

Toshiba adopted use of the drywell water wall as the passive containment cooling system for their TOSBWR-900P. TOSBWR-900P is a steam drum-type natural circulation BWR with 300 MW electrical power [N-1]. The containment, partly made of steel, includes the pressure suppression pool which is located above the reactor pressure vessel. The upper part of the suppression pool serves as the water source for the gravity driven core cooling system (GDCS), and the lower part of the pool can be utilized as the water source for the gravity driven drywell spray. The reactor pressure vessel can be flooded completely by the spray water due to the shortened pressure vessel and the smaller cavity volume of the lower drywell associated with the adoption of a top-mounted control rod drive.

The water wall is placed around the lower part of the reactor cavity. The reactor cavity is filled after a loss of coolant accident by the hot water flowing through the break and by emergency coolant communicating through an equalizing line which is installed between the drywell and the reactor pressure vessel. The flow within this drywell pool is driven by natural circulation. Baffle plates near the steel wall promote natural circulation in the drywell pool. The cooling water from the ultimate heat sink, such as the sea, is introduced into the water wall by opening the valves on the connecting pipes to the ultimate heat sink during a loss of coolant accident. The cold water enters into the water wall from the lower pipes and cools the steel containment by natural convective heat transfer. The heated water flows out to the ultimate heat sink through the upper pipes, thereby providing the natural circulation flow to the steel containment wall.

To evaluate the heat transfer performance of the drywell water wall passive containment cooling system, a safety evaluation code, TOSPAC, was developed by Toshiba. The analyses show that the peak containment pressure is well below the design pressure under a postulated severe loss of coolant accident. Researchers also claim that the heat removal performance of the drywell water wall is relatively good compared with the water wall placed around the suppression chamber, even if the ultimate heat sink for the water wall is not used, mainly due to high partial pressure of noncondensables in the suppression chamber, and low suppression pool temperature.

2.2.4 Drywell Cooler

As shown in Figure 2.1, the drywell cooler is submerged in the pool of the gravity driven core cooling system, and located close to the depressurization valve discharge lines which are introduced into the air space of the pool. The openings between the air space of the pool and drywell provide a noncondensables venting function. The operation of the drywell cooler is similar to the isolation condenser; however, the decay heat steam is guided to the shell side of the cooler. When the reactor vessel pressure approaches drywell pressure during a loss of coolant accident, the gravity driven core cooling system starts to deliver pool water into the reactor vessel. The water level in the pool gradually decreases and the outer surface of drywell cooler tubes is exposed to the steam jet from depressurization valve discharge lines. The drywell coolers start to operate automatically, and heat up the cooling water inside the tubes. The cooling water is supplied to the tube bundles from the makeup pool located at the outside of the containment. The cooling flow

is, then, maintained by natural circulation. The steam jet along with lower concentration of noncondensables and high steam temperature assure effective steam condensation heat transfer by the drywell cooler. Analysis by the researchers [O-2] show that the heat transfer performance of the drywell cooler may be comparable to the isolation condenser.

2.3 Passive Containment Cooling System for Pressurized Water Reactors

An air annulus passive containment cooling design for a high power rated reactor – the proposed KfK composite containment, and an air annulus with water film passive containment cooling design for the Westinghouse AP600 are described in the following subsections. The experiments or analyses to demonstrate the applicability of each design are also discussed. Figure 2.2 shows a schematic of each of these designs. The topical passive containment cooling concept of this thesis study – the prefilled water-air annulus – was described in Section 1.1. The prefilled water-air annulus passive containment cooling concept, which is similar in some respects to the "water wall" approach which has been discussed in the previous sections, involves innovation regarding the location of the water and the means and geometry for heat transfer to circumvent the heat transfer limitations of the previous approaches. The major differences between the prefilled water-air annulus and the water wall are: (1) there is no in-containment water pool in the heat transfer path for the prefilled water-air annulus, that is, the heat is directly transferred by steam condensation through the containment wall to the outer pool; and (2) the prefilled water-air annulus preserves the natural air convection cooling capability for outside containment heat removal.

2.3.1 Air Annulus

A composite containment for pressurized water reactors has been proposed in Germany to cope with beyond design basis accidents, e.g. severe core meltdown accidents [E-1]. The containment consists of two individual shells similar to the present large dry containment designs. The inner steel shell is of 60 m diameter and 38 mm wall thickness, the outer reinforced concrete shell is of 2 m wall thickness. The annulus of 80 cm radial gap width is bridged by longitudinal support ribs fixed in the concrete shell. The ribs are placed at intervals on the circumference with 50 cm spacing to form a circulation chimney and to transfer the load of the expanding and deflecting steel containment to the reinforced

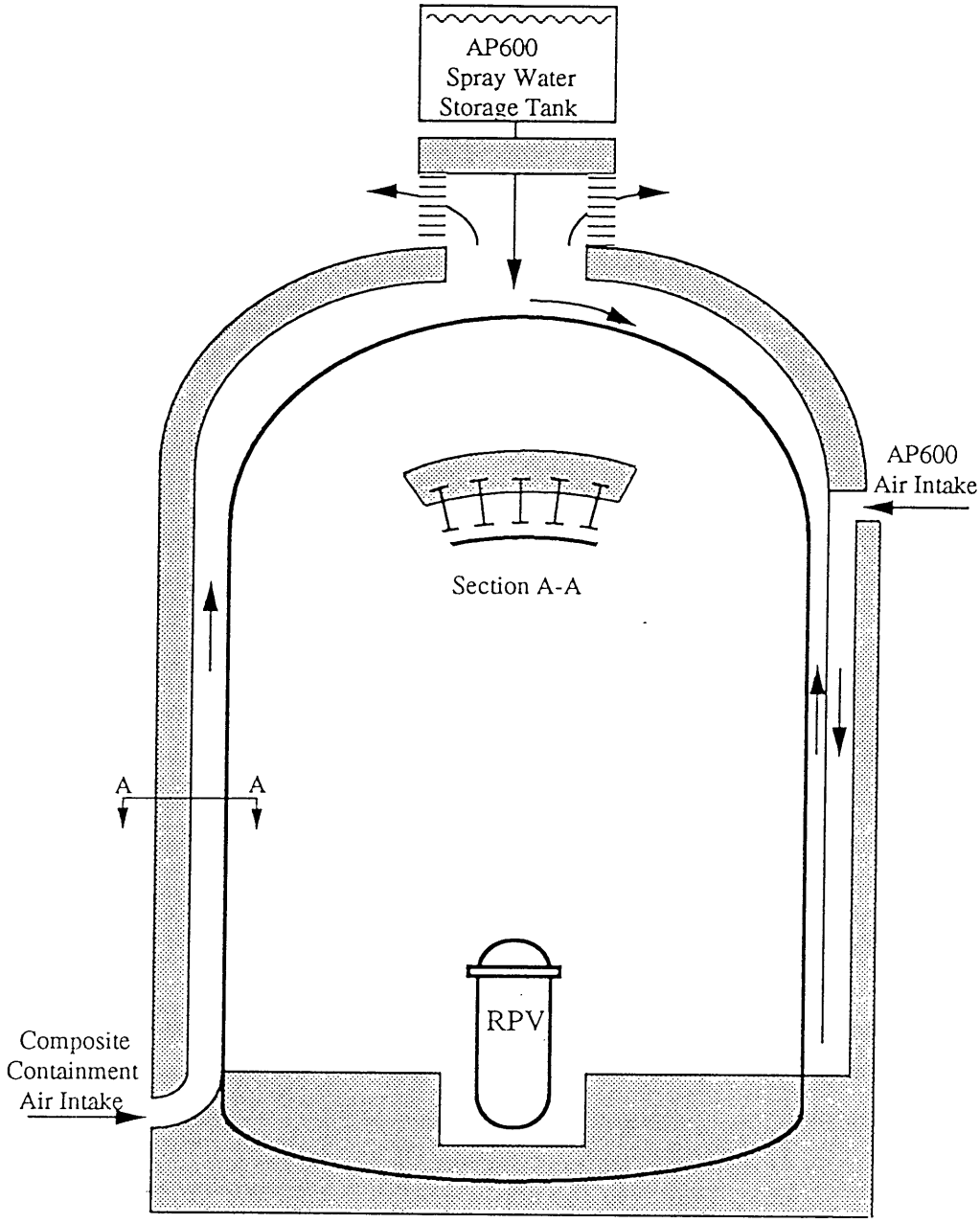

Figure 2.2 Composite Schematic of Passive Containment Cooling Designs for PWRs

concrete wall in a potential hydrogen detonation. There is a core catcher (ex-vessel) in this new design. Filters, atop of the chimney, are also proposed to prevent potential fission gas release to the environment.

The decay heat removal is achieved as follows. In a core meltdown accident the decay heat is converted into steam by direct water contact of the melt with the water. The steam produced condenses on the inner surface of the externally cooled containment shell and the internal structures. Reflux of the steam condensate to the core catcher establishes a passive self-circulating steam/water flow. The heat transfer from the containment to the air is accomplished via the following mechanisms: the heat is transferred by conduction across the steel shell, then the heat transfer from the containment to the air takes place by natural convection at the four side walls of the chimney (see section A-A in Figure 2.2) where radiant heat transfer occurs between the individual walls.

The heat transfer performance of the composite containment has been analyzed by KfK and others [E-1]. In their analysis, they assumed a uniform temperature distribution on the inner steel wall surface and adiabatic conditions at the concrete wall due to its large wall thickness and poor thermal conductivity. To calculate convective heat transfer the following Nusselt-correlation, valid for vertical flat walls of infinite extension and turbulent flow, has been used: $Nu = 0.104\ Ra^{1/3}$. This correlation is claimed to be validated for a range of Rayleigh numbers from $2 \cdot 10^9$ to 10^{12}.

Their results show, based on CONTAIN code calculations, a decay heat of about 8 MWth can be removed, with high emissivities of the chimney walls and no filter atop, by natural air convection for a 1300 MWe pressurized water reactor. The temperature of the steel containment reaches about 150 °C in the analysis. They claim that the heat transfer capability of the proposed composite containment is sufficient due to the high heat storage capability of the internal structures in the containment (approximately 13200 m^3 of concrete, 490 m^3 of steel).

2.3.2 Air Annulus with Water Film

The Westinghouse AP600 reactor, 600 MWe rated power, adopts an air annulus with water film design as its passive containment cooling system [S-4, W-4]. The containment consists of a steel shell, a baffle plate, and concrete structure to form an annulus providing

natural air circulation passages. To enhance the heat removal capability of the design, a water storage tank is proposed atop of the containment. The passive containment cooling is activated in case the normal containment fan coolers are not available, or an accident has occurred that requires containment heat removal at elevated pressures and temperatures. The heat removal on the outside of the containment is achieved through natural air convection associated with radiative heat transfer in the annulus and evaporation of a thin water film flowing, by gravity, from the water storage tank onto the containment dome and down its sides. Cooling on the outside of the containment causes the in-containment steam to condense and remove heat from the reactor system.

To demonstrate the applicability of the passive containment cooling design, many tests have been performed that included [S-2]: a wind tunnel test, water film test, air flow resistance test, heated plate test, and integral test. The wind tunnel test, using a small scale model, is to assure that air inlets and outlets are arranged so that wind will aid, not reduce, natural circulation. The results showed that the wind always tends to increase the flow in the cooling annulus around the containment. The water film test provides guidance for the design of the water addition and distribution system. The air flow path resistance test, using a one-sixth scale of a prototype air flow path, suggests an optimum configuration to reduce the flow resistance and maximize air velocity. Researchers found that the rounded perforated inlet vanes at the bottom of the annulus, and fairing over the support posts could significantly reduce the air flow resistance. The heated plate test, using a two feet wide, six feet long, and one inch thick steel plate coated with prototypic paint, is to investigate the water film behavior and to obtain convection and evaporation heat transfer correlations. They found that the water film flow was wavy laminar flow, not susceptible to instabilities which induce dry patch formation, and the water film evaporation showed no tendency to form rivulets even in high air velocity conditions. The integral tests, including small scale and large scale, are to simulate the entire heat transfer process of the passive containment cooling system. The results indicated that the heat removal capacity of the AP600 passive containment cooling system would meet or exceed its designed objectives.

2.4 Summary of Chapter 2

- Several passive containment cooling designs have been discussed. These include: General Electric's isolation condenser, Hitachi's suppression chamber water wall, Toshiba's drywell water wall, and a drywell cooler for boiling water reactors; the KfK's

composite containment with air annulus, and Westinghouse's air annulus with water film for pressurized water reactors.

- General Electric has extended the use of isolation condenser technology in their SBWR, 600 MWe rated power, as a passive containment cooling system. An isolation condenser removes decay heat efficiently, since it absorbs decay heat steam directly from the hottest portion inside the containment. The technical issue that affects the performance of the isolation condenser is noncondensable gas accumulation inside heat transfer tubes.

- Toshiba (Oikawa et al.) made a performance comparison of the suppression chamber water wall, drywell water wall, isolation condenser, and drywell cooler for SBWR. Their result suggests that the isolation condenser has the best heat removal capability among passive containment cooling concepts evaluated in their analysis. They also concluded that the suppression chamber water wall is ineffective, mainly due to high noncondensable gas partial pressure in the suppression chamber, and low suppression pool temperature.

- Erbacher et al. (KfK), estimated, based on containment calculations with the CONTAIN code, that a decay heat of about 8 MWth can be removed by natural air convection in an air annulus containment cooling geometry, and concluded that it is sufficient for a 1300 MWe reactor, due to the high heat storage capacity of the internal structures within the composite containment.

- Westinghouse demonstrated, by the conduct of wind tunnel tests, water film tests, air flow resistance tests, heated plate tests, and integral tests, that an air annulus combined with a water film (supplied by a tank atop the containment building) provides suitable decay heat removal capability for the AP600.

CHAPTER 3

PROOF-OF-PRINCIPLE EXPERIMENT DESIGN

3.1 Introduction

The objective of this thesis research is to explore the high heat removal performance of a prefilled water-air annulus passive containment cooling system that can allow a high power rating reactor design. This study, therefore, focuses on experimentally demonstrating the heat transfer performance of the passive cooling design for a prototype power reactor system. This chapter will address the issues concerning details of the design of the experiment. To achieve the desired functions of the experiment, a scaling analysis for the selection of the test apparatus dimensions has been performed. To evaluate the heat transfer performance of the design, a set of parameters has been selected, and the experimental determination of these parameters will be discussed in detail. This chapter also provides a detailed description of the test apparatus experimental setup and the instrumentation calibration.

3.2 Selection of the Test Apparatus Dimensions

The scale of an experiment is a trade-off between its goal and the experimental constraints. The goal of the experimental part of this research is defined as a proof-of-principle test. The key consideration is the power removal capability of the design under conditions which simulate or are confidently extrapolatable to a full-scale application. The selection of the test apparatus dimensions, then, is based on the scaling analysis and the experimental constraints as will be discussed in the following sections.

3.2.1 Scaling of Natural Air Convection

Referring to equation 6 of Fu's work on mixed convection for vertical air flow [F-2], a pressure balance on a heated channel with an adiabatic chimney gives:

$$\frac{2Gr_{q''}}{Re^3Pr}\frac{L}{D_e}\frac{L+2L_c}{D_e}=\frac{f}{2}\frac{L+L_c+L_u}{D_e}, \tag{3.1}$$

where

f: friction factor,

L: heated length,

L_c: chimney length,

L_u: unheated entrance length.

Solving for Re,

$$Re=\left(\frac{4Gr_{q''}}{fPr}\frac{L}{D_e}\frac{L+2L_c}{L+L_c+L_u}\right)^{1/3}. \tag{3.2}$$

But

$$Gr_{q''}=\frac{g\beta q''D_e^4}{kv^2}. \tag{3.3}$$

Hence, in terms of system design variables, and assuming a constant friction factor,

$$Re \sim D_e(q''L)^{1/3}\left(\frac{2+L/L_c}{1+L/L_c+L_u/L_c}\right)^{1/3}. \tag{3.4}$$

For a tall chimney ($L_c >> L$ and L_u), the last term of the above equation is approximately a constant.

$$Re \sim D_e(q''L)^{1/3} \tag{3.5}$$

Assume Reynolds analogy, that is,

$$\frac{Nu}{RePr}=\frac{f}{2}\sim \text{constant}. \tag{3.6}$$

Thus

$$\frac{hD_e}{k}=Nu \sim Re \sim D_e(q''L)^{1/3}, \tag{3.7}$$

$$h \sim (q''L)^{1/3}=(h\Delta TL)^{1/3}. \tag{3.8}$$

Hence

$$h \sim (L\Delta T)^{1/2}, \text{ and} \tag{3.9}$$

$$Re \sim D_e(L\Delta T)^{1/2}. \tag{3.10}$$

Therefore, the heat transfer coefficient and the Reynolds number are only moderately sensitive to heated length, and the Reynolds number is sensitive to the hydraulic diameter. This analysis suggests that reducing heated length rather than hydraulic diameter should be more effective in reducing scale for the experiment. Moreover, the input heat flux or heat source temperature can be increased for the reduced scale experiment to ensure attainment of the applicable turbulence regime and to achieve the simulation of the heat transfer coefficient.

3.2.2 Scaling of Heat Transfer to the Pool

For free convection on a vertical plate, the Nusselt number can be expressed as:

$$Nu_{FC} = (\frac{hL}{k})_{FC} \sim Gr_{FC}^{1/3} \sim (L\Delta T^{1/3})_{FC}, \tag{3.11}$$

$$h_{FC} \sim \Delta T^{1/3}. \tag{3.12}$$

Therefore, the free convection heat transfer coefficient is independent of characteristic length. For nucleate boiling heat transfer on a vertical plate, the heat transfer coefficient can be expressed as [R-1]:

$$h_{NB} = (\frac{C_{pf}\Delta T}{C_{sf}h_{fg}\,Pr_f})^{\frac{1}{0.33}} \cdot \frac{\mu_f h_{fg}}{\Delta T[\frac{\sigma}{g(\rho_f - \rho_g)}]^{0.5}}, \tag{3.13}$$

$$h_{NB} \sim \Delta T^2. \tag{3.14}$$

The nucleate boiling heat transfer coefficient is not directly dependent on the characteristic length. However, the fluid properties in the heat transfer correlation are a function of pressure, and hence pool depth; this effect should be taken into account.

3.2.3 Constraints in the Laboratory

Although the height of the shaft available for emplacement of the test apparatus is 20.73 m (72 ft), the cross-section is 2.6 m by 1.8 m. Hence if a larger test cross-section is desired, the height of the ceiling in the laboratory, 3.8 m, will limit the integral dimensions of the test apparatus. In addition, the capability of the laboratory steam supply (used as the heat source in the experiment), which is 0.138 kg/sec of 0.48 MPa saturated steam (about 290 kw), imposes another constraint on the selection of the dimensions. We chose to make use of the full shaft height (72 ft) and therefore accepted the 2.6 m by 1.8 m cross-section constraint on the apparatus.

3.3 Design and Construction of Test Apparatus

The subject small scale proof-of-principle experiment – the prefilled water-air annulus passive containment cooling experiment was performed at the High-Bay Test Facility in the W.M. Rohsenow Heat Transfer Laboratory at MIT. A constant temperature has been selected as the boundary condition of the experiment. The test apparatus is composed of four concentric pipes (steam distributor, heated vessel, inner annulus wall and outer annulus wall) and a long chimney. The four concentric pipes are assembled together on a bottom plate. This configuration ensures the heat loss of the experiment will be minimized, as estimated in Appendix A. Figures 3.1.a and 3.1.b show the schematic diagram and photographs of the test apparatus. Table 3.1 and Figure 3.2 show the dimensions of each component. To ensure the symmetry of the apparatus, there are four lateral supports, made of aluminum bar, 0.63 inches in outer diameter, in each of the annuli, as shown in Figure 3.3. The following subsections provide the detailed description of each component.

3.3.1 Heated Vessel

The heated vessel is a 6.096 m (20 ft) long, 304 stainless steel pipe, 11.43 cm (4.5 in) in outer diameter, serving as a containment steel vessel. It is equipped with a steam distributor, a safety relief valve, a sight glass, and vent pipes. The safety relief valve and top vent are located at the top of the heated pipe which is capped with a 22.86 cm (9 in) blind flange. The bottom of the heated pipe, which is also equipped with a bottom vent, a condensate drain line and a sight glass, is connected to a 0.91 m by 0.91 m (3 ft by 3 ft)

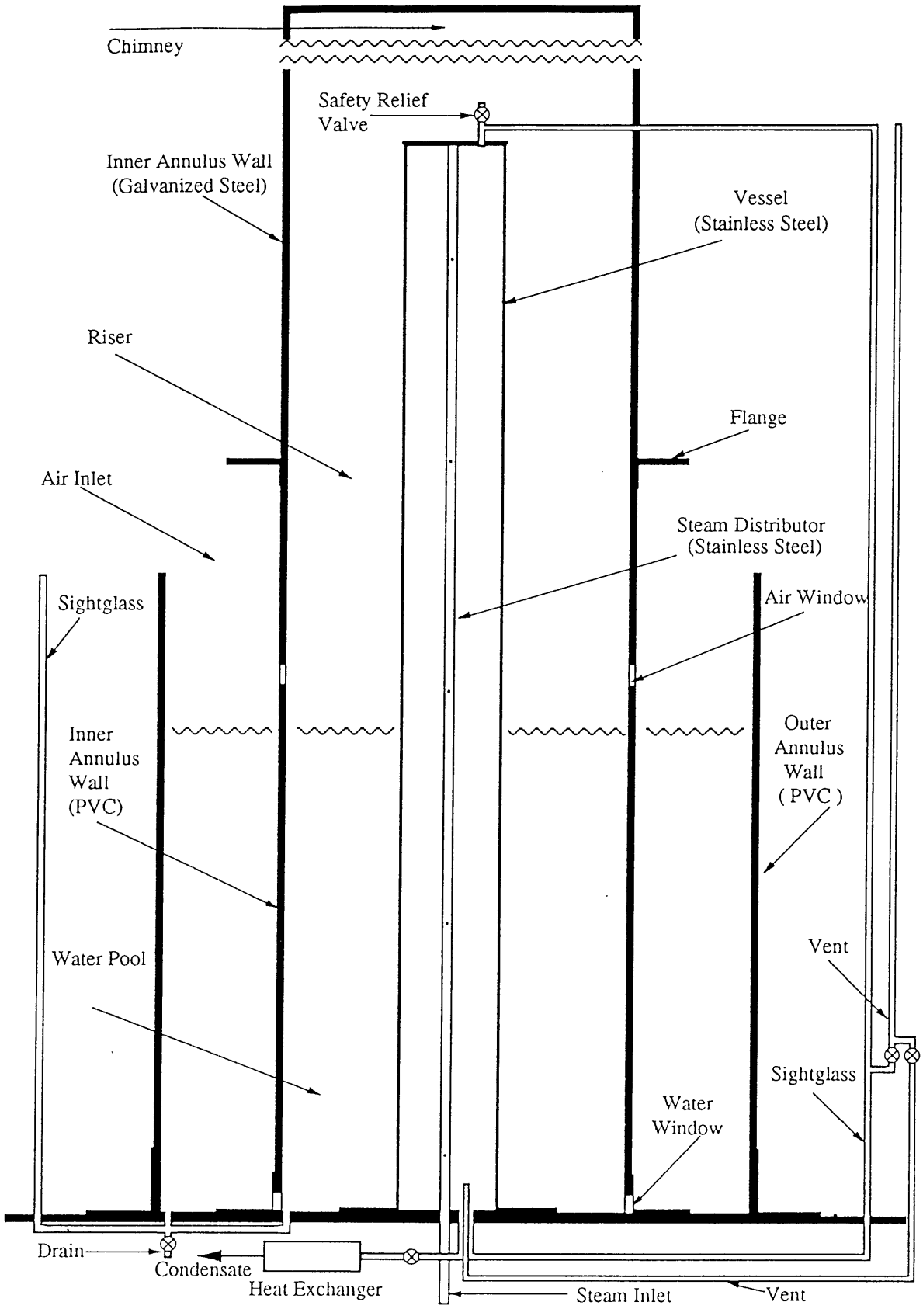

Figure 3.1.a Schematic of Test Apparatus

Figure 3.1.b Photographs of Test Apparatus

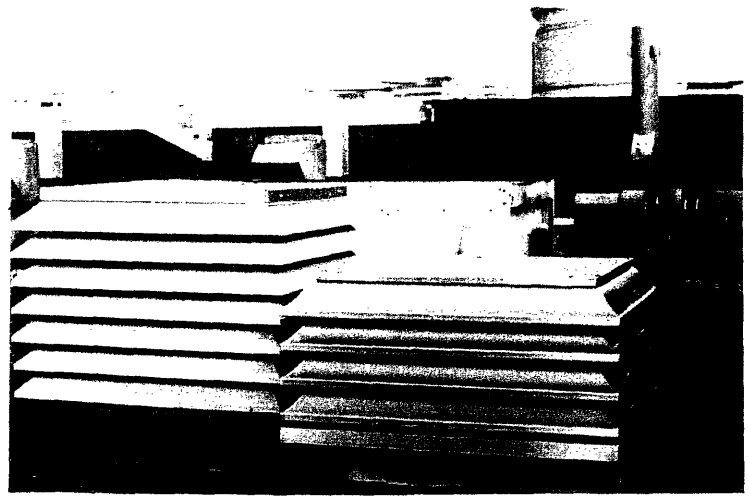

Chimney Before Insulation Viewed From Bottom

Roof Vent

Bottom of Test Apparatus

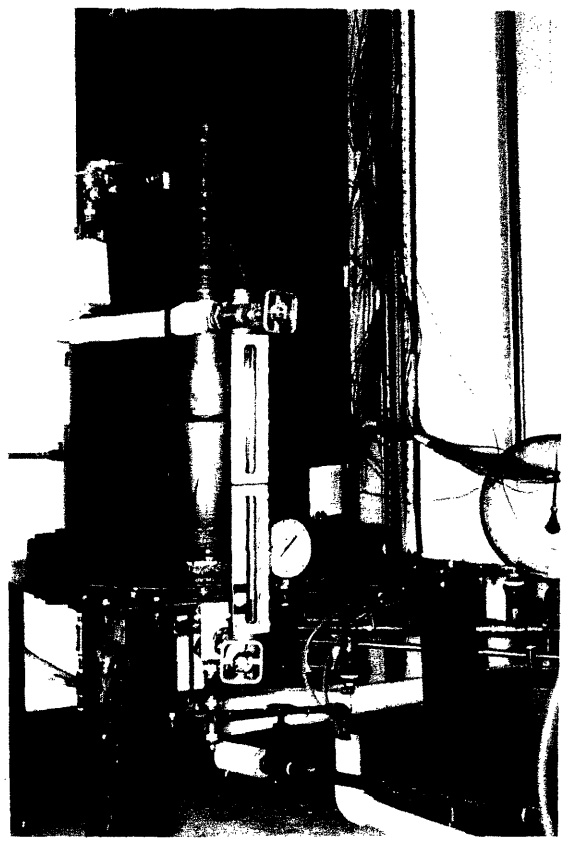

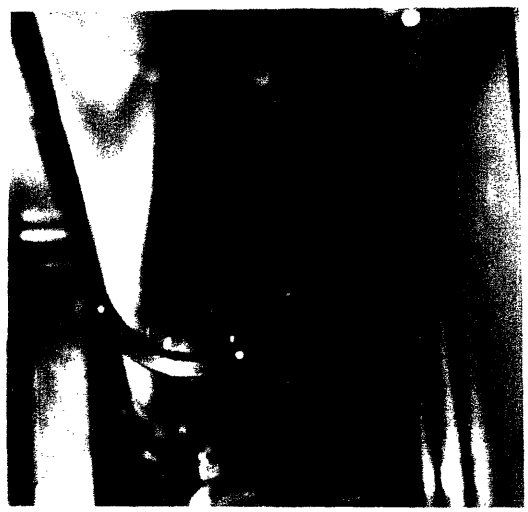

Chimney Before Insulation Viewed From Top

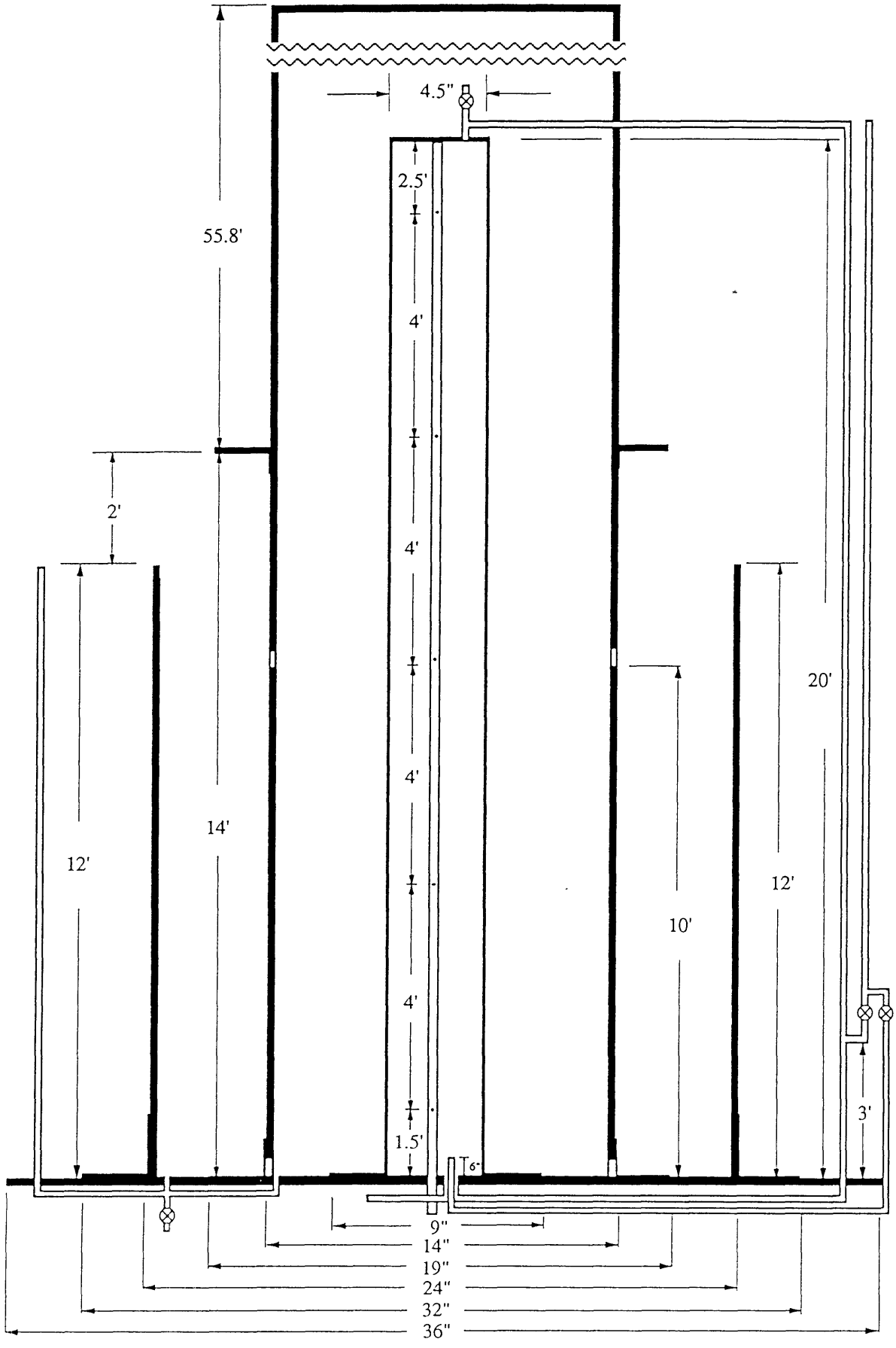

Figure 3.2 Dimensions of Test Apparatus

Table 3.1 Dimensions of the Test Apparatus

	Geometry, Material	Outer Diameter or Gap Width (in)	Wall Thickness (in)	Insulation Material, Thickness(in)	Height (feet)
Steel Vessel	hollow cylinder 304 S.S. (Sch.40S)	4.5	0.237	-	20
Steam Distributor	perforated tube 304 S.S. (Sch. 40S)	1.05	0.113	-	20
Inner	hollow cylinder PVC (Sch. 80)	14	0.79	-	14
Annulus Wall	hollow cylinder galvanized steel	12	0.024	2" fiberglass	6
Inner Water Pool	annulus	3.95	-	-	-
Outer Annulus Wall	hollow cylinder PVC (SDR 41)	24	0.663	-	12
Outer Water Pool	annulus	4.33	-	-	-
Chimney (Lower Section)	hollow cylinder galvanized steel	12	0.024	2" fiberglass	29.8
Chimney (Upper Section)	hollow cylinder PVC	14	-	0.75" fiberglass	20
Bottom Plate	square 304 S.S.	36"*36"	0.5	-	-

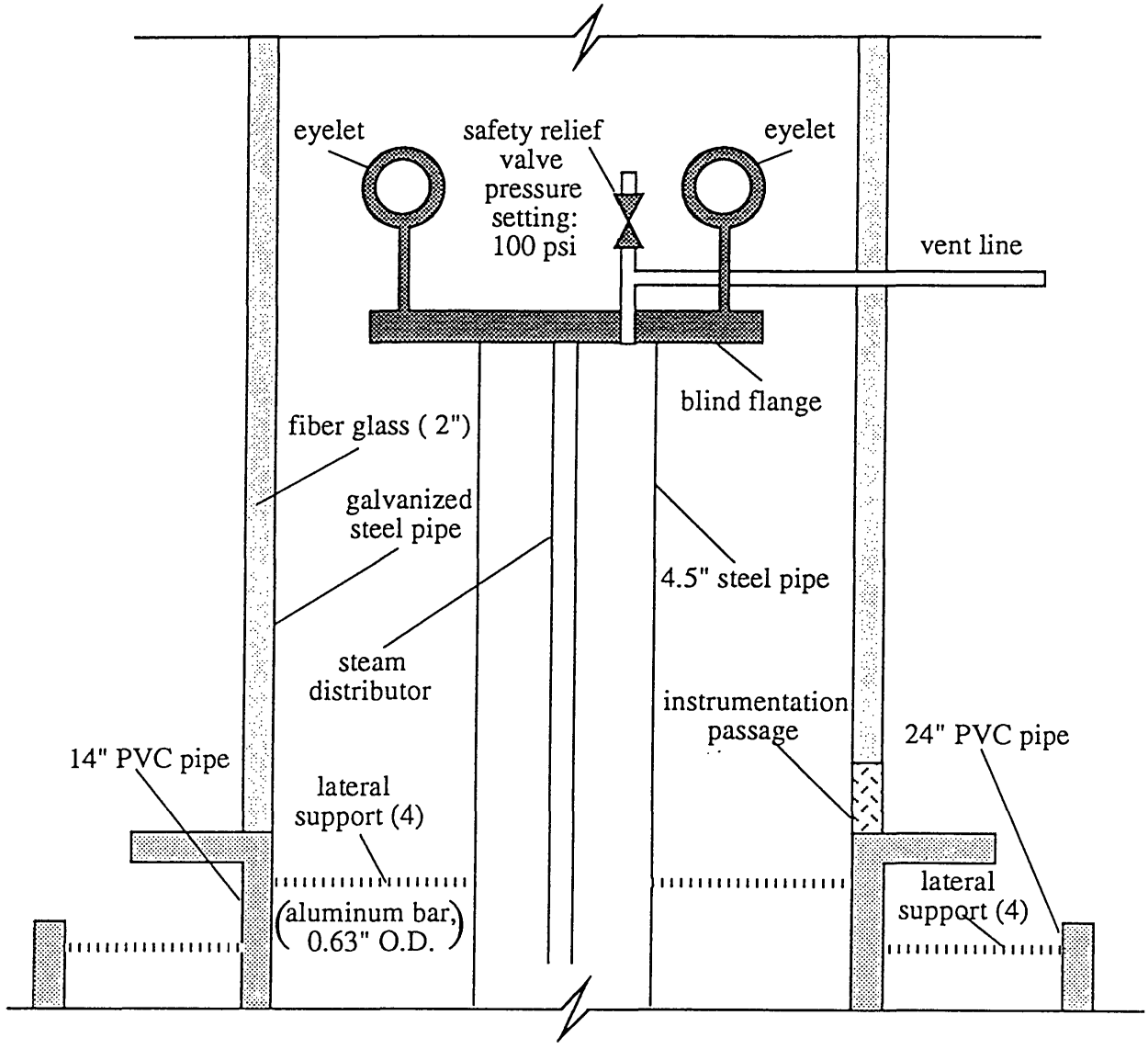

Figure 3.3 Top Portion of Heated Vessel

square stainless steel plate. The function of the top and bottom vent pipes is to vent the noncondensable (air) present in the steam supply source. The condensate drain line is run through a water-cooled heat exchanger to prevent flashing of the hot water. The condensate is then collected in a container which is located on a scale. The sight glass, marked with a level, serves to monitor the condensate accumulation in the heated vessel.

3.3.2 Steam Supply System

Saturated steam is selected as the power source for the experiment to simulate the environment of a prototype containment under accident conditions. The steam is from the MIT steam supply system which provides nominal 0.138 kg/sec of 0.48 MPa saturated steam to the heat transfer laboratory. The steam is further passed through a fiberglass insulated hot water tank, as shown in Figure 3.4, to ensure the quality of the steam before entering the heated vessel. The hot water tank is a gravity driven steam-water separator. Studies [G-1] show the general good performance of a gravity driven steam-water separator in low flowrate applications. To run the experiment at various steam pressure conditions, a steam pressure regulator is installed at the inlet of the hot water tank. The outlet of the hot water tank is connected to the steam distributor. The function of the steam distributor is to provide uniform axial steam distribution in the heated vessel. It is a 6.096 m (20 ft) long, 304 stainless steel pipe, 2.67 cm (1.05 in) in outer diameter, located at the center of the heated pipe. To achieve the desired function, there are nineteen 3.175 mm (1/8 in), staggered (90° rotation) flow holes uniformly distributed along the pipe, as shown in Figure 3.5. The total flow area of the holes is 1.5 cm^2 (0.233 in^2), which is less than half of the cross sectional area of the steam distributor, 3.44 cm^2 (0.533 in^2), to ensure a near-equal distribution of steam throughout the distributor.

3.3.3 Inner Annulus Wall

The function of the inner annulus wall is to form a flow channel and to limit the amount of directly heated fluid. The inner annulus wall is made up of two kinds of material, 4.27 m (14 ft) long PVC and 1.83 m (6 ft) long galvanized steel. The PVC section is located at the bottom of the inner annulus wall. The galvanized section is insulated with 5.08 cm (2 in) thick fiberglass. The outer diameter of the inner annulus wall is 35.56 cm (14 in). Two air and/or water windows on the PVC section provide air inlet or

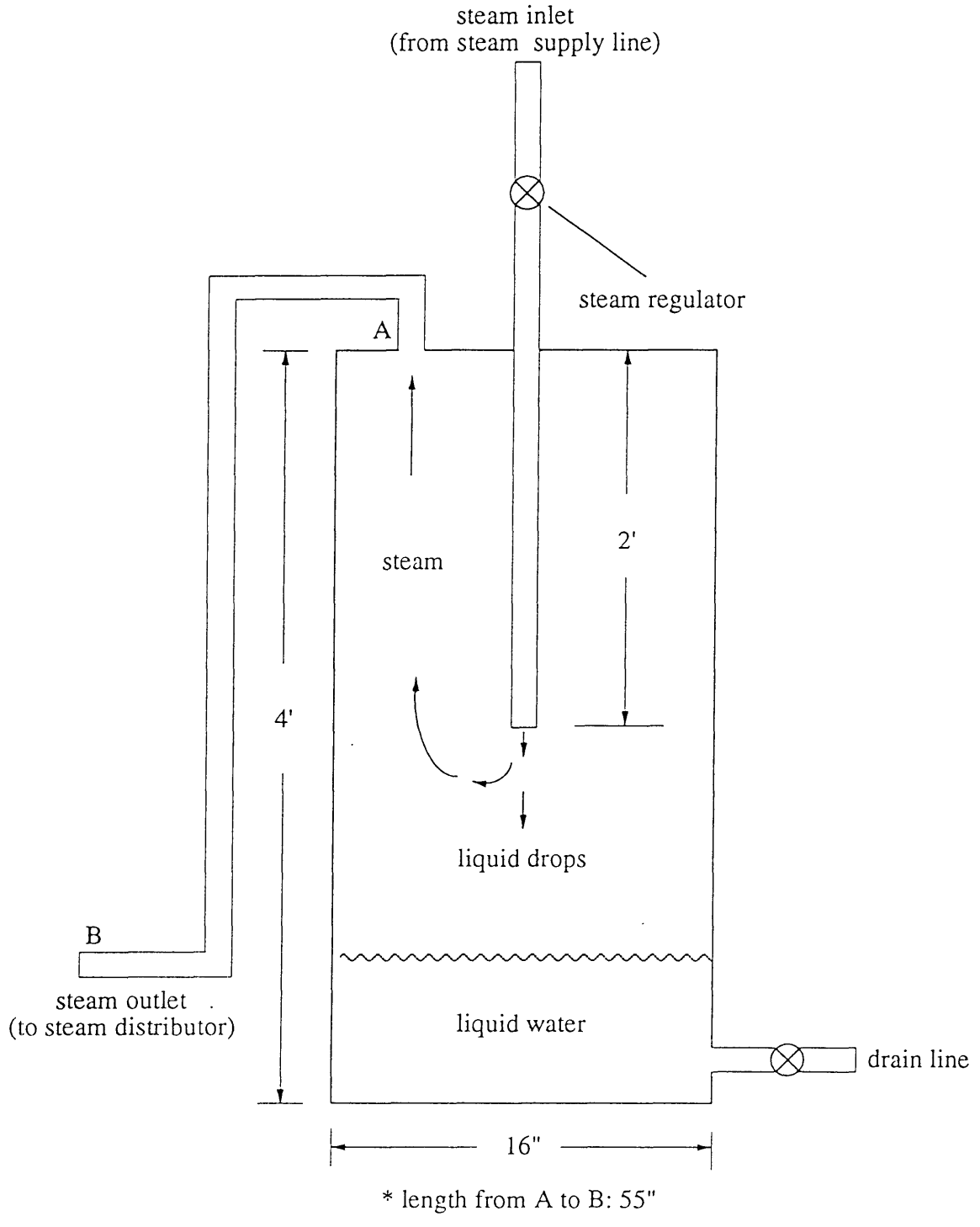

Figure 3.4 Hot Water Tank

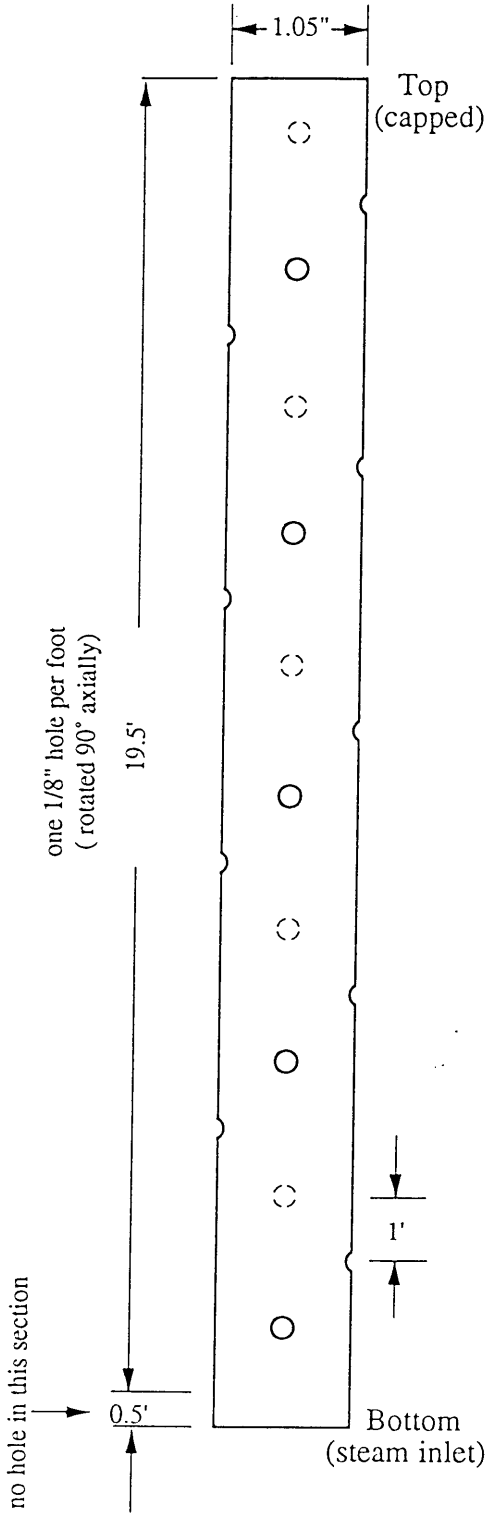

Figure 3.5 Steam Distribuor

water passages between the inner and outer annuli. One of the windows is located at the bottom of the wall and the other is located 3.048 m (10 ft) height above the bottom, as shown in Figure 3.6. Each of the windows is composed of three 16.5 cm by 16.5 cm (6.5 in by 6.5 in) square, rounded-edge and corner openings.

3.3.4 Outer Annulus Wall

The outer annulus wall confines the non-direct-heated fluid. It is a 3.66 m (12 ft) long, PVC pipe, 60.96 cm (24 in) in outer diameter. The outer annulus is equipped with a sight glass which has a ruler taped to it to indicate water level.

3.3.5 Chimney

The chimney vents the steam generated from pool water evaporation out of the test facility and provides length to achieve a fully developed flow. This is the condition at which exit flow stream measurements are made as well as that achieved in a prototype containment, that is, the length from the top of the heated vessel flange to the chimney diameter, L/D, is 22.5. The chimney is 15.2 m (49 ft, 10 in) long, composed of a permanently mounted 6 m long, 35.6 cm (14 in) outer diameter, PVC pipe section (upper) and 9.1 m long galvanized steel pipe section (lower). The PVC pipe is insulated with 1.9 cm thick fiberglass. The galvanized steel pipe is 1.524 m (5 ft) long apiece, 30.48 cm (12 in) inner diameter. The gap between two pipes is sealed by silicon rubber (RTV). The galvanized steel pipe section is insulated with 5.08 cm (2 in) thick fiberglass to reduce the heat loss. The outlet of the chimney is connected to a chimney cap (3 ft by 3 ft), provided by Norman Associates Inc., type RLX - aluminum louvered penthouse, as shown in Figure 3.1.b. The chimney cap is surrounded by a plywood enclosure box to minimize wind effects.

3.3.6 Instrumentation

There are forty-seven thermocouples, one velocity meter, two relative humidity meters, one scale, one pressure gauge, and two level indicators used in the experiment to measure the data of our interest. Table 3.2 shows the nomenclature of the instruments.

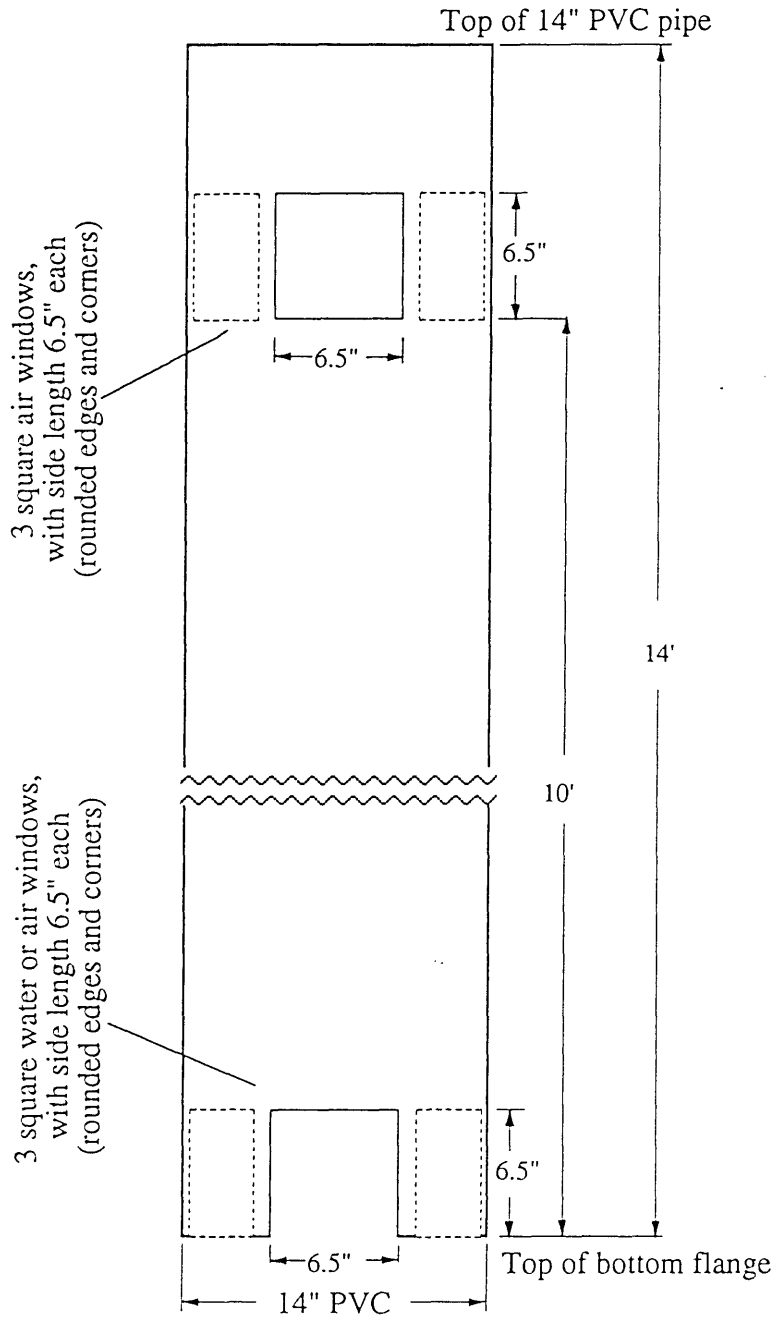

Figure 3.6 Air and/or Water Windows of Inner Annulus Wall

Table 3.2 Nomenclature for the Instrumentation

Symbol	Description
TC1 ~ TC10	thermocouples for the heated pipe's wall outer surface temperature; $T_{wo,pool}$ or $T_{wo,mix}$
TC11 ~ TC15	thermocouples for the heated pipe's inner (steam) temperature
TC16 ~ TC20	thermocouples for the inner annulus steam-air mixture or
TC26 ~ TC30	pool water temperature; T_{mix} or T_{pi}
TC21 ~ TC25	thermocouples for the outer annulus pool water temperature; T_{po}
TC31	thermocouple for the exit steam-air mixture temperature (at the same location for the velocity meter and the exit humidity meter); $T_{mix,o}$
TC32	thermocouple for the supplied steam temperature
TC33, TC34	thermocouples for the condensate temperature
TC35 ~ TC39	thermocouples for the wet bulb temperature
TC40 ~ TC42	thermocouples for heat loss estimation
TC43	thermocouple for the inlet air temperature; T_{in}
TC44, TC45	thermocouples for the inner wall surface temperature of the PVC inner annulus wall, T_{PVC}
TC46, TC47	thermocouples for the inner wall surface temperature of the galvanized steel inner annulus wall, T_{gal}
RH1	humidity meter for the exit steam-air mixture; ϕ_{mix}
RH2	humidity meter for the inlet air; ϕ_{in}
V1	velocity meter for the steam-air mixture; V_{mix}
L1	level indicator for the water pool; H_{pool}
L2	level indicator for the condensate

The arrangement of the instruments is shown in Figures 3.7 and 3.8. The level indicators, which are essentially rulers, and the standard bourdon tube pressure gauge are not discussed further. The barometric pressure, used to estimate the vapor contained in the intake air flow, is obtained from a local weather station.

3.3.6.1 Thermocouples

Ten thermocouples (TC1 through TC10) are mounted on the surface of the heated vessel to measure the wall outer surface temperature. The thermocouples are arranged in a staggered manner, 180° separation in the circumferential direction and one thermocouple per two-foot axial height, to ensure the symmetric measurement of the experimental data. Five thermocouples (TC11 through TC15) are mounted in the center of the heated vessel to measure the axial steam temperature distribution. Ten thermocouples (TC16 through TC20 and TC26 through TC30) are mounted in the center of the inner annulus, positioned in the same direction as those of TC1 through TC10, to measure the fluid temperature in the inner annulus. Another five thermocouples (TC21 through TC25) are mounted in the center of the outer annulus, positioned in the same staggered manner as those of TC16 through TC20, to measure the fluid temperature in the outer annulus.

To measure the temperature of the fully developed fluid stream, one thermocouple (TC31) is mounted at the center of the chimney and 6.86 m (22.5 ft) above the top of the heated vessel, which is 22.5 times the inner diameter of the chimney. There is one thermocouple (TC32) mounted at the inlet of the steam supply line which together with a pressure gauge mounted at the same location, monitor the thermodynamic state of the input steam. To monitor the condensate temperature, thermocouples, TC33 and TC34, are mounted at the inlet and outlet of the heat exchanger, respectively . To estimate the heat loss, there are two thermocouples (TC40 and TC41) mounted in the chimney, 2.74 m (9 ft) below TC31, and one thermocouple (TC42) mounted at the outer surface of the chimney insulation at the same elevation as TC40 and TC41. Another thermocouple (TC43) is mounted at the entrance of the outer annulus to measure the inlet air temperature. In addition, there are four thermocouples (TC44 through TC47) mounted at the inner surface of the inner annulus wall, positioned at the same circumferential orientation and elevation as TC26 through TC29, respectively, to estimate radiative heat transfer.

All thermocouples, except TC35 through TC39 and TC41 through TC43, are of the

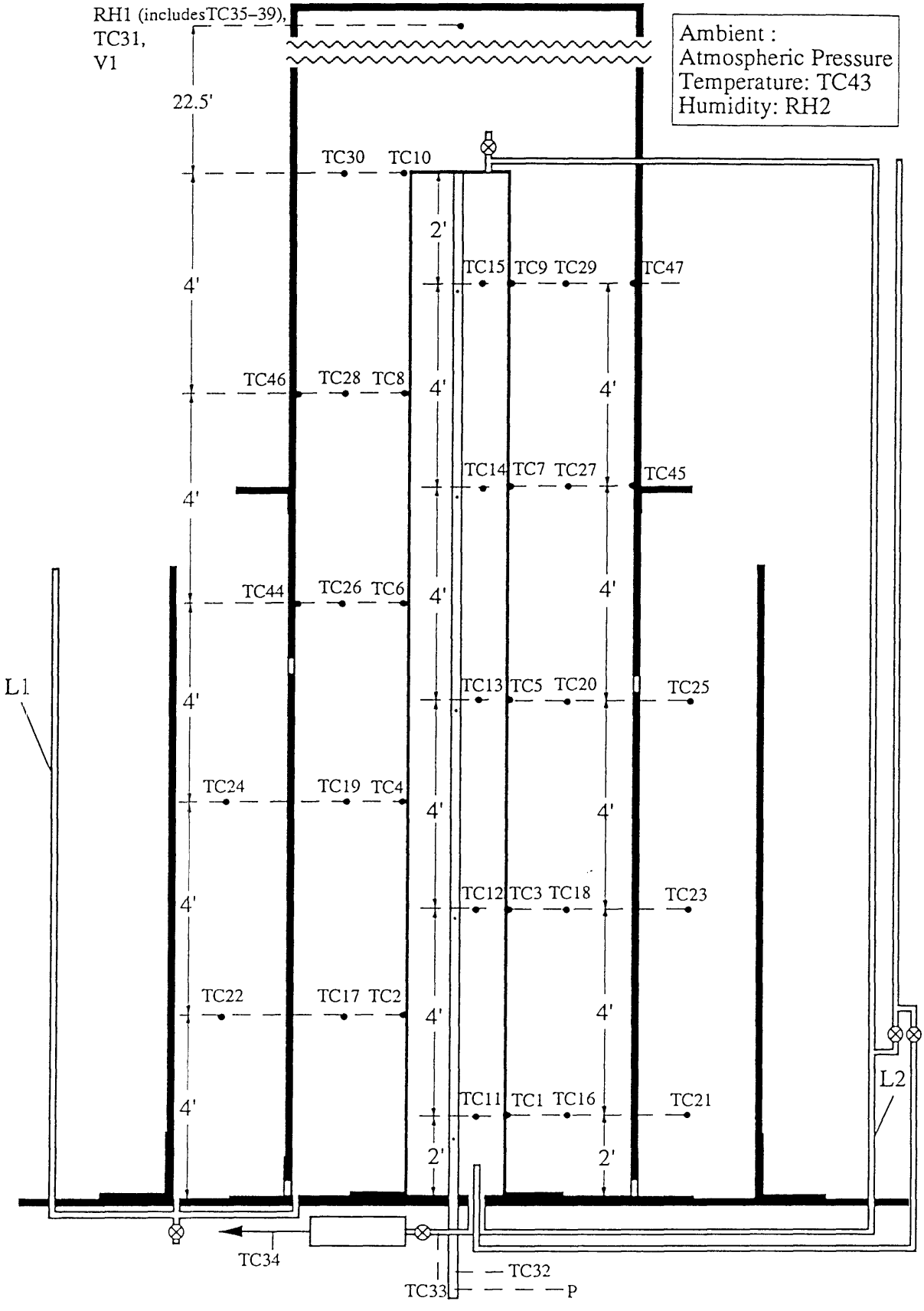

Figure 3.7 Instrumentation Arrangement

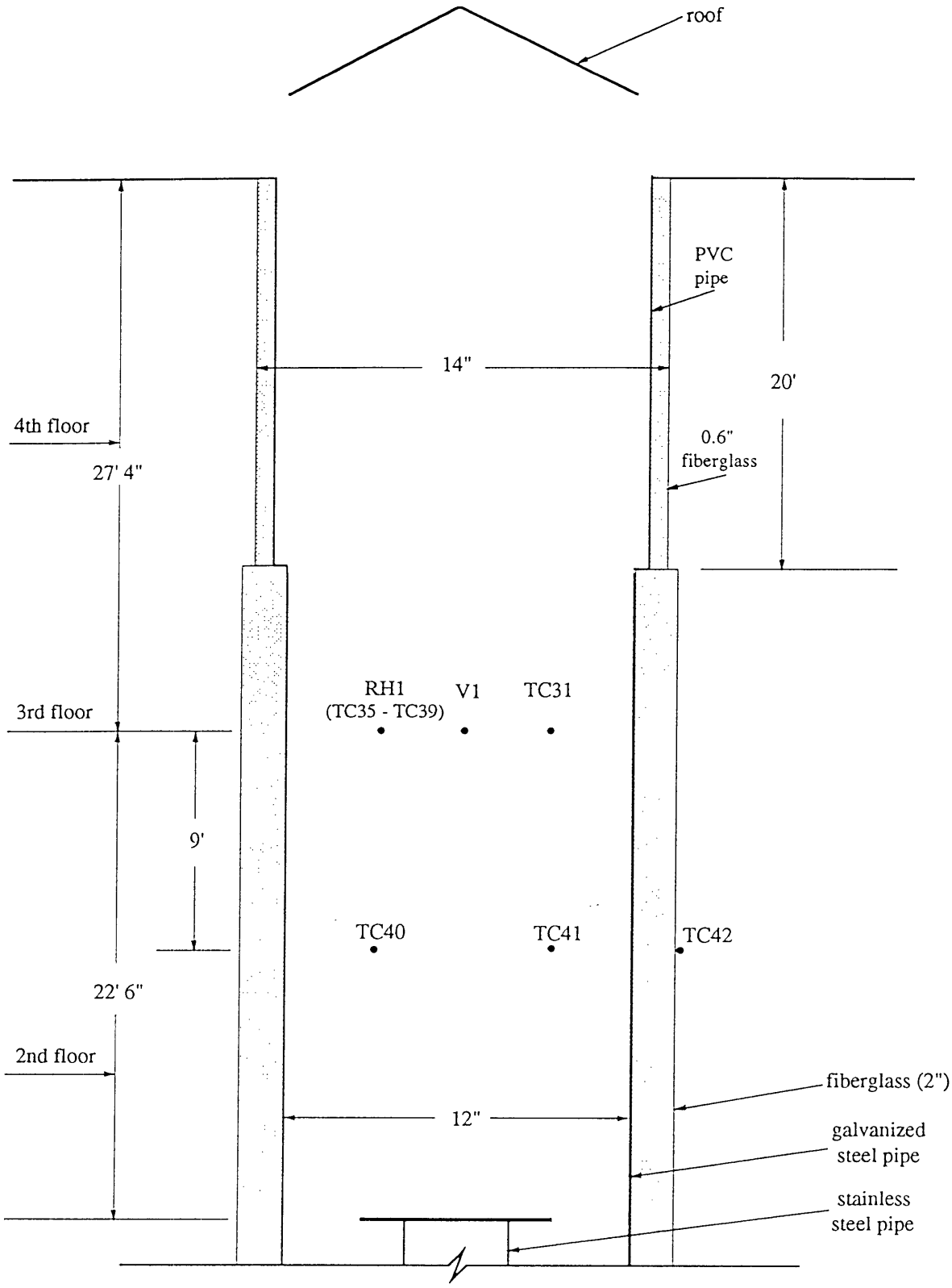

Figure 3.8 Chimney – Instrumentation Layout

stainless steel sheathed copper-constantan type with a diameter of about 1.5 mm. Thermocouples TC35 through TC39 and TC41 through TC43, which are also of copper-constantan type, are made in the laboratory from 0.056 in diameter thermocouple wire by using a thermocouple welder. All thermocouples which penetrate the pipe wall are equipped with a brass-made thermocouple port. Three O-rings prevent leakage for each thermocouple port. All thermocouples and the thermocouple wires used to make thermocouples, as well as thermocouple extension wires, are purchased from OMEGA Engineering Inc. located at 1 Omega Drive, Stamford, Connecticut 06906. Note that the accuracy of the copper-constantan thermocouples, which are used in the experiment in the region of our interest, is about 0.5 °C. All thermocouples were calibrated in an isothermal condition, and exhibited adequate agreement (within ± 0.5 °C at a given station). Table 3.3 shows the thermocouple readings at various locations under adiabatic/isothermal conditions.

3.3.6.2 Velocity Meter

A velocity meter (V1) is mounted near TC31 to estimate the mass flow rate of the steam-air mixture in association with TC31 and humidity meter RH1. To prevent flow disturbance, the velocity meter is placed below RH1. The velocity meter, purchased from OMEGA Engineering Inc., model HH-F10, is based on the principal that a freely turning turbine will rotate at a speed directly proportional to the speed of the air flow. The signal wires and power supply wires have been extended to fit the geometry of the apparatus and provide convenient readout at the basement level. The calibration of the velocity meter is discussed in section 3.4.1.

3.3.6.3 Relative Humidity Meter

To estimate the vapor content in the steam-air mixture flow, one relative humidity meter (RH1) is mounted just above the velocity meter. The relative humidity meter is a wet bulb-dry bulb type humidity meter. The wet bulb temperature measurement device of RH1 is shown in Figure 3.9. The design of the meter is described in the work of J. Bowman and P. Griffith [B-1]. Bowman has demonstrated that the wet bulb-dry bulb humidity meter will behave properly in both forced convection and natural convection. To mitigate

Table 3.3 Thermocouple Readings under Adiabatic/Isothermal Conditions

Heated Vessel Wall Surface Temperature	TC1	TC2	TC3	TC4	TC5
	25.24	25.17	25.08	25.06	25.57
	TC6	TC7	TC8	TC9	TC10
	25.96	25.99	25.92	25.92	25.91
In-Vessel Steam Temperature	TC11	TC12	TC13	TC14	TC15
	25.34	25.16	25.73	26.04	26.00
Inner Annulus Fluid Temperature	TC16	TC17	TC18	TC19	TC20
	25.63	25.64	25.62	25.63	25.35
	TC26	TC27	TC28	TC29	TC30
	26.05	25.93	26.01	25.91	25.93
Outer Annulus Fluid Temperature	TC21	TC22	TC23	TC24	TC25
	25.65	25.74	25.91	26.06	26.21
Chimney Fluid Temperature	TC31	TC40	TC41	-	-
	25.83	26.04	26.04	-	-
Humidity Meter Temperature	TC35	TC36	TC37	TC38	TC39
	25.84	25.84	25.84	25.84	25.91
Duct Wall Temperature	TC44	TC45	TC46	TC47	-
	26.18	25.83	25.78	25.54	-

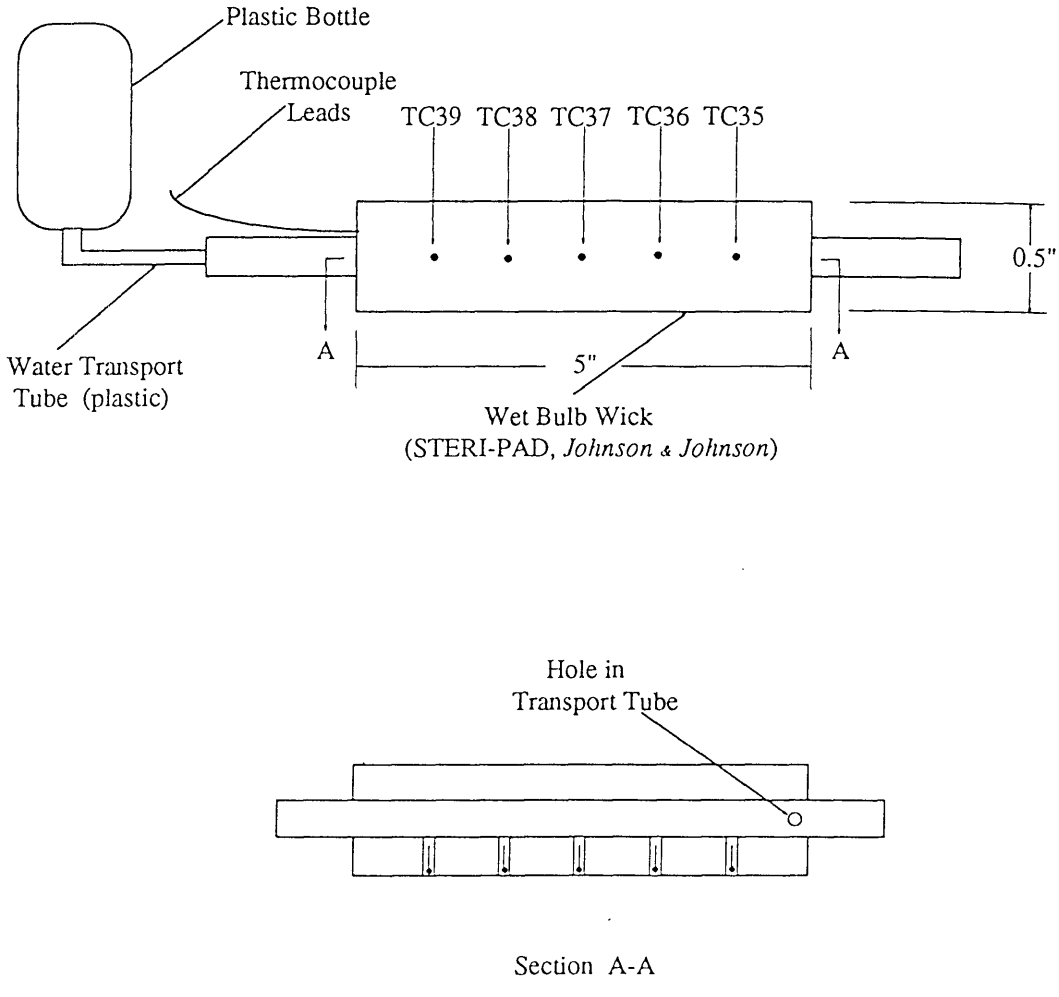

Figure 3.9 RH1 – Wet Bulb Temperature Measurement Device

the effects from the supplied subcooled water and/or dryout of the wick, five copper-constantan type thermocouples (TC35 through TC39) are embedded in the cotton wick. In addition, one humidity meter (RH2), purchased from Industrial Instruments & Supplies Company, model: PSYCHRO-DYNE, is used to estimate the vapor contained in the inlet air flow. The RH2 meter is also a wet bulb-dry bulb type humidity meter. It is manufactured and calibrated according to Weather Bureau and Navy specifications.

3.3.6.4 Scale

A scale is used to weigh the condensate collected from the steam condensation in the heated vessel to provide a redundant parameter to check the total heat transfer rate. The scale, model OHAUS DS5-M, is purchased from Caley & Whitmore Co., located at 18 Highland Av., Somerville, MA 02143. The scale had been calibrated against NIST (National Institute of Standards and Technology) standards by the supplier. The accuracy of the scale is $\pm$ 0.02 kg. It is also periodically checked using secondary standard weights.

3.4 Calibration of Velocity Meter, Humidity Meter and Data Acquisition System

3.4.1 Velocity Meter Calibration

The signal wires and power supply wires of the velocity meter have been extended to fit the geometry of the apparatus and for the purpose of convenient readout. Therefore, it has been recalibrated in the wind tunnel located at Room 33-012, Aeronautics and Astronautics Department. The model numbers and the accuracy of the wind tunnel instrumentation are as follows.

(1) MKS Baratron Differential Pressure Transducer, model 310B-10 torr
(2) Readout Box, model 170
(3) Accuracy
- 0.08 % of reading for the transducer
- resolution : 1E-5 torr
- 0 (zero) coefficient : 5E-6 of full scale per °C
- span coefficient : less than 0.002 % of reading per °C

The calibration data and curves are shown in Table 3.4, Figures 3.10, 3.11, and 3.12. Because of the high accuracy of the wind tunnel instrumentation (less than 0.2 % of the reading, in the range of our interest of 1.5 m/s to 3 m/s), the uncertainty associated with the velocity measurement is due to the limitation of the velocity meter readout capability, that is, 0.1 m/sec or 10 ft/min. As can be seen, the meter has a quite linear response and good absolute accuracy.

3.4.2 Relative Humidity Meter Calibration

The relative humidity meter, RH1, was calibrated against another wet bulb-dry bulb humidity meter, RH2, which is also referred to as the standard meter. The accuracy of the RH2 is 1 %, as addressed in the technical manual. The calibration of RH1 was performed over a long period of time to obtain a wide range of humidity data (30 % to 90 % relative humidity). The uncertainty of the RH1 meter is 2 %. Table 3.5 and Figure 3.13 show the calibration data and curve. Since RH1 is essentially a wet bulb-dry bulb relative humidity meter, it can be used outside of the calibrated range without introducing extra uncertainty.

3.4.3 Data Acquisition System Calibration

A Hewlett-Packard data acquisition system, HP-3497A, together with an IBM/XT personal computer, is used to measure the temperature. LOTUS 123 with MEASURE software is used to record and preprocess the data. The data acquisition system was calibrated against NIST standards on Jan. 28, 1994 by Hewlett-Packard Co., located at W 120 Century Road, Paramus, New Jersey. The instrument was found to be within its manufacturer's specified accuracy (less than $\pm$ 0.01% deviation), which is far beyond the requirements of this experiment.

3.5 Procedure for Experimental Determination of Heat Transfer Performance

One of the key parameters to evaluate the performance of a passive containment cooling design is the power removal capability. Therefore, in the prefilled water-air annulus passive containment cooling experiment, the parameters of interest are the total heat transfer rate and heat flux, the heat transfer coefficient and the Reynolds number of the

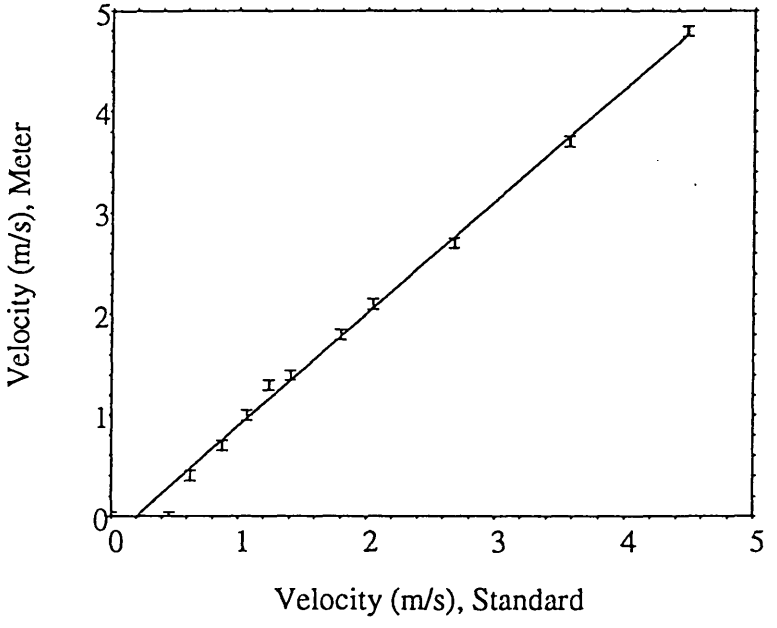

Figure 3.10 Velocity Meter Calibration Curve — Meters Per Second

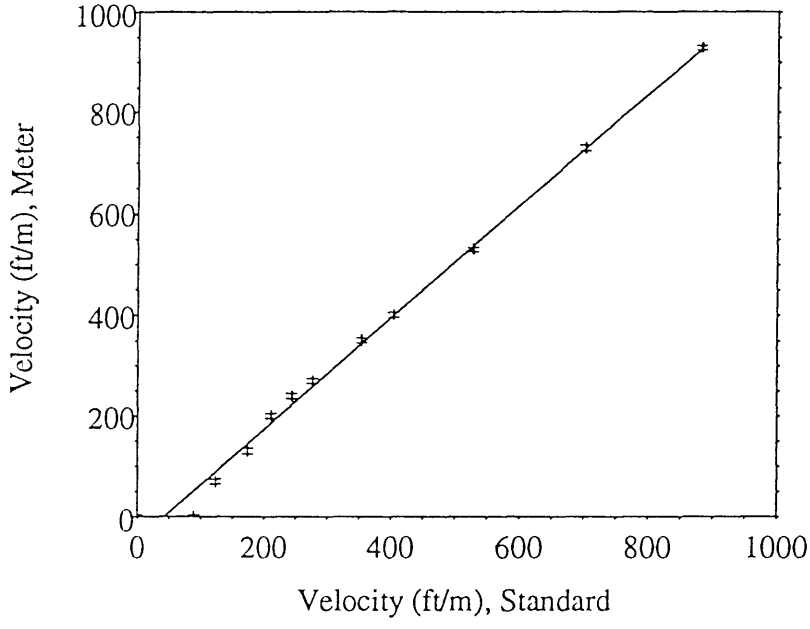

Figure 3.11 Velocity Meter Calibration Curve — Feet Per Minute

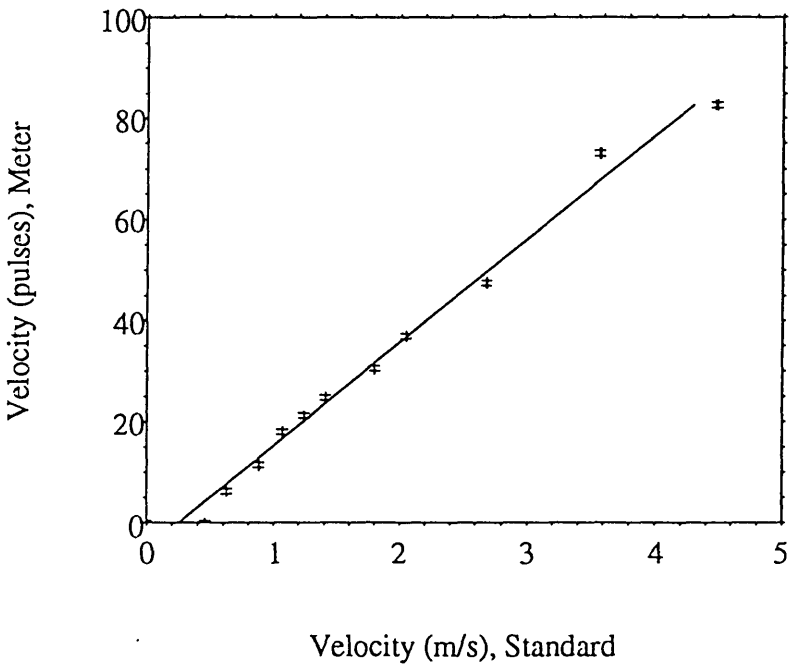

Figure 3.12 Velocity Meter Calibration Curve — No. of Pulses

Note : No. of pulses — No. of signals detected by the meter

Table 3.4 Velocity Meter Calibration Data

Pressure (torr)	0	0.0009	0.002	0.0037	0.006	0.008	0.01	0.0147	0.02	0.033	0.0588	0.0918
Velocity (m/s) Standard	0	0.46	0.625	0.88	1.07	1.24	1.41	1.8	2.05	2.68	3.75	4.48
Velocity (m/s) Meter	0	0	0.4	0.7	1.0	1.3	1.4	1.8	2.1	2.7	3.7	4.8
Velocity (ft/m) Standard	0	90	123	174	211	244	277	354	404	528	702	882
Velocity (ft/m) Meter	0	0	70	130	200	240	270	350	400	530	730	930
Velocity (pulse) Meter	0	0	6.3	11.5	18.0	21.2	24.8	30.5	36.9	47.5	64.6	82.6

Table 3.5 Humidity Meter , RH1, Calibration Data

Relative Humidity (%), Standard	30.0	37.0	50.0	66.0	68.0	71.5	72.0	75.5	81.5	83.0	87.0	89.0
Relative Humidity (%), RH1 Meter	30.0	37.0	51.0	65.0	69.0	70.5	70.0	77.0	82.5	84.0	88.0	90.0

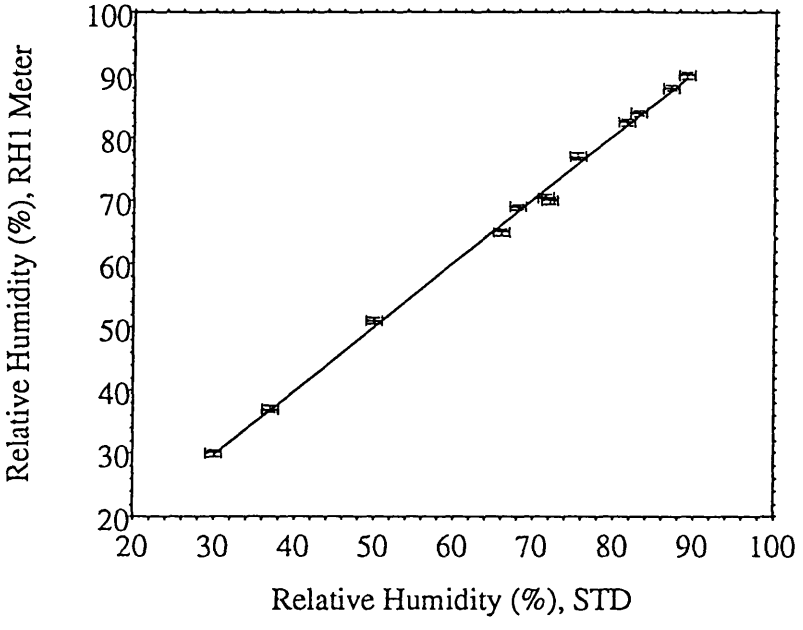

Figure 3.13 Humidity Meter, RH1, Calibration Curve

steam-air mixture flow. The total heat transfer rate is the summation of the heat transfer rates to the pool water and to the flowing steam-air mixture. The heat transfer mechanisms in the pool can be free convection and/or subcooled or saturated boiling. The heat transfer mechanism in the air section of the annulus is mixed air (or steam-air mixture) convection. These performance indicators can be derived from the measured heated wall surface temperatures, fluid temperatures, temperature rise of the mixture along the heated surface, temperature rise of the pool water over a certain amount of time, flow velocity, humidity, and condensate weight.

3.5.1 Heat Transfer Rate to Steam-Air Mixture

To calculate the heat transfer rate to the steam-air mixture, the steam-air mixture flow rate is measured using a velocity meter, a humidity meter and a thermocouple. Assuming further that air and steam are perfect gases, the heat transfer rate can be evaluated as follows by applying the heat balance equation.

$$\dot{Q}_{mix} = \dot{m}_{mix} \overline{C}_{p,mix} (T_{mix,o} - T_{mix,in}), \tag{3.15}$$

where

$$\dot{m}_{mix} = \dot{m}_{stm} + \dot{m}_{air}$$

$$= (\rho_{stm} + \rho_{air}) V_{mix} A_{mix}$$

$$= [\frac{\phi_{mix} P_{sat}(T_{mix})}{R_{stm} T_{mix}} + \frac{P_{atm} - \phi_{mix} P_{sat}(T_{mix})}{R_{air} T_{mix}}] V_{mix} A_{mix} \tag{3.16}$$

An alternative approach to determining the steam generation rate is to measure the rate of level decrease in the water pool.

$$\dot{m}_{stm} = \frac{1}{\Delta t} (H_{pool,1} - H_{pool,2})(\overline{\rho}_{f,pi} A_{pi} + \overline{\rho}_{f,po} A_{po}) \tag{3.17}$$

In the case of no water in the pool, $\dot{m}_{mix}$ is the summation of $\dot{m}_{air}$ and $\dot{m}_{vapor,in}$. $\dot{m}_{vapor,in}$ is the vapor content in the intake air flow. It can be expressed as:

$$\dot{m}_{vapor,in} = [\frac{\phi P_{sat}(T)}{RT}(VA)]_{vapor,in}$$

$$= [\frac{\phi P_{sat}(T)}{RT}]_{vapor,in} \frac{\dot{m}_{air}}{[\frac{P_{atm} - \phi P_{sat}(T)}{RT}]_{air,in}} . \quad (3.18)$$

The heat transfer in the steam-air mixture section can be further split into two parts, that is, convective heat transfer and radiative heat transfer. In addition, the duct wall is made up of two kinds of material: galvanized steel and PVC. The radiative heat transfer should be treated separately.

$$\dot{Q}_{mix} = \dot{m}_{mix} \overline{C}_{p,mix} (T_{mix,o} - T_{mix,in})$$

$$= \dot{Q}_{conv} + \dot{Q}_{rad}, \quad (3.19)$$

where

$$\dot{Q}_{conv} = \overline{h}_{mix} \pi D_{vessel} (H_{vessel} - H_{pool})(\overline{T}_{wo} - \overline{T})_{mix} \quad (3.20)$$

$$\dot{Q}_{rad} = \dot{Q}_{rad,PVC} + \dot{Q}_{rad,gal} \quad (3.21)$$

$$\dot{Q}_{rad,gal} = \pi D_{vessel} H_{gal} \frac{\sigma}{[\frac{1}{\varepsilon_{ss}} + \frac{D_{vessel}}{D_{gal}}(\frac{1}{\varepsilon_{gal}} - 1)]} (\overline{T}^4_{wo} - \overline{T}^4_{wi})_{gal} \quad (3.22)$$

$$\dot{Q}_{rad,PVC} = \pi D_{vessel} (H_{vessel} - H_{pool} - H_{gal}) \frac{\sigma}{[\frac{1}{\varepsilon_{ss}} + \frac{D_{vessel}}{D_{PVC}}(\frac{1}{\varepsilon_{PVC}} - 1)]} (\overline{T}^4_{wo} - \overline{T}^4_{wi})_{PVC} \quad (3.23)$$

The averaged effective heat transfer coefficient of the steam-air mixture which combines the convective heat transfer and radiative heat transfer can be expressed as:

$$\overline{h}_{mix,eff} = \frac{\overline{q}''_{mix}}{(\overline{T}_{wo} - \overline{T})_{mix}}, \quad (3.24)$$

where

$$\bar{q}''_{mix} = \frac{\dot{Q}_{mix}}{\pi D_{vessel}(H_{vessel} - H_{pool})}. \tag{3.25}$$

The averaged convective heat transfer coefficient, $\bar{h}_{mix}$, can be evaluated by applying Equations 3.19 and 3.20.

$$\bar{h}_{mix} = \frac{\dot{Q}_{mix} - \dot{Q}_{rad}}{\pi D_{vessel}(H_{vessel} - H_{pool})(\bar{T}_{wo} - \bar{T})_{mix}} \tag{3.26}$$

The Reynolds number of the flowing mixture, which is used to check the flow regime of the buoyancy driven air or mixture flow, can be evaluated by

$$Re = (\frac{\dot{m}D_e}{\mu A})_{mix}. \tag{3.27}$$

3.5.2 Heat Transfer Rate to Water Pool

The heat transfer rate to the water pool is the summation of the heat transfer rates due to free convection or subcooled boiling and saturated boiling or evaporation.

$$\dot{Q}_{pool} = (\dot{Q}_{pool})_{FC\ or\ SCB} + (\dot{Q}_{pool})_B \tag{3.28}$$

To find the free convection or subcooled boiling heat transfer rate in the water pool, the temperature increase rate of the inner and outer pool are measured before saturated boiling commences. By applying the heat balance equation, the heat transfer rate due to free convection or subcooled boiling can be expressed as:

$$\{\dot{Q}_{pool} = \frac{1}{\Delta t}\{[m_{wtr}(\bar{C}_{pf,2}\bar{T}_2 - \bar{C}_{pf,1}\bar{T}_1)]_{pi} + [m_{wtr}(\bar{C}_{pf,2}\bar{T}_2 - \bar{C}_{pf,1}\bar{T}_1)]_{po}\}\}_{FC\ or\ SCB}, \tag{3.29}$$

where

$$[m_{wtr,pi} = \rho_{f,pi}A_{pi}H_{pi}]_{FC\ or\ SCB}, \tag{3.30}$$

$$[m_{wtr,po} = \rho_{f,po}A_{po}H_{po}]_{FC\ or\ SCB}, \tag{3.31}$$

and subscripts 1, 2 represent times.

To find the heat transfer rate due to saturated boiling or evaporation, the steam generation rate is evaluated by measuring either the humidity of the flowing mixture or the water level decrease rates as discussed in the previous section. The heat transfer rate is expressed as:

$$[\dot{Q}_{pool} = (\dot{m}h_{fg})_{pool}]_{B}, \tag{3.32}$$

where

$$\dot{m}_{pool} = \dot{m}_{stm} - \dot{m}_{vapor,in}, \text{ and} \tag{3.33}$$

$\dot{m}_{stm}$ and $\dot{m}_{vapor,in}$ are the same as evaluated in Section 3.5 1, Equations 3.16 to 3.18.

The averaged heat transfer coefficient to the pool water can be expressed as:

$$[\bar{h}_{pool} = \frac{\bar{q}''_{pool}}{(\bar{T}_{wo} - \bar{T})_{pool}}]_{FC,\ SCB\ or\ B}, \tag{3.34}$$

where

$$[\bar{q}''_{pool} = \frac{\dot{Q}_{pool}}{\pi D_{vessel} H_{pool}}]_{FC,\ SCB\ or\ B}. \tag{3.35}$$

3.5.3 Total Heat Transfer Rate

The total heat transfer rate is the summation of the heat transfer rates to the pool water by free convection and/or subcooled or saturated boiling and to the flowing steam-air mixture. It can be expressed as:

$$\dot{Q}_{total} = \dot{Q}_{pool} + \dot{Q}_{mix}. \tag{3.36}$$

There is a redundant parameter to check the heat transfer performance of the system, that is, the heat transfer inferred from steam condensation, $\dot{Q}_{cond}$. It can be evaluated by weighing the condensate collected from the steam condensation in the heated stainless steel pipe, and can be expressed as:

$$\dot{Q}_{cond} = \frac{m_{cond}}{\Delta t} h_{fg}. \tag{3.37}$$

3.6 Summary of Chapter 3

Design considerations and experimental setup are discussed in this chapter. The major points are as follows:

- The performance indicators of the prefilled water-air annulus experiment are the total heat transfer rate and heat flux, the heat transfer coefficient and the Reynolds number of the flowing steam-air mixture. The total heat transfer rate is the summation of the heat transfer rates to the pool water and to the flowing steam-air mixture. The heat transfer mechanisms in the pool can be free convection and/or subcooled or saturated boiling. The heat transfer mechanism in the air section of the annulus is the mixed air (or steam-air mixture) convection. The steam condensation heat transfer provides a redundant parameter to check the total heat transfer rate.

- For the scaling of air convection, the heat transfer coefficient and Reynolds number are only moderately sensitive to heated length; and Reynolds number is sensitive to hydraulic diameter. This analysis suggests that reducing heated length rather than hydraulic diameter should be more effective in reducing scale for the experiment. Moreover, the input heat flux or temperature can be increased for the reduced scale experiment to ensure achievement of the appropriate turbulence regime and to achieve the simulation of the heat transfer coefficient.

- For the scaling of the heat transfer in the pool, the free convection heat transfer coefficient is independent of the characteristic length. The nucleate boiling heat transfer coefficient is not directly dependent on the characteristic length. However, the fluid properties in the heat transfer correlation are a function of pressure, hence pool depth. This effect should be taken into account.

- The test apparatus is composed of four concentric pipes and a long chimney. A steam distributor ensures a uniform axial temperature distribution in the heated vessel. The air and/or water windows provide passages for fluid communication between the inner and outer annulus. The selection of the test apparatus dimensions is based on the scaling analysis and the constraints of the laboratory. The tall chimney helps in the data acquisition for the fully developed flow stream, and ensures attainment of the same flow regime as in a prototype containment.

- There are ten thermocouples mounted at the heated surface to measure wall surface temperature, seventeen thermocouples mounted in the inner annulus, outer annulus and chimney to measure the flow stream or fluid temperature, five thermocouples mounted in the heated vessel to measure the axial temperature distribution, and four thermocouples mounted at the inner surface of the inner annulus wall to estimate radiative heat transfer. To measure the heat loss, three additional thermocouples are mounted in the chimney.

- The relative humidity meter is a wet bulb-dry bulb type, and calibrated against another standard wet bulb-dry bulb relative humidity meter. The fan type velocity meter, located at 22.5 times the diameter of the chimney from the top of the heated vessel, to measure the developed flow velocity, was recalibrated at the MIT wind tunnel.

- Saturated steam is selected as the power source for the experiment to simulate the environment of a prototype containment under accident conditions. The boundary condition of the experiment is the constant steam temperature in the heated vessel. The steam pressure is set by a regulator. The effect of noncondensables is mitigated by venting. The heat transfer capability of the design is evaluated from the measured heated wall surface temperatures, fluid temperatures, temperature rise of the mixture along the heated surface, temperature rise of the pool water within a certain amount of time, flow velocity, humidity, and condensate weight. There are two methods to determine the steam generation rate of the experiment, that is, by relative humidity measurement associated with the velocity measurement of the flow stream, and by measuring the water pool level decrease rate.

CHAPTER 4

DOCUMENTATION AND ANALYSIS OF EXPERIMENTAL RESULTS

This chapter deals with the documentation and analysis of the proof-of-principle experimental results. The experiments were run for both air-only and water-filled conditions to provide the basic data for application to the proposed passive water cooled containment concept. For air-only cases, there is no water in the pool, and the tests were run for various interior containment steam temperature conditions. For water-filled cases, the pool is filled to a 1.524 m (5 ft) height of water, and the tests are also run for various steam temperature conditions. This chapter also documents a sensitivity study of heat transfer performance to the heated vessel surface emissivity , the form loss coefficient in the air path, noncondensables in the supplied steam, and the pool temperature distribution. The test results are compared with predictions by a simplified analytical model – PREWAS (see Appendix C for details).

4.1 Documentation of Test Results

A total of sixteen air-only and water-filled tests, eight tests for each kind, were run, as summarized in Table 4.1. Detailed experimental results for each test is presented in Appendix B. This section presents the procedures used to run the tests, and to evaluate the results.

In the air-only tests, the apparatus is heated by steam supplied to the heated vessel, and the data is taken after the steady state condition has been reached. Steady state is defined as that condition for which the deviation of the individual thermocouple readings are within ± 0.5 °C, which is the as-manufactured uncertainty of the thermocouples, over a period of one hour. Five sets of data were taken for each test. The time interval between two sets of data in the same test run ranged from ten minutes to two hours. The time duration to acquire a data set is about 20 seconds.

Because of the dynamic behavior in a water-filled test, particularly when the pool temperature changes with time, a fixed heated vessel internal temperature boundary

Table 4.1 Summary of Test Runs

TEST ID	$\overline{T}_{stm}$ (°C)	H_{pool} (m)	NO. OF DATA SETS	NOTE
A0301-11~15	150.1~150.4	0	5	-
A0304-11~15	150.2~150.3	0	5	-
A0429-11~15	108.7~109.3	0	5	-
A0429-21~25	104.1~104.3	0	5	-
A0430-11~15	120.1~120.8	0	5	-
A0502-11~15	120.0~120.1	0	5	sealed upper air windows
A0503-11~15	130.1~130.2	0	5	-
A0503-21~25	140.2~140.6	0	5	-
W0222	143.3~145.9	1.524	9	-
W0304	132.9~134.6	1.524	8	-
W0315	116.3~121.6	1.524	10	-
W0401	108.4~109.2	1.524	10	-
W0405	104.1~105.0	1.524	9	-
W0408	108.1~108.9	1.524	10	-
W0412	113.1~114.0	1.524	9	-
W0430	109.6~110.6	1.524	9	-

KEY TO TEST ID:

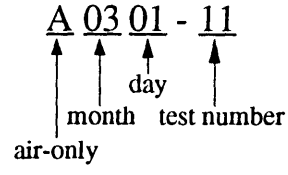

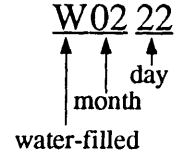

condition is hard to achieve. However, the difficulty of control is circumvented to a maximum degree by the following procedure. The apparatus is heated up without water in the pool until a steady state condition is reached as in the air-only tests. Then, the steam is turned off and water added into the pool to the desired height. Thereafter, the test is initiated by re-introducing the steam into the heated vessel, and the steam pressure is manually controlled to a fixed level via the steam regulator. Eight to ten sets of data are taken for each water test. Each data set in the same test run represents the surface temperature conditions and the thermodynamic states of the fluids for a specific time interval. Therefore, each test run documents the progress of the test with time for a given set of initial conditions and boundary conditions. Figure 4.1 shows a typical run sequence for a water-filled test.

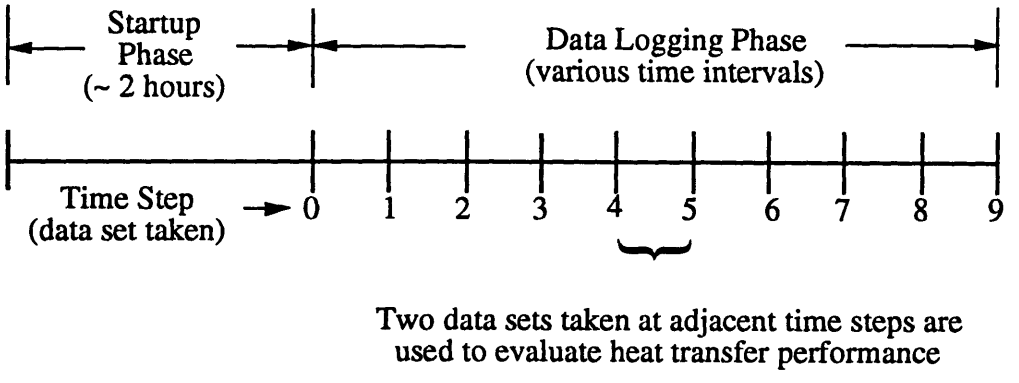

Figure 4.1 Typical Run Sequence

The procedures used to calculate the heat transfer performance in the steam-air mixture section which is located above the water pool, are presented in Section 3.5.1, Equations 3.15 to 3.27; and the procedures to calculate the heat transfer performance in the water pool are presented in Section 3.5.2, Equations 3.28 to 3.35. For air-only tests, the heat transfer in the steam-air mixture section represents the total heat transfer of the test, and the term "steam-air mixture" should be read as "air". The required input parameters for the heat transfer performance calculation are the space and/or time averaged value of the corresponding instrumentation readings. An illustration of the averaging method for a water-filled test is as follows.

Required Input Parameter	Data Taken for Averaging
$\overline{T}_{stm}$	TC11 ~ TC15
$\overline{T}_{wo,pl}$	TC1 ~ TC2
$\overline{T}_{wo,mix}$	TC3 ~ TC10
$\overline{T}_{pi}$	TC16 ~ TC17
$\overline{T}_{po}$	TC21 ~ TC22
$\overline{T}_{mix,o}$	TC31
$\overline{T}_{air,in}$	TC43
$\overline{T}_{wi,PVC}$	TC44 ~ TC45
$\overline{T}_{wi,gal}$	TC46 ~ TC47
$\overline{V}_{mix}$	V1

If there are multiple thermocouples for the parameter of interest, they are summed to provide a space-averaged value. Although there is only one thermocouple each for both intake air temperature and flowing mixture outlet temperature measurement, the data acquisition unit is set to cycle five times to read the data from the process instruments per trigger, and to thereby provide time averaged data (over on the order of 20 seconds). In the meantime, TC40 and TC41, for the purpose of heat loss estimation, can also provide redundant indications for the flowing mixture outlet temperature. The velocity of the flowing mixture is the average of six readings taken from velocity flow meter V1 at an interval of approximately ten seconds.

Each data set of the air-only tests can be reduced to evaluate the heat transfer performance since they are essentially independent tests. However, the data sets in the same run of the water-filled tests are dependent upon each other. Two data sets taken at adjacent time steps should be used to evaluate the heat transfer performance. Detailed data reduction and error analysis of the experiment are presented in Appendix A.

4.2 Evaluation of Heat Transfer Performance

This section presents the evaluation of the heat transfer performance for the air-only tests and the water-filled tests. The heat transfer performance cited in this section includes

pool and/or flowing mixture heat fluxes and pool and/or flowing mixture heat transfer coefficients. The test results are compared with the prediction by a simplified analytical model – PREWAS (see Appendix C for details). Comparisons between the air-only test, Westinghouse's small scale test for AP600 [W-4], and Argonne National Laboratory's (ANL's) natural convection test for advanced liquid metal reactors [H-1] are also included. For the water-filled tests, there is no low pressure pool boiling data for a similar test geometry available for comparison.

4.2.1 Air-Only Tests

The air-only tests were run under fixed geometry, at different steam temperature levels, except A0502-11~15 in which the upper air windows (located at 3.048 m above the bottom plate) were sealed. Table 4.2 summarizes the heat transfer performance of all the air-only tests. Detailed air-only test results are presented in Appendix B.

As shown in Table 4.2, the radiative heat transfer rate accounts for one third of the total heat transfer rate. Thus the magnitude of the surface emissivity may play a major role. A sensitivity study to the emissivity will be presented in the next section (Section 4.3.1). The deviation of the as-measured test results in each test run on the same day under the same test conditions is less than ± 5 %. The major contribution to the deviation is the steam temperature change during the test, although the magnitude is small.

Tests A0301-11~15 and A0304-11~15 are directly comparable since they were run at approximately the same steam temperature, 150 °C, and the same geometry. The results show they are in good agreement, since the deviation of the heat transfer performance between these two runs is less than 5 %, which is within the magnitude of experimental uncertainty. Tests A0430-11~15 and A0502-11~15 are worth comparison because they were run with different geometry but approximately the same steam temperature 120 °C. The heat transfer performance of A0502-11~15 (sealed upper windows) is consistently about 5 % higher than that of A0430-11~15 (nominal geometry). The reason for the degraded heat transfer performance, although small in magnitude, for A0430-11~15 is that the upper air windows provide another in-coming air flow passage which bypasses part of the heated surface.

The comparisons of the test results with the predictions by PREWAS are shown in Figure 4.2 and 4.3. Figure 4.2 shows the heat flux comparison as a function of heated

Table 4.2 Summary of Air-Only Tests Heat Transfer Performance

TEST ID	A0301-11~15	A0304-11~15	A0429-11~15	A0429-21~25	A0430-11~15	A0502-11~15	A0503-11~15	A0503-21~25
$\overline{T}_{stm}$ (°C)	150.1 ~ 150.4	150.2 ~ 150.3	108.7 ~ 109.3	104.1 ~ 104.3	120.1 ~ 120.8	120.0 ~ 120.1	130.1 ~ 130.2	140.2 ~ 140.6
$\dot{Q}_{cond}$ (kw)	4.12 ~ 4.28	4.16 ~ 4.34	2.29 ~ 2.38	2.25 ~ 2.34	2.83 ~ 2.90	2.82 ~ 2.87	3.07 ~ 3.13	3.54 ~ 3.63
$\dot{Q}_{air}$ (kw)	3.93 ~ 4.09	3.79 ~ 3.90	2.07 ~ 2.17	1.97 ~ 2.22	2.53 ~ 2.58	2.58 ~ 2.66	2.90 ~ 2.97	3.33 ~ 3.41
$\dot{Q}_{rad}$ (kw)	1.43 ~ 1.44	1.43 ~ 1.44	0.78 ~ 0.80	0.72	0.93 ~ 0.94	0.93	1.08	1.24 ~ 1.25
$\frac{\dot{Q}_{cond}}{\dot{Q}_{air}}$	1.02 ~ 1.09	1.06 ~ 1.14	1.10 ~ 1.14	1.13 ~ 1.17	1.10 ~ 1.13	1.07 ~ 1.09	1.04 ~ 1.07	1.05 ~ 1.08
$\overline{q}''_{air}$ (kw/m^2)	1.79 ~ 1.85	1.72 ~ 1.77	0.94 ~ 0.98	0.89 ~ 0.92	1.15 ~ 1.17	1.17 ~ 1.21	1.32 ~ 1.35	1.51 ~ 1.55
$\overline{h}_{air,eff}$ (w/m^2°C)	15.74 ~ 16.33	15.14 ~ 15.86	12.33 ~ 13.09	12.62 ~ 13.01	13.47 ~ 13.82	14.03 ~ 14.46	14.06 ~ 14.37	14.75 ~ 15.08
$\overline{h}_{air,conv}$ (w/m^2°C)	10.02 ~ 11.12	9.39 ~ 10.13	7.57 ~ 8.35	8.00 ~ 8.39	8.45 ~ 8.79	8.96 ~ 9.39	8.81 ~ 9.13	9.24 ~ 9.56
Re ($\times 10^4$)	2.60 ~ 2.64	2.57 ~ 2.64	2.14 ~ 2.23	2.10 ~ 2.13	2.16 ~ 2.20	1.30 ~ 1.33	2.35 ~ 2.39	2.40 ~ 2.46

Note: "~" denotes the range of the data.

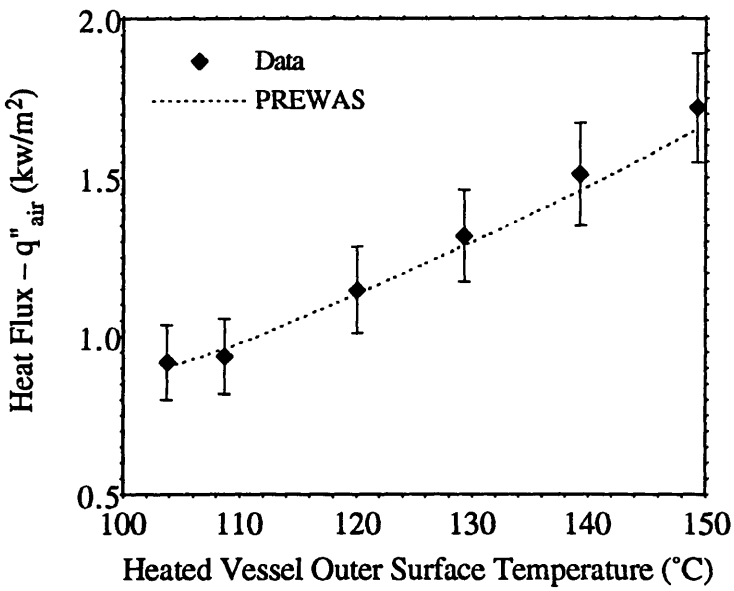

Figure 4.2 Air-Only Test Results Comparison – Heat Flux

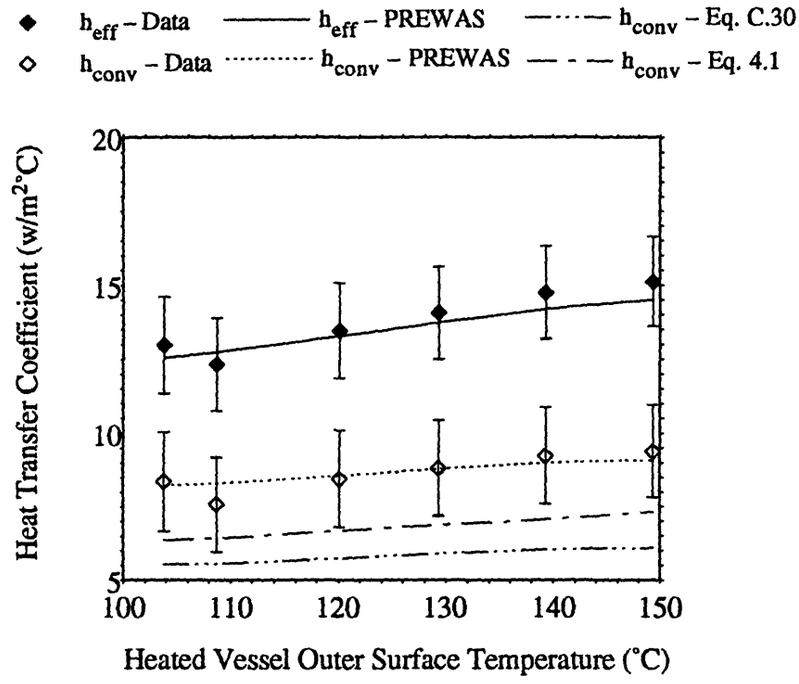

Figure 4.3 Air-only Test Results Comparison – Heat Transfer Coefficient

vessel outer surface temperature, while Figure 4.3 shows the heat transfer coefficient comparison as a function of heated vessel outer surface temperature. The effective heat transfer coefficient is evaluated using the total heat flux, which includes radiative heat transfer. The heat flux used to evaluate the convective heat transfer coefficient does not include the heat flux contribution from radiation. The data shown in the figures are typical values for each test. Appendix B provides comparisons for each data set of the tests. As shown in the figures, the test data and the predictions are in good agreement. Furthermore, the change in the convective heat transfer coefficient with heated vessel outer surface temperature is rather small over the range of the tests. The heat transfer correlation adopted in PREWAS is the ANL-proposed heat transfer correlation developed in their natural convection test rig for advanced liquid metal reactors [H-1]. Detailed description of PREWAS is presented in Appendix C.

Also shown in Figure 4.3 is the comparison for predicted convective heat transfer coefficient using PREWAS (Equation C.29), Equation C.30, and Equation 4.1 (shown below).

$$h_{conv} = 0.13\frac{k_{air}}{D}Ra^{1/3} \tag{4.1}$$

Equation 4.1 is the turbulent natural convection heat transfer correlation. Equation C.30 is Gang Fu's heat transfer correlation [F-3]. Both Equations 4.1 and C.30 under-predict the experimental results.

The air-only test results are next compared with other similar experimental data. Table 4.3 shows the reference dimensions and the heat transfer performance of this experiment, the Westinghouse small scale test, and the ANL natural convection test. Note that the characteristic length in the Reynolds number and the Grashof number evaluations is the equivalent hydraulic diameter of the gap. As shown in the table, the heat transfer regime in all tests of this experiment fall in the mixed convection range ($0.1 < Gr/Re^2 < 10$) where both free convection and forced convection heat transfer mechanisms are significant. Moreover, the test geometry of this experiment and ANL's are quite similar. These similarities may explain why the predictions by PREWAS, which adopts ANL's heat transfer correlation, are in good agreement with the air-only test results. Note also that , in the Westinghouse small scale test, the higher heat transfer coefficients correspond to the tests with narrow gap width, which also fall in the mixed convection heat transfer regime.

Table 4.3 Heat Transfer Performance Comparison –
Air-Only Test, Westinghouse Small Scale Test, and ANL's Test

	Air-Only Test	Westinghouse	ANL
Heated Height, m (ft)	6.1 (20)	6.4 (21)	6.7 (22)
Chimney Height, m (ft)	15.2 (50)	-	15.2 (50)
Gap Width, cm (ft)	10 (0.33)	7.6 (0.25)~39.6 (1.3)	15.2 (0.5)~45.7 (1.5)
Ambient Temp., (°C)	23.7~26.4	4.5~32.2	-1.7~21.7
Wall-Air Temp. Diff., (°C)	71~114	47~91	95~286
Air Velocity, (m/s)	1.6~2.1	0.61~2.1	1.3~5.3
Heat Transfer Coeff., ($w/m^2°C$)	7.6~11.1	5.7~9.7	6.8~14.2
Form Loss Coeff.	8.7	2~50	1.5~20
Prandtl Number,	0.7	0.7	0.7
Reynolds Number, $\times 10^4$	2.0~2.6	0.75~3.6	3.5~12.6
Gr/Re^2	0.15~0.17	0.063~3.6	0.1~1.0

As can be seen, the heat transfer coefficients are quite similar for the three experiments, which validates the MIT apparatus as suitable for its intended purpose as a containment cooling simulation.

4.2.2 Water-Filled Tests

All the water-filled tests were run at the same initial height of water. They differ primarily in the input steam temperature. The selection of the initial water level is a trade-off between the steam supply capability and the controllability of the condensate flow. The higher temperature runs, W0222 (145 °C) and W0304 (134 °C), are for the purpose of providing basic data for pool boiling at low pressure. They are not directly applicable to a prototype containment unless usual design pressure limits are exceeded. This section will present a typical low temperature test result. Detailed experimental results for each test are presented in Appendix B.

Shown in Figures 4.4 and 4.5 (also as Figures B.16.a and B.16.b, respectively) are the test results of W0430 which was run at a steam temperature of 110 °C. The pool heat flux is high (about 60 kw/m^2) at the beginning, when the pool temperature is still low, and the pool is in the free convection heat transfer regime. Then, the pool heat flux decreases rapidly as the pool temperature increases due to heat addition. Transition from free convection to subcooled boiling heat transfer is suspected to occur during this period of time since the pool heat transfer coefficient is increasing, as shown in Figure 4.5. As the pool temperature reaches the corresponding saturation temperature, saturated pool boiling heat transfer takes place, and the pool heat flux levels off (at about 12.5 kw/m^2) consistent with the imposed constant steam temperature and the constant pool temperature and heat transfer coefficients.

Note that the pool heat transfer coefficients are evaluated without taking into account the swelling effect due to void generation. The pool level increase due to void induced swelling is small based on the observation of the heated vessel outer surface temperature readings. Assuming that the pool is in a bubbly flow regime and an uniform void distribution, the total pool level (H_T) which includes the void effect can be evaluated by

$$H_L = H_T - \frac{q''' H_T^2}{2 V_\infty h_{fg} \rho_g}, \tag{4.2}$$

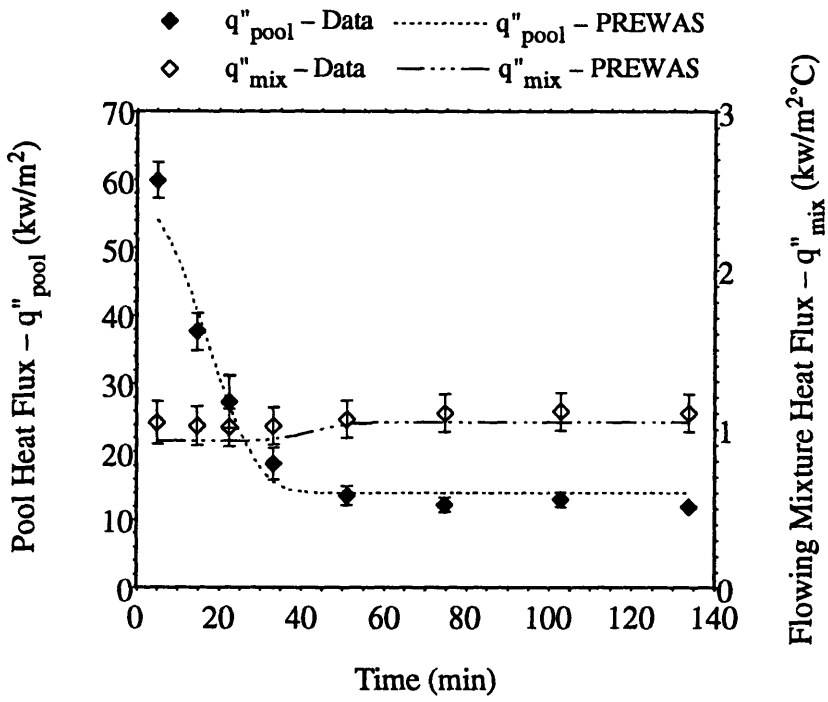

Figure 4.4 W0430 Test Results – Heat Flux

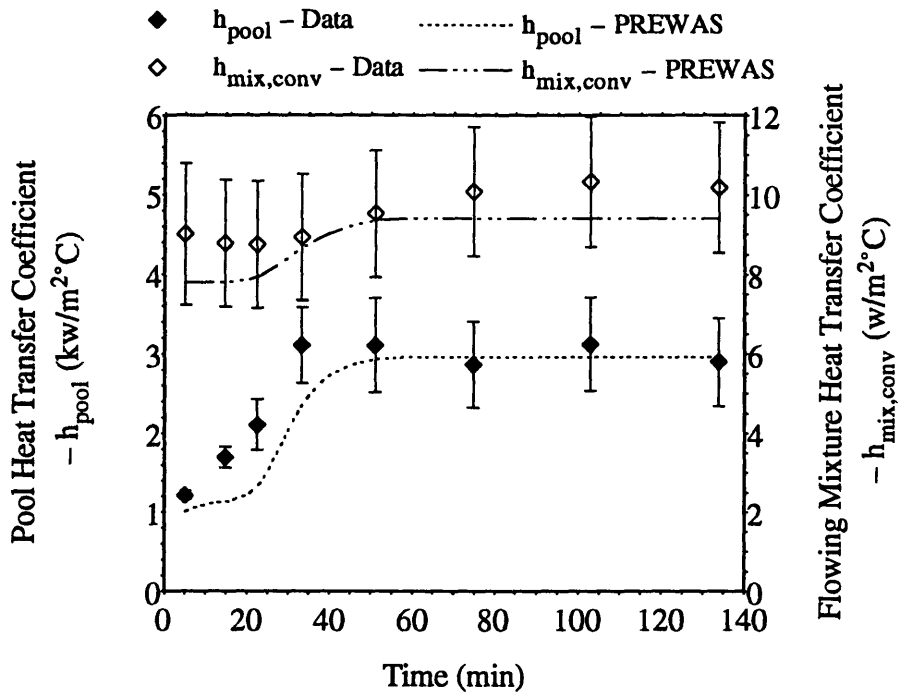

Figure 4.5 W0430 Test Results – Heat Transfer Coefficient

where

$$V_\infty = 1.53\left(\frac{g\sigma}{\rho_f}\right)^{0.25}, \tag{4.3}$$

H_L is the liquid-only level, and q''' is the heat addition rate per unit volume. The estimated increased level is 8.5 cm, and the void fraction is 0.053. The pool heat transfer coefficient evaluated at this new level is 5 % less than the previous value, hence the correction is negligible.

The convective heat transfer coefficient and the heat flux to the flowing vapor phase mixture stay at approximately constant levels (9 w/m^2°C and 1 kw/m^2, respectively) before saturated boiling occurs in the pool section. When the pool is in the saturated boiling heat transfer regime, the heat transfer coefficient and the heat flux increase about 10 %. The reason for the increase of the air heat transfer performance in the presence of steam could be that the hot steam enhances the buoyancy-induced air flow rate (the molecular weight of steam, 18, is less than that of air, 29).

All eight water-filled tests follow the same trend as discussed above. The comparison between the test data and the prediction by PREWAS for test W0430 are also shown in Figures 4.4 and 4.5. The predictions are in good agreement with the test data. The test results show higher flowing mixture heat transfer performance than the prediction before saturated boiling occurs in the pool section because PREWAS does not account for water evaporation when the pool is in a subcooled condition. The comparisons for each test are presented in Appendix B. The predictions are generally in good agreement with the test data. However, there are deviations between the predictions and the test data, especially before saturated pool boiling occurs. Factors that contribute to the deviation are: (1) the space-averaging method used to derive desired quantities may not be appropriate when the deviation among the parameters of interest is large; (2) the steam temperature and/or ambient conditions (for example, atmospheric pressure) changes during the test, which can not be simulated by PREWAS, (3) the dissolved gases in the water, which tend to decrease the required wall superheat for nucleation [R-1], and (4) for high temperature tests, the wall inner surface temperature may be decreased to a non-negligible degree by the noncondensables contained in the supplied steam, which degrades the heat transfer (see Section 4.3.3 for detailed discussion). Figure 4.6 shows the ratio of the derived saturated nucleate pool boiling heat transfer coefficients from the test data to the predictions by PREWAS. Note that the predictions are based on Rohsenow's nucleate boiling heat transfer correlation (Equation C.16). The deviation of the data from the prediction is large

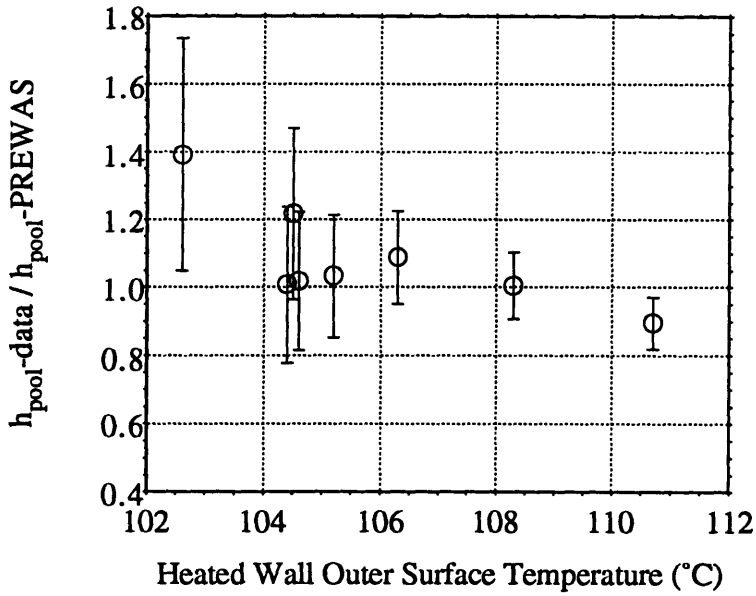

Figure 4.6 Ratio of Measured Pool Heat Transfer Coefficients to Predictions

at wall outer surface temperature of 102.6 °C (test W0405) due to the steam temperature control problem (intermittent higher steam temperature).

4.3 Sensitivity Study of Heat Transfer Performance

This section presents the sensitivity of the test results and the predictions to uncertainties in the surface emissivity, the form loss coefficient of the apparatus, the noncondensables contained in the supplied steam, and the pool temperature distribution.

4.3.1 Sensitivity to Emissivity

As discussed in Section 4.2, radiative heat transfer accounts for approximately one third of the total heat transfer rate in the air-only tests. Therefore, the magnitude of the surface emissivity may have a significant effect on the evaluation of the convective heat transfer coefficient. Figure 4.7 shows the sensitivity of the convective heat transfer coefficient for test A0304-15 to the heated wall surface emissivity, which is made of stainless steel, and to the inner annulus wall surface emissivity, which is composed of PVC and galvanized steel. The heat transfer coefficient is insensitive to the PVC and the galvanized steel emissivity in the range of our application, but is sensitive to the stainless steel emissivity, in part because the diameter of the heated vessel (4.5 in) is much smaller than the diameter of the inner annulus wall (14 in). The arrows in the figure mark the estimated range of the stainless steel emissivity, which is ± 10 % of the nominal value [T-1]. The uncertainty in the stainless steel emissivity contributes approximately 5 % error in the evaluation of the convective heat transfer coefficient.

The surface emissivity also affects the prediction of the heat transfer performance for the air-only test. Figures 4.8 and 4.9 show the sensitivity of the heat transfer performance prediction (by PREWAS) for test A0304-15 to the emissivity. The heat flux and both the effective and the convective heat transfer coefficients are insensitive to the duct wall emissivity for the same reason as above. However, the effective heat transfer coefficient and hence the heat flux are sensitive to the heated wall surface emissivity since the effective heat transfer coefficient includes the radiation effect. The proposed ± 10 % uncertainty in the heated wall emissivity contributes ± 3 % uncertainty in the prediction of the heat flux and the effective heat transfer coefficient.

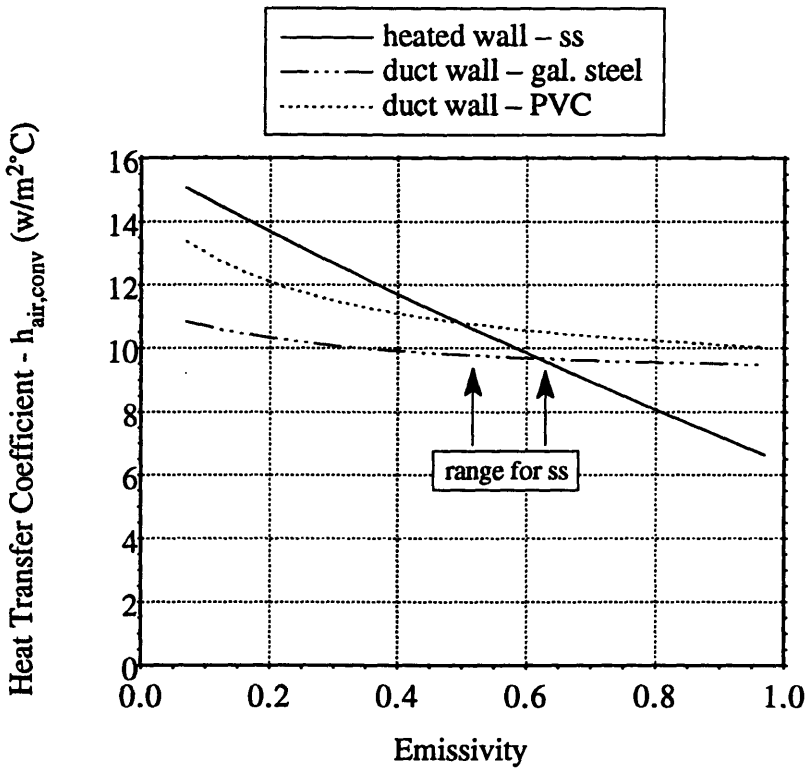

Figure 4.7 Sensitivity to Emissivity – Test Data : A0304-15

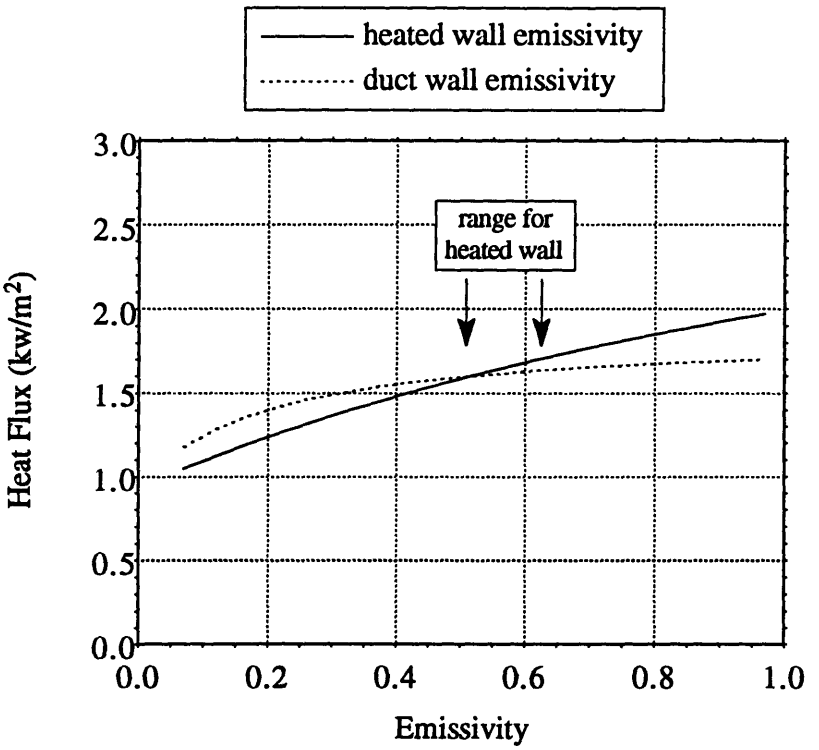

Figure 4.8 Sensitivity to Emissivity – Heat Flux Prediction

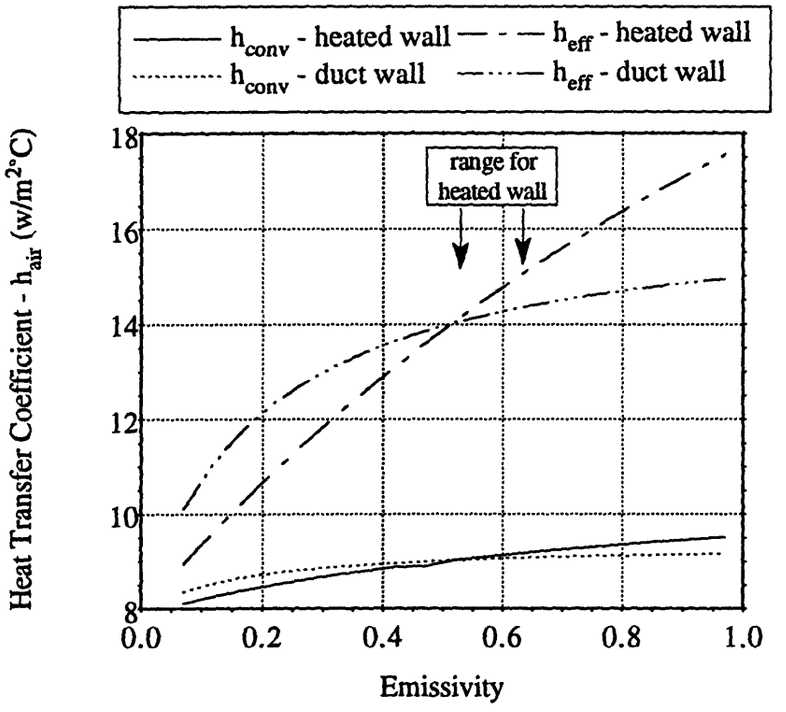

Figure 4.9 Sensitivity to Emissivity – Heat Transfer Coefficient Prediction

4.3.2 Sensitivity to Form Loss Coefficient

The form loss coefficients of the apparatus are calculated analytically by referring to the manufacturer's data and/or to Idelchik's hydraulic resistance handbook [I-1] at similar flow geometry (see Appendix D for details). Therefore, a sensitivity analysis of the form loss coefficient to the heat transfer performance of the air-only test is needed. The calculated inlet and outlet form loss coefficients are 4.2 and 3.7, respectively.

The sensitivity to the form loss coefficient of the heat transfer performance predictions for test A0304-15 are shown in Figures 4.10 and 4.11. The error due to the uncertainty of the form loss coefficient in the heat transfer performance prediction for the air-only test is less than 5 % in the range of our interest. The predicted heat flux and the heat transfer coefficient are relatively less sensitive to the inlet form loss coefficient than to the outlet form loss coefficient, as discussed in the following analysis.

The pressure drop due to form loss can be expressed as

$$(\Delta P)_{\text{in or out}} = (K_c \frac{\dot{m}^2}{2\rho A^2})_{\text{in or out}}, \tag{4.4}$$

hence

$$(K_c)_{\text{in or out}} = (\frac{2\rho A^2 \Delta P}{\dot{m}^2})_{\text{in or out}}, \tag{4.5}$$

where in and out denote inlet and outlet, respectively. The derivative of the form loss coefficient at fixed pressure drop with respect to the buoyancy induced air flow is

$$\left|\frac{\partial K_c}{\partial \dot{m}}\right|_{\text{in or out}} = (\frac{4\rho A^2 \Delta P}{\dot{m}^3})_{\text{in or out}}. \tag{4.6}$$

For this experiment,

$$(\rho A^2)_{\text{out}} < (\rho A^2)_{\text{in}}. \tag{4.7}$$

Therefore, for a reference air flowrate,

$$\left|\frac{\partial K_c}{\partial \dot{m}}\right|_{\text{out}} < \left|\frac{\partial K_c}{\partial \dot{m}}\right|_{\text{in}}, \text{ or} \tag{4.8}$$

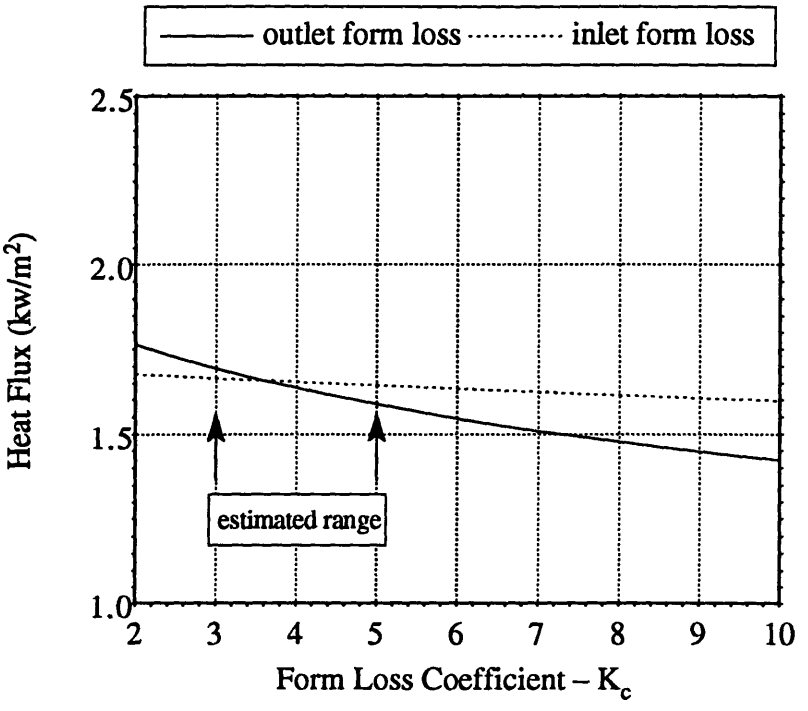

Figure 4.10 Sensitivity to Form Loss – Heat Flux Prediction

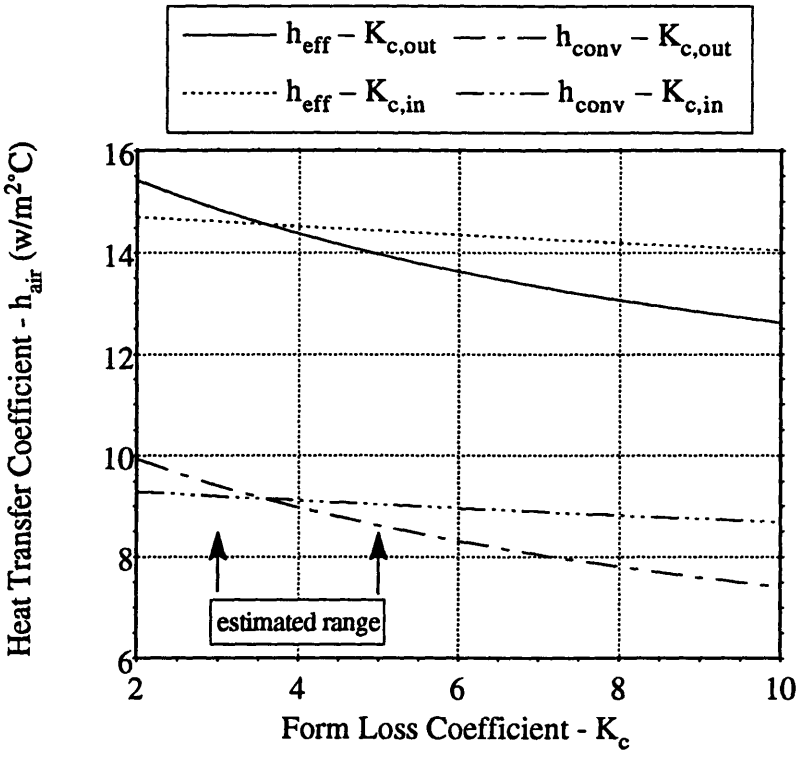

Figure 4.11 Sensitivity to Form Loss – Heat Transfer Coefficient Prediction

$$\left|\frac{\partial \dot{m}}{\partial K_c}\right|_{out} > \left|\frac{\partial \dot{m}}{\partial K_c}\right|_{in}. \tag{4.9}$$

Since the air mass flowrate is a key indicator of the heat transfer performance, the rate of the heat transfer performance change due to change in outlet form loss coefficient is higher than that due to inlet form loss coefficient change.

4.3.3 Sensitivity to Noncondensables

The noncondensables (air) contained in the supplied steam are vented to the maximum degree practicable during the tests. Axial steam temperature and heated wall outer surface temperature distribution are monitored continuously to assess the need for and effectiveness of venting. However, complete de-gassing of the steam is impossible and impractical, particularly, during the high temperature water-filled tests. The effect of the non-condensables on both the air-only tests and water-filled tests are discussed in the paragraphs which follow.

The actual heated vessel inner wall surface temperature in the presence of noncondensables for the air-only tests and the water-filled test (W0430) are shown in Figure 4.12 and 4.13, respectively. For a thin wall heated vessel, the heat flux can be expressed as

$$q'' = U(T_{stm} - T_f), \text{ or} \tag{4.10}$$

$$q'' = h_{cond}(T_{stm} - T_{wi}), \tag{4.11}$$

where

$$U = \frac{1}{\frac{1}{h_{cond}} + \frac{\Delta}{k_w} + \frac{1}{h_f}}, \tag{4.12}$$

$$h_{cond} = 450\left(\frac{m_{air}}{m_{stm}}\right)^{-0.8}, \tag{4.13}$$

T_f is the average air temperature for the air-only tests, or the average inner pool temperature for the water-filled tests, and h_f is the heat transfer coefficient to the air or to the pool water.

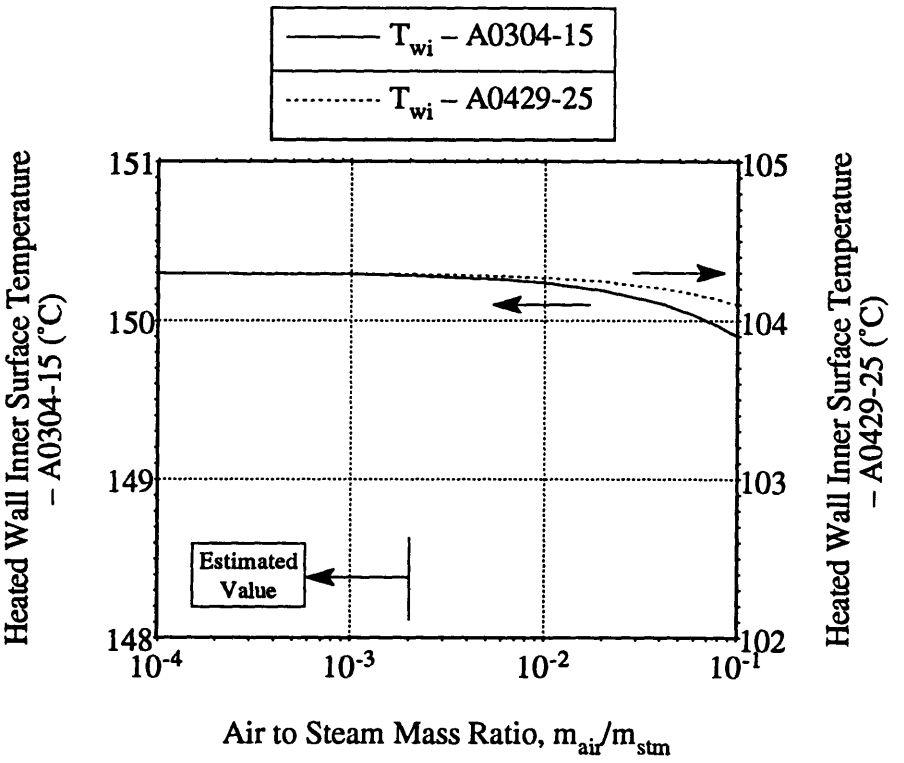

Figure 4.12 Sensitivity to Noncondensables – Air-Only Test

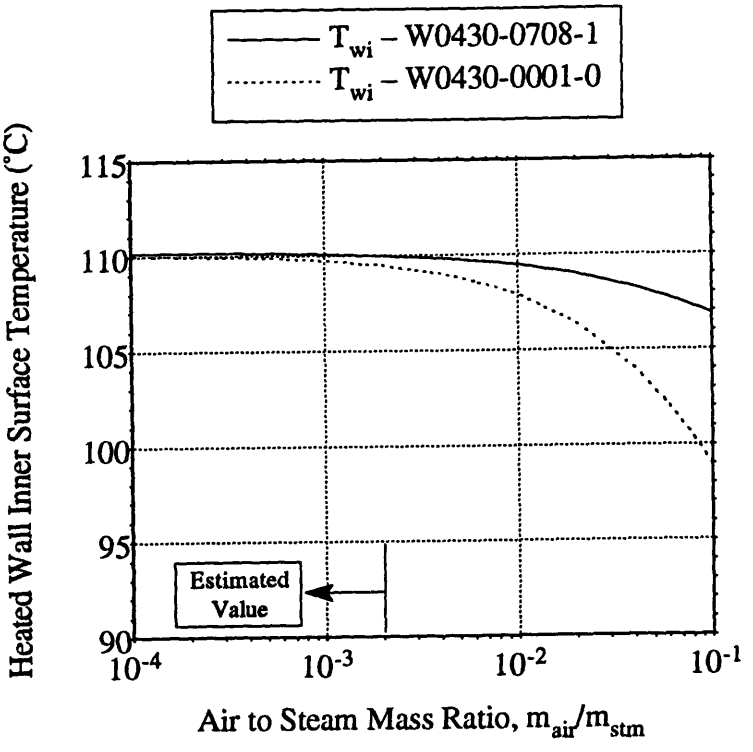

Figure 4.13 Sensitivity to Noncondensables – Water-Filled Test: W0430

Note that Uchida's condensation heat transfer correlation [U-1, G-3] is adopted here. The inner wall surface temperature can be evaluated by

$$T_{wi} = T_{stm} - \frac{U}{h_{cond}}(T_{stm} - T_f). \tag{4.14}$$

Figure 4.12 shows the noncondensable effect for two extreme test temperature cases of the air-only test. As shown in the figure, the decrease in the inner wall surface temperature is less than 1 °C in the temperature range of our tests even for an air to steam mass ratio equal to 0.1, which is an implausibly high value for the air-only tests.

Figure 4.13 shows the decrease in the inner wall surface temperature in the presence of noncondensables for water test W0430 from the beginning of the test to the end of the test. The temperature decrease is significant at high air to steam ratios and pronounced when coupled with high heat flux (W0430-0001-0). The estimated mass ratio of air to steam is approximately 0.002 in the W0401, W0405, W0408, W0412, and W0430 tests; 0.02 in test W0315; 0.035 in test W0304; and 0.04 in test W0222. The higher noncondensable concentration for the high temperature tests (W0222, W0304, and W0315) arises from the fact that the pool section heated wall outer surface temperature shows an axial variation which is inferred as due to concentration of noncondensables in the lower axial portion of the heated vessel.

The reason for the more pronounced noncondensables effect on the water tests than on the air tests can be explained using Equation 4.12. In the air tests, the total thermal resistance is controlled by the thermal resistance due to the air ($1/h_f$), while the total thermal resistance is controlled by the noncondensables via $1/h_{cond}$ in the water tests. Meanwhile, the higher steam demand in the water tests, particularly in the high temperature tests, gives rise to a higher noncondensable concentration accumulation inside the heated vessel.

4.3.4 Sensitivity to Pool Temperature Distribution

As addressed in Section 4.2.2, the space-averaging method used to derive desired quantities may introduce a large uncertainty into the test results, particularly when the deviation among the parameters of interest is large. This situation can occur during the free convection or subcooled boiling heat transfer regimes in the water-filled tests. The pool

temperature difference between two axially mounted thermocouples may be higher than 10 °C (see Appendix B for details).

Figure 4.14 shows the sensitivity of the pool heat transfer coefficient to the pool temperature distribution for part of the W0430 test group, for which the pool temperature is still subcooled. The "high", "low", and "average" in the figure denote that the heat transfer coefficients are evaluated using the high temperature reading, the low temperature reading and by the space-averaging method, respectively. The ratios shown in the figure represent the possible range of the heat transfer coefficients due to a non-uniform axial pool temperature distribution. The deviation of the high and low values from the average value ranges from 5 % to 15 %, depending on the magnitude of the temperature difference.

4.4 Summary of Chapter 4

The documentation and analysis of the proof-of-principle experimental results are presented in this Chapter. The major points are listed as follows.

- A total of sixteen air-only and water-filled tests, eight tests for each kind, were run to provide the basic data for application to the proposed passive water cooled containment concept. Detailed experimental results for each test are presented in Appendix B.

- The air-only tests were run at steady state conditions. The steady state condition is assumed to be achieved when the deviations of the individual thermocouple readings are within ± 0.5 °C over one hour, which is the uncertainty of the thermocouples. Five sets of data are taken for each test. The time interval between two sets of data in the same test run ranges from ten minutes to two hours.

- Because of the dynamic behavior in a water-filled test, special test procedures are followed to circumvent control difficulties. The apparatus is heated up without water in the pool until the steady state condition is reached. Then, the steam is turned off and water is introduced into the pool to a desired height. Thereafter, the test is initiated by re-introducing the steam into the heated vessel, and the steam pressure is manually controlled to a fixed level via the steam regulator. Eight to ten sets of data are taken for each water test. Each test run documents the progress of the test with time for a given set of initial conditions and boundary conditions.

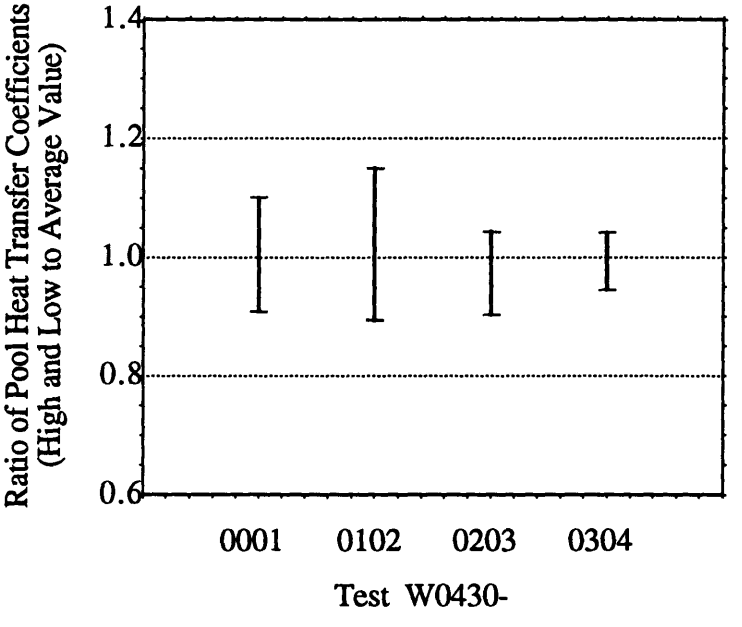

Figure 4.14 Sensitivity to Pool Temperature Distribution
(Note: see Appendix B for test ID description)

- The deviation of the heat transfer performance in each group of the air-only tests run on the same day under the same test conditions is less than ± 5 %. Tests A0301-11~15 and A0304-11~15 were run at approximately the same steam temperature 150 °C, and the same geometry. The results show good agreement, since the deviation of the heat transfer performance between these two tests is less than ± 5 %, which is within the magnitude of the experimental uncertainty. Tests A0430-11~15 and A0502-11~15 were run under different geometry but approximately the same steam temperature 120 °C. The heat transfer performance of A0502-11~15 (sealed upper windows) is consistently about 5 % higher than that of A0430-11~15 (nominal geometry). The reason for the degraded heat transfer performance of A0430-11~15, although small in magnitude, is that the upper air windows provide another in-coming air flow passage which bypasses part of the heated surface.

- The comparisons of the test results with predictions by PREWAS shows that they are in good agreement. Meanwhile, the change in the convective heat transfer coefficient with temperature is rather small over the range of the tests. The air-only test results are also compared with the Westinghouse small scale test, and the ANL natural convection test. The heat transfer regime in this experiment and the ANL test fall in the mixed convection region ($0.1 < Gr/Re^2 < 10$) where both free convection and forced convection heat transfer effects are significant. Moreover, the test geometry of this experiment and ANL's are quite similar. These factors may explain why the predictions by PREWAS, which adopts ANL's heat transfer correlation, are in good agreement with the air-only test results. All these tests yield similar values for the heat transfer coefficient, which validates the MIT apparatus as suitable for its intended purpose as a containment cooling proof-of-principle test.

- All the water-filled tests were run at the same initial height of water. They differ primarily in the input steam temperature. An illustration of water-filled test results, for run W0430, which was run at 110 °C steam temperature, shows that the pool heat flux is high (about 60 kw/m^2) at the beginning when the pool temperature is still low and the pool is in the free convection heat transfer regime. Then the pool heat flux decreases rapidly as the pool temperature increases due to heat addition. Transition from free convection to subcooled boiling heat transfer is suspected to occur during this period of time since the pool heat transfer coefficient is increasing. As the pool temperature reaches the corresponding saturation temperature, saturated pool boiling heat transfer takes place, and the pool heat flux levels off (at about 12.5 kw/m^2) as the pool heat transfer coefficient remains approximately constant (3 $kw/m^2°C$). The convective heat transfer coefficient and

the heat flux to the flowing vapor phase mixture (air plus steam) stay at an approximately constant level (9 w/m^2°C and 1 kw/m^2, respectively) before saturated boiling occurs in the pool section. When the pool is in the saturated boiling heat transfer regime, the heat transfer coefficient and the heat flux in this region increase about 10 %. The reason for the increase of the air heat transfer performance in the presence of steam is that the hot steam enhances the buoyancy-induced air flowrate.

- All eight water-filled tests follow the same trend as in test W0430. The predictions are generally in good agreement with the test data. However, deviations between the predictions and the test data still exist, especially before saturated pool boiling occurs. Factors that contribute to the deviation are: (1) the space-averaging method to derive desired quantities may not be appropriate when the deviation between the parameters of interest is large; (2) the steam temperature and/or ambient conditions (for example, atmospheric pressure) changes during the test, which can not be simulated by PREWAS, (3) the dissolved gases in the water, which tend to decrease the required wall superheat for nucleation [R-1], and (4) for high temperature tests, the wall inner surface temperature may be decreased to a non-negligible degree by the noncondensables contained in the supplied steam, which degrades the heat transfer.

- The radiative heat transfer rate accounts for approximately one third of the total heat transfer rate in the air-only tests. A sensitivity analysis shows that the convective heat transfer coefficient is insensitive to the emissivity of the inner annulus wall, which is composed of PVC and galvanized steel, in the range of our application, but is sensitive to the emissivity of the heated wall which is made of stainless steel, in part because the diameter of the heated vessel (4.5 in) is much smaller than the diameter of the inner annulus wall (14 in). The uncertainty in the stainless steel emissivity contributes approximately $\pm$ 5 % uncertainty in the evaluation of the convective heat transfer coefficient.

- The surface emissivity also affects the prediction of the heat transfer performance for the air-only test. Analysis shows that the heat flux and both the effective and the convective heat transfer coefficients are insensitive to the duct wall emissivity. However the effective heat transfer coefficient and hence the heat flux are sensitive to the heated wall surface emissivity since the effective heat transfer coefficient includes the radiation effect. The proposed 10 % uncertainty in the heated wall emissivity contributes 3 % uncertainty in the prediction of the heat flux and the effective heat transfer coefficient.

- The form loss coefficients of the apparatus are estimated by referring to manufacturer's data and/or to Idelchik's hydraulic resistance handbook [I-1] for similar flow geometry. The uncertainty in the heat transfer performance prediction due to the uncertainty of the form loss coefficient for the air-only test is less than 5 % in the range of our interest. The predicted heat flux and the heat transfer coefficient are relatively less sensitive to the inlet form loss coefficient than to the outlet form loss coefficient.

- The noncondensables contained in the supplied steam are vented during the tests, and the axial steam temperature and the heated wall outer surface temperature distribution are monitored continuously to guide the need for and effectiveness of venting. However, complete de-gassing of the steam is impossible and impractical, particularly, during the high temperature water-filled tests.

- Analysis of the noncondensable effect for two extreme test temperature cases of the air-only test shows that the decrease in the inner wall surface temperature is less than 1 °C in the temperature range of our tests even for an air to steam mass ratio equal to 0.1 which is an implausibly high value for the air-only tests. Analysis of the decrease in the inner wall surface temperature in the presence of noncondensables for water test run W0430 shows that the degree of temperature decrease is significant only at high air to steam mass ratios and more pronounced when coupled with high heat flux (W0430-0001-0). From the observed temperature decrements, the estimated mass ratio of air to steam is approximately 0.002 in the W0401, W0405, W0408, W0412, and W0430 tests; 0.02 in test W0315; 0.035 in test W0304; and 0.04 in test W0222. The higher noncondensable concentration for the high temperature tests (W0222, W0304, and W0315) arises from the fact that the pool section heated wall outer surface temperature shows an axial variation which is inferred as due to concentration of noncondensables in the lower axial portion of the heated vessel.

CHAPTER 5

APPLICATION OF FINDINGS

5.1 Introduction

The purpose of this research is to explore the applicability of the proposed passive water cooled containment concept – a prefilled water-air annulus – to a high power rating PWR reactor, for example 1300 MWe. The proposed containment cooling geometry is shown in Figure 5.1 (also as Figure 1.1). The prefilled water-air annulus arrangement preserves the cooling capability of natural air convection heat transfer, and enhances the heat removal capability by means of the prefilled water pool. The prefilled water pool consists of an inner and an outer pool. The windows at the bottom of the pools provide water communication passages between the two pools. The inner pool provides the direct heat sink, while the outer pool replaces the inner pool inventory loss due to evaporation. The heat transfer mechanisms in the water pool can be free convection and/or nucleate pool boiling, depending on the heat flux. The application of the proof-of-principle experimental results to a prototype containment is presented in this chapter. The proposed containment in this analysis is a right circular cylinder, 60 m in both diameter and height, having a 4.45 cm thick steel wall pressure boundary. The free volume of the containment is $1.0 \cdot 10^5$ m^3 The proposed design pressure and temperature are 0.47 MPa (53 psig) and 143 °C (290 °F), respectively, which are typical large dry containment design values.

5.2 Analysis for Application to a High Power Rating Reactor

5.2.1 Air-Only Application

The air-only test results presented in Chapter 4 are not directly applicable to a prototype containment since the heat transfer performance is dimensionally dependent as discussed in Section 3.2.1. In particular, the heat transfer coefficient is dependent on heated length and gap width. However, the analysis in Chapter 4 shows that the predictions by PREWAS are in good agreement with the test data. Therefore, the PREWAS model can be used to evaluate the heat transfer capability of the proposed

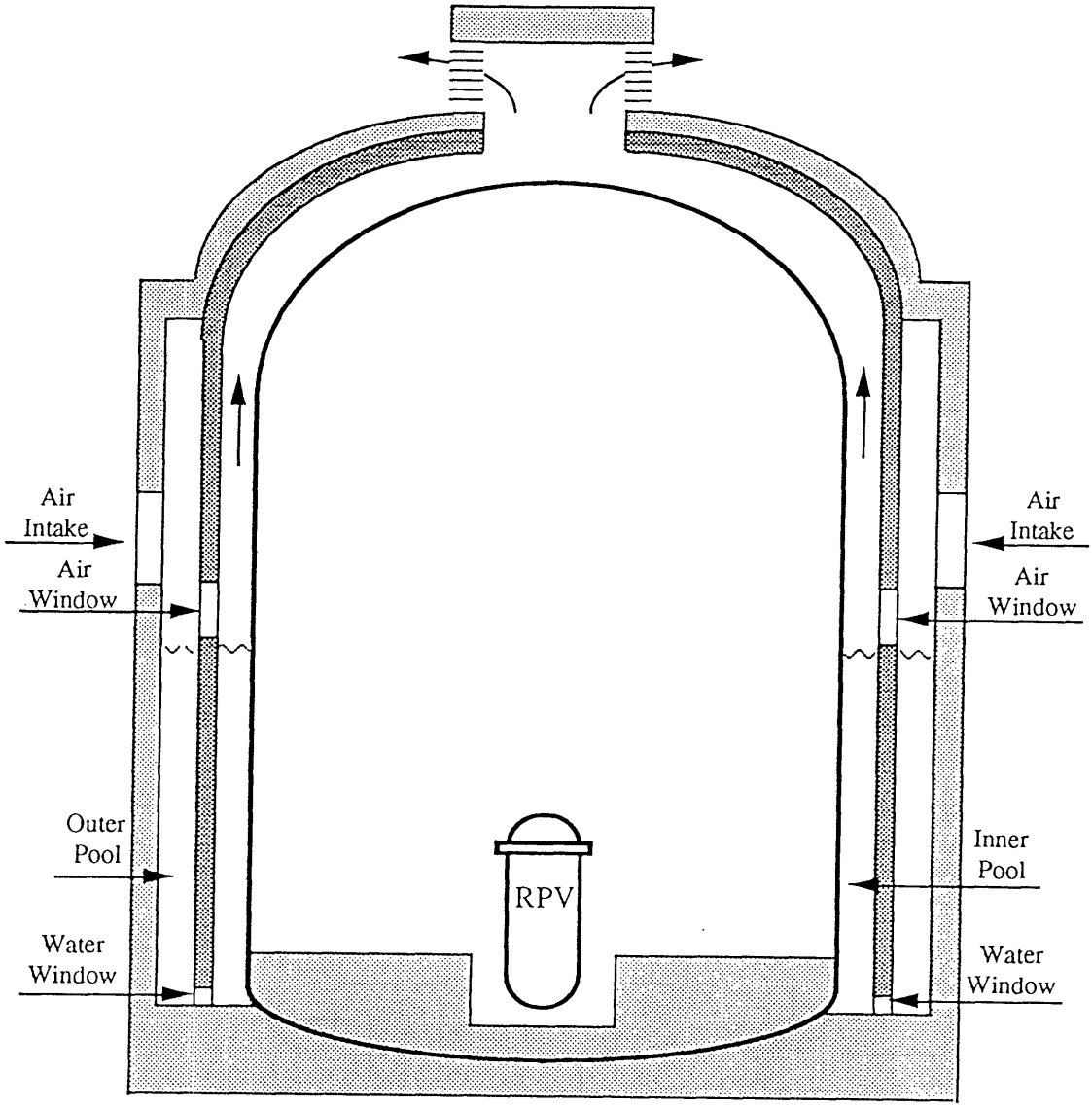

Figure 5.1 Schematic of Prefilled Water-Air Annulus Passive Containment Cooling System

containment under steady state natural air convection conditions. Figure 5.2 shows the gap width dependent heat transfer performance. The assumptions for Figure 5.2 are: (1) uniform containment atmosphere temperature at 137.5 °C; (2) uniform mixing of noncondensable (air) and steam inside the containment, and a mass ratio of air to steam of 0.63; (3) containment wall thermal resistance of 0.0011 m²°C/w (which may also implicitly include a fouling factor); (4) 0.7 emissivity for all surfaces; (5) a total air path form loss coefficient of 30; and (6) the annulus wall in which the windows are located has an insulated outer surface boundary condition.

As shown in Figure 5.2, the maximum heat removal capability for this specific geometry and boundary conditions is approximately 8.8 MWth which occurs at a gap width of about 40 cm. The maximum convective heat transfer coefficient, which excludes the effect of radiation, is 7 w/m²°C at a gap width of 20 cm (about 100 % larger than in our scale-down experiment). The difference in the gap width for the maximum value of the removal power and the heat transfer coefficient is due to the fact that the radiative heat transfer is independent of the gap width.

5.2.2 Water-Cooled Application

In the saturated pool boiling heat transfer regime, researchers have shown that the heat transfer is independent of, or at least less sensitive to, the dimensions and the orientation of the heating surface [K-8]. Therefore, to a first approximation, the water-filled test data can be applied directly to a prototype containment. The following analysis will be based on W0430 test results (the heat flux and the heat transfer coefficient, specifically).

Assuming a steady state saturated pool boiling condition in the inner pool, the containment temperature can be expressed as:

$$T_{cont} = T_{sat} + \frac{q''_{pool}}{U}, \tag{5.1}$$

where

$$U = \frac{1}{\frac{1}{h_{cond}} + \frac{\Delta}{k} + \frac{1}{h_{pool}}}. \tag{5.2}$$

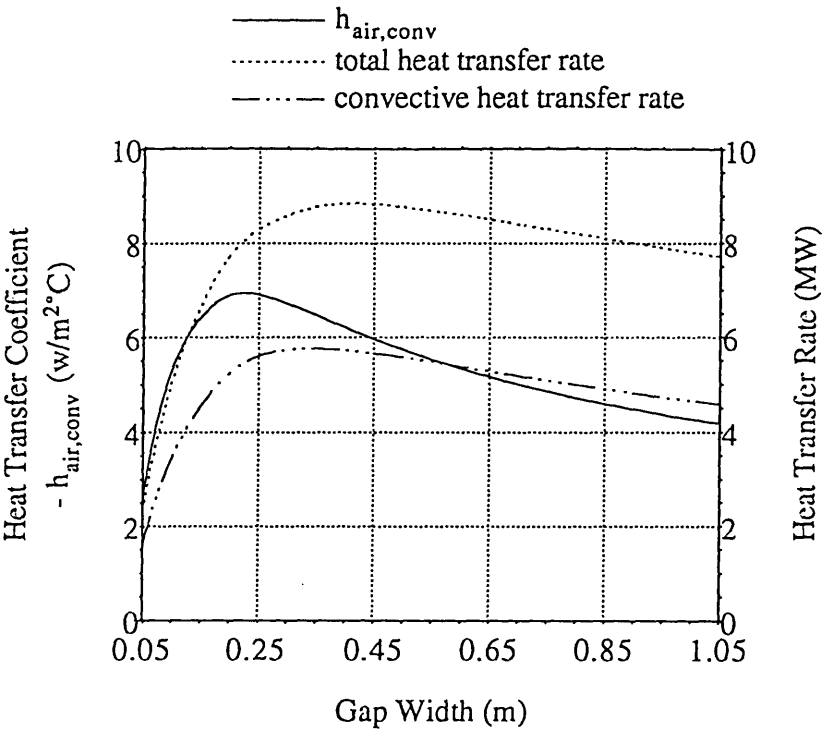

Figure 5.2 Containment Performance as a Function of Gap Width

Note that the heat transfer by natural convection to air has been neglected. Uchida's condensation heat transfer correlation (Equation 4.13) is adopted in this analysis. Assuming further that Dalton's law of partial pressure is applicable; and air is a perfect gas, the containment pressure in the presence of noncondensables can be expressed as:

$$P_{cont} = P_{sat}(\text{at } T_{cont}) + P_{air}(\text{at } T_{cont}), \tag{5.3}$$

where

$$P_{air}(\text{at } T_{cont}) = \frac{m_{air} R T_{cont}}{V_{cont}} = \frac{\frac{m_{air}}{m_{stm}} R T_{cont}}{v_{stm}}. \tag{5.4}$$

For the same heat transfer capability as in W0430 (the heat flux and the heat transfer coefficient are 12.5 kw/m^2 and 3 kw/m^2°C, respectively), the containment temperature and the corresponding pressure as a function of containment wall thermal resistance (Δ/k) and mass ratio of air to steam inside containment are shown in Figures 5.3 and 5.4. In other words, for a typical containment wall thermal resistance (Δ/k equals 0.0011), the heat removal capability (the heat flux) is 12.5 kw/m^2 at a containment temperature of 137.5 °C and 0.63 mass ratio of air to steam. The corresponding containment pressure is 0.47 MPa, which is the design pressure of the containment. The containment wall thermal resistance dependent curves shown in the figures provide an indication of the importance of the wall thermal properties to the total performance.

An alternative cooling mechanism for the proposed passive water cooled containment is the "moat cooling mode". In the moat cooling geometry, the water pool temperature is assumed to be kept essentially constant by installing a sufficiently large pool around the containment. The heat transfer regime in the moat cooling geometry is free convection in the water pool. The test data in this regime can not be applied directly to the proposed containment since the data taken in the water-filled tests in this regime was not obtained under steady state conditions. Nevertheless, the analysis in Chapter 4 shows that the predictions by PREWAS are in good agreement with the test results in the free convection heat transfer regime (although only a limited amount of data is available for comparison). The predicted heat transfer performance is then used to evaluate the applicability of the moat cooling geometry. Specifically, the predicted heat flux and heat transfer coefficient are approximately 25.6 kw/m^2 and 800 w/m^2°C, respectively.

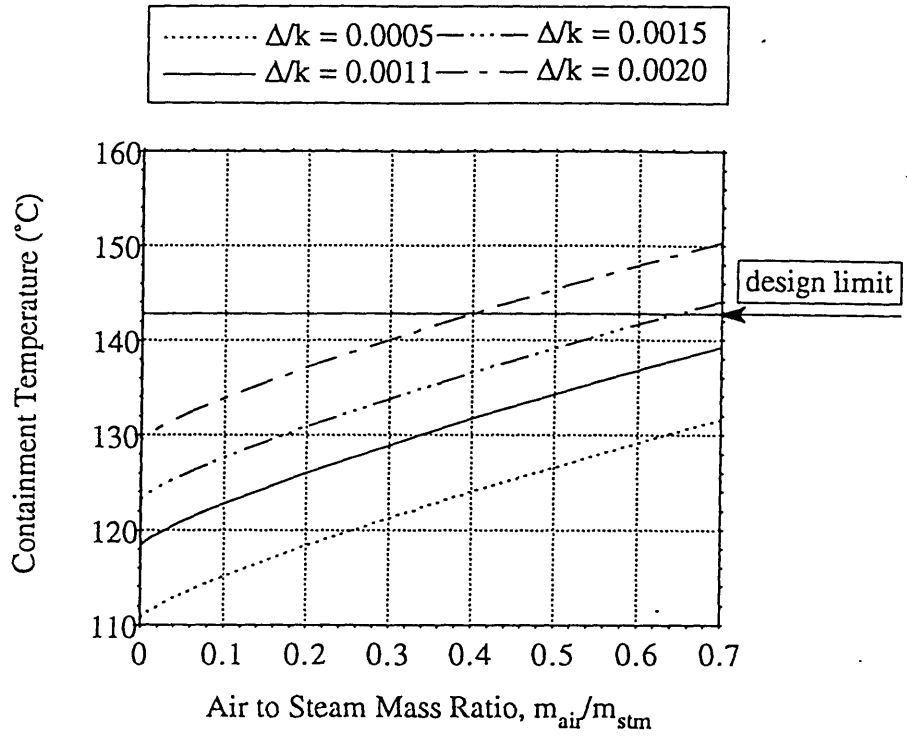

Figure 5.3 Predicted Steady State Containment Temperature for Cooling by a Boiling Water Pool

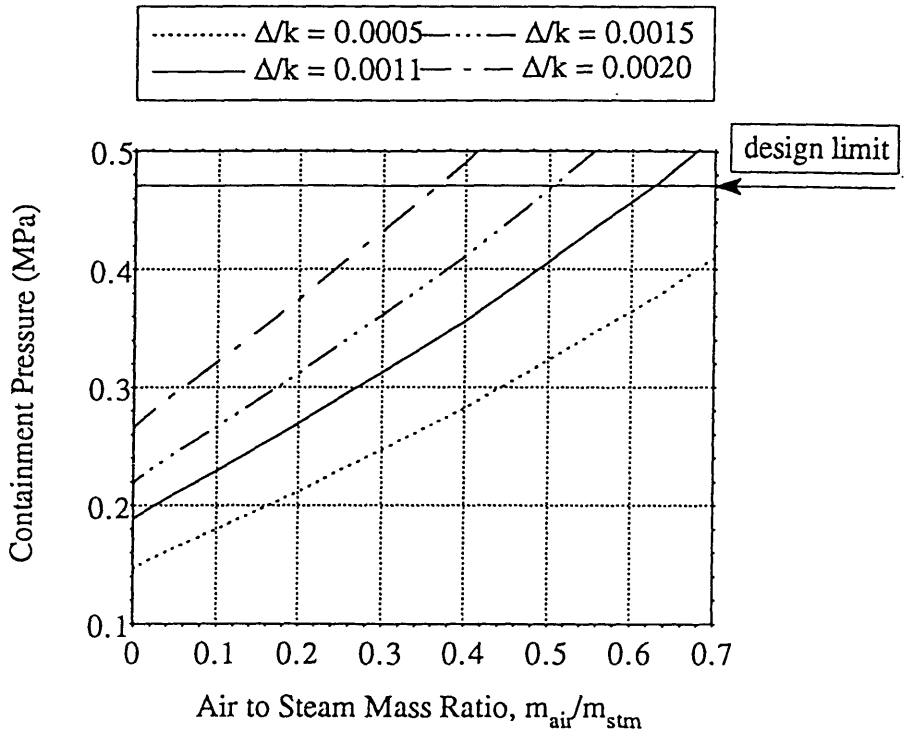

Figure 5.4 Predicted Steady State Containment Pressure for Cooling by a Boiling Water Pool

Figure 5.5 shows the containment temperature and the corresponding pressure, as a function of the mass ratio of air to steam at the containment wall utilizing these heat flux and heat transfer coefficient values. The assumptions adopted in Figure 5.5 are: (1) constant water pool temperature of 35 °C; (2) a 32 °C temperature difference between wall outer surface and the pool; and (3) the total wall thermal resistance is 0.0011 m^2°C/w. Equation 5.1 is again used to evaluate the containment temperature, but T_{sat} is replaced by T_{pool}. Also included in Figure 5.5 is the saturated pool boiling case discussed in the previous paragraph. The containment wall thermal resistance for the boiling case is the same as in the moat case.

The air to steam mass ratio shown in Figure 5.5 is assumed to be a local value evaluated at the interface of the containment wall and the mixture. It is possible in a stratified containment to have this interface ratio higher than the fully mixed homogeneous value. Alternately a design to promote natural circulation flow of steam over the interface could achieve a local air to steam ratio less than the homogeneous containment value.

To evaluate the heat removal capability of the proposed water cooled containment, the ratio of the steady state integral removal power to the integral decay power is shown in Figure 5.6. The containment atmospheric temperature is assumed to be 137.5 °C, and the mass ratio of air to steam is 0.63. The corresponding containment pressure is 0.47 MPa. The decay power fraction is as given in ORNL-6554 [F-1]. The reference reactor power is 1300 MWe (4000 MWth). The heat fluxes in Figure 5.5 for the boiling case and the moat case are the same as in Figure 5.5. The removal power for the air-only case is 8.8 MWth. On Figure 5.6, when the plotted cooling trajectory exceeds 1.0 on the vertical axis, containment cooling alone can hold containment pressure below its design limit; prior to that the energy must be stored in internal heat sinks.

Figure 5.6 indicates that (1) the air only heat removal case will not catch up with the decay heat production within the time scale of the figure, (2) the boiling case will balance the decay heat production within 1 hour (0.4 hour) for 30 m (on 40 m) pool height, (3) the moat case can almost match the decay heat production at LOCA initiation. This suggests that heat storage capability inside containment is needed for one hour after LOCA initiation for the boiling-cooled case. This is well within the normal capability of typical PWR units.

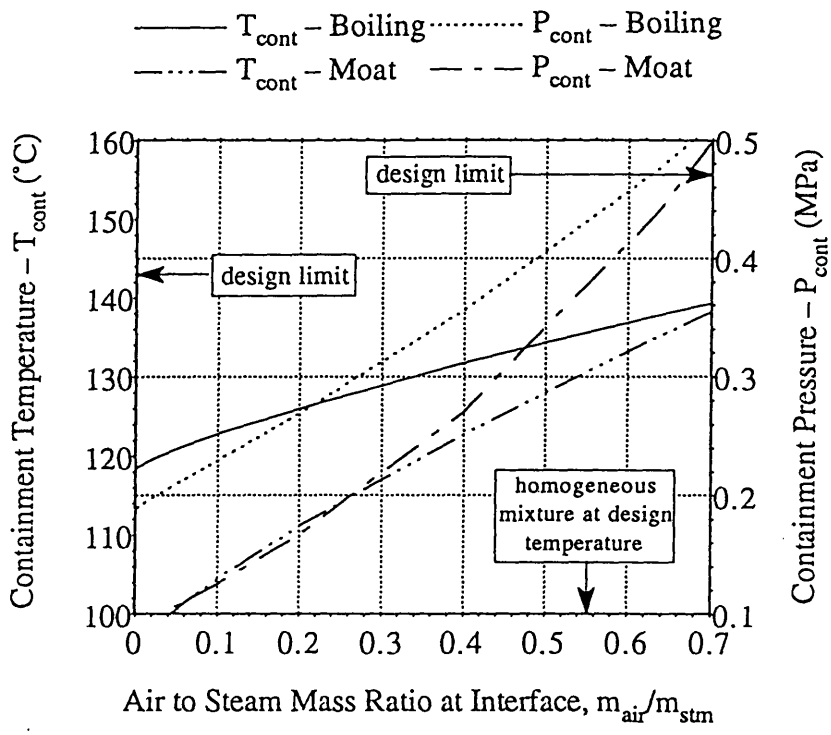

Figure 5.5 Comparison of Boiling Pool and Moat Performance

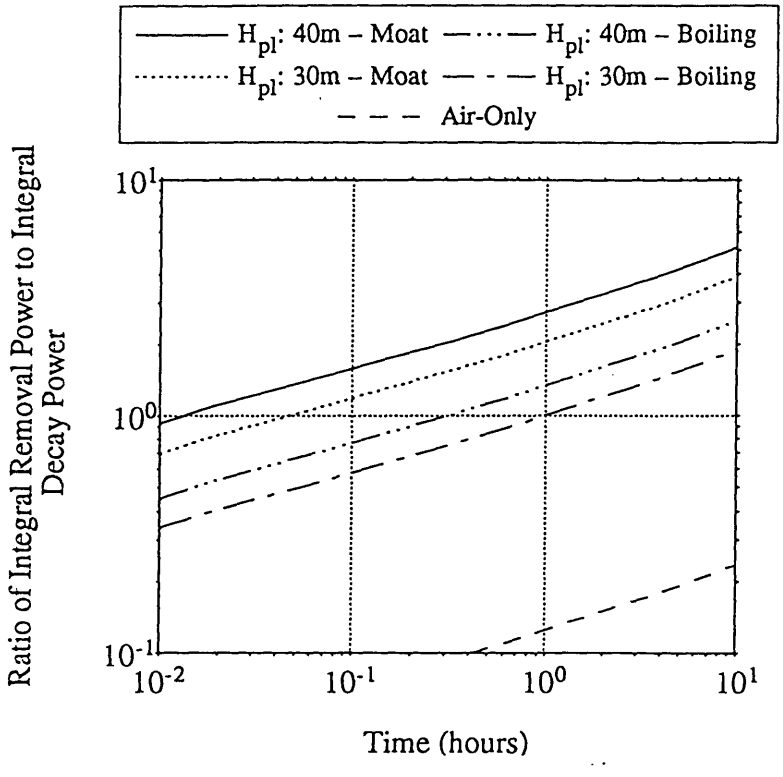

Figure 5.6 Passive Water Cooled Containment Performance – Constant Removal Power

Figures 5.7 and 5.8 provide other indicators of the heat removal capability of a boiling pool. The containment atmosphere temperature at fixed wall outer surface temperature can be expressed as:

$$T_{cont}(t) = T_{wo} + \frac{\dot{Q}_{decay}(t)}{\pi D_{cont} H_{pl} U}, \tag{5.5}$$

where

$$U = \frac{1}{\frac{1}{h_{cond}} + \frac{\Delta}{k}}. \tag{5.6}$$

Assuming the same wall thermal resistance and decay heat level as in Figure 5.6, with pressure evaluated at a fixed containment free volume of $1.0 \cdot 10^5$ m^3, and without credit for internal energy storage, Figures 5.7 and 5.8 show the containment temperature and pressure as a function of time, hence also implicitly as a function of decay power. For 30 m pool height and a wall outer surface temperature of 105°C, which is about the same wall outer surface temperature as in the W0430 test in the saturated pool boiling regime, the containment design limits will not be exceeded after 0.4 hour from LOCA initiation. Also shown in the figures is a wall outer surface temperature of 100 °C case, which corresponds to a non-boiling case. Comparing Figures 5.6 and 5.8, it is suggested that the heat removal capability of the pool imposes the major limitation (under preset conditions) on the performance of the proposed containment.

An overall evaluation of the proposed water cooled containment performance, based on PREWAS calculation, is shown in Figure 5.9. The assumptions in the calculation are: (1) the initial condition is an after-blowdown, well mixed containment at 125 °C saturation temperature; (2) the initial pool height is 40 m, and the inner pool and the outer pool gap width are 0.5 m and 1 m, respectively; (3) the initial pool temperature is 35 °C; (4) no credit for heat storage inside containment is taken; and (5) the pool swelling effect is neglected. For the time scale of interest, the pool inventory is still large. Approximately, 10 m height of water are evaporated at the end point shown in Figure 5.9.

The containment pressure shown in Figure 5.9 is the total pressure of steam and air. The mass ratio of air to steam is in the range of 0.66 to 2 within the time scale of the figure. The containment pressure first increases above the post-blowdown pressure due to the high

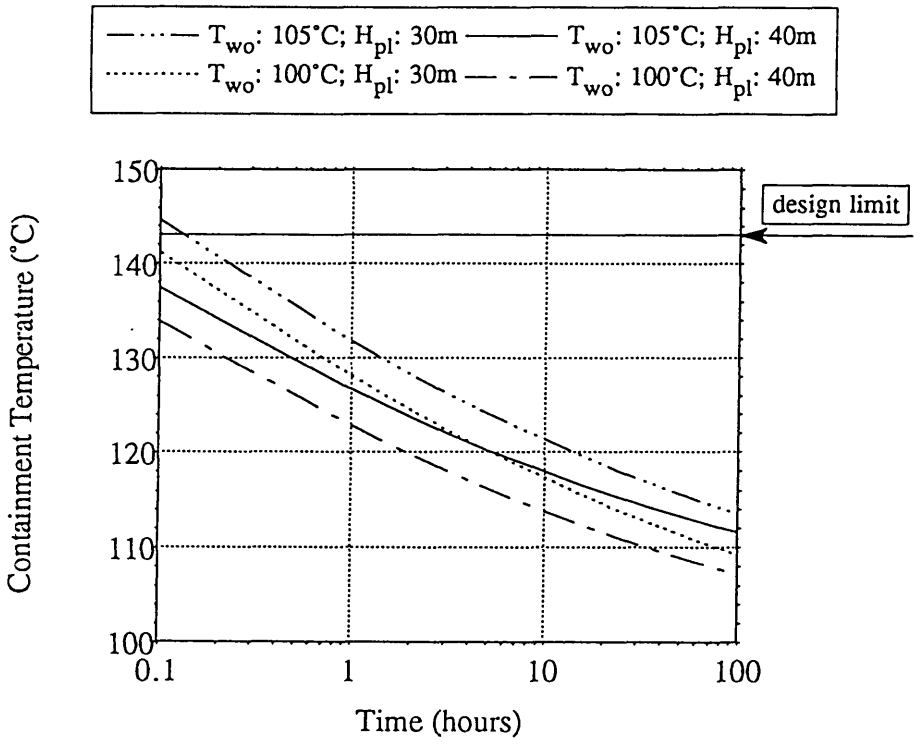

Figure 5.7 Containment Temperature at Fixed Outer Wall Surface Temperature for Cooling by Water Pool

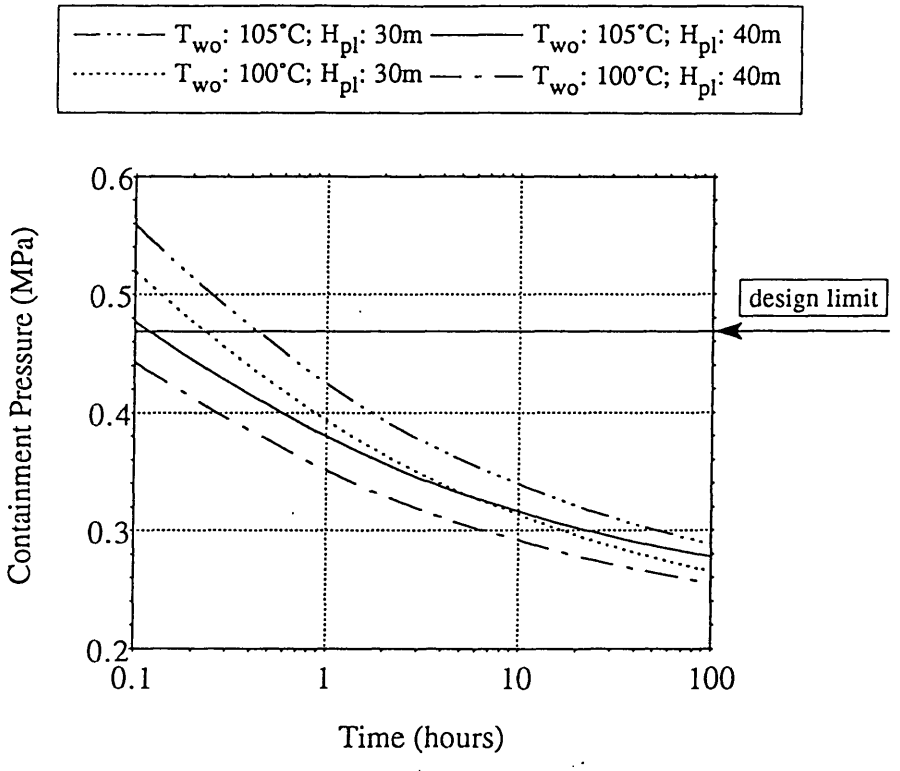

Figure 5.8 Containment Pressure at Fixed Outer Wall Surface Temperature for Cooling by Water Pool

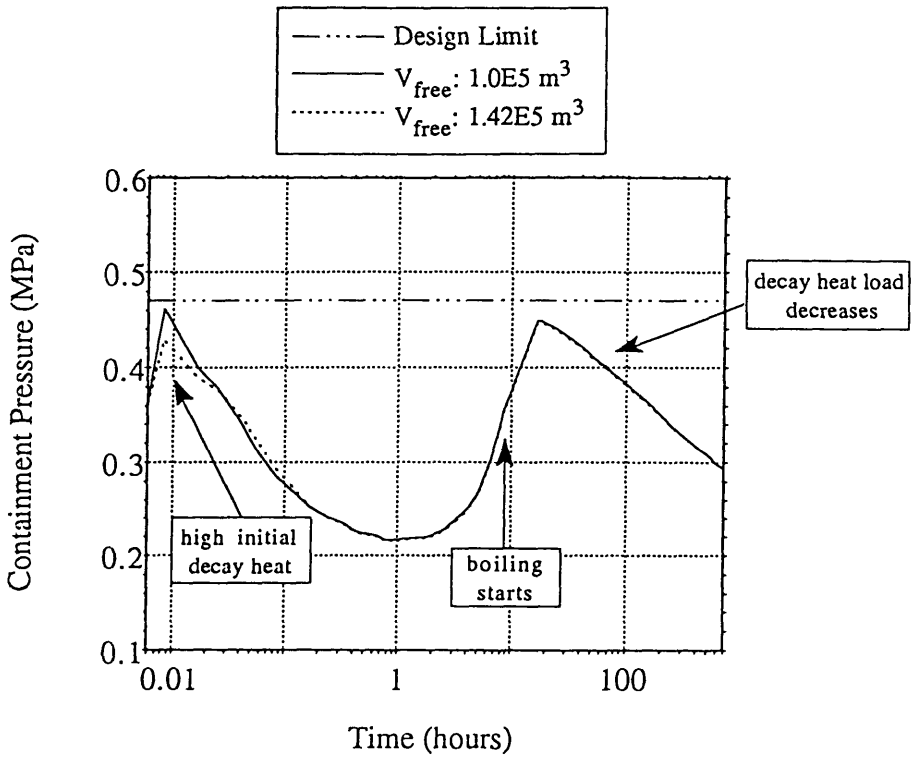

Figure 5.9 Containment Performance for Cooling by Boiling Pool

initial decay heat level, and then decreases due to the high heat removal capability of the cold water pool. When the pool temperature increases and approaches saturation conditions, the heat removal rate, while still good, is lower, and thus the pressure inside the containment increases. The pressure increase is reversed by the decreasing decay heat generation rate. The peak pressure for a $1.42 \cdot 10^5$ m³ free containment volume is approximately 0.45 MPa and the corresponding peak temperature is 134 °C, which are within the proposed containment design limits. However, for the smaller reference case free containment volume ($1.0 \cdot 10^5$ m³), the peak pressure is close to the design pressure. Therefore, in-containment heat storage should be provided in a smaller containment.

The containment performance for cooling by a moat is shown in Figure 5.10. The assumptions in Figure 5.10 are the same as in Figure 5.9. However, the inner pool is kept sufficiently large that the pool temperature is still low within the time scale as shown in the figure. The containment pressure decreases from the after-blowdown peak to a reasonably low level.

5.3 Summary of Chapter 5

The analysis for the application of the proof-of-principle experimental results to a prototype containment is presented in this Chapter. The major points are as follows.

- The proposed containment in the analysis is a right circular cylinder, 60 m in both diameter and height, with a 4.45 cm thick steel wall as a pressure boundary. The free volume of the containment is $1.0 \cdot 10^5$ m³. The stipulated design pressure and temperature are 0.47 MPa (53 psig) and 143 °C (290 °F), respectively.

- Gap width dependent heat transfer performance for the natural air convection cooled containment is shown in Figure 5.2. The maximum heat removal capability is approximately 8.8 MWth which occurs at a gap width of about 40 cm. The maximum convective heat transfer coefficient, which excludes the effect of radiation, is 7 w/m²°C at the gap width of 20 cm.

- Within the saturated pool boiling heat transfer regime, Figures 5.3 and 5.4 show the containment temperature and the corresponding pressure as a function of the containment wall thermal resistance and the mass ratio of air to steam inside containment to achieve the

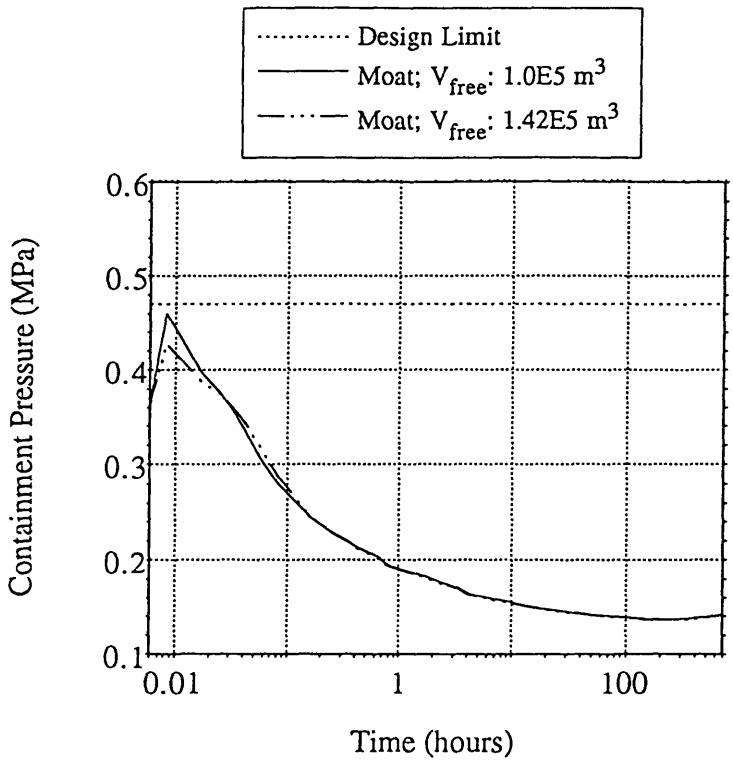

Figure 5.10 Containment Performance for Cooling by Moat

same heat transfer capability as in experimental run W0430. For a typical wall thermal resistance (Δ/k equals 0.0011), the heat removal capability (the heat flux) is 12.5 kw/m^2 at a containment atmospheric temperature of 137.5 °C and 0.63 mass ratio of air to steam. The corresponding containment pressure is 0.47 MPa, which is the design pressure of the containment.

- An alternative cooling mechanism for the proposed passive water cooled containment is the "moat cooling mode". In the moat cooling geometry, the water pool temperature is assumed to be kept effectively constant by installing a sufficiently large pool around the containment. Figure 5.5 shows the containment temperature and the corresponding pressure, as a function of mass ratio of air to steam, to achieve the predicted heat transfer performance. The predicted heat flux and heat transfer coefficient are approximately 25.6 kw/m^2 and 800 w/m^2°C, respectively.

- The ratio of the steady state integral removal power to the integral decay power is shown in Figure 5.6. The analysis indicates that (1) the air-only heat removal case will not match the decay heat production within the time scale of the figure, (2) the boiling cooling case will balance the decay heat production within one hour for 30 m pool height, (3) the moat case can almost accommodate the decay heat production at the beginning. This suggests that heat storage capability inside the containment is needed for almost one hour for cooling by a boiling water pool.

- An overall evaluation of the proposed water cooled containment performance, based on PREWAS calculation, is shown in Figure 5.9. Note that no credit is taken for heat storage inside containment. The containment pressure first increases due to the high initial decay heat level, and then decreases due to high heat removal capability of the cold water pool. When the pool temperature increases and approaches saturation conditions, the pressure again increases. The pressure increase is reversed by the decreasing decay heat generation rate. The performance of an alternative cooling geometry – a moat, is shown in Figure 5.10. The containment pressure decreases monotonously from the after-blowdown peak to a reasonably low level.

CHAPTER 6

SUMMARY, CONCLUSIONS AND FUTURE WORK

The objective of this thesis research is to explore a high heat removal capability passive containment cooling concept – a prefilled water-air annulus – that can allow a high power rating reactor design. The prefilled water-air annulus passive containment cooling concept, which is similar in some respects to the "water wall" approach explored by others, preserves the cooling capability of natural air convection heat transfer, and enhances the heat transfer capability by means of the prefilled water pool. The prefilled water pool consists of an inner and an outer pool. A small scale proof-of-principle containment test was designed and constructed to provide data in verification of the concept. Experiments were conducted for both air-only and water-filled cases at various steam temperature conditions to simulate the environment of a prototype containment under accident conditions. This chapter presents an overview of the thesis, which has as its goal the evaluation, both experimentally and analytically, of a water/air hybrid containment cooling system. Sections 6.1 through 6.4 summarize the contents of Chapter 2 through Chapter 5, respectively. The conclusions of the thesis and the recommendations for future work follow the summaries.

6.1 Summary of Advanced Light Water Reactor Passive Containment Cooling Design

Chapter 2 review advanced light water reactor passive containment cooling designs. The major points of this chapter are as follows:

- Containment, being one of the heat transfer barriers, while also serving as the last barrier to confine fission products, should be designed in a manner to enhance passive decay heat removal, while still maintaining its integrity during normal and accident conditions. Several passive containment cooling systems have been developed for advanced reactors. These passive containment cooling systems differ in cooling location and methods.

- Several passive containment cooling designs have been discussed. These include: General Electric's isolation condenser, Hitachi's suppression chamber water wall, Toshiba's drywell water wall, and a drywell cooler for boiling water reactors; KfK's composite containment with air annulus, and Westinghouse's air annulus with water film for pressurized water reactors.

- General Electric has extended the use of isolation condenser technology in their SBWR, having 600 MWe rated power, as a passive containment cooling system. An isolation condenser removes decay heat efficiently, since it absorbs decay heat steam directly from the hottest portion inside the containment. The technical issue that affects the performance of the isolation condenser is noncondensable gas accumulation inside heat transfer tubes.

- Toshiba (Oikawa et al.) made a performance comparison of the suppression chamber water wall, drywell water wall, isolation condenser, and drywell cooler for SBWR. Their result suggests that the isolation condenser has the best heat removal capability among passive containment cooling concepts evaluated in their analysis. They also concluded that the suppression chamber water wall is ineffective, mainly due to high noncondensable gas partial pressure in the suppression chamber, and low suppression pool temperature.

- Erbacher et al. (KfK), estimated, based on containment calculations with the CONTAIN code, that a decay heat rate of about 8 MWth can be removed by natural air convection in an air annulus containment cooling geometry, and concluded that it is sufficient for a 1300 MWe reactor, due to the high heat storage capacity of the internal structures within the composite containment.

- Westinghouse demonstrated, by the conduction of wind tunnel tests, water film tests, air flow resistance tests, heated plate tests, and integral tests, that an air annulus combined with a water film (supplied by a tank atop the containment building) provides suitable decay heat removal capability for the AP600.

6.2 Summary of Proof-of-Principle Experiment Design

Design considerations and the experimental setup are discussed in chapter 3. Figure 6.1 outlines the key features of the experiment. The major points are as follows:

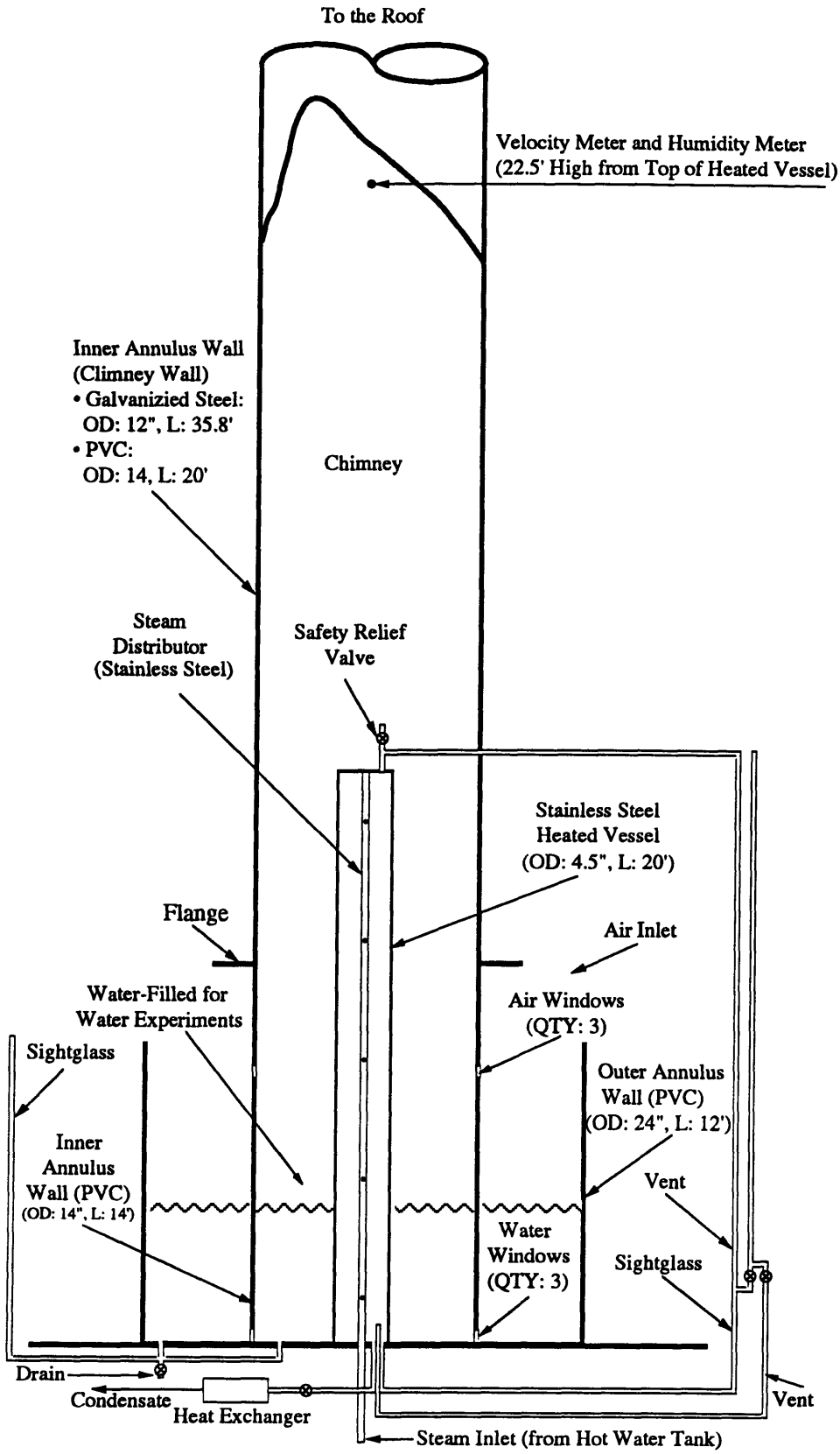

Figure 6.1 Key Features of Test Apparatus

• The performance indicators of the prefilled water-air annulus experiment are the heat flux, the heat transfer coefficient and the Reynolds number of the flowing steam-air mixture. The heat transfer mechanisms in the pool can be free convection and/or subcooled or saturated boiling. The heat transfer mechanism in the air section of the annulus is mixed air (or steam-air mixture) convection.

• For the scaling of air convection, the heat transfer coefficient and Reynolds number are only moderately sensitive to heated length; and Reynolds number is sensitive to hydraulic diameter. This analysis suggests that reducing the heated length rather than the hydraulic diameter is the proper method to reduce scale for the air portion of the experiment. Moreover, the input heat flux or temperature can be increased for the reduced scale experiment to ensure achievement of the appropriate turbulence regime and to achieve the simulation of the heat transfer coefficient.

For the scaling of the heat transfer in the pool, the free convection heat transfer coefficient is independent of the characteristic length. The nucleate boiling heat transfer coefficient is not directly dependent on the characteristic length. However, the fluid properties in the heat transfer correlation are a function of pressure, hence pool depth. This effect should be taken into account.

• The test apparatus is composed of four concentric pipes and a long chimney. A steam distributor ensures a uniform axial temperature distribution in the heated vessel. The air and/or water windows provide passages for fluid communication between the inner and outer annulus. A 6.1 m (20 ft) long heated length and a 10 cm (0.33 in) wide gap width are selected. The selection of the test apparatus dimensions is based on the scaling analysis and the constraints of the laboratory. The tall chimney helps in the data acquisition for the fully developed flow stream, and ensures attainment of the same flow regime as in a prototype containment. A 1.524 m (5 ft) height of the initial pool level is selected, based on a trade-off between the steam supply capability and the controllability of the condensate flow, for all the water-filled tests.

• There are ten thermocouples mounted at the heated surface to measure wall surface temperature, seventeen thermocouples mounted in the inner annulus, outer annulus and chimney to measure the flow stream or fluid temperature, five thermocouples mounted in the heated vessel to measure the axial temperature distribution, and four thermocouples

mounted at the inner surface of the inner annulus wall to estimate radiative heat transfer. To measure the heat loss, three additional thermocouples are mounted in the chimney. A wet bulb-dry bulb type relative humidity meter, associated with a fan type velocity meter, located at 22.5 times the diameter of the chimney from the top of the heated vessel, are used to measure the flowing mixture mass flowrate.

- Saturated steam is selected as the power source for the experiment to simulate the environment of a prototype containment under accident conditions. The boundary condition of the experiment is the constant steam temperature in the heated vessel. The steam pressure is set by a regulator. The effect of noncondensables is mitigated by venting. The heat transfer capability of the design is evaluated from the measured heated wall surface temperatures, fluid temperatures, temperature rise of the mixture along the heated surface, temperature rise of the pool water within a certain amount of time, flow velocity, humidity, and condensate weight.

6.3 Summary of Documentation and Analysis of Experimental Results

The documentation and analysis of the proof-of-principle experimental results are presented in Chapter 4. The major points are listed as follows.

- A total of sixteen air-only and water-filled tests, eight tests for each kind, were run to provide the basic data for application to the proposed passive water cooled containment concept as summarized in Table 6.1. Detailed experimental results for each test is presented in Appendix B.

- The air-only tests were run at steady state conditions. Five sets of data are taken for each test. The time interval between two sets of data in the same test run ranges from ten minutes to two hours. Because of the dynamic behavior in a water-filled test, special test procedures are followed to circumvent control difficulties. Eight to ten sets of data are taken for each water test. Each test run documents the progress of the test with time for a given set of initial conditions and boundary conditions.

- The deviation of the heat transfer performance in each air-only test run on the same day under the same test conditions is less than ± 5 % (shown in Table 4.2). Tests A0301-

Table 6.1 Summary of Test Results

TEST ID	$\overline{T}_{stm}$ (°C)	H_{pool} (m)	$h_{air,conv}$ or h_B (w/m²°C)	$\frac{\dot{Q}_{cond}}{\dot{Q}_{air} + \dot{Q}_{pool}}$	NO. OF DATA SETS	NOTE
A0301-11~15	150.1~150.4	0	10.02~11.12	1.02~1.09	5	-
A0304-11~15	150.2~150.3	0	9.39~10.13	1.07~1.14	5	-
A0429-11~15	108.7~109.3	0	7.57~8.35	1.10~1.14	5	-
A0429-21~25	104.1~104.3	0	8.00~8.39	1.13~1.17	5	-
A0430-11~15	120.1~120.8	0	8.45~8.79	1.10~1.14	5	-
A0502-11~15	120.0~120.1	0	8.96~9.39	1.07~1.09	5	sealed upper air windows
A0503-11~15	130.1~130.2	0	8.81~9.13	1.04~1.07	5	-
A0503-21~25	140.2~140.6	0	9.24~9.56	1.05~1.08	5	-
W0222	143.3~145.9	1.524	6670~7360	0.88~1.34	9	-
W0304	132.9~134.6	1.524	5740~6580	1.11~1.31	8	-
W0315	116.3~121.6	1.524	4840~5190	0.91~1.41	10	-
W0401	108.4~109.2	1.524	2850~3560	0.83~1.22	10	-
W0405	104.1~105.0	1.524	1470~2230	0.89~1.26	9	-
W0408	108.1~108.9	1.524	2070~2490	0.84~1.28	10	-
W0412	113.1~114.0	1.524	3660~4130	0.87~1.24	9	-
W0430	109.6~110.6	1.524	2870~3140	0.94~1.23	9	-

KEY TO TEST ID:

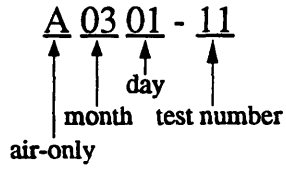

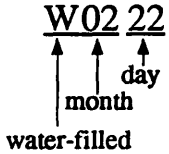

11~15 and A0304-11~15 were run at approximately the same steam temperature 150 °C, and the same geometry. The results show good agreement, since the deviation of the heat transfer performance between these two tests is less than ± 5 %, which is within the magnitude of the experimental uncertainty. Tests A0430-11~15 and A0502-11~15 were run under different geometry but approximately the same steam temperature 120 °C. The heat transfer performance of A0502-11~15 (sealed upper windows) is consistently about 5 % higher than that of A0430-11~15 (nominal geometry). The reason for the degraded heat transfer performance of A0430-11~15, although small in magnitude, is that the upper air windows provide another in-coming air flow passage which bypasses part of the heated surface.

- The comparisons of the test results with predictions by a simplified analytical model – PREWAS – shows that they are in good agreement (shown in Figures 4.2 and 4.3). Meanwhile, the change in the convective heat transfer coefficient with temperature is rather small over the range of the tests. The air-only test results are also compared with the Westinghouse small scale test, and the ANL natural convection test (shown in Table 4.3). All these tests yield similar values for the heat transfer coefficient, which validates the MIT apparatus as suitable for its intended purpose as a containment cooling proof-of-principle test. The heat transfer regime in this experiment and the ANL test fall in the mixed convection region ($0.1 < Gr/Re^2 < 10$). Moreover, the test geometry of this experiment and ANL's are quite similar. These factors may explain why the predictions by PREWAS, which adopts ANL's heat transfer correlation, are in good agreement with the air-only test results.

- In the PREWAS model, heat transfer to the water-filled section and the air-filled section are coupled together through the steam generation rate in the water pool. The steam flow is considered to be uniformly mixed at the beginning of the air section with incoming air flow from an air window. In the air section, momentum balance equations are employed to evaluate air mass flow rate, and energy balance equations are applied to the steam-air mixture flow to evaluate the heat transfer rate. In the water-filled section, continuity equations and energy balance equations are applied to evaluate the heat transfer rate and the steam generation rate. For the air-only case, the vapor contained in the air is also taken into consideration.

- All the water-filled tests were run at the same initial height of water. They differ

primarily in the input steam temperature. An illustration of water-filled test results, for run W0430 (Figures 4.4 and 4.5), which was run at 110 °C steam temperature, shows that the pool heat flux is high (about 60 kw/m^2) at the beginning when the pool temperature is still low and the pool is in the free convection heat transfer regime. Then the pool heat flux decreases rapidly as the pool temperature increases due to heat addition. Transition from free convection to subcooled boiling heat transfer is suspected to occur during this period of time since the pool heat transfer coefficient is increasing. As the pool temperature reaches the corresponding saturation temperature, saturated pool boiling heat transfer takes place, and the pool heat flux levels off (at about 12.5 kw/m^2) as the pool heat transfer coefficient remains approximately constant (3 kw/m^2°C). The convective heat transfer coefficient and the heat flux to the flowing vapor phase mixture (air plus steam) stay at an approximately constant level (9 w/m^2°C and 1 kw/m^2, respectively) before saturated boiling occurs in the pool section. When the pool is in the saturated boiling heat transfer regime, the heat transfer coefficient and the heat flux in this region increase about 10 %. The reason for the increase of the air heat transfer performance in the presence of steam is that the hot steam enhances the buoyancy-induced air flowrate.

- All eight water-filled tests follow the same trend as in test W0430. The predictions are generally in good agreement with the test data. However, deviations between the predictions and the test data still exist, especially before saturated pool boiling occurs. Factors that contribute to the deviation are: (1) the space-averaging method to derive desired quantities may not be appropriate when the deviation between the parameters of interest is large; (2) the steam temperature and/or ambient conditions (for example, atmospheric pressure) changes during the test, which can not be simulated by PREWAS, (3) the dissolved gases in the water, which tend to decrease the required wall superheat for nucleation [R-1], and (4) for high temperature tests, the wall inner surface temperature may be decreased to a non-negligible degree by the noncondensables contained in the supplied steam, which degrades the heat transfer.

- The radiative heat transfer rate accounts for approximately one third of the total heat transfer rate in the air-only tests. A sensitivity analysis shows that the convective heat transfer coefficient is insensitive to the emissivity of the inner annulus wall in the range of our application, but is sensitive to the emissivity of the heated wall, in part because the

diameter of the heated vessel (4.5 in) is much smaller than the diameter of the inner annulus wall (14 in). The uncertainty in the heated wall surface emissivity contributes approximately ± 5 % uncertainty in the evaluation of the convective heat transfer coefficient.

- The surface emissivity also affects the prediction of the heat transfer performance for the air-only test. Analysis shows that the heat flux and both the effective and the convective heat transfer coefficients are insensitive to the duct wall emissivity. However the effective heat transfer coefficient and hence the heat flux are sensitive to the heated wall surface emissivity since the effective heat transfer coefficient includes the radiation effect. The proposed 10 % uncertainty in the heated wall emissivity contributes 3 % uncertainty in the prediction of the heat flux and the effective heat transfer coefficient.

- The form loss coefficients of the apparatus are estimated by referring to manufacturer's data and/or to Idelchik's hydraulic resistance handbook [I-1] for similar flow geometry. The uncertainty in the heat transfer performance prediction due to the uncertainty of the form loss coefficient for the air-only test is less than 5 % in the range of our interest. The predicted heat flux and the heat transfer coefficient are relatively less sensitive to the inlet form loss coefficient than to the outlet form loss coefficient.

- Analysis of the noncondensable effect for two extreme test temperature cases of the air-only test shows that the decrease in the inner wall surface temperature is less than 1 °C in the temperature range of our tests even for an air to steam mass ratio equal to 0.1 which is an implausibly high value for the air-only tests. Analysis of the decrease in the inner wall surface temperature in the presence of noncondensables for water test run W0430 shows that the degree of temperature decrease is significant only at high air to steam mass ratios and more pronounced when coupled with high heat flux (W0430-0001-0). From the observed temperature decrements, the estimated mass ratio of air to steam is approximately 0.002 in the W0401, W0405, W0408, W0412, and W0430 tests; 0.02 in test W0315; 0.035 in test W0304; and 0.04 in test W0222. The higher noncondensable concentration for the high temperature tests (W0222, W0304, and W0315) arises from the fact that the pool section heated wall outer surface temperature shows an axial variation which is inferred as due to concentration of noncondensables in the lower axial portion of the heated vessel.

6.4 Summary of Application of Findings

The analysis for the application of the proof-of-principle experimental results to a prototype containment is presented Chapter 5. The major points are as follows.

- The proposed containment in the analysis is a right circular cylinder, 60 m in both diameter and height, with a 4.45 cm thick steel wall as a pressure boundary. The free volume of the containment is $1.0 \cdot 10^5$ m^3. The stipulated design pressure and temperature are 0.47 MPa (53 psig) and 143 °C (290 °F), respectively. A schematic diagram of the passive water cooled containment is shown in Figure 5.1.

- Gap width dependence of heat transfer performance for the natural air convection cooled containment is shown in Figure 5.2. The maximum heat removal capability is approximately 8.8 MWth which occurs at a gap width of about 40 cm. The maximum convective heat transfer coefficient, which excludes the effect of radiation, is 7 $w/m^2°C$ at a gap width of 20 cm.

- Within the saturated pool boiling heat transfer regime, Figures 5.3 and 5.4 show the containment temperature and the corresponding pressure as a function of the containment wall thermal resistance and the mass ratio of air to steam inside containment to achieve the same heat transfer capability as in experimental run W0430. For a typical wall thermal resistance (Δ/k equals 0.0011), the heat removal capability (the heat flux) is 12.5 kw/m^2 at a containment atmospheric temperature of 137.5 °C and 0.63 mass ratio of air to steam. The corresponding containment pressure is 0.47 MPa, which is the design pressure of the containment.

- An alternative cooling mechanism for the proposed passive water cooled containment is the "moat cooling mode". In the moat cooling geometry, the water pool temperature is assumed to be kept effectively constant by installing a sufficiently large pool around the containment. Figure 5.5 shows the containment temperature and the corresponding pressure, as a function of mass ratio of air to steam, to achieve the predicted heat transfer performance. The predicted heat flux and heat transfer coefficient are approximately 25.6 kw/m^2 and 800 $w/m^2°C$, respectively.

- The ratio of the steady state integral removal power to the integral decay power is shown in Figure 5.6. The analysis indicates that (1) the air-only heat removal case will not

match the decay heat production within the time scale of the figure, (2) the boiling cooling case will balance the decay heat production within one hour for 30 m pool height, (3) the moat case can almost accommodate the decay heat production at the beginning. This suggests that heat storage capability inside the containment is needed for on the order of one hour for cooling by a boiling water pool. Figure 6.2 shows the achievable reactor power for a given heat transfer surface area without in-containment heat storage.

- An overall evaluation of the proposed water cooled containment performance, based on PREWAS calculation, is shown in Figure 6.3. Note that no credit is taken for heat storage inside containment. For cooling by a normal water pool (the boiling case), the containment pressure first increases due to the high initial decay heat level, and then decreases due to high heat removal capability of the cold water pool. When the pool temperature increases and approaches saturation conditions, the pressure again increases. The pressure increase is reversed by the decreasing decay heat generation rate. For cooling by a moat, the containment pressure decreases from the after-blowdown peak to a reasonably low level. The peak pressure for both two cooling approaches is approximately 0.46 MPa which is slightly less than the design limit. It suggests that in-containment heat storage and/or increased containment free volume should be provided to increase the containment safety margin.

6.5 Conclusions and Recommendations for Future Work

A proof-of-principle experiment has been conducted to evaluate the feasibility of a proposed passive water cooled containment concept which can accommodate a high power rating reactor design. The experiments were run for both air-cooled-only and water-cooled conditions to provide the basic data for application to a prototype containment.

The air-cooled-only tests were run in the mixed convection heat transfer regime. The test results agree with ANL natural convection tests for advanced liquid metal reactors and Westinghouse small scale tests for their AP600 in the range of our interest. The water-cooled tests were run in a dynamic manner in which the water pool temperature changes with time until a quasi-steady state condition, that is a saturated pool, is reached. The water-cooled test results in the saturated pool boiling regime agree with Rohsenow's nucleate pool boiling heat transfer correlation. The test results in the free convection regime

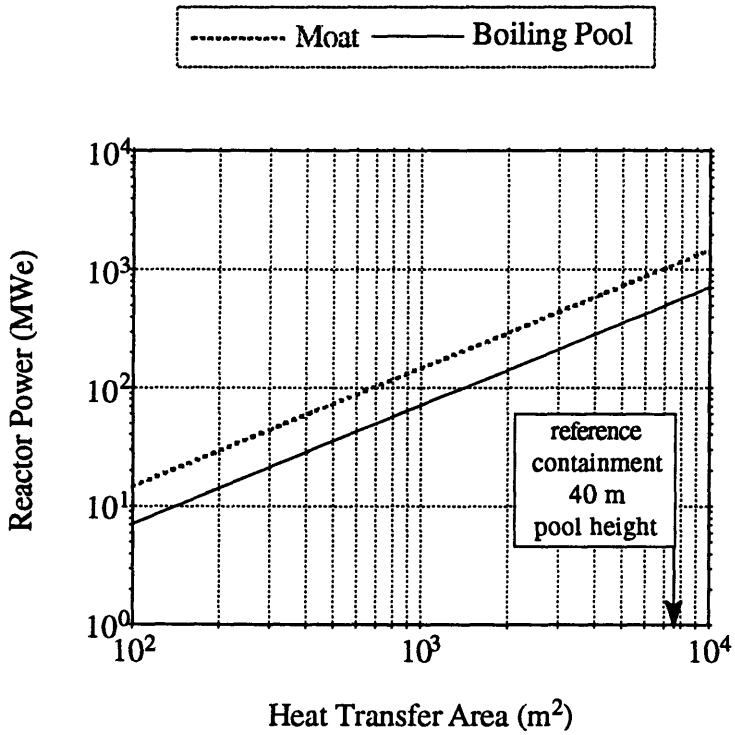

Figure 6.2 Achievable Reactor Power for a Given Heat Transfer Area

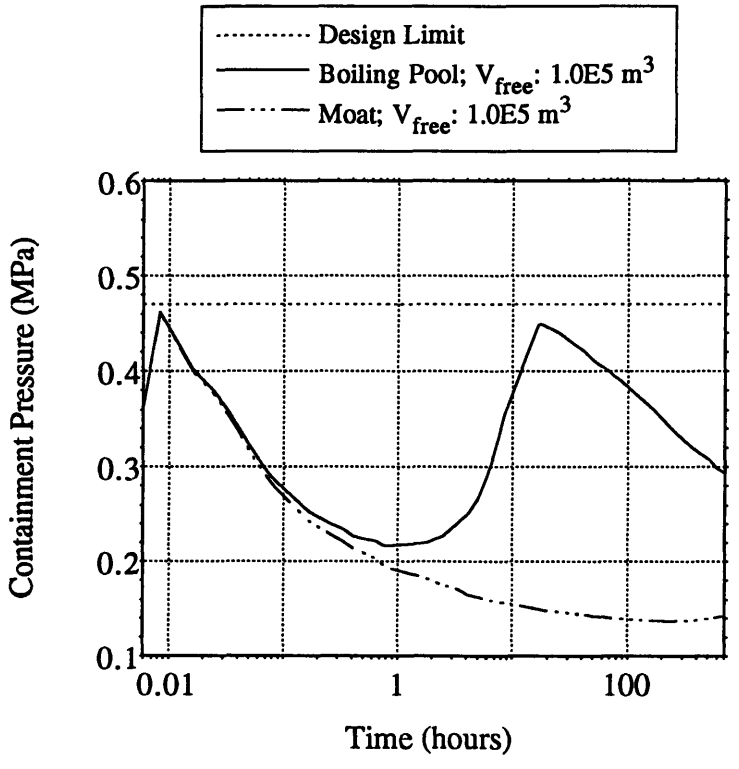

Figure 6.3 Passive Water Cooled Containment Performance

are in good agreement with the prediction by a typical natural turbulent heat transfer correlation, although only a limited amount of data is available. However, in the subcooled pool boiling regime, the test results show higher values than the prediction. The water-cooled tests also show an increase in the heat transfer performance in the air-cooled section of the heated vessel due to the enhancement of the buoyancy force by mixing steam with air.

The analysis shows that the capability of an air-cooled-only containment can not accommodate the decay heat production without extensive heat storage inside containment. For a water-cooled containment, on the other hand, only a small amount of heat storage capacity is needed during the initial phase of the decay heat generation. Furthermore, the heat transfer capability of a moat having constant pool temperature is predicted to be better than a boiling pool.

The proposed passive water cooled containment preserves air cooling capability and enhances the heat transfer performance using a prefilled water pool. The analysis, assuming a well mixed containment atmospheric condition, shows that the containment pressure is kept within the design limit (a typical value for an advanced PWR design) in a loss of coolant accident.

An axially averaged condensation heat transfer correlation has been adopted in this analysis. However, thickening of the condensate film as water flows down the containment steel shell, which is the major heat transfer area for the proposed water cooled containment, may degrade the heat transfer performance. Further evaluation using a local condensation heat transfer correlation should be considered. The condensation heat transfer model developed by Siddique et al. [S-5] can be applied to the analysis.

Thermal stratification in the presence of noncondensables and nonuniform heat distribution inside containment during accident conditions affect the performance of a passive cooled containment. Circulation of the containment atmosphere, especially near-wall circulation, is desirable to ensure the achievement of the high heat removal capability of the proposed water cooled containment. A baffle close to the inner containment wall may help to form a thermosyphon circulation loop. Furthermore, an internal or external passive containment spray may also help to break thermal stratification. However, the effectiveness of the circulation loop and the capability of the passive containment spray should be demonstrated. Computer simulation and ultimately a large scale containment test

are, therefore, recommended to investigate the heat transfer mechanisms inside containment.

The analysis shows that the moat cooling geometry can provide better heat transfer performance than the boiling cooling geometry. However, the water-filled tests provide limited data in the free convection mode and the subcooled boiling heat transfer regime due to limitations of the apparatus. Modifying the experiment to explore more extensively the cooling capability of a moat should be considered.

The structural integrity of the prefilled water-air annulus configuration under static and/or dynamic loads (for example, seismic events) should be demonstrated. A normally-dry moat concept, which is flooded at the onset of a severe accident scenario (for example, from the cooling tower basin) should be evaluated.

REFERENCES

[A-1] A.A. Ahmad et at., " PWR Severe Accident Delineation and Assessment," NUREG/CR-2666, University of California, Los Angeles, 1983.

[A-2] " Decay Heat Power in Light Water Reactors," ANSI/ANS-5.1, 1979.

[B-1] J. Bowman and P. Griffith, " Non-Condensable Gas Fraction Predictions Using Wet and Dry Bulb Temperature Measurements," NUREG/CR-2853, 1983.

[C-1] J.J. Carbajo, " Heat Transfer Coefficients under LOCA Conditions in Containment Buildings," Nuclear Engineering and Design 65, 1981.

[C-2] J.G. Collier, " Convective Boiling and Condensation," McGraw-Hill, 1981.

[C-3] A.G. Croff, " ORIGEN2 - A Revised and Updated Version of the Oak Ridge Isotope Generation and Depletion Code," ORNL-5621, Oak Ridge National Laboratory, July 1980.

[D-1] A. Dehbi, M. Golay, M. Kazimi, " The Effects of Noncondensable Gases on Steam Condensation under Turbulent Natural Convection Conditions," MIT-ANP-TR-004, 1991.

[E-1] F.J. Erbacher and H.J. Neitzel, " Passive Containment Cooling by Natural Air Convection for Next Generation LWRs," KfK, NURETH-5, Vol. IV, pp. 1235~1241, 1992.

[F-1] C.W. Forsberg et al., " Proposed and Existing Passive and Inherent Safety-Related Structures, Systems, and Components (building blocks) for Advanced Light Water Reactors," ORNL-6554, 1989.

[F-2] G. Fu et. al., " Heat Transfer and Friction Factor Behavior in the Mixed Convection Regime for Air Up-Flow in a Heated Vertical Pipe," AIChE Heat Transfer Conf., Minneapolis, Symp. Series, 382, Vol. 87, 1991a.

[F-3] G. Fu et al., " Heat Transfer Correlation for Reactor Riser in Mixed Convection Air Flow," Journal of Heat Transfer, Vol. 116, pp. 489~492, 1994.

[F-4] T. Fujii et al., " Natural Convection Induced by Steam Condensation and Mitigation of Thermal Stratification in Water Pool," Hitachi, NURETH-5, 1992.

[F-5] W. Frost and G.S. Dzakowic, " An Extension of the Method for Predicting Incipient Boiling on Commercially Finished Surfaces," ASME Paper 67-HT-61, 1967.

[G-1] Peter Griffith, " Steam-Water Separation," Massachusetts Institute of Technology, Feb., 1990.

[G-2] S.V. Garimella and R.N. Christensen, " Transient Condensation in the Presence of Noncondensables at a Vertical Wall," Nuclear Technology Vol. 89, 1990.

[G-3] T.L. George et al., " GOTHIC - Containment Analysis Package Technical Manual for GOTHIC_S," Version 3.4e, NAI 8907-06 Rev. 2, pp. 8-3, Numerical Applications Inc., 1993.

[G-4] T.L. George et al., " GOTHIC - Containment Analysis Package User's Manual," Version 3.4e, NAI 8907-02 Rev. 3, Numerical Applications Inc., 1993.

[H-1] J. Heineman et al., " Experimental and Analytical Studies of a Passive Shutdown Heat Removal System for Advanced LMRs," Proc. of Intl. Topical Meeting on Safety of Next Generation Power Reactors, Seattle, 1991.

[H-2] P. Hejzlar, N.E. Todreas, M.J. Driscoll, " Passive Decay Heat Removal in Advanced Reactor Concepts," Nucl. Eng. Des., Vol. 139, No. 1, 1993a.

[H-3] Gad Hetsroni, " Handbook of Multiphase Systems," Hemisphere Publishing Co., 1982.

[I-1] I. E. Idelchik, " Handbook of Hydraulic Resistance," Second Edition, Hemisphere Publishing Co., 1986.

[I-2] PSYCHRO-DYNE Relative Humidity Meter Instruction Manual, Industrial Instruments & Supplies, Southampton, PA, 1993.

[I-3] T.F. Irvine, Jr and P.E. Liley, " Steam and Gas Tables with Computer Equations," Academic Press Inc., 1984.

[K-1] S. Kakac et al., " Handbook of Single-Phase Convective Heat Transfer," John Wiley & Son Inc., 1987.

[K-2] Y. Kataoka et al., "Thermal Hydraulic Characteristics and Heat Removal Capability of Containment Cooling System with External Water Wall," Hitachi, J.N.S.T., 1990.

[K-3] Y. Katoaka et al., " Experiments on Convection Heat Transfer Along a Vertical Flat Plate Between Pools with Different Temperatures," Nuclear Technology, Vol. 99, 1992.

[K-4] J.H. Keenan et al., " Steam Tables - Thermodynamic Properties of Water Including Vapor, Liquid, and Solid Phases," John Wiley & Sons Inc., 1978.

[K-5] John Keffer, " Passive Cooling of a Sealed BWR Containment," M.S. Thesis, Department of Nuclear Engineering, MIT, 1987.

[K-6] G.E. Kendall and W.H. Rohsenow, " Heat Transfer to Impacting Drops and Post Critical Heat Flux Dispersed Flow," Report No. 85694-100, MIT, 1978.

[K-7] M.D. Kennedy et al., " Westinghouse-GOTHIC Comparisons with 1/10 Passive Containment Cooling Tests," Intl. Conf. on New Trends in Nuclear System Thermohydraulics, Vol. II, pp. 535~540, Pisa, Italy, 1994

[K-8] Frank Kreith, " Heat Transfer Data Book," Genium Publishing Co., 1984.

[K-9] G.E. Kulynych and J.E. Lemon, " Babcock and Wilcox Advanced PWR Development," Nuclear Europe, 4, 1986.

[L-1] J.H. Lienhard et al., " A Heat Transfer Textbook," Prentice-Hall Inc., 1987.

[L-2] G.S.H. Lock, " The Tubular Thermosyphon," Oxford Science Publications, 1992.

[M-1] R.J. McCandless and J.R. Redding, " Simplicity: the Key to Improved Safety, Performance and Economics," Nuclear Engineering Intl., Nov., 1989.

[M-2] Wade R. McGills et. al., " Pool Boiling on Small Heat Dissipating Elements in Water at Subatmospheric Pressure," HTD-Vol. 159, Phase Change Heat Transfer, ASME, 1991.

[N-1] H. Nagasaka et al., " Study of a Natural-Circulation Boiling Water Reactor with Passive Safety," Toshiba, Nuclear Technology, Vol. 92, 1990.

[O-1] OHAUS DS Series Electronic Digital Bench Scales Instruction Manual, Ohaus Co., 1992.

[O-2] H. Oikawa et al., " Heat Removal Performance Evaluation of Several Passive Containment Cooling Systems during Loss of Coolant Accident," Toshiba, J.N.S.T., 1991.

[O-3] Temperature Catalog of Omega Engineering, Stamford, Connecticut, 1993.

[P-1] A. Pernsteiner, I. Huhtiniemi, M. Corradini, " Condensation in the Presence of Noncondensable Gases--Effect of Helium," NURETH-5, Vol. IV, pp. 1071~1078, 1992.

[P-2] F.E. Peters et al., " Advanced PWR Passive Containment Cooling Experimental Program," Intl. Conf. on New Trends in Reactor Thermodynamics, Vol. II, pp. 37~43, Pisa, Italy, 1994.

[P-3] Y. Parlatan, " Friction Factor and Nusselt Number Behavior in Turbulent Mixed Convection in Vertical Pipes," Ph.D. Thesis, Department of Nuclear Engineering, MIT, 1993.

[R-1] W.M. Rohsenow and H. Y. Choi, " Heat, Mass, and Momentum Transfer," Prentice-Hall Inc., 1961.

[S-1] D.S. Selengut, " Diffusion Coefficients for Heterogeneous Systems," Trans. Am. Nucl. Soc., Vol. 4, No. 2, 1991.

[S-2] R.S. Sirohi and H.C.R. Krishna, " Mechanical Measurements," Wiley, New York, 1983.

[S-3] N.J. Spinks and J.E. Dick, " Passive Design Options for CANDU," Trans. ANS Vol. 64, 1991.

[S-4] D. Squarer et al., " Test Program in Support of the Westinghouse Advanced Light Water Reactor," NURETH-4, Vol. 2, pp. 812~817, 1989.

[S-5] M. Siddique et. al., " Theoretical Modeling of Forced Convection Condensation of Steam in a Vertical Tube in the Presence of a Noncondensable Gas," Nuclear Technology, Vol. 106, 1994.

[T-1] J.K. Thomas et. al., " Stainless Steel 304L Oxidation and Emittance," WSRC-MS-93-602X, ANS Summer Conference, 1994.

[T-2] Neil E. Todreas and Mujid S. Kazimi, " Nuclear Systems I - Thermal Hydraulic Fundamentals," Hemisphere Publishing Co., 1990.

[T-3] Neil E. Todreas and Mujid S. Kazimi, " Nuclear Systems II - Elements of Thermal Hydraulic Design," Hemisphere Publishing Co., 1990.

[U-1] H. Uchida, A. Oyama, and Y. Togo, " Evaluation of Post-Incident Cooling Systems of Light-Water Power Reactors," Proc. of the 3rd Intl. Conf. on the Peaceful Uses of Atomic Energy, 1964.

[U-2] T. Ueda and T. Miyashita, " On the Performance Limit of Closed Two-Phase Thermosiphons," Heat Transfer: Japanese Research, Vol. 20, No. 6, 1991.

[V-1] Theo van de Venne et al., " The Westinghouse AP600 Passive Containment Cooling Test Analysis Program," Intl. Conf. on Design and Safety of Advanced Nuclear Power Plants, Vol. II, pp. 17.1-1~8, Tokyo, Japan, 1992.

[W-1] P.B. Whalley, " Boiling, Condensation and Gas-Liquid Flow," Oxford Science Publications, 1987.

[W-2] L. Wolf et al., " Comparisons Between Multi-Dimensional and Lumped-Parameter GOTHIC-Containment Analyses with Data," Intl. Conf. on New Trends in Reactor Thermodynamics, Vol. II, pp. 321~330, Pisa, Italy, 1994.

[W-3] L. Wolf et al., " Hydrogen Mixing Experiments in the HDR-Containment Under Severe Accident Conditions," 21st Water Reactor Safety Information Meeting, 1993.

[W-4] R.F. Wright, D.R. Spencer, F. Delose, " Reactor Passive Containment Cooling System Small Scale Containment Test," Westinghouse Electric Corporation, 1992.

[W-5] R.F. Wright et al., " Comparisons of the Westinghouse-GOTHIC Containment Code Predictions to Free Convection Heat Transfer Tests," Intl. Conf. on New Trends in Reactor Thermodynamics, Vol. II, pp. 541~546, Pisa, Italy, 1994.

[Z-1] O.T. Zimmerman and I. Lavine, " Psychrometric Tables and Charts," Industrial Research Service Inc., 1964.

APPENDIX A

DATA REDUCTION AND EXPERIMENTAL ERROR ANALYSIS

A.1 Introduction

The determination of experimental parameters, either from direct measurements or derived from direct measurements, is subject to error or uncertainty. The error stems from the capability of the experimental equipment, which can have only certain precision, and may also have systematic bias. Error also arises due to variations in the quantities being measured. In the prefilled water-air annulus passive containment cooling experiment, the parameters of our interest are the total heat transfer rate and heat flux, the heat transfer rate to the flowing mixture, the heat transfer rate to the pool water, the heat transfer coefficient for moist air convection, the heat transfer coefficient of pool boiling and free convection, and the Reynolds number of the flowing mixture. These values are derived from the measured heated wall surface temperatures, fluid temperatures, temperature rise of the mixture along the heated surface, temperature rise of the pool water over a certain period of time, flow velocity, humidity, and condensate weight.

To estimate the uncertainty associated with a derived quantity from the uncertainties of directly measured parameters, a general rule can be used for the expected error in the derived quantity. For any function

$$y = f(x_1, x_2, \cdots, x_i, \cdots, x_n), \tag{A.1}$$

the square of the uncertainty in y, E_y, can be expressed as

$$E_y^2 = \sum_i^n \left(\frac{\partial y}{\partial x_i}\right)^2 E_{x_i}^2, \tag{A.2}$$

where x_i, i = 1, 2, ····, n, are the directly measured parameters, y is the derived quantity from the directly measured parameters, and E represents the uncertainty [S-2].

Equation A.2 is valid only if the errors due to measured parameters are due to random, independent error or due to systematic errors of unknown sign. If the errors are of systematic nature with known sign, the error due to each component must be added. That is

$$E_y = \sum_i^n \left(\frac{\partial y}{\partial x_i}\right) E_{x_i} . \tag{A.3}$$

The method used in the error analysis is as follows: (1) The random errors and systematic errors with unknown sign are combined by Equation A.2. (2) The systematic errors with known sign are combined by Equation A.3. (3) The total error due to combined random and systematic errors of both kind, the results of (1) and (2) are then summed using Equation A.2 [S-2].

In the experiment, y represents the total heat transfer rate, the heat transfer rate or heat flux to the steam-air mixture, the heat transfer rate or heat flux to the pool water, the heat transfer coefficient of the mixed air convection, the heat transfer coefficient of the nucleate boiling and/or free convection, and the Reynolds number. Expressions for these quantities are given in Chapter 3, and reproduced in the following sections.

A.1.1 Heat Transfer Rate to Steam-Air Mixture

To calculate the heat transfer rate to the steam-air mixture, the steam-air mixture flow rate is measured using a velocity meter and a humidity meter. Assuming further that air and steam are perfect gases, the heat transfer rate can be evaluated as follows by applying the heat balance equation.

$$\dot{Q}_{mix} = \dot{m}_{mix} \overline{C}_{p,mix} (T_{mix,o} - T_{mix,in}), \tag{3.15}$$

where

$$\dot{m}_{mix} = \dot{m}_{stm} + \dot{m}_{air}$$

$$= (\rho_{stm} + \rho_{air}) V_{mix} A_{mix}$$

$$\dot{m}_{mix} = [\frac{\phi_{mix} P_{sat}(T_{mix})}{R_{stm} T_{mix}} + \frac{P_{atm} - \phi_{mix} P_{sat}(T_{mix})}{R_{air} T_{mix}}] V_{mix} A_{mix}. \quad (3.16)$$

An alternative approach to determining the steam generation rate is to measure the level decrease rate of the water pool.

$$\dot{m}_{stm} = \frac{1}{\Delta t}(H_{pool,1} - H_{pool,2})(\overline{\rho}_{f,pi} A_{pi} + \overline{\rho}_{f,po} A_{po}) \quad (3.17)$$

In the case of no water in the pool, $\dot{m}_{mix}$ is the summation of $\dot{m}_{air}$ and $\dot{m}_{vapor,in}$. $\dot{m}_{vapor,in}$ is the vapor content in the intake air flow. It can be expressed as:

$$\dot{m}_{vapor,in} = [\frac{\phi P_{sat}(T)}{RT}(VA)]_{vapor,in}$$

$$= [\frac{\phi P_{sat}(T)}{RT}]_{vapor,in} \frac{\dot{m}_{air}}{[\frac{P_{atm} - \phi P_{sat}(T)}{RT}]_{air,in}}. \quad (3.18)$$

The heat transfer in the steam-air mixture section can be further split into two parts, that is, convective heat transfer and radiative heat transfer. In addition, the duct wall is made up of two kinds of material: galvanized steel and PVC. The radiative heat transfer should be treated separately.

$$\dot{Q}_{mix} = \dot{m}_{mix} \overline{C}_{p,mix}(T_{mix,o} - T_{mix,in})$$

$$= \dot{Q}_{conv} + \dot{Q}_{rad}, \quad (3.19)$$

where

$$\dot{Q}_{conv} = \overline{h}_{mix} \pi D_{vessel}(H_{vessel} - H_{pool})(\overline{T}_{wo} - \overline{T})_{mix}, \quad (3.20)$$

$$\dot{Q}_{rad} = \dot{Q}_{rad,PVC} + \dot{Q}_{rad,gal}, \quad (3.21)$$

$$\dot{Q}_{rad,gal} = \pi D_{vessel} H_{gal} \frac{\sigma}{[\frac{1}{\varepsilon_{ss}} + \frac{D_{vessel}}{D_{gal}}(\frac{1}{\varepsilon_{gal}} - 1)]}(\overline{T}^4_{wo} - \overline{T}^4_{wi})_{gal}, \quad (3.22)$$

$$\dot{Q}_{rad,PVC} = \pi D_{vessel}(H_{vessel} - H_{pool} - H_{gal}) \frac{\sigma}{[\frac{1}{\varepsilon_{ss}} + \frac{D_{vessel}}{D_{PVC}}(\frac{1}{\varepsilon_{PVC}} - 1)]} (\overline{T}_{wo}^4 - \overline{T}_{wi}^4)_{PVC}. \tag{3.23}$$

The averaged effective heat transfer coefficient of the steam-air mixture which combines the convective heat transfer and radiative heat transfer can be expressed as:

$$\overline{h}_{mix,eff} = \frac{\overline{q}''_{mix}}{(\overline{T}_{wo} - \overline{T})_{mix}}, \tag{3.24}$$

where

$$\overline{q}''_{mix} = \frac{\dot{Q}_{mix}}{\pi D_{vessel}(H_{vessel} - H_{pool})}. \tag{3.25}$$

The averaged convective heat transfer coefficient, $\overline{h}_{mix}$, can be evaluated by applying Equations 3.19 and 3.20.

$$\overline{h}_{mix} = \frac{\dot{Q}_{mix} - \dot{Q}_{rad}}{\pi D_{vessel}(H_{vessel} - H_{pool})(\overline{T}_{wo} - \overline{T})_{mix}} \tag{3.26}$$

The Reynolds number of the flowing mixture, which is used to check the flow regime of the buoyancy driven air or mixture flow, can be evaluated by

$$Re = (\frac{\dot{m} D_e}{\mu A})_{mix}. \tag{3.27}$$

A.1.2 Heat Transfer Rate to Water Pool

The heat transfer rate to the water pool is the summation of the heat transfer rates due to free convection or subcooled boiling and saturated boiling or evaporation.

$$\dot{Q}_{pool} = (\dot{Q}_{pool})_{FC\ or\ SCB} + (\dot{Q}_{pool})_B \tag{3.28}$$

To find the free convection or subcooled boiling heat transfer rate in the water pool, the temperature increase rate of the inner and outer pool are measured. By applying the heat balance equation, the heat transfer rate due to free convection or subcooled boiling can be expressed as:

$$\{\dot{Q}_{pool} = \frac{1}{\Delta t}\{[m_{wtr}(\overline{C}_{pf,2}\overline{T}_2 - \overline{C}_{pf,1}\overline{T}_1)]_{pi} + [m_{wtr}(\overline{C}_{pf,2}\overline{T}_2 - \overline{C}_{pf,1}\overline{T}_1)]_{po}\}\}_{FC \text{ or } SCB}, \quad (3.29)$$

where

$$[m_{wtr,pi} = \rho_{f,pi} A_{pi} H_{pi}]_{FC \text{ or } SCB}, \quad (3.30)$$

$$[m_{wtr,po} = \rho_{f,po} A_{po} H_{po}]_{FC \text{ or } SCB}. \quad (3.31)$$

To find the heat transfer rate due to saturated boiling or evaporation, the steam generation rate is evaluated by measuring either the humidity of the flowing mixture or the water level decrease rates as discussed in the previous section. The heat transfer rate is expressed as:

$$[\dot{Q}_{pool} = (\dot{m} h_{fg})_{pool}]_B, \quad (3.32)$$

where

$$\dot{m}_{pool} = \dot{m}_{stm} - \dot{m}_{vapor,in}, \text{ and} \quad (3.33)$$

$\dot{m}_{stm}$ and $\dot{m}_{vapor,in}$ are the same as evaluated in Section 3.5 1, Equations 3-16 to 3-18.

The averaged heat transfer coefficient to the pool water can be expressed as:

$$[\overline{h}_{pool} = \frac{\overline{q}''_{pool}}{(\overline{T}_{wo} - \overline{T})_{pool}}]_{FC,\ SCB \text{ or } B}, \quad (3.34)$$

where

$$[\overline{q}''_{pool} = \frac{\dot{Q}_{pool}}{\pi D_{vessel} H_{pool}}]_{FC,\ SCB \text{ or } B}. \quad (3.35)$$

A.1.3 Total Heat Transfer Rate

The total heat transfer rate is the summation of the heat transfer rates to the pool water by free convection and/or subcooled or saturated boiling and to the flowing steam-air mixture. It can be expressed as:

$$\dot{Q}_{total} = \dot{Q}_{pool} + \dot{Q}_{mix}. \tag{3.36}$$

There is a redundant parameter to check the heat transfer performance of the system, that is, the heat transfer inferred from steam condensation, $\dot{Q}_{cond}$. It can be evaluated by weighing the condensate collected from the steam condensation in the heated stainless steel pipe, and can be expressed as:

$$\dot{Q}_{cond} = \frac{m_{cond}}{\Delta t} h_{fg}. \tag{3.37}$$

A.2 Analysis of the Experimental Error

A.2.1 Uncertainty in the Total Heat Transfer Rate

The uncertainty associated with the total condensation heat transfer rate, $\partial\dot{Q}_{cond}$, can be evaluated by applying Equation A.2 to Equation 3.37.

$$\frac{\partial\dot{Q}_{cond}}{\dot{Q}_{cond}} = [(\frac{\partial\Delta t}{\Delta t})^2 + (\frac{\partial m_{cond}}{m_{cond}})^2 + (\frac{\partial h_{fg}}{h_{fg}})^2]^{.5}, \tag{A.4}$$

where Δt and m_{cond} are directly measured parameters. The enthalpy difference between the vapor phase and liquid phase of water in the temperature range of our interest can be expressed as:

$$h_{fg} \approx 2532.8 - 2.7929T \quad (kJ/kg). \tag{A.5}$$

Therefore

$$(\partial h_{fg})^2 = 2.7929^2(\partial T)^2 + h_{fg}^2\sigma_{h_{fg}}^2, \tag{A.6}$$

where $\sigma^2_{h_{fg}}$ represents the systematic error with unknown sign. If this systematic error is taken as 1%, and ∂T is assumed to be 1 °C, we then obtain

$$(\frac{\partial h_{fg}}{h_{fg}})^2 = (\frac{2.7929}{h_{fg}})^2 + 0.01^2. \tag{A.7}$$

At the typical steam supply temperature of the heat transfer laboratory, that is 150 °C,

$$(\frac{\partial h_{fg}}{h_{fg}})^2 = 0.0013^2 + 0.01^2, \tag{A.8}$$

or

$$\frac{\partial h_{fg}}{h_{fg}} = 0.01009 \approx 0.01, \tag{A.9}$$

which shows that the uncertainty in the enthalpy difference between the vapor phase and liquid phase of the water due to the uncertainty in the temperature can be neglected, compared to the systematic error in the last item of Equation A.8. By the same procedure, we can demonstrate that the systematic error associated with most of the physical properties of our interest, which we have taken as 1%, is the dominant source of the total uncertainty (that is, the uncertainty in the temperature measurement can be neglected). However, for the density of water vapor, dynamic viscosity of air, and saturation pressure of steam, the total uncertainty should include the uncertainty in the temperature measurement and the systematic error.

A.2.2 Uncertainty in the Heat Transfer Rate to the Steam-Air Mixture

The uncertainty associated with the heat transfer rate to the steam-air mixture (Equation 3.15) can be expressed as:

$$\frac{\partial \dot{Q}_{mix}}{\dot{Q}_{mix}} = \{(\frac{\partial \dot{m}_{mix}}{\dot{m}_{mix}})^2 + (\frac{\partial \overline{C}_{p,mix}}{\overline{C}_{p,mix}})^2 + [\frac{\partial (T_{mix,o} - T_{mix,in})}{(T_{mix,o} - T_{mix,in})}]^2\}^{.5}. \tag{A.10}$$

If $\dot{m}_{stm}$ is evaluated by humidity measurement (Equation 3.16),

$$\frac{\partial \dot{m}_{mix}}{\dot{m}_{mix}} = \{(\frac{\partial V}{V})^2 + (\frac{\partial T}{T})^2$$

$$+ \frac{(\frac{1}{R_{stm}} - \frac{1}{R_{air}})^2[\frac{P_{sat}(T)\partial\phi}{T}]^2 + [\frac{\partial P_{atm}}{R_{air}T}]^2 + (\frac{1}{R_{stm}} - \frac{1}{R_{air}})^2[\frac{\phi\partial P_{sat}(T)}{T}]^2}{[\frac{\phi P_{sat}(T)}{R_{stm}T} + \frac{P_{atm} - \phi P_{sat}(T)}{R_{air}T}]^2}\}^{.5}_{mix}, \quad (A.11)$$

$$\frac{\partial \dot{m}_{stm}}{\dot{m}_{stm}} = \{(\frac{\partial \phi_{mix}}{\phi_{mix}})^2 + (\frac{\partial T_{mix}}{T_{mix}})^2 + [\frac{\partial P_{sat}(T_{mix})}{P_{sat}(T_{mix})}]^2 + (\frac{\partial V_{mix}}{V_{mix}})^2\}^{.5}. \quad (A.12)$$

If $\dot{m}_{stm}$ is evaluated by water pool measurement (Equation 3.17),

$$\partial \dot{m}_{mix} = [(\partial \dot{m}_{stm})^2 + (\partial \dot{m}_{air})^2]^{.5}, \quad (A.13)$$

$$\frac{\partial \dot{m}_{air}}{\dot{m}_{air}} = \{\frac{(\partial P_{atm})^2 + [P_{sat}(T_{mix})\partial\phi_{mix}]^2 + [\phi_{mix}\partial P_{sat}(T_{mix})]^2}{[P_{atm} - \phi_{mix}P_{sat}(T_{mix})]^2} + (\frac{\partial T_{mix}}{T_{mix}})^2 + (\frac{\partial V_{mix}}{V_{mix}})^2\}^{.5},$$

(A.14)

$$\frac{\partial \dot{m}_{stm}}{\dot{m}_{stm}} = [(\frac{\partial \Delta t}{\Delta t})^2 + \frac{(\partial H_{pool,1})^2 + (\partial H_{pool,2})^2}{(H_{pool,1} - H_{pool,2})^2} + \frac{(A_{pi}\partial \overline{\rho}_{f,pi})^2 + (A_{po}\partial \overline{\rho}_{f,po})^2}{(\overline{\rho}_{f,po}A_{pi} + \overline{\rho}_{f,po}A_{po})^2}]^{.5}.$$

(A.15)

P_{atm}, T_{mix}, $T_{mix,o}$, $T_{mix,in}$, V_{mix}, ϕ_{mix}, and H_{pool} are directly measured parameters. T_{mix} represents the measured temperature at the location of the humidity measurement of the steam-air mixture. $P_{sat}(T_{mix})$ represents the corresponding saturation steam pressure at T_{mix}. The specific heat of the mixture is evaluated using a simplified mixing law as discussed in the description of the PREWAS computer program (see Appendix C for details). The uncertainty associated with all the temperature measurements comes from the accuracy of the copper-constantan thermocouples, which is taken as 0.5 °C, [Omega Catalog, 1993]. The uncertainty associated with V_{mix} and ϕ_{mix} are 0.051 m/s and 2%, respectively, as discussed in Chapter 3. The uncertainty associated with $P_{sat}(T_{mix})$ should combine the assumed systematic error and the uncertainty in temperature measurement, as

discussed in the previous section. The uncertainty associated with H_{pool} is one readable scale division of the ruler which is 1.59 mm (0.0625 in). The uncertainty associated with the flow area, ∂A_{mix}, or cross sectional area, ∂A_{pi} and ∂A_{po}, can be neglected, since they have been determined very accurately (less than 0.5 % error).

The uncertainty associated with the radiative heat transfer (Equations 3.22 and 3.23) can be expressed as:

$$\frac{\partial \dot{Q}_{rad,PVC}}{\dot{Q}_{rad,PVC}} = \{[\frac{\partial(\overline{T}_{wo}^4 - \overline{T}_{wi}^4)}{(\overline{T}_{wo}^4 - \overline{T}_{wi}^4)}]_{PVC}^2 + [\frac{\partial(H_{vessel} - H_{pool} - H_{gal})}{(H_{vessel} - H_{pool} - H_{gal})}]^2 + \frac{(\frac{\partial \varepsilon_{ss}}{\varepsilon_{ss}^2})^2 + (\frac{D_{vessel}}{D_{PVC}} \frac{\partial \varepsilon_{PVC}}{\varepsilon_{PVC}^2})^2}{[\frac{1}{\varepsilon_{ss}} + \frac{D_{vessel}}{D_{PVC}}(\frac{1}{\varepsilon_{PVC}} - 1)]^2}\}^{0.5}, \quad \text{(A.16)}$$

$$\frac{\partial \dot{Q}_{rad,gal}}{\dot{Q}_{rad,gal}} = \{[\frac{\partial(\overline{T}_{wo}^4 - \overline{T}_{wi}^4)}{(\overline{T}_{wo}^4 - \overline{T}_{wi}^4)}]_{gal}^2 + (\frac{\partial H_{gal}}{H_{gal}})^2 + \frac{(\frac{\partial \varepsilon_{ss}}{\varepsilon_{ss}^2})^2 + (\frac{D_{vessel}}{D_{gal}} \frac{\partial \varepsilon_{gal}}{\varepsilon_{gal}^2})^2}{[\frac{1}{\varepsilon_{ss}} + \frac{D_{vessel}}{D_{gal}}(\frac{1}{\varepsilon_{gal}} - 1)]^2}\}^{0.5}, \quad \text{(A.17)}$$

$$\partial \dot{Q}_{rad} = (\partial \dot{Q}_{rad,PVC} + \partial \dot{Q}_{rad,gal})^{0.5}. \quad \text{(A.18)}$$

All the temperatures and wall heights in Equations A.16 and A.17 are directly measured parameters. The uncertainty associated with the averaged temperature can be evaluated by applying Equations A.2 and A.3. The emissivity of the stainless steel pipe, the PVC pipe, and the galvanized steel pipe are as given by Kreith's heat transfer data book [K-8], which are: 0.57 for the stainless steel pipe; 0.89 for the PVC pipe; 0.28 for the galvanized steel pipe. The uncertainty associated with the emissivities are 10% for the stainless steel pipe and the galvanized steel pipe, and 5% for the PVC pipe [T-1]. The uncertainty associated with the diameter of the heated wall and the duct wall are neglected since they have been determined very accurately (less than 0.5 % error).

A.2.3 Uncertainty in the Mixed Air Convection Heat Transfer Coefficient

The uncertainty associated with the averaged effective heat transfer coefficient (equation 3.24) and averaged convective heat transfer coefficient (equation 3.26) to the steam-air mixture can be evaluated as:

$$\frac{\partial h_{mix,eff}}{h_{mix,eff}} = \{(\frac{\partial q''_{mix}}{q''_{mix}})^2 + [\frac{\partial(\overline{T}_{wo} - \overline{T})}{(\overline{T}_{wo} - \overline{T})}]^2_{mix}\}^{0.5}, \tag{A.19}$$

$$\frac{\partial h_{mix}}{h_{mix}} = \{[\frac{\partial(\dot{Q}_{mix} - \dot{Q}_{rad})}{(\dot{Q}_{mix} - \dot{Q}_{rad})}]^2 + [\frac{\partial(\overline{T}_{wo} - \overline{T})}{(\overline{T}_{wo} - \overline{T})}]^2_{mix} + [\frac{\partial(H_{vessel} - H_{pool})}{(H_{vessel} - H_{pool})}]^2\}^{0.5}, \tag{A.20}$$

where

$$\frac{\partial \overline{q}''_{mix}}{\overline{q}''_{mix}} = \{(\frac{\partial \dot{Q}_{mix}}{\dot{Q}_{mix}})^2 + [\frac{\partial(H_{vessel} - H_{pool})}{(H_{vessel} - H_{pool})}]^2\}^{.5}. \tag{A.21}$$

H_{vessel} and H_{pool} are directly measured parameters. The uncertainty in $\overline{T}_{wo}$ and $\overline{T}_{mix}$ can be evaluated by applying equations A.2 and A.3. The uncertainty in the heat transfer rate to the flowing mixture can be evaluated by equation A.10.

A.2.4 Uncertainty in the Flowing Mixture Reynolds Number

The uncertainty associated with the Reynolds number of the flowing mixture (equation 3.27) can be evaluated as:

$$\frac{\partial Re}{Re} = [(\frac{\partial \dot{m}_{mix}}{\dot{m}_{mix}})^2 + (\frac{\partial \mu_{mix}}{\mu_{mix}})^2]^{.5}. \tag{A.21}$$

The uncertainty in the flowing mixture mass flowrate can be evaluated by Equations A.11 or A.13. The dynamic viscosity of the mixture is evaluated using a simplified mixing law as discussed in the description of the PREWAS computer program (see Appendix C).

A.2.5 Uncertainty in the Heat Transfer Rate to the Pool Water

The uncertainty associated with the heat transfer rate to the pool water can be expressed as:

$$\partial \dot{Q}_{pool} = [(\partial \dot{Q}_{pool})^2_{FC \text{ or } SCB} + (\partial \dot{Q}_{pool})^2_B]^{.5}. \tag{A.22}$$

If no appreciable evaporation occurs in the water pool, the uncertainty associated with the heat transfer rate to the pool water (Equation 3.29) can be evaluated as:

$$\begin{aligned}\{\partial \dot{Q}_{pool} = \{&\frac{(\partial \Delta t)^2}{(\Delta t)^4}\{[m_{wtr}(\overline{C}_{pf,2}\overline{T}_2 - \overline{C}_{pf,1}\overline{T}_1)]_{pi} + [m_{wtr}(\overline{C}_{pf,2}\overline{T}_2 - \overline{C}_{pf,1}\overline{T}_1)]_{po}\}^2 \\ &+\frac{1}{(\Delta t)^2}\{[(m_{wtr}\overline{C}_{pf,2}\partial\overline{T}_2)^2 + (m_{wtr}\overline{T}_2\partial\overline{C}_{pf,2})^2 + (\overline{C}_{pf,2}\overline{T}_2\partial m_{wtr})^2 \\ &+(m_{wtr}\overline{C}_{pf,1}\partial\overline{T}_1)^2 + (m_{wtr}\overline{T}_1\partial\overline{C}_{pf,1})^2 + (\overline{C}_{pf,1}\overline{T}_1\partial m_{wtr})^2]_{pi} \\ &+[(m_{wtr}\overline{C}_{pf,2}\partial\overline{T}_2)^2 + (m_{wtr}\overline{T}_2\partial\overline{C}_{pf,2})^2 + (\overline{C}_{pf,2}\overline{T}_2\partial m_{wtr})^2 \\ &+(m_{wtr}\overline{C}_{pf,1}\partial\overline{T}_1)^2 + (m_{wtr}\overline{T}_1\partial\overline{C}_{pf,1})^2 + (\overline{C}_{pf,1}\overline{T}_1\partial m_{wtr})^2]_{po}\}^{.5}\}_{FC \text{ or } SCB},\end{aligned} \tag{A.23}$$

where

$$\{\frac{\partial m_{wtr,pi}}{m_{wtr,pi}} = [(\frac{\partial \rho_{f,pi}}{\rho_{f,pi}})^2 + (\frac{\partial H_{pi}}{H_{pi}})^2]^{.5}\}_{FC \text{ or } SCB}, \tag{A.24}$$

$$\{\frac{\partial m_{wtr,po}}{m_{wtr,po}} = [(\frac{\partial \rho_{f,po}}{\rho_{f,po}})^2 + (\frac{\partial H_{po}}{H_{po}})^2]^{.5}\}_{FC \text{ or } SCB}. \tag{A.25}$$

$(H_{pi})_{FC \text{ or } SCB}$ and $(H_{po})_{FC \text{ or } SCB}$ are the height of the inner and the outer pool in which the heat transfer mechanism is free convection or subcooled boiling. However , there is no subcooled boiling heat transfer in the outer pool. $(H_{pi})_{FC \text{ or } SCB}$ and $(H_{po})_{FC}$ can be estimated by observing the changes of T_{pi} and T_{po} from the thermocouples at different elevations. It is assumed that the heat transfer mechanism in a certain section of the pool is free

convection or subcooled boiling if the associated T_{pi} or T_{po} changes with time. The uncertainty associated with $(H_{pi})_{FC\ or\ SCB}$ and $(H_{po})_{FC}$ are the same as that of H_{pool} (1.59 mm), if no saturated boiling occurs. In case free convection or subcooled boiling and saturated boiling heat transfer occur in the pool at the same time (although, at different locations), the uncertainty associated with $(H_{pi})_{FC\ or\ SCB}$ is assumed to be half of the distance between two thermocouples.

If evaporation occurs in the water pool, the uncertainty associated with the heat transfer rate to the pool water (Equation 3.32) can be evaluated as:

$$\{\frac{\partial \dot{Q}_{pool}}{\dot{Q}_{pool}} = [(\frac{\partial \dot{m}_{pool}}{\dot{m}_{pool}})^2 + (\frac{\partial h_{fg}}{h_{fg}})^2_{pool}]^{.5}\ \}_B, \tag{A.26}$$

where

$$\partial \dot{m}_{pool} = [(\partial \dot{m}_{stm})^2 + (\partial \dot{m}_{vapor,in})^2]^{.5}, \tag{A.27}$$

$$(\frac{\partial \dot{m}}{\dot{m}})_{vapor,in} = \{(\frac{\partial \phi}{\phi})^2 + [\frac{\partial P_{sat}(T)}{P_{sat}(T)}]^2 + (\frac{\partial \dot{m}_{air}}{\dot{m}_{air}})^2 + \frac{(\partial P_{atm})^2 + [P_{sat}(T)\partial\phi]^2 + [\phi \partial P_{sat}(T)]^2}{[P_{atm} - \phi P_{sat}(T)]^2}\}^{.5}_{vapor,in}. \tag{A.28}$$

The uncertainty associated with the air flow rate can be evaluated by equation A.14. The uncertainty associated with the steam flow rate can be evaluated by Equations A.12 or A.15. The uncertainty associated with the cross-sectional area of the water pool, ∂A_{pi} and ∂A_{po}, can be neglected since they have been determined very accurately (less than 0.5 % error).

A.2.6 Uncertainty in the Pool Heat Transfer Coefficient

The uncertainty associated with the heat transfer coefficient to the pool water in free convection, subcooled or saturated boiling conditions (Equations 3.34) can be evaluated as:

$$\{\frac{\partial \bar{h}_{pool}}{\bar{h}_{pool}} = \{(\frac{\partial \bar{q}''_{pool}}{\bar{q}''_{pool}})^2 + [\frac{\partial(\bar{T}_{wo} - \bar{T})_{pool}}{(\bar{T}_{wo} - \bar{T})_{pool}}]^2\}^{.5}\}_{FC,\ SCB\ or\ B}, \tag{A.29}$$

where

$$\left\{\frac{\partial \overline{q}''_{pool}}{\overline{q}''_{pool}} = \left[\left(\frac{\partial \dot{Q}_{pool}}{\dot{Q}_{pool}}\right)^2 + \left(\frac{\partial H_{pool}}{H_{pool}}\right)^2\right]^{.5}\right\}_{FC,\ SCB\ or\ NB} \tag{A.30}$$

H_{pool} is a directly measured parameter. The uncertainty in $\overline{T}_{wo}$ and $\overline{T}_{pool}$ can be evaluated by applying Equations A.2 and A.3. The uncertainty in the heat transfer rate to the pool water can be evaluated by Equations A.23 or A.26.

A.3 Heat Loss Calculation

There are three locations that can contribute significantly to heat loss in the experiment. They are: (1) the connecting pipe of the level indicator L1, (2) part of the galvanized steel pipe, and (3) part of the inner annulus wall. The first item will affect the accuracy of the condensate measurement, m_{cond}, while the last two items impose uncertainties on the flowing mixture heat transfer rate estimation, $\dot{Q}_{mix}$ (or $\dot{Q}_{air}$).

(1) Heat loss through connecting pipe of the level indicator L1

The function of the level indicator connecting pipe is to balance the pressure between the heated vessel and the level indicator L1. The connecting pipe is a fiberglass insulated stainless steel pipe, 255 inches long. Figure A.1 shows detailed dimensions of the pipe. Heat loss through the pipe, $\dot{Q}_{loss,L1}$, can be estimated by applying the conduction equation.

$$\dot{Q}_{loss,L1} = \frac{(T_{stm} - T_{fg,wo})L}{\frac{1}{\pi D_1 h_{cond}} + \frac{1}{2\pi k_{ss}}\ln\left(\frac{D_2}{D_1}\right) + \frac{1}{2\pi k_{fg}}\ln\left(\frac{D_3}{D_2}\right)} \tag{A.31}$$

The thermal resistance due to condensation heat transfer can be neglected since the noncondensables are controlled to a negligible level. The average wall outer surface temperature of fiberglass, $T_{fg,wo}$, measured by a portable thermometer, is 35 °C. The typical thermal conductivity of stainless steel and fiberglass are 17 w/m°C and 0.035 w/m°C [K-8], respectively. It follows that, at 150.5 °C steam temperature, the calculated heat loss through the connecting pipe is about 202 W. Typical magnitudes of the heat loss contribution to the condensate measurement are listed as follows:

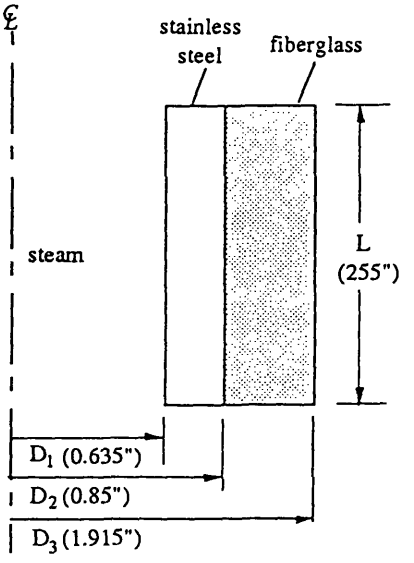

Figure A.1 Dimensions of Level Indicator L1 Connecting Pipe

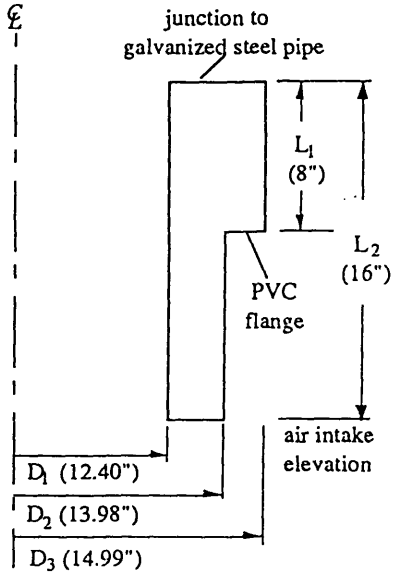

Figure A.2 Dimensions of Inner Annulus Wall Heat Loss Section

$$\frac{\dot{Q}_{loss,L1}}{\dot{Q}_{cond}} = 4.8\% \qquad \text{for A0304-15 air-only test,}$$

$$\frac{\dot{Q}_{loss,L1}}{\dot{Q}_{cond}} = 2\% \qquad \text{for W0401-05 water-filled test.}$$

(2) Heat loss through galvanized steel pipe

Heat loss from the section of the galvanized steel pipe that affects the evaluation of the heat transfer rate to the flowing mixture, $\dot{Q}_{mix}$ (or $\dot{Q}_{air}$), is from the top flange of the inner annulus wall to the location of thermocouple TC31 which is used to measure the outlet temperature of the flow. As shown in Figures 3.2 and 3.8, the distance from the top flange of the inner annulus wall to TC31 is 8.72 m (28.6 feet). A heat balance equation can be used to estimate the heat loss.

$$\dot{Q}_{loss,gal} = \dot{m}_{mix}\overline{C}_{p,mix}\Delta T \tag{A.32}$$

where: $\dot{m}_{mix}$ is obtained from the test; ΔT is the temperature drop from TC40 and/or TC41 to TC31. A typical value of ΔT is about 0.2 °C. Equation A.32 only accounts for the heat loss between TC40 and TC31 which are located 2.74 m (9 feet) apart. Therefore, equation A.32 should be multiplied by a factor of (8.72/2.74) to calculate the total effective heat loss. The heat loss through the galvanized steel pipe is 11.5 W.

(3) Heat loss through inner annulus wall

As discussed in Chapter 3, there is an outer annulus wall to form the intake air flow passage. The heat loss through most of the inner annulus wall will be re-absorbed by the intake air flow. Figure A.2 shows the section of the inner annulus wall which is above the air intake, and hence is that section that should be taken into account in the heat loss estimation. A heat conduction equation can be applied to estimate the heat loss.

$$\dot{Q}_{loss,PVC} = 2\pi k_{PVC}\left[\frac{L_1(T_{1,wi} - T_{1,wo})}{\ln\frac{D_3}{D_1}} + \frac{L_2(T_{2,wi} - T_{2,wo})}{\ln\frac{D_2}{D_1}}\right] \tag{A.33}$$

where: $T_{1,wi}$ and $T_{2,wi}$ are the wall inner surface temperature of the thick and thin sections, respectively; $T_{1,wo}$ and $T_{2,wo}$ are the wall outer surface temperature of the thick and thin sections, respectively. $T_{1,wi}$ and $T_{2,wi}$ are obtained from TC45 and TC44, respectively. The wall outer surface temperatures are measured by a portable thermometer. Typical thermal conductivity of the PVC pipe is 0.3 w/m²°C [K-8]. The measured temperatures and the heat loss are as follows.

$$T_{1,wi} = 31.4\ ^\circ C;\ T_{2,wi} = 31.0\ ^\circ C$$

$$T_{1,wo} = 27.2\ ^\circ C;\ T_{2,wo} = 27.3\ ^\circ C$$

$$\dot{Q}_{loss,PVC} = 18.6\ W$$

Heat loss through the galvanized steel pipe and the inner annulus wall will affect the accuracy in the calculation of the heat transfer rate to the flowing mixture, $\dot{Q}_{mix}$, which is nominally 2.53 kw (see test A0430-11). The contribution of the heat loss to $\dot{Q}_{mix}$ is

$$\frac{\dot{Q}_{loss,gal} + \dot{Q}_{loss,PVC}}{\dot{Q}_{mix}} = \frac{11.5 + 18.6}{2530} = 1.2\%$$

A.4 Results of Data Reduction and Error Analysis

A simple computer program written in FORTRAN 77 has been developed, based on the equations given above, for data reduction and experimental error calculation. The properties of water and steam are from Keenan's steam tables [K-4]. The properties of air are from Irvine's steam and gas tables with computer equations [I-3]. The input data of the program for each test are listed in the tables of Appendix B (raw data of the tests). Appendix B also summarizes the test results. Tables A.1 to A.10 show the results of the uncertainty analysis for the derived quantities.

The major measurement contributions to the uncertainty of the air-only test results are from the uncertainties associated with the emissivities (surface emissivity of stainless steel, in particular), humidity measurement, and velocity measurement. The uncertainty associated with the convective heat transfer coefficient, which is the key derived parameter for the air-only tests, and has the largest uncertainty in the test, ranges from 16 percent to

21 percent. The higher value of the uncertainty applies to low steam temperature tests due to the smaller temperature rise of the air flow. For the water-filled tests, the major contribution to the uncertainty of the test is from the steam generation rate measurement, which is accomplished either by using a humidity meter associated with a velocity meter and thermocouples or by measuring pool level decrease rate. In case of no steam generation, the uncertainty associated with the pool temperature increase rate measurement, which is accomplished by using thermocouples and a timer, imposes the major contribution to the total uncertainty. The uncertainty associated with the heat transfer coefficient to the pool water ranges from 5 percent to 25 percent. The higher value occurs during the transition of the heat transfer mechanism in the pool from free convection or subcooled boiling to saturated pool boiling.

Table A.1 Results of the Uncertainty Analysis – A0301-11 to A0429-25

TEST ID	$\frac{\partial \dot{Q}_{cond}}{\dot{Q}_{cond}}$ (%)	$\frac{\partial \dot{Q}_{air}}{\dot{Q}_{air}}$ (%)	$\frac{\partial \dot{Q}_{rad}}{\dot{Q}_{rad}}$ (%)	$\frac{\partial \bar{q}''_{air}}{\bar{q}''_{air}}$ (%)	$\frac{\partial \bar{h}_{air,eff}}{\bar{h}_{air,eff}}$ (%)	$\frac{\partial \bar{h}_{air,conv}}{\bar{h}_{air,conv}}$ (%)	$\frac{\partial Re}{Re}$ (%)	$\frac{\partial \dot{m}_{air}}{\dot{m}_{air}}$ (%)
A0301-11	6.18	9.96	7.93	9.96	9.97	15.95	8.69	2.49
A0301-12	6.12	9.95	7.93	9.95	9.97	16.23	8.65	2.48
A0301-13	5.74	10.09	7.93	10.09	10.11	16.49	8.79	2.52
A0301-14	5.64	9.98	7.93	9.98	10.00	16.20	8.69	2.49
A0301-15	5.60	10.03	7.93	10.03	10.04	16.41	8.72	2.50
A0304-11	12.6	9.95	7.93	9.95	9.96	16.77	8.64	2.48
A0304-12	8.68	9.91	7.93	9.91	9.92	16.55	8.61	2.47
A0304-13	4.81	9.87	7.93	9.87	9.88	16.41	8.57	2.46
A0304-14	5.81	9.82	7.93	9.82	9.84	16.20	8.54	2.45
A0304-15	6.38	9.69	7.93	9.69	9.70	15.83	8.41	2.41
A0429-11	6.42	12.68	7.96	12.68	12.71	21.27	10.80	3.12
A0429-12	3.57	12.30	7.96	12.30	12.32	20.10	10.43	3.01
A0429-13	2.92	12.53	7.96	12.53	12.56	20.45	10.69	3.09
A0429-14	2.45	12.23	7.96	12.23	12.26	19.71	10.38	3.00
A0429-15	2.14	12.66	7.96	12.66	12.68	20.83	10.80	3.12
A0429-21	7.32	12.74	7.97	12.74	12.77	20.28	10.84	3.14
A0429-22	5.72	12.83	7.97	12.83	12.86	20.39	10.96	3.17
A0429-23	5.94	12.90	7.97	12.90	12.93	20.63	11.02	3.19
A0429-24	5.83	12.81	7.97	12.81	12.84	20.54	10.90	3.15
A0429-25	6.05	12.93	7.97	12.93	12.96	20.95	11.01	3.19

Table A.2 Results of the Uncertainty Analysis – A0430-11 to A0503-25

TEST ID	$\frac{\partial \dot{Q}_{cond}}{\dot{Q}_{cond}}$ (%)	$\frac{\partial \dot{Q}_{air}}{\dot{Q}_{air}}$ (%)	$\frac{\partial \dot{Q}_{rad}}{\dot{Q}_{rad}}$ (%)	$\frac{\partial \bar{q}''_{air}}{\bar{q}''_{air}}$ (%)	$\frac{\partial \bar{h}_{air,eff}}{\bar{h}_{air,eff}}$ (%)	$\frac{\partial \bar{h}_{air,conv}}{\bar{h}_{air,conv}}$ (%)	$\frac{\partial Re}{Re}$ (%)	$\frac{\partial \dot{m}_{air}}{\dot{m}_{air}}$ (%)
A0430-11	6.10	11.94	7.95	11.94	11.96	19.63	10.35	3.00
A0430-12	3.71	11.83	7.95	11.83	11.85	19.22	10.25	2.97
A0430-13	2.37	11.87	7.95	11.87	11.90	19.34	10.30	2.98
A0430-14	2.05	11.87	7.95	11.87	11.89	19.22	10.30	2.98
A0430-15	2.89	12.03	7.95	12.03	12.05	19.63	10.45	3.03
A0502-11	4.69	12.39	7.96	12.39	12.41	19.56	10.84	3.12
A0502-12	4.82	12.63	7.96	12.63	12.66	20.30	11.07	3.19
A0502-13	2.51	12.63	7.96	12.63	12.65	20.22	11.07	3.19
A0502-14	3.69	12.68	7.96	12.68	12.70	20.28	11.13	3.20
A0502-15	2.56	12.39	7.96	12.39	12.41	19.59	10.84	3.12
A0503-11	3.72	11.11	7.94	11.11	11.13	16.18	9.57	2.76
A0503-12	3.18	11.15	7.94	11.15	11.17	16.28	9.61	2.77
A0503-13	2.45	11.17	7.94	11.17	11.19	18.27	9.66	2.78
A0503-14	2.10	11.05	7.94	10.05	11.07	17.98	9.53	2.74
A0503-15	1.92	11.22	7.94	11.22	11.24	18.45	9.70	2.79
A0503-21	6.56	10.64	7.94	10.64	10.66	17.64	9.24	2.66
A0503-22	4.17	10.60	7.94	10.60	10.61	17.52	9.20	2.65
A0503-23	2.55	10.67	7.94	10.67	10.68	17.57	9.28	2.67
A0503-24	2.16	10.77	7.94	10.77	10.79	17.60	9.40	2.71
A0503-25	1.82	10.67	7.94	10.67	10.69	17.58	9.28	2.67

Table A.3 Results of the Uncertainty Analysis – W0222

TEST ID W0222-	$\frac{\partial \dot{Q}_{cond}}{\dot{Q}_{cond}}$ (%)	$\frac{\partial \dot{Q}_{pool}}{\dot{Q}_{pool}}$ (%)	$\frac{\partial \dot{Q}_{mix}}{\dot{Q}_{mix}}$ (%)	$\frac{\partial \dot{Q}_{rad}}{\dot{Q}_{rad}}$ (%)	$\frac{\partial \bar{q}''_{pool}}{\bar{q}''_{pool}}$ (%)	$\frac{\partial \bar{q}''_{mix}}{\bar{q}''_{mix}}$ (%)	$\frac{\partial \bar{h}_{pool}}{\bar{h}_{pool}}$ (%)	$\frac{\partial \bar{h}_{mix,eff}}{\bar{h}_{mix,eff}}$ (%)	$\frac{\partial \bar{h}_{mix,conv}}{\bar{h}_{mix,conv}}$ (%)	$\frac{\partial Re_{mix}}{Re_{mix}}$ (%)	$\frac{\partial \dot{m}_{mix}}{\dot{m}_{mix}}$ (%)
0001-0	8.37	6.50	9.75	7.28	6.51	9.75	6.62	9.76	15.92	8.02	2.64
0102-0	7.68	5.52	9.61	7.30	5.52	9.61	5.89	9.62	15.47	7.91	2.60
0203-0	10.55	9.54	8.50	7.31	9.54	8.50	10.38	8.52	13.01	6.86	2.31
0304-0	4.01	5.70	7.76	7.33	5.70	7.76	9.12	7.78	11.65	5.96	2.10
0304-1	4.01	7.87	8.70	7.33	7.87	8.70	10.61	8.73	13.40	4.80	1.52
0405-0	2.54	4.26	7.50	7.36	4.27	7.50	8.10	7.52	11.11	5.67	2.03
0405-1	2.54	6.19	7.30	7.36	6.19	7.30	9.26	7.33	10.63	4.63	1.44
0506-0	1.70	3.92	7.37	7.38	3.93	7.37	7.88	7.40	10.76	5.65	2.02
0506-1	1.70	5.51	6.86	7.38	5.51	6.86	8.78	6.89	9.87	4.59	1.41
0607-0	1.72	3.31	7.58	7.43	3.31	7.58	7.64	7.61	11.63	5.74	2.08
0607-1	1.72	5.51	6.85	7.43	5.51	6.85	8.82	6.88	10.10	4.73	1.45
0708-0	2.04	2.87	7.49	7.40	2.87	7.52	7.52	7.52	11.62	5.50	2.02
0708-1	2.04	6.34	7.19	7.47	6.35	7.19	9.41	7.22	10.83	4.51	1.42

Table A.4 Results of the Uncertainty Analysis – W0304

TEST ID W0304-	$\frac{\partial \dot{Q}_{cond}}{\dot{Q}_{cond}}$ (%)	$\frac{\partial \dot{Q}_{pool}}{\dot{Q}_{pool}}$ (%)	$\frac{\partial \dot{Q}_{mix}}{\dot{Q}_{mix}}$ (%)	$\frac{\partial \dot{Q}_{rad}}{\dot{Q}_{rad}}$ (%)	$\frac{\partial \bar{q}''_{pool}}{\bar{q}''_{pool}}$ (%)	$\frac{\partial \bar{q}''_{mix}}{\bar{q}''_{mix}}$ (%)	$\frac{\partial \bar{h}_{pool}}{\bar{h}_{pool}}$ (%)	$\frac{\partial \bar{h}_{mix,eff}}{\bar{h}_{mix,eff}}$ (%)	$\frac{\partial \bar{h}_{mix,conv}}{\bar{h}_{mix,conv}}$ (%)	$\frac{\partial Re_{mix}}{Re_{mix}}$ (%)	$\frac{\partial \dot{m}_{mix}}{\dot{m}_{mix}}$ (%)
0001-0	5.52	4.50	10.31	7.32	4.50	10.31	4.65	10.32	17.38	8.16	2.67
0102-0	6.99	5.94	9.95	7.32	5.94	9.95	6.33	9.97	15.24	8.21	2.69
0203-0	8.83	7.77	9.14	7.33	7.77	9.14	8.87	9.16	13.68	7.39	2.47
0304-0	5.10	6.33	8.21	7.34	6.33	8.21	8.73	8.24	12.01	6.27	2.17
0304-1	5.10	10.00	8.66	7.33	10.00	8.67	11.67	8.69	12.62	5.12	1.57
0405-0	2.49	3.98	7.96	7.36	3.99	7.96	9.38	7.99	11.56	5.96	2.10
0405-1	2.49	6.11	7.50	7.36	6.11	7.50	10.46	7.53	10.75	4.82	1.47
0506-0	1.92	3.70	7.82	7.39	3.70	7.82	9.18	7.85	11.18	5.94	2.08
0506-1	1.92	5.66	7.19	7.39	5.67	7.19	10.14	7.22	10.19	4.80	1.45
0607-0	1.90	3.52	7.76	7.42	3.53	7.76	9.14	7.79	11.08	5.90	2.06
0607-1	1.90	5.66	7.02	7.42	5.66	7.02	10.16	7.05	9.91	4.78	1.43

Table A.5 Results of the Uncertainty Analysis – W0315

TEST ID W0315-	$\frac{\partial \dot{Q}_{cond}}{\dot{Q}_{cond}}$ (%)	$\frac{\partial \dot{Q}_{pool}}{\dot{Q}_{pool}}$ (%)	$\frac{\partial \dot{Q}_{mix}}{\dot{Q}_{mix}}$ (%)	$\frac{\partial \dot{Q}_{rad}}{\dot{Q}_{rad}}$ (%)	$\frac{\partial \bar{q}''_{pool}}{\bar{q}''_{pool}}$ (%)	$\frac{\partial \bar{q}''_{mix}}{\bar{q}''_{mix}}$ (%)	$\frac{\partial \bar{h}_{pool}}{\bar{h}_{pool}}$ (%)	$\frac{\partial \bar{h}_{mix,eff}}{\bar{h}_{mix,eff}}$ (%)	$\frac{\partial \bar{h}_{mix,conv}}{\bar{h}_{mix,conv}}$ (%)	$\frac{\partial Re_{mix}}{Re_{mix}}$ (%)	$\frac{\partial \dot{m}_{mix}}{\dot{m}_{mix}}$ (%)
0001-0	11.43	7.93	13.88	7.33	7.93	13.88	8.04	13.90	23.17	12.04	3.96
0102-0	9.92	6.99	13.43	7.34	6.99	13.43	7.28	13.45	21.83	11.65	3.83
0203-0	11.58	10.17	13.09	7.34	10.07	13.09	10.49	13.11	20.88	11.38	3.75
0304-0	10.78	15.44	12.76	7.34	25.27	12.77	25.76	12.79	20.21	11.12	3.68
0405-0	12.63	15.16	11.09	7.34	15.16	11.09	16.89	11.11	17.81	9.28	3.14
0405-1	12.63	24.20	14.26	7.34	24.20	14.26	25.32	14.31	22.54	7.86	2.42
0506-0	2.89	4.70	9.80	7.36	4.70	9.80	12.15	9.82	14.78	7.91	2.73
0506-1	2.89	6.64	8.76	7.36	6.64	8.76	13.03	8.79	13.21	6.33	1.89
0607-0	2.85	4.32	9.48	7.38	4.33	9.48	12.07	9.15	14.12	7.58	2.63
0607-1	2.85	6.53	8.43	7.38	6.53	8.43	13.02	8.47	13.43	6.10	1.82
0708-0	3.20	4.30	9.44	7.40	4.30	9.44	12.09	9.47	14.15	7.48	2.59
0708-1	3.20	6.99	8.40	7.40	6.99	8.40	13.29	8.43	12.38	6.04	1.80
0809-0	3.22	4.32	9.45	7.42	4.32	9.45	12.13	9.48	14.14	7.57	2.62
0809-1	3.22	6.98	8.40	7.42	6.99	8.40	13.31	8.43	12.45	6.10	1.82

Table A.6 Results of the Uncertainty Analysis – W0401

TEST ID W0401-	$\frac{\partial \dot{Q}_{cond}}{\dot{Q}_{cond}}$ (%)	$\frac{\partial \dot{Q}_{pool}}{\dot{Q}_{pool}}$ (%)	$\frac{\partial \dot{Q}_{mix}}{\dot{Q}_{mix}}$ (%)	$\frac{\partial \dot{Q}_{rad}}{\dot{Q}_{rad}}$ (%)	$\frac{\partial \bar{q}''_{pool}}{\bar{q}''_{pool}}$ (%)	$\frac{\partial \bar{q}''_{mix}}{\bar{q}''_{mix}}$ (%)	$\frac{\partial \bar{h}_{pool}}{\bar{h}_{pool}}$ (%)	$\frac{\partial \bar{h}_{mix,eff}}{\bar{h}_{mix,eff}}$ (%)	$\frac{\partial \bar{h}_{mix,conv}}{\bar{h}_{mix,conv}}$ (%)	$\frac{\partial Re_{mix}}{Re_{mix}}$ (%)	$\frac{\partial \dot{m}_{mix}}{\dot{m}_{mix}}$ (%)
0001-0	5.66	4.85	11.85	7.34	4.85	11.85	5.02	11.88	19.18	8.98	2.96
0102-0	8.59	5.72	11.39	7.34	5.72	11.39	6.31	11.42	16.97	9.13	3.01
0203-0	9.81	8.71	11.42	7.35	8.71	11.42	10.13	11.45	16.91	9.26	3.05
0304-0	8.76	10.72	11.19	7.35	10.72	11.19	15.01	11.22	16.78	8.84	2.93
0304-1	8.76	10.72	10.18	7.35	10.72	10.18	15.01	10.22	15.53	7.21	2.08
0405-0	10.15	10.73	11.12	7.36	10.73	11.12	19.99	11.15	16.68	8.79	2.93
0405-1	10.15	18.25	10.24	7.36	24.86	10.24	24.86	10.30	15.10	7.17	2.08
0506-0	8.18	8.88	10.73	7.36	8.88	10.73	19.65	10.76	15.74	8.38	2.79
0506-1	8.18	14.43	9.60	7.36	14.44	9.60	22.71	9.64	13.88	6.81	1.97
0607-0	6.31	7.96	10.49	7.37	7.97	10.49	19.14	10.52	15.16	8.12	2.71
0607-1	6.31	13.43	9.22	7.37	13.43	9.22	21.99	9.26	13.06	6.63	1.91
0708-0	6.56	7.95	10.47	7.37	7.95	10.47	19.00	10.50	15.12	8.12	2.71
0708-1	6.56	11.90	9.29	7.37	11.90	9.29	20.96	9.32	13.29	6.58	1.91
0809-0	5.56	7.14	10.23	7.38	7.14	10.23	19.08	10.27	14.58	7.88	2.63
0809-1	5.56	11.44	8.96	7.38	11.44	8.96	21.07	8.99	12.54	6.42	1.85

Table A.7 Results of the Uncertainty Analysis – W0405

TEST ID W0405-	$\frac{\partial \dot{Q}_{cond}}{\dot{Q}_{cond}}$ (%)	$\frac{\partial \dot{Q}_{pool}}{\dot{Q}_{pool}}$ (%)	$\frac{\partial \dot{Q}_{mix}}{\dot{Q}_{mix}}$ (%)	$\frac{\partial \dot{Q}_{rad}}{\dot{Q}_{rad}}$ (%)	$\frac{\partial \bar{q}''_{pool}}{\bar{q}''_{pool}}$ (%)	$\frac{\partial \bar{q}''_{mix}}{\bar{q}''_{mix}}$ (%)	$\frac{\partial \bar{h}_{pool}}{\bar{h}_{pool}}$ (%)	$\frac{\partial \bar{h}_{mix,eff}}{\bar{h}_{mix,eff}}$ (%)	$\frac{\partial \bar{h}_{mix,conv}}{\bar{h}_{mix,conv}}$ (%)	$\frac{\partial Re_{mix}}{Re_{mix}}$ (%)	$\frac{\partial \dot{m}_{mix}}{\dot{m}_{mix}}$ (%)
0001-0	6.53	5.84	12.51	7.35	5.84	12.51	6.00	12.54	19.34	10.14	3.33
0102-0	3.66	4.55	12.34	7.34	4.55	12.34	5.39	12.37	19.23	9.86	3.24
0203-0	5.81	9.09	12.16	7.34	9.09	12.16	11.52	12.18	18.88	9.59	3.16
0304-0	5.22	14.56	12.19	7.35	14.56	12.19	18.55	12.22	18.77	9.73	3.21
0405-0	4.89	14.57	12.19	7.36	14.57	12.19	19.28	12.22	18.53	9.86	3.26
0405-1	4.89	22.51	11.03	7.36	22.51	11.03	25.81	11.07	16.53	8.04	2.32
0506-0	4.47	13.89	12.27	7.36	13.89	12.27	18.75	12.30	18.70	9.96	3.29
0506-1	4.47	22.38	10.87	7.36	22.38	10.87	25.68	10.90	16.26	8.12	2.34
0607-0	5.50	15.52	12.41	7.36	15.52	12.41	21.09	12.44	19.05	10.10	3.34
0607-1	5.50	24.81	11.09	7.36	24.81	11.09	28.62	11.13	16.75	8.23	2.37
0708-0	4.67	17.06	12.26	7.37	17.06	12.26	22.19	12.29	18.65	9.96	3.29
0708-1	4.67	25.48	10.71	7.37	25.48	10.71	29.16	10.75	16.08	8.10	2.33

Table A.8 Results of the Uncertainty Analysis – W0408

TEST ID W0408-	$\frac{\partial \dot{Q}_{cond}}{\dot{Q}_{cond}}$ (%)	$\frac{\partial \dot{Q}_{pool}}{\dot{Q}_{pool}}$ (%)	$\frac{\partial \dot{Q}_{mix}}{\dot{Q}_{mix}}$ (%)	$\frac{\partial \dot{Q}_{rad}}{\dot{Q}_{rad}}$ (%)	$\frac{\partial \bar{q}''_{pool}}{\bar{q}''_{pool}}$ (%)	$\frac{\partial \bar{q}''_{mix}}{\bar{q}''_{mix}}$ (%)	$\frac{\partial \bar{h}_{pool}}{\bar{h}_{pool}}$ (%)	$\frac{\partial \bar{h}_{mix,eff}}{\bar{h}_{mix,eff}}$ (%)	$\frac{\partial \bar{h}_{mix,conv}}{\bar{h}_{mix,conv}}$ (%)	$\frac{\partial Re_{mix}}{Re_{mix}}$ (%)	$\frac{\partial \dot{m}_{mix}}{\dot{m}_{mix}}$ (%)
0001-0	6.48	5.08	13.18	7.34	5.08	13.18	5.26	13.21	21.68	10.81	3.54
0102-0	8.80	6.06	12.87	7.34	6.06	12.87	6.61	12.89	21.03	10.47	3.43
0203-0	11.90	9.90	12.45	7.34	9.90	12.45	10.92	12.47	19.71	10.11	3.32
0304-0	16.72	14.13	12.37	7.33	14.13	12.37	16.18	12.40	19.44	10.10	3.32
0405-0	4.31	17.56	12.28	7.35	17.56	12.28	21.95	12.31	19.22	10.03	3.31
0405-1	4.31	17.56	11.48	7.35	17.56	11.48	21.95	11.51	18.05	8.11	2.36
0506-0	5.98	10.79	11.96	7.36	10.79	11.96	20.67	11.99	18.21	9.76	3.23
0506-1	5.98	15.27	10.36	7.36	15.27	10.36	23.32	10.40	15.74	7.89	2.28
0607-0	4.92	9.88	11.84	7.37	9.88	11.84	20.43	11.87	18.07	9.59	3.18
0607-1	4.92	13.85	10.28	7.37	13.85	10.28	22.62	10.32	15.65	7.75	2.24
0708-0	5.04	11.60	11.77	7.37	11.06	11.77	21.37	11.80	17.94	9.51	3.16
0708-1	5.04	17.69	10.37	7.37	17.69	10.37	25.44	10.41	15.67	7.71	2.23
0809-0	4.97	10.38	11.62	7.37	10.38	11.62	21.36	11.65	17.48	9.39	3.12
0809-1	4.97	15.68	10.18	7.37	15.69	10.18	24.38	10.22	15.24	7.59	2.20

Table A.9 Results of the Uncertainty Analysis – W0412

TEST ID W0412-	$\frac{\partial \dot{Q}_{cond}}{\dot{Q}_{cond}}$ (%)	$\frac{\partial \dot{Q}_{pool}}{\dot{Q}_{pool}}$ (%)	$\frac{\partial \dot{Q}_{mix}}{\dot{Q}_{mix}}$ (%)	$\frac{\partial \dot{Q}_{rad}}{\dot{Q}_{rad}}$ (%)	$\frac{\partial \bar{q}''_{pool}}{\bar{q}''_{pool}}$ (%)	$\frac{\partial \bar{q}''_{mix}}{\bar{q}''_{mix}}$ (%)	$\frac{\partial \bar{h}_{pool}}{\bar{h}_{pool}}$ (%)	$\frac{\partial \bar{h}_{mix,eff}}{\bar{h}_{mix,eff}}$ (%)	$\frac{\partial \bar{h}_{mix,conv}}{\bar{h}_{mix,conv}}$ (%)	$\frac{\partial Re_{mix}}{Re_{mix}}$ (%)	$\frac{\partial \dot{m}_{mix}}{\dot{m}_{mix}}$ (%)
0001-0	7.59	5.47	11.46	7.33	5.47	11.46	5.62	11.49	17.33	9.36	3.08
0102-0	8.31	5.89	11.36	7.34	5.89	11.36	6.35	11.39	17.20	9.22	3.03
0203-0	11.54	9.01	11.01	7.34	9.01	11.01	9.90	11.04	16.52	8.80	2.90
0304-0	10.06	15.40	10.84	7.34	15.40	10.84	17.02	10.87	16.26	8.60	2.85
0304-1	10.06	20.05	10.98	7.34	20.05	10.98	21.33	11.02	16.31	7.08	2.07
0405-0	4.50	7.06	10.90	7.35	7.06	10.90	16.02	10.92	16.88	8.54	2.86
0405-1	4.50	8.75	9.75	7.35	8.75	9.75	16.84	9.78	15.18	6.86	2.00
0506-0	4.16	5.96	10.69	7.37	5.96	10.69	15.96	10.71	16.42	8.32	2.80
0506-1	4.16	8.02	9.44	7.37	8.03	9.44	16.84	9.47	14.42	6.70	1.96
0607-0	6.06	7.14	10.29	7.38	7.14	10.30	16.94	10.32	15.04	8.20	2.76
0607-1	6.06	11.22	9.24	7.38	11.22	9.24	19.02	9.27	13.38	6.63	1.94
0708-0	4.80	6.18	10.15	7.39	6.19	10.15	16.87	10.18	14.64	8.10	2.73
0708-1	4.80	9.16	8.94	7.39	9.16	8.94	18.17	8.98	12.85	6.53	1.91

Table A.10 Results of the Uncertainty Analysis – W0430

TEST ID W0430-	$\frac{\partial \dot{Q}_{cond}}{\dot{Q}_{cond}}$ (%)	$\frac{\partial \dot{Q}_{pool}}{\dot{Q}_{pool}}$ (%)	$\frac{\partial \dot{Q}_{mix}}{\dot{Q}_{mix}}$ (%)	$\frac{\partial \dot{Q}_{rad}}{\dot{Q}_{rad}}$ (%)	$\frac{\partial \bar{q}''_{pool}}{\bar{q}''_{pool}}$ (%)	$\frac{\partial \bar{q}''_{mix}}{\bar{q}''_{mix}}$ (%)	$\frac{\partial \bar{h}_{pool}}{\bar{h}_{pool}}$ (%)	$\frac{\partial \bar{h}_{mix,eff}}{\bar{h}_{mix,eff}}$ (%)	$\frac{\partial \bar{h}_{mix,conv}}{\bar{h}_{mix,conv}}$ (%)	$\frac{\partial Re_{mix}}{Re_{mix}}$ (%)	$\frac{\partial \dot{m}_{mix}}{\dot{m}_{mix}}$ (%)
0001-0	5.67	4.48	12.94	7.34	4.49	12.94	4.71	12.97	19.83	10.70	3.11
0102-0	9.64	7.24	11.71	7.34	7.25	11.71	7.92	11.74	18.22	9.40	3.11
0203-0	10.10	14.15	11.70	7.34	14.15	11.70	15.17	11.73	18.25	9.34	3.10
0304-0	9.45	12.79	11.43	7.35	12.79	11.43	15.38	11.45	17.75	9.03	3.01
0304-1	9.45	16.36	10.81	7.35	16.36	11.81	18.45	10.85	16.41	7.39	2.15
0405-0	8.12	10.01	10.96	7.35	10.01	10.96	19.11	10.99	16.72	8.52	2.86
0405-1	8.12	15.74	9.89	7.35	15.74	9.89	22.64	9.93	14.60	6.98	2.03
0506-0	7.46	8.89	10.76	7.36	8.89	10.76	18.87	10.79	16.11	8.39	2.82
0506-1	7.46	13.10	9.51	7.36	13.10	9.51	21.18	9.55	13.88	6.84	1.99
0607-0	6.58	8.12	10.74	7.37	8.12	10.74	18.82	10.77	15.96	8.46	2.85
0607-1	6.58	12.18	9.39	7.37	12.18	9.39	20.89	9.43	13.56	6.91	2.00
0708-0	6.14	8.05	10.77	7.38	8.05	10.77	19.03	10.80	16.09	8.45	2.85
0708-1	6.14	11.42	9.40	7.38	11.42	9.40	20.68	9.44	13.70	6.90	2.00

```
$DEBUG
C      PREWAT EXPERIMENT DATA REDUCTION AND ERROR ANALYSIS
C
       IMPLICIT REAL*8(A-H,O-Z)
       CHARACTER*24 INDAT,OUTPT
       CHARACTER*72 ITITLE
C   INPUT DATA
       PI=3.14159D0
       SIG=5.669D-8
       RAIR=287.04
       RSTM=462.
       WRITE(*,1000)
 1000  FORMAT(' ENTER INPUT FILE NAME-------')
       READ(*,1010) INDAT
 1010  FORMAT(A16)
       OPEN(5,FILE=INDAT,STATUS='OLD',ERR=8888)
       WRITE(*,1020)
 1020  FORMAT(' ENTER OUTPUT FILE NAME-------')
       READ(*,1010) OUTPT
       OPEN(6,FILE=OUTPT,STATUS='NEW',ERR=9999)
       READ(5,100) ITITLE
  100  FORMAT(A72)
       WRITE(6,100) ITITLE
C-----------------------------------------------------------------------
C  TMIXEX1,TMIXEX2 - MIXTURE TEMP AT CHIMNEY EXIT AT TIME 1 AND 2
C  TMIXO - MIXTURE TEMP AT RISER OUT    TMIXI - MIXTURE TEMP AT RISER IN
C  TMIX - AVERAGED MIXTURE TEMP         TWA - AVERAGED AIR SECT TWO
C  TPI1,TPI2,TPO1,TPO2 - AVERAGED INNER; OUTER POOL TEMP AT TIME 1 AND 2
C  TPLF - AVERAGED INNER POOL T (FC)    TPLN - AVERAGED INNER POOL T (NB)
C  TWPF - AVERAGED POOL SEC TWO (FC)    TWPN - AVERAGED POOL SEC TWO (NB)
C  TWO - WALL SURFACE TEMP              TWDG - AVERAGED GALVANIC TWO
C  TWDP - AVERAGED PVC TWO              TIN - ATM TEMP
C  TSTM - SUPPLY STEAM TEMP             TSP - AVERAGED STEAM TEMP IN POOL
C  HPOOL - POOL HEIGHT                  HPLF - POOL HEIGHT (FC)
C  HPL1 - POOL HEIGHT AT TIME 1         HPL2 - POOL HEIGHT AT TIME 2
C  MS=0 - CAL. STMFR BY HUMIDITY        MS=1 - CAL. STMFR BY LEVEL
C  VEL1 - MIXTURE VELOCITY AT TIME 1    VEL2 - MIXTURE VELOCITY AT TIME 2
C  CONDM - CONDENSATE MASS              DT - TIME STEP btw 2 DATA POINT
C  RHI - RELATIVE HUMIDITY AT ATM       PATM - ATM PRESSURE
C  RHO1,RHO2 - RELATIVE HUMIDITY AT OUTLET AT TIME 1 AND 2
C  ELT - VESSEL HEIGHT                  HGAL - GALVANIC STEEL LENGTH
C  DTR - VESSEL OD                      DID - DUCT (14" PVC) ID
C  D - EQUIVELENT DIA OF RISER          ACH - CHIMNEY FLOW AREA
C  API - INNER POOL CROSS SECTION       APO - OUTER POOL CROSS SECTION
C  EMS - EMISSIVITY OF STAINLESS STEEL  EMP - EMISSIVITY OF PVC
C  EMG - EMISSIVITY OF GALVANIC STEEL   SIG - BOLTZMAN CONSTANT
C  D**** - UNCERTAINTY OF ****          F**** - FRACTIONAL UNCERTAINTY
C  ALL IN SI UNITS
C-----------------------------------------------------------------------
       READ(5,200) TMIXEX1,TMIXEX2,TMIXO,TSP,TIN
  200  FORMAT(6D12.5)
       WRITE(6,201) TMIXEX1,TMIXEX2,TMIXO,TSP,TIN
  201  FORMAT(' Tmix,e,1, Tmix,e,2, Tmix,o, Tstm,pl, Tin'/6(1X,1PD12.5))
       READ(5,200) TPLF,TPLN,TPI1,TPI2,TPO1,TPO2
       WRITE(6,202) TPLF,TPLN,TPI1,TPI2,TPO1,TPO2
  202  FORMAT(' Tpl(FC),Tpl(NB), TPI1, TPI2, TPO1, TPO2'/6(1X,1PD12.5))
       READ(5,200) TSTM,TWA,TWPF,TWPN,TWDP,TWDG
```

```
      WRITE(6,203) TSTM,TWA,TWPF,TWPN,TWDP,TWDG
  203 FORMAT(' Tstm, Two,air, Two,pl(FC),Two,pl(NB), Two,pvc, Two,gal'/6
     /(1X,1PD12.5))
      READ(5,200) HPOOL,HPLF,HPL1,HPL2,HGAL,DID
      WRITE(6,204) HPOOL,HPLF,HPL1,HPL2,HGAL,DID
  204 FORMAT(' Hpool, Hpl(FC), Hpl1, Hpl2, Hgal, Dduct'/6(1X,1PD12.5))
      READ(5,200) RHI,RHO1,RHO2,VEL1,VEL2
      WRITE(6,205) RHI,RHO1,RHO2,VEL1,VEL2
  205 FORMAT(' RHI, RHO1, RHO2, Vel,1, Vel,2'/6(1X,1PD12.5))
      READ(5,200) PATM,CONDM,DT
      WRITE(6,206) PATM,CONDM,DT
  206 FORMAT(' Patm, Mcond, DTime'/6(1X,1PD12.5))
      READ(5,200) ELT,DTR,D,API,APO,ACH
      WRITE(6,207) ELT,DTR,D,API,APO,ACH
  207 FORMAT(' ELT, DTR, D, API, APO, ACH'/6(1X,1PD12.5))
      READ(5,200) DTMIXEX,DTMIXO,DTSP,DTIN
      WRITE(6,208) DTMIXEX,DTMIXO,DTSP,DTIN
  208 FORMAT(' DTmix,ex, DTmix,o, DTstm,pl, DTin'/6(1X,1PD12.5))
      READ(5,200) DTPLF,DTPLN,DTPI1,DTPI2,DTPO1,DTPO2
      WRITE(6,209) DTPLF,DTPLN,DTPI1,DTPI2,DTPO1,DTPO2
  209 FORMAT(' DTpl(FC), DTpl(NB), DTPI1, DTPI2, DTPO1, DTPO2'/6(1X,1PD1
     /2.5))
      READ(5,200) DTSTM,DTWA,DTWPF,DTWPN,DTWDP,DTWDG
      WRITE(6,210) DTSTM,DTWA,DTWPF,DTWPN,DTWDP,DTWDG
  210 FORMAT(' DTstm;DTwo,a;DTwo,pl(FC);DTwo,pl(NB);DTwo,pvc;DTwo,gal'/6
     /(1X,1PD12.5))
      READ(5,200) DRHI,DRHO,DPATM,DVEL,DCONDM
      WRITE(6,211) DRHI,DRHO,DPATM,DVEL,DCONDM
  211 FORMAT(' DRHI, DRHO, DPatm, DVel, DMcond'/6(1X,1PD12.5))
      READ(5,200) DHPOOL,DHPLF,DHPL1,DHPL2,DHGAL
      WRITE(6,212) DHPOOL,DHPLF,DHPL1,DHPL2,DHGAL
  212 FORMAT(' DHpool, DHpl(FC), DHpl1, DHpl2, DHgal'/6(1X,1PD12.5))
      READ(5,200) DAPI,DAPO,DACH,DDT
      WRITE(6,213) DAPI,DAPO,DACH,DDT
  213 FORMAT(' DAPI, DAPO, DACH, DDT'/6(1X,1PD12.5))
      READ(5,200) FHFG,FHFGP,FPR,FPRI,FDVS,FDVA
      WRITE(6,214) FHFG,FHFGP,FPR,FPRI,FDVS,FDVA
  214 FORMAT(' FHFG, FHFGP, FPR, FPRI, FDVS, FDVA'/6(1X,1PD12.5))
      READ(5,200) FCPS,FCPA,FCPI,FCPO,FROI,FROO
      WRITE(6,215) FCPS,FCPA,FCPI,FCPO,FROI,FROO
  215 FORMAT(' FCPS, FCPA, FCPI, FCPO, FROI, FROO'/6(1X,1PD12.5))
      READ(5,200) EMS,DEMS,EMP,DEMP,EMG,DEMG
      WRITE(6,216) EMS,DEMS,EMP,DEMP,EMG,DEMG
  216 FORMAT(' EM-SS, DEM-SS, EM-PVC, DEM-PVC, EM-GAL, DEM-GAL'/6(1X,1PD
     /12.5))
      READ(5,217) MS
  217 FORMAT(14I5)
      WRITE(6,218) MS
  218 FORMAT(' MS',1X,12I5)
C
C TOTAL HEAT TRANSFER RATE, QT, AND UNCERTAINTY
C
      CALL SATWP(TSTM,HFG,XX)
      QT=CONDM*HFG/DT
      DQT=QT*((DCONDM/CONDM)**2+FHFG**2+(DDT/DT)**2)**.5
      FQT=DQT/QT
C
C HEAT TRANSFER RATE TO MIXTURE FLOW, QMIX, AND UNCERTAINTY
```

```
C
      CALL PSAT(PR1,TMIXEX1)
      CALL PSAT(PR2,TMIXEX2)
      IF(MS.EQ.0) GOTO 1
C EVALUATE STEAM FLOW RATE BY LEVEL
      CALL SATWP(TPI1,XI1,ROI1)
      CALL SATWP(TPI2,XI2,ROI2)
      CALL SATWP(TPO1,XO1,ROO1)
      CALL SATWP(TPO2,XO2,ROO2)
      ROI=(ROI1+ROI2)/2.
      ROO=(ROO1+ROO2)/2.
      DRI=.5*((FROI*ROI1)**2+(FROI*ROI2)**2)**.5
      DRO=.5*((FROO*ROO1)**2+(FROO*ROO2)**2)**.5
      STMFR=(HPL1-HPL2)*(ROI*API+ROO*APO)/DT
      FSTMFR=((DDT/DT)**2+(DHPL1**2+DHPL2**2)/(HPL1-HPL2)**2+((API*DRI)*
     /*2+(DAPI*ROI)**2+(DAPO*ROO)**2+(APO*DRO)**2)/(ROI*API+ROO*APO)**2)
     /**.5
      DSTMFR=FSTMFR*STMFR
      GOTO 2
    1 IF(RHO1.EQ.0..AND.RHO2.EQ.0.) GOTO 2
C EVALUATE STEAM FLOW RATE BY HUMIDITY
      STMFR1=(RHO1*PR1/RSTM/TMIXEX1)*VEL1*ACH
      DSTMFR1=STMFR1*((DRHO/RHO1)**2+(DTMIXEX/TMIXEX1)**2+FPR**2+
     /(DVEL/VEL1)**2)**.5
      STMFR2=(RHO2*PR2/RSTM/TMIXEX2)*VEL2*ACH
      DSTMFR2=STMFR2*((DRHO/RHO2)**2+(DTMIXEX/TMIXEX2)**2+FPR**2+
     /(DVEL/VEL2)**2)**.5
      STMFR=(STMFR1+STMFR2)/2.
      DSTMFR=.5*(DSTMFR1**2+DSTMFR2**2)**.5
      IF(STMFR1.EQ.STMFR2.AND.DSTMFR1.EQ.DSTMFR2) DSTMFR=DSTMFR1
      FSTMFR=DSTMFR/STMFR
C EVALUATE AIR FLOW RATE
    2 AIRFR1=((PATM-RHO1*PR1)/RAIR/TMIXEX1)*VEL1*ACH
      DPR=PR1*FPR
      DAIRFR1=AIRFR1*(((DPATM**2+(PR1*DRHO)**2+(RHO1*DPR)**2)
     //(PATM-RHO1*PR1)**2)+(DTMIXEX/TMIXEX1)**2+(DVEL/VEL1)**2)**.5
      AIRFR2=((PATM-RHO2*PR2)/RAIR/TMIXEX2)*VEL2*ACH
      DPR=PR2*FPR
      DAIRFR2=AIRFR2*(((DPATM**2+(PR2*DRHO)**2+(RHO2*DPR)**2)
     //(PATM-RHO2*PR2)**2)+(DTMIXEX/TMIXEX2)**2+(DVEL/VEL2)**2)**.5
      AIRFR=(AIRFR1+AIRFR2)/2.
      DAIRFR=.5*(DAIRFR1**2+DAIRFR2**2)**.5
      IF(AIRFR1.EQ.AIRFR2.AND.DAIRFR1.EQ.DAIRFR2) DAIRFR=DAIRFR1
      FAIRFR=DAIRFR/AIRFR
C EVALUATE VAPOR CONTENT IN THE INTAKE AIR (FOR AIR ONLY, DRHO=0.)
      IF(DRHO.NE.0.)  GOTO 3
      CALL PSAT(PRI,TIN)
      STMFR=(RHI*PRI/RSTM/TIN)*(AIRFR*RAIR*TIN/(PATM-RHI*PRI))
      DPRI=FPRI*PRI
      DSTMFR=((DPATM**2+(PRI*DRHI)**2+(RHI*DPRI)**2)/(PATM-RHI*PRI)**2
     /+(DRHI/RHI)**2+(DPRI/PRI)**2+FAIRFR**2)**.5*STMFR
    3 CMIX=AIRFR+STMFR
      TMIXEX=(TMIXEX1+TMIXEX2)/2.
      CALL PSAT(PR,TMIXEX)
      VEL=(VEL1+VEL2)/2.
      RHO=RSTM*TMIXEX*STMFR/VEL/ACH/PR
      IF(MS.EQ.1) DCMIX=(DAIRFR**2+DSTMFR**2)**.5
      IF(MS.EQ.0) DCMIX=CMIX*((DVEL/VEL)**2+(DTMIXEX/TMIXEX)**2+((DRHO*P
```

```
     /R/TMIXEX)**2*(1./RSTM-1./RAIR)**2+(DPATM/RAIR/TMIXEX)**2+(DPR*RHO/
     /TMIXEX)**2*(1./RSTM-1./RAIR)**2)/(RHO*PR/RSTM/TMIXEX+(PATM-RHO*PR)
     //RAIR/TMIXEX)**2)**.5
      FCMIX=DCMIX/CMIX
      XAIR=AIRFR/CMIX
      FXAIR=(FCMIX**2+FAIRFR**2)**.5
C EVALUATE INLET STEAM-AIR MIXTURE TEMPERATURE, TMIXI
      IF(TSP.NE.0.) GOTO 4
      TMIXI=TIN
      DTMIXI=DTIN
      GOTO 5
    4 CALL CPVAIR(CPA,CX,TIN)
      CALL CPVSTM(CPS,CXX,TSP)
      TMIXI=(TIN+STMFR*CPS*TSP/AIRFR/CPA)/(1+STMFR*CPS/AIRFR/CPA)
      CONT=CPA*AIRFR+CPS*STMFR
      DCPA=CPA*FCPA
      DCPS=CPS*FCPS
      DTMIXI=((DTIN*AIRFR*CPA/CONT)**2+(DTSP*STMFR*CPS/CONT)**2+(TSP-TIN
     /)**2/CONT**4*((DSTMFR*CPS*AIRFR*CPA)**2+(STMFR*DCPS*AIRFR*CPA)**2+
     /(STMFR*CPS*DAIRFR*CPA)**2+(STMFR*CPS*AIRFR*DCPA)**2))**.5
    5 CALL ASMP(TMIXO,DTMIXO,XAIR,FXAIR,DVMO,DDVMO,FDVS,FDVA,
     /CPMO,DCPMO,FCPS,FCPA)
      CALL ASMP(TMIXI,DTMIXI,XAIR,FXAIR,DVMI,DDVMI,FDVS,FDVA,
     /CPMI,DCPMI,FCPS,FCPA)
      CPM=(CPMO+CPMI)/2.
      DCPM=.5*(DCPMO**2+DCPMI**2)**.5
      QMIX=CMIX*CPM*(TMIXO-TMIXI)
      FQMIX=((DTMIXO**2+DTMIXI**2)/(TMIXO-TMIXI)**2+(DCPM/CPM)**2
     /+FCMIX**2)**.5
      DQMIX=FQMIX*QMIX
C
C EVALUATE RADIATIVE HEAT TRANSFER, QPVC AND QGAL, AND UNCERTAINTY
C
      QPVC=PI*DTR*(ELT-HPOOL-HGAL)*SIG/(1./EMS+DTR/DID*(1./EMP-1.))*(TWA
     /**4-TWDP**4)
      FQPVC=((16.*TWA**6*DTWA**2+16.*TWDP**6*DTWDP**2)/(TWA**4-TWDP**4)*
     /*2+(DHPOOL**2+DHGAL**2)/(ELT-HPOOL-HGAL)**2+((DEMS/EMS**2)**2+(DTR
     //DID*DEMP/EMP**2)**2)/(1./EMS+DTR/DID*(1./EMP-1.))**2)**.5
      DQPVC=FQPVC*QPVC
      QGAL=PI*DTR*HGAL*SIG/(1./EMS+DTR/DID*(1./EMG-1.))*(TWA**4-TWDG**4)
      FQGAL=((16*TWA**6*DTWA**2+16*TWDG**6*DTWDG**2)/(TWA**4-TWDG**4)**2
     /+(DHGAL/HGAL)**2+((DEMS/EMS**2)**2+(DTR/DID*DEMG/EMG**2)**2)/(1./E
     /MS+DTR/DID*(1./EMG-1.))**2)**.5
      DQGAL=FQGAL*QGAL
      QRAD=QPVC+QGAL
      DQRAD=(DQPVC**2+DQGAL**2)**.5
      FQRAD=DQRAD/QRAD
C
C EVALUATE REYNOLDS NUMBER AND UNCERTAINTY
C
      DVM=(DVMO+DVMI)/2.
      DDVM=.5*(DDVMO**2+DDVMI**2)**.5
      RE=CMIX*D/API/DVM
      DRE=RE*(FCMIX**2+(DDVM/DVM)**2)**.5
      FRE=DRE/RE
C
C EVALUATE HEAT TRANSFER RATE TO POOL WATER AND UNCERTAINTY
C
```

```
      IF(HPOOL.EQ.0.) GOTO 30
C
C NO EVAPORATION IN WATER POOL
      CALL SUBWP(TPI1,CPI1,ROI1)
      CALL SUBWP(TPI2,CPI2,ROI2)
      CALL SUBWP(TPO1,CPO1,ROO1)
      CALL SUBWP(TPO2,CPO2,ROO2)
      CPI=(CPI1+CPI2)/2.
      CPO=(CPO1+CPO2)/2.
      ROI=(ROI1+ROI2)/2.
      ROO=(ROO1+ROO2)/2.
      FRI=.5*((FROI*ROI1)**2+(FROI*ROI2)**2)**.5/ROI
      FRO=.5*((FROO*ROO1)**2+(FROO*ROO2)**2)**.5/ROO
C INNER AND OUTER POOL WATER MASS, WMI AND WMO
      IF(HPLF.EQ.0.) GOTO 6
      WMI=ROI*HPLF*API
      DWMI=WMI*(FRI**2+(DHPLF/HPLF)**2+(DAPI/API)**2)**.5
    6 WMO=ROO*HPOOL*APO
      DWMO=WMO*(FRO**2+(DHPOOL/HPOOL)**2+(DAPO/APO)**2)**.5
      QPFC=(WMI*CPI*(TPI2-TPI1)+WMO*CPO*(TPO2-TPO1))/DT
      DCPI=.5*((FCPI*CPI1)**2+(FCPI*CPI2)**2)**.5
      DCPO=.5*((FCPO*CPO1)**2+(FCPO*CPO2)**2)**.5
      DQPFC=(((WMI*CPI)**2*(DTPI2**2+DTPI1**2)+(WMI*DCPI*(TPI2-TPI1))**2
     /+(DWMI*CPI*(TPI2-TPI1))**2+(WMO*CPO)**2*(DTPO1**2+DTPO2**2)
     /+(WMO*DCPO*(TPO2-TPO1))**2+(DWMO*CPO*(TPO2-TPO1))**2)/DT**2+(DDT**
     /2/DT**4)*(WMI*CPI*(TPI2-TPI1)+WMO*CPO*(TPO2-TPO1))**2)**.5
      FQPFC=DQPFC/QPFC
C
C IN CASE OF EVAPORATION IN WATER POOL
      HPLN=HPOOL-HPLF
      IF(HPLN.EQ.0.) GOTO 10
      CALL PSAT(PRI,TIN)
      IF(RHI.EQ.0.) GOTO 11
      VAPI=(RHI*PRI/RSTM/TIN)*(AIRFR*RAIR*TIN/(PATM-RHI*PRI))
      DPRI=FPRI*PRI
      DVAPI=((DPATM**2+(PRI*DRHI)**2+(RHI*DPRI)**2)/(PATM-RHI*PRI)**2
     /+(DRHI/RHI)**2+(DPRI/PRI)**2+FAIRFR**2)**.5*VAPI
   11 IF(MS.EQ.1) STMFR=STMFR+VAPI
      PLFR=STMFR-VAPI
      DPLFR=(DSTMFR**2+DVAPI**2)**.5
      IF(MS.EQ.1) DPLFR=DSTMFR
      FPLFR=DPLFR/PLFR
      CALL SATWP(TPLN,HFGP,XR)
      QPNB=PLFR*HFGP
      DQPNB=QPNB*(FPLFR**2+FHFGP**2)**.5
      FQPNB=DQPNB/QPNB
C TOTAL HEAT TRANSFER RATE AND UNCERTAINTY TO POOL
   10 QP=QPFC+QPNB
      DQP=(DQPFC**2+DQPNB**2)**.5
      FQP=DQP/QP
      IF(HPLF.NE.0.) GOTO 30
      QPFC=0.
      QPNB=QP
      DQPNB=DQP
      FQPNB=FQP
   30 RQ=QT/(QP+QMIX)
C
C EVALUATE HEAT FLUX TO MIXTURE FLOW AND UNCERTAINTY
```

```
C
      HFMIX=QMIX/(PI*DTR*(ELT-HPOOL))
      DHFMIX=HFMIX*((DHPOOL/(ELT-HPOOL))**2+FQMIX**2)**.5
      FHFMIX=DHFMIX/HFMIX
C
      IF(HPOOL.EQ.0.) GOTO 21
C
C EVALUATE HEAT FLUX TO POOL WATER (FC) AND UNCERTAINTY
C
      IF(QPFC.EQ.0..OR.HPLF.EQ.0.) GOTO 22
      HFPLF=QPFC/(PI*DTR*HPLF)
      DHFPLF=HFPLF*(FQPFC**2+(DHPLF/HPLF)**2)**.5
      FHFPLF=DHFPLF/HFPLF
C
C EVALUATE HEAT FLUX TO POOL WATER (NB) AND UNCERTAINTY
C
   22 IF(HPLN.EQ.0.) GOTO 21
      DHPLN=(DHPOOL**2+DHPLF**2)**.5
      HFPLN=QPNB/(PI*DTR*HPLN)
      DHFPLN=HFPLN*(FQPNB**2+(DHPLN/HPLN)**2)**.5
      FHFPLN=DHFPLN/HFPLN
C
C EVALUATE HTC TO MIXTURE AND UNCERTAINTY
C
   21 TMIX=(TMIXO+TMIXI)/2.
      DTMIX=0.5*(DTMIXO**2+DTMIXI**2)**0.5
C EVALUATE EFFECTIVE HTC, HCMIXE
      HCMIXE=HFMIX/(TWA-TMIX)
      DHCMIXE=HCMIXE*(FHFMIX**2+(DTWA**2+DTMIX**2)/(TWA-TMIX)**2)**.5
      FHCMIXE=DHCMIXE/HCMIXE
C EVALUATE CONVECTIVE HTC, HCMIX
      HCMIX=(QMIX-QRAD)/(PI*DTR*(ELT-HPOOL))/(TWA-TMIX)
      FHCMIX=((DQMIX**2+DQRAD**2)/(QMIX-QRAD)**2+(DTWA**2+DTMIX**2)/(TWA
     /-TMIX)**2+DHPOOL**2/(ELT-HPOOL)**2)**0.5
      DHCMIX=FHCMIX*HCMIX
C
      IF(HPOOL.EQ.0.) GOTO 24
C
C EVALUATE HTC TO POOL WATER (FC) AND UNCERTAINTY
C
      IF(QPFC.EQ.0..OR.HPLF.EQ.0.) GOTO 23
      HCPLF=HFPLF/(TWPF-TPLF)
      DHCPLF=HCPLF*(FHFPLF**2+(DTWPF**2+DTPLF**2)/(TWPF-TPLF)**2)**.5
      FHCPLF=DHCPLF/HCPLF
C
C EVALUATE HTC TO POOL WATER (NB) AND UNCERTAINTY
C
   23 IF(QPNB.EQ.0..OR.HPLN.EQ.0.) GOTO 24
      HCPLN=HFPLN/(TWPN-TPLN)
      DHCPLN=HCPLN*(FHFPLN**2+(DTWPN**2+DTPLN**2)/(TWPN-TPLN)**2)**.5
      FHCPLN=DHCPLN/HCPLN
C
   24 IF(QPFC.EQ.0..OR.QPNB.EQ.0.) GOTO 25
      HPLT=QP/(PI*DTR*HPOOL)/((TWPF+TWPN)/2.-(TPLF+TPLN)/2.)
      DHPLT=HPLT*((DHPOOL/HPOOL)**2+(DQP/QP)**2+(DTWPF**2+DTWPN**2+DTPLF
     /**2+DTPLN**2)/(TWPF+TWPN-TPLF-TPLN)**2)**.5
C
   25 WRITE(6,300)
```

```
  300 FORMAT(///'    Qcond,       Qpool,       Qp(FC),      Qp(NB),
     / Qmix,        Qrad')
      WRITE(6,301) QT,QP,QPFC,QPNB,QMIX,QRAD
  301 FORMAT(1X,6(1X,1PD12.4))
      WRITE(6,302)
  302 FORMAT(/'    q"pl(FC),    q"pl(NB),    q"mix,       Hmix,eff,    R
     /E,          Qcond/Q')
      WRITE(6,301) HFPLF,HFPLN,HFMIX,HCMIXE,RE,RQ
      WRITE(6,303)
  303 FORMAT(/'    Hp(FC),      Hp(NB)       Hmix,        Mair,        M
     /stm,        Mmix')
      WRITE(6,301) HCPLF,HCPLN,HCMIX,AIRFR,STMFR,CMIX
      WRITE(6,304)
  304 FORMAT(/'    DQt/Qt,      DQp/Qp(T),   DQp/Qp(FC),  DQp/Qp(NB),  D
     /Qm/Qm,      DQrad/Qrad')
      WRITE(6,301) FQT,FQP,FQPFC,FQPNB,FQMIX,FQRAD
      WRITE(6,305)
  305 FORMAT(/'    DQt,         DQp(T),      DQp(FC),     DQp(NB),     D
     /Qmix,       DQrad')
      WRITE(6,301) DQT,DQP,DQPFC,DQPNB,DQMIX,DQRAD
      WRITE(6,306)
  306 FORMAT(/'    (Dq"/q")FC,  (Dq"/q")NB,  (Dq"/q")m,   (DH/H)m,eff  D
     /RE/RE       Hp(T)')
      WRITE(6,301) FHFPLF,FHFPLN,FHFMIX,FHCMIXE,FRE,HPLT
      WRITE(6,307)
  307 FORMAT(/'    Dq"(FC),     Dq"(NB),     Dq"mix,      DHm,eff,     D
     /RE,         DHp(T)')
      WRITE(6,301) DHFPLF,DHFPLN,DHFMIX,DHCMIXE,DRE,DHPLT
      WRITE(6,308)
  308 FORMAT(/'    (DHp/Hp)FC,  (DHp/Hp)NB,  DHm/Hm,      DMair/Mair,  D
     /Mstm/Mstm,  DMm/Mm')
      WRITE(6,301) FHCPLF,FHCPLN,FHCMIX,FAIRFR,FSTMFR,FCMIX
      WRITE(6,309)
  309 FORMAT(/'    DHp(FC),     DHp(NB),     DHm,         DMair,       D
     /Mstm,       DMm')
      WRITE(6,301) DHCPLF,DHCPLN,DHCMIX,DAIRFR,DSTMFR,DCMIX
      GOTO 7777
 8888 WRITE(6,8000)
 8000 FORMAT(' NO FILE BY THAT NAME')
      GOTO 7777
 9999 WRITE(6,9000)
 9000 FORMAT(' THIS FILE ALREADY EXISTS')
 7777 STOP
      END
C
C  DYNAMIC VISCOSITY OF AIR  EMI(KG/M-S), T(K)
C  IRVINE T.F. STEAM AND GAS TABLES WITH COMP. EQS., NY., 1984
      SUBROUTINE VISAIR(EMI,T)
      IMPLICIT REAL*8(A-H,O-Z)
      DIMENSION B1(5),B2(5)
      DATA B1/-9.8601D-1, 9.080125D-2, -1.17635575D-4, 1.2349703D-7,
     /        -5.7971299D-11/
      DATA B2/4.8856745, 5.43232D-2, -2.4261775D-5, 7.9306D-9,
     /        -1.10398D-12/
      IF(T.LT.250.OR.T.GT.1050) GOTO 3
      EMI=0.
      IF(T.GE.600.) GOTO 2
      DO 10 I=1,5
```

```
   10 EMI=EMI+B1(I)*T**(I-1)
      EMI=EMI*1.D-6
      RETURN
    2 DO 20 I=1,5
   20 EMI=EMI+B2(I)*T**(I-1)
      EMI=EMI*1.D-6
      RETURN
    3 WRITE(6,100) T
  100 FORMAT(' **ERROR IN VISAIR T(K)=',1PD11.4)
      STOP 333
      END
C
C DYNAMIC VISCOSITY OF STEAM
      SUBROUTINE VISSTM(EMI,T)
      IMPLICIT REAL*8(A-H,O-Z)
      DIMENSION TM(26),DV(26)
      DATA TM/1.D-2,1.D1, 2.D1, 3.D1, 4.D1, 5.D1, 6.D1, 7.D1, 8.D1,
     /        9.D1,1.D2,1.1D2,1.2D2,1.3D2,1.4D2,1.5D2,1.6D2,1.7D2,
     /        1.8D2,1.9D2,2.D2,2.1D2,2.2D2,2.3D2,2.4D2,2.5D2/
      DATA DV/8.105D-6,8.504D-6,8.903D-6,9.305D-6,9.701D-6,1.010D-5,
     /        1.050D-5,1.089D-5,1.129D-5,1.167D-5,1.206D-5,1.245D-5,
     /        1.283D-5,1.320D-5,1.357D-5,1.394D-5,1.430D-5,1.466D-5,
     /        1.502D-5,1.537D-5,1.572D-5,1.607D-5,1.642D-5,1.678D-5,
     /        1.714D-5,1.751D-5/
      TT=T-273.15
      DO 1 I=2,26
      IF(TM(I-1).LE.TT.AND.TM(I).GE.TT) GOTO 2
    1 CONTINUE
      WRITE(6,100) T
  100 FORMAT(' TEMPERATURE IS OUTSIDE RANGE', 1PD11.4)
      STOP
    2 T1=TM(I-1)
      T2=TM(I)
      EMI1=DV(I-1)
      EMI2=DV(I)
      EMI=EMI1+(EMI2-EMI1)/(T2-T1)*(TT-T1)
      RETURN
      END
C
C  SPECIF.HEAT AT CONST.PRESSURE OF AIR  CP(J/KG-K), T(K)
C  SPECIF.HEAT AT CONST.VOLUME OF AIR  CV(J/KG-K), T(K)
C  IRVINE T.F. STEAM AND GAS TABLES WITH COMP. EQS., NY., 1984
      SUBROUTINE CPVAIR(CP,CV,T)
      IMPLICIT REAL*8(A-H,O-Z)
      DIMENSION B(5)
      DATA B/0.103409D1, -0.2848870D-3,  0.7816818D-6, -0.4970786D-9,
     /       0.1077024D-12/,            R/287.04/
      IF(T.LT.250.OR.T.GT.2000) GOTO 3
      CP=0.
      DO 10 I=1,5
   10 CP=CP+B(I)*T**(I-1)
      CP=CP*1000.
      CV=CP-R
      RETURN
    3 WRITE(6,100) T
  100 FORMAT(' **ERROR IN CPAIR T(K)=',1PD11.4)
      STOP 333
      END
```

```
C
C  SPECIFIC HEAT OF STEAM
      SUBROUTINE CPVSTM(CP,CV,T)
      IMPLICIT REAL*8(A-H,O-Z)
      DIMENSION TM(26),CG(26)
      DATA TM/1.D-2,1.D1, 2.D1, 3.D1, 4.D1, 5.D1, 6.D1, 7.D1, 8.D1,
     /        9.D1,1.D2,1.1D2,1.2D2,1.3D2,1.4D2,1.5D2,1.6D2,1.7D2,
     /        1.8D2,1.9D2,2.D2,2.1D2,2.2D2,2.3D2,2.4D2,2.5D2/
      DATA CG/1.863D+3,1.870D+3,1.880D+3,1.890D+3,1.900D+3,1.912D+3,
     /        1.924D+3,1.946D+3,1.970D+3,1.999D+3,2.034D+3,
     /        2.076D+3,2.125D+3,2.180D+3,2.245D+3,2.320D+3,
     /        2.406D+3,2.504D+3,2.615D+3,2.741D+3,2.883D+3,
     /        3.043D+3,3.223D+3,3.426D+3,3.656D+3,3.918D+3/
      DATA R/462/
      TT=T-273.15
      DO 1 I=2,26
      IF(TM(I-1).LE.TT.AND.TM(I).GE.TT) GOTO 2
    1 CONTINUE
      WRITE(6,100) T
  100 FORMAT(' TEMPERATURE IS OUTSIDE RANGE', 1PD11.4)
      STOP
    2 T1=TM(I-1)
      T2=TM(I)
      CP1=CG(I-1)
      CP2=CG(I)
      CP=CP1+(CP2-CP1)/(T2-T1)*(TT-T1)
      CV=CP-R
      RETURN
      END
C
C AIR-STAEAM MIXTURE PROPERTIES
      SUBROUTINE ASMP(T,DT,XA,FXA,DV,DDV,FDVS,FDVA,CP,DCP,FCPS,FCPA)
      IMPLICIT REAL*8(A-H,O-Z)
      AIRM=2.897D-2
      STMM=1.8D-2
      CALL VISAIR(DVA,T)
      CALL VISSTM(DVS,T)
      CALL CPVAIR(CPA,CVA,T)
      CALL CPVSTM(CPS,CVS,T)
      YAIR=XA/AIRM/(XA/AIRM+(1.-XA)/STMM)
      YSTM=(1.-XA)/STMM/(XA/AIRM+(1.-XA)/STMM)
      DV1=YAIR*DVA*AIRM**.5+YSTM*DVS*STMM**.5
      DV2=YAIR*AIRM**.5+YSTM*STMM**.5
      DV=DV1/DV2
      CP=YAIR*CPA+YSTM*CPS
C
C CALC. UNCERTAINTY IN DV (TEMP INCLUDED) AND CP
      T1=T-273.15
      DDVAI=DVA*(FDVA**2+((2.2404D-8+2*8.5329D-11*T1*DT)/DVA)**2)**.5
      IF(XA.NE.1.) GOTO 1
      DDV=DDVAI
      DCP=FCPA*CPA
      GOTO 2
    1 DXA=FXA*XA
      DYAIR=YAIR*(FXA**2+((DXA/AIRM)**2+(DXA/STMM)**2)
     //(XA/AIRM+(1.-XA)/STMM)**2)**.5
      DYSTM=YSTM*((DXA/(1.-XA))**2+((DXA/STMM)**2+(DXA/AIRM)**2)
     //(XA/AIRM+(1.-XA)/STMM)**2)**.5
```

```
      DDVS=FDVS*DVS
      DDV1=(AIRM*((YAIR*DDVAI)**2+(DYAIR*DVA)**2)
     /+STMM*((YSTM*DDVS)**2+(DYSTM*DVS)**2))**.5
      DDV2=(STMM*DYSTM**2+AIRM*DYAIR**2)**.5
      DDV=DV*((DDV1/DV1)**2+(DDV2/DV2)**2)**.5
      DCPS=FCPS*CPS
      DCPA=FCPA*CPA
      DCP=((YAIR*DCPA)**2+(DYAIR*CPA)**2
     /+(YSTM*DCPS)**2+(DYSTM*CPS)**2)**.5
    2 RETURN
      END
C
C  SATURATION PRESSURE OF STEAM (Pa)
C  IRVINE T.F. STEAM AND GAS TABLES WITH COMP. EQS., NY, 1984
      SUBROUTINE PSAT(P,T)
      IMPLICIT REAL*8(A-H,O-Z)
      DIMENSION B(12)
      DATA B/0.104592D2,  -0.404897D-2,  -0.417520D-4,   0.368510D-6,
     /      -0.101520D-8,  0.865310D-12,  0.903668D-15, -0.199690D-17,
     /       0.779287D-21, 0.191482D-24, -0.396806D4,    0.395735D2/
      IF(T.LT.273.15.OR.T.GT.647.3)  GOTO 3
      P=0.0
      DO 10 I=1,10
   10 P=P+B(I)*T**(I-1)
      P=P+B(11)/(T-B(12))
      P=EXP(P)
      P=P*1.D+6
      RETURN
    3 WRITE(6,100) T
  100 FORMAT('**ERROR IN STEAM TEMP.',1PD11.4)
      STOP 333
      END
C
C
C SATURATION WATER PROPERTIES
      SUBROUTINE SATWP(T,HD,RF)
      IMPLICIT REAL*8(A-H,O-Z)
      DIMENSION TM(26),ED(26),VL(26)
      DATA TM/1.D-2,1.D1, 2.D1, 3.D1, 4.D1, 5.D1, 6.D1, 7.D1, 8.D1,
     /        9.D1,1.D2,1.1D2,1.2D2,1.3D2,1.4D2,1.5D2,1.6D2,1.7D2,
     /        1.8D2,1.9D2,2.D2,2.1D2,2.2D2,2.3D2,2.4D2,2.5D2/
      DATA ED/2.5013D+6,2.4777D+6,2.4541D+6,2.4305D+6,2.4067D+6,
     /        2.3827D+6,2.3585D+6,2.3338D+6,2.3088D+6,2.2832D+6,
     /        2.2570D+6,2.2302D+6,2.2026D+6,2.1742D+6,2.1447D+6,
     /        2.1143D+6,2.0826D+6,2.0495D+6,2.0150D+6,1.9788D+6,
     /        1.9407D+6,1.9007D+6,1.8585D+6,1.8138D+6,1.7665D+6,
     /        1.7162D+6/
      DATA VL/1.0002D-3,1.0004D-3,1.0018D-3,1.0043D-3,1.0078D-3,
     /        1.0121D-3,1.0172D-3,1.0228D-3,1.0291D-3,1.0360D-3,
     /        1.0435D-3,1.0516D-3,1.0603D-3,1.0697D-3,1.0797D-3,
     /        1.0905D-3,1.1020D-3,1.1143D-3,1.1274D-3,1.1414D-3,
     /        1.1565D-3,1.1726D-3,1.1900D-3,1.2088D-3,1.2291D-3,
     /        1.2512D-3/
C
      TT=T-273.15
      DO 1 I=2,26
      IF(TM(I-1).LE.TT.AND.TM(I).GE.TT) GOTO 2
    1 CONTINUE
```

```
      WRITE(6,100) T
  100 FORMAT(' TEMPERATURE IS OUTSIDE RANGE', 1PD11.4)
      STOP
    2 T1=TM(I-1)
      T2=TM(I)
      T3=(TT-T1)/(T2-T1)
      HD1=ED(I-1)
      HD2=ED(I)
      HD=HD1+(HD2-HD1)*T3
      RF1=VL(I-1)
      RF2=VL(I)
      RF3=RF1+(RF2-RF1)*T3
      RF=1./RF3
      RETURN
      END
C
      SUBROUTINE SUBWP(T,CP,RF)
      IMPLICIT REAL*8(A-H,O-Z)
      DIMENSION TM(26),CF(26),VL(26)
      DATA TM/1.D-2,1.D1, 2.D1, 3.D1, 4.D1, 5.D1, 6.D1, 7.D1, 8.D1,
     /        9.D1,1.D2,1.1D2,1.2D2,1.3D2,1.4D2,1.5D2,1.6D2,1.7D2,
     /        1.8D2,1.9D2,2.D2,2.1D2,2.2D2,2.3D2,2.4D2,2.5D2/
      DATA VL/1.0002D-3,1.0004D-3,1.0018D-3,1.0043D-3,1.0078D-3,
     /        1.0121D-3,1.0172D-3,1.0228D-3,1.0291D-3,1.0360D-3,
     /        1.0435D-3,1.0516D-3,1.0603D-3,1.0697D-3,1.0797D-3,
     /        1.0905D-3,1.1020D-3,1.1143D-3,1.1274D-3,1.1414D-3,
     /        1.1565D-3,1.1726D-3,1.1900D-3,1.2088D-3,1.2291D-3,
     /        1.2512D-3/
      DATA CF/4.218D+3,4.194D+3,4.182D+3,4.179D+3,4.179D+3,4.181D+3,
     /        4.185D+3,4.191D+3,4.198D+3,4.207D+3,4.218D+3,
     /        4.230D+3,4.244D+3,4.262D+3,4.282D+3,4.306D+3,
     /        4.334D+3,4.366D+3,4.403D+3,4.446D+3,4.494D+3,
     /        4.550D+3,4.613D+3,4.685D+3,4.769D+3,4.866D+3/
C
      TT=T-273.15
      DO 1 I=2,26
      IF(TM(I-1).LE.TT.AND.TM(I).GE.TT) GOTO 2
    1 CONTINUE
      WRITE(6,100) T
  100 FORMAT(' TEMPERATURE IS OUTSIDE RANGE', 1PD11.4)
      STOP
    2 T1=TM(I-1)
      T2=TM(I)
      RF1=VL(I-1)
      RF2=VL(I)
      RF3=RF1+(RF2-RF1)/(T2-T1)*(TT-T1)
      RF=1./RF3
      CP1=CF(I-1)
      CP2=CF(I)
      CP=CP1+(CP2-CP1)/(T2-T1)*(TT-T1)
      RETURN
      END
```

APPENDIX B

SUMMARY OF EXPERIMENTAL RESULTS

B.1 Summary of Air-only Tests

The results of the air-only tests are presented in this section. There are eight groups of test results, which were obtained between March 1, 1994 and May 3, 1994. All the tests, except A0502-11 to A0502-15, were run for the same geometry of the test apparatus as described in Chapter 3. In A0502-11 to A0502-15, the upper air windows (located 10 feet above the bottom plate) were sealed, therefore, the lower air windows provide the only flow passages. Each test consists of five sets of data, which were run under the same conditions. The notation of the test identification number is as follows.

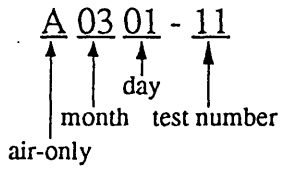

The results of each air-only test are presented in three tables and two figures. The first two tables show the raw data of the test. The third table shows the results of the data analysis. The figures show the heat flux and the heat transfer coefficient, with their associated uncertainty. Also included in these figures are the predictions of the heat flux and the heat transfer coefficient by PREWAS (see Appendix C for details). PREWAS simulates the same conditions as in the tests. The heat transfer coefficient adopted in PREWAS is the ANL (Argonne National Laboratory) heat transfer correlation (Equation C.29). The input form loss coefficients for each section are as presented in Appendix D. The emissivity of each surface, taken from Kreith's heat transfer data book [K-8], are 0.57 for stainless steel, 0.89 for PVC, and 0.28 for galvanized steel. The thermal conductivity of the stainless steel heated vessel is assumed to be 17 w/m°C [K-8].

Table B.1.a Air-Only Tests Thermocouple Raw Data – A0301-11 to A0301-15

TC ID	Function	A0301-11 (°C)	A0301-12 (°C)	A0301-13 (°C)	A0301-14 (°C)	A0301-15 (°C)
TC1	T_{wo}	149.1	148.6	148.7	148.4	148.1
TC2	T_{wo}	149.5	149.5	149.5	149.5	149.4
TC3	T_{wo}	149.7	149.6	149.7	149.6	149.6
TC4	T_{wo}	149.7	149.6	149.7	149.7	149.6
TC5	T_{wo}	149.2	149.1	149.2	149.2	149.1
TC6	T_{wo}	149.1	149.0	149.1	149.1	149.0
TC7	T_{wo}	149.2	149.1	149.2	149.2	149.1
TC8	T_{wo}	149.5	149.4	149.5	149.5	149.4
TC9	T_{wo}	149.2	149.2	149.2	149.2	149.2
TC10	T_{wo}	149.4	149.3	149.4	149.4	149.3
TC11	T_{stm}	150.4	150.2	150.2	149.8	149.7
TC12	T_{stm}	150.4	150.3	150.3	150.3	150.2
TC13	T_{stm}	150.3	150.2	150.3	150.3	150.2
TC14	T_{stm}	150.5	150.4	150.5	150.5	150.4
TC15	T_{stm}	150.3	150.2	150.3	150.3	150.2
TC31	$T_{air,o}$	47.9	47.2	47.5	47.5	47.4
TC40	heat loss estimation	48.3	47.6	47.9	48.0	47.8
TC41	heat loss estimation	48.1	47.7	47.9	48.0	47.9
TC43	$T_{air,in}$	23.7	23.9	24.0	24.0	24.1
TC44	$T_{wi,PVC}$	31.3	31.4	31.5	31.5	31.5
TC45	$T_{wi,PVC}$	32.5	32.7	32.9	33.0	33.1
TC46	$T_{wi,gal}$	40.4	40.1	40.0	39.9	40.1
TC47	$T_{wi,gal}$	41.9	41.4	41.7	41.8	41.7

Notes: (1) see Figure 3.7 and Figure 3.8 for thermocouple (TC) location

(2) see Table 3.2 for T_i notation

Table B.1.b Air-Only Tests Raw Data – A0301-11 to A0301-15

TEST ID	P_{atm} (kPa)	ϕ_{in} (%)	$\overline{T}_{stm}$ (°C)	$\overline{T}_{wo}$ (°C)	$\overline{T}_{air,in}$ (°C)
A0301-11	103.0	19.0	150.4	149.4	23.7
A0301-12	103.0	19.0	150.3	149.2	23.9
A0301-13	103.0	19.0	150.3	149.3	24.0
A0301-14	103.0	19.0	150.2	149.3	24.0
A0301-15	103.0	19.0	150.1	149.2	24.1
TEST ID	$\overline{T}_{air,o}$ (°C)	$\overline{T}_{wi,PVC}$ (°C)	$\overline{T}_{wi,gal}$ (°C)	$\overline{V}_{air}$ (m/s)	$\dot{m}_{cond}$ (10^{-3}kg/s)
A0301-11	47.9	31.9	41.1	2.06	1.98
A0301-12	47.2	32.0	40.7	2.07	1.97
A0301-13	47.5	32.2	40.9	2.03	2.02
A0301-14	47.5	32.2	40.9	2.06	2.03
A0301-15	47.4	32.3	40.9	2.05	2.03

Table B.1.c Air-Only Test Results – A0301-11 to A0301-15

TEST ID	$\overline{T}_{stm}$ (°C)	$\dot{Q}_{cond}$ (kw)	$\dot{Q}_{air}$ (kw)	$\dot{Q}_{rad}$ (kw)	$\overline{q}''_{air}$ (kw/m^2)
A0301-11	150.4	4.12	4.09	1.44	1.85
A0301-12	150.3	4.17	3.97	1.43	1.80
A0301-13	150.3	4.27	3.95	1.43	1.79
A0301-14	150.2	4.28	3.99	1.43	1.81
A0301-15	150.1	4.28	3.93	1.43	1.79
TEST ID	$\overline{h}_{air,eff}$ (w/m^2°C)	$\overline{h}_{air,conv}$ (w/m^2°C)	Re ($\times 10^4$)	$\dot{m}_{air}$ (10^{-1}kg/s)	$\frac{\dot{Q}_{cond}}{\dot{Q}_{air}}$
A0301-11	16.33	10.59	2.63	1.67	1.02
A0301-12	15.84	11.12	2.64	1.69	1.05
A0301-13	15.78	10.05	2.60	1.66	1.08
A0301-14	15.96	10.23	2.63	1.68	1.07
A0301-15	15.74	10.02	2.62	1.67	1.09

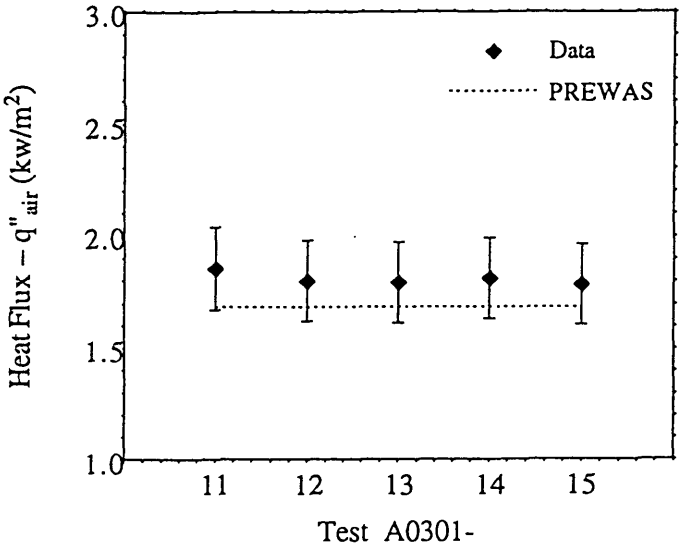

Figure B.1 a A0301 Test Results – Heat Flux

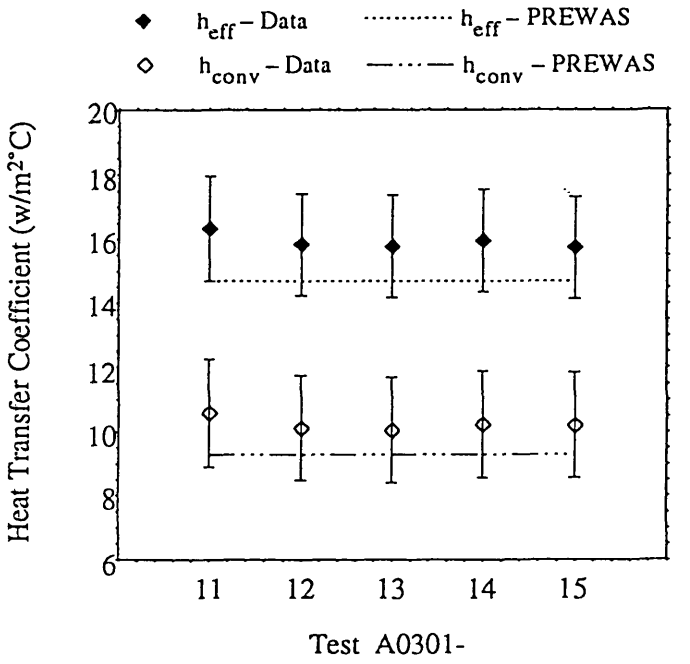

Figure B.1.b A0301 Test Results – Heat Transfer Coefficient

Table B.2.a Air-Only Tests Thermocouple Raw Data – A0304-11 to A0304-15

TC ID	Function	A0304-11 (°C)	A0304-12 (°C)	A0304-13 (°C)	A0304-14 (°C)	A0304-15 (°C)
TC1	T_{wo}	149.0	148.8	148.8	149.0	149.1
TC2	T_{wo}	149.5	149.4	149.4	149.5	149.5
TC3	T_{wo}	149.6	149.4	149.5	149.6	149.6
TC4	T_{wo}	149.6	149.5	149.6	149.6	149.7
TC5	T_{wo}	14148.8	148.9	149.1	148.9	149.0
TC6	T_{wo}	149.1	149.0	149.0	149.1	149.1
TC7	T_{wo}	149.1	149.0	149.1	149.1	149.2
TC8	T_{wo}	149.5	149.3	149.4	149.4	149.5
TC9	T_{wo}	149.2	149.1	149.2	149.2	149.2
TC10	T_{wo}	149.3	149.2	149.3	149.3	149.3
TC11	T_{stm}	150.3	150.2	150.3	150.3	150.3
TC12	T_{stm}	150.3	150.2	150.3	150.3	150.3
TC13	T_{stm}	150.3	150.1	150.2	150.2	150.3
TC14	T_{stm}	150.5	150.3	150.4	150.4	150.5
TC15	T_{stm}	150.3	150.1	150.2	150.3	150.3
TC31	$T_{air,o}$	47.1	47.2	47.3	47.5	47.4
TC40	heat loss estimation	47.6	47.8	47.8	47.9	47.9
TC41	heat loss estimation	47.6	47.8	47.8	48.0	47.8
TC43	$T_{air,in}$	24.2	24.3	24.3	24.2	24.2
TC44	$T_{wi,PVC}$	31.3	31.6	31.7	31.8	31.8
TC45	$T_{wi,PVC}$	31.1	32.1	32.2	32.4	32.5
TC46	$T_{wi,gal}$	40.4	40.7	41.0	41.0	41.0
TC47	$T_{wi,gal}$	40.8	41.0	41.0	41.2	41.2

Notes: (1) see Figure 3.7 and Figure 3.8 for thermocouple (TC) location

(2) see Table 3.2 for T_i notation

Table B.2.b Air-Only Tests Raw Data – A0304-11 to A0304-15

TEST ID	P_{atm} (kPa)	ϕ_{in} (%)	$\overline{T}_{stm}$ (°C)	$\overline{T}_{wo}$ (°C)	$\overline{T}_{air,in}$ (°C)
A0304-11	100.2	19.0	150.3	149.3	24.2
A0304-12	100.2	19.0	150.2	149.2	24.3
A0304-13	100.2	19.0	150.3	149.2	24.3
A0304-14	100.2	19.0	150.3	149.3	24.2
A0304-15	100.2	19.0	150.3	149.3	24.2
TEST ID	$\overline{T}_{air,o}$ (°C)	$\overline{T}_{wi,PVC}$ (°C)	$\overline{T}_{wi,gal}$ (°C)	$\overline{V}_{air}$ (m/s)	$\dot{m}_{cond}$ (10^{-3}kg/s)
A0304-11	47.1	31.2	40.6	2.07	2.05
A0304-12	47.2	31.8	40.8	2.07	1.97
A0304-13	47.3	32.0	41.0	2.08	1.99
A0304-14	47.5	32.1	41.1	2.09	1.97
A0304-15	47.4	32.1	41.1	2.13	2.00

Table B.2.c Air-Only Test Results – A0304-11 to A0304-15

TEST ID	$\overline{T}_{stm}$ (°C)	$\dot{Q}_{cond}$ (kw)	$\dot{Q}_{air}$ (kw)	$\dot{Q}_{rad}$ (kw)	$\overline{q}''_{air}$ (kw/m^2)
A0304-11	150.3	4.34	3.79	1.44	1.72
A0304-12	150.2	4.17	3.82	1.44	1.74
A0304-13	150.3	4.21	3.85	1.43	1.75
A0304-14	150.3	4.16	3.90	1.43	1.77
A0304-15	150.3	4.23	3.97	1.44	1.80
TEST ID	$\overline{h}_{air,eff}$ (w/m^2°C)	$\overline{h}_{air,conv}$ (w/m^2°C)	Re ($\times 10^4$)	$\dot{m}_{air}$ (10^{-1}kg/s)	$\frac{\dot{Q}_{cond}}{\dot{Q}_{air}}$
A0304-11	15.14	9.39	2.57	1.64	1.14
A0304-12	15.30	9.57	2.58	1.64	1.09
A0304-13	15.42	9.68	2.59	1.65	1.09
A0304-14	15.62	9.88	2.60	1.66	1.06
A0304-15	15.86	10.13	2.64	1.68	1.07

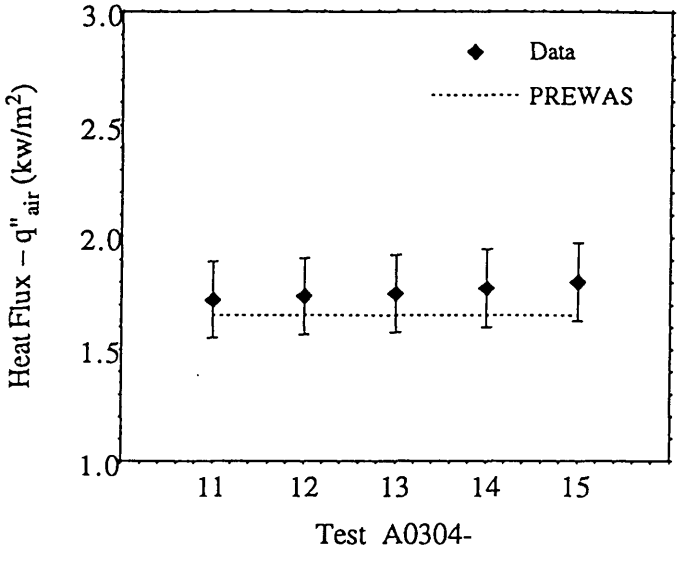

Figure B.2.a A0304 Test Results – Heat Flux

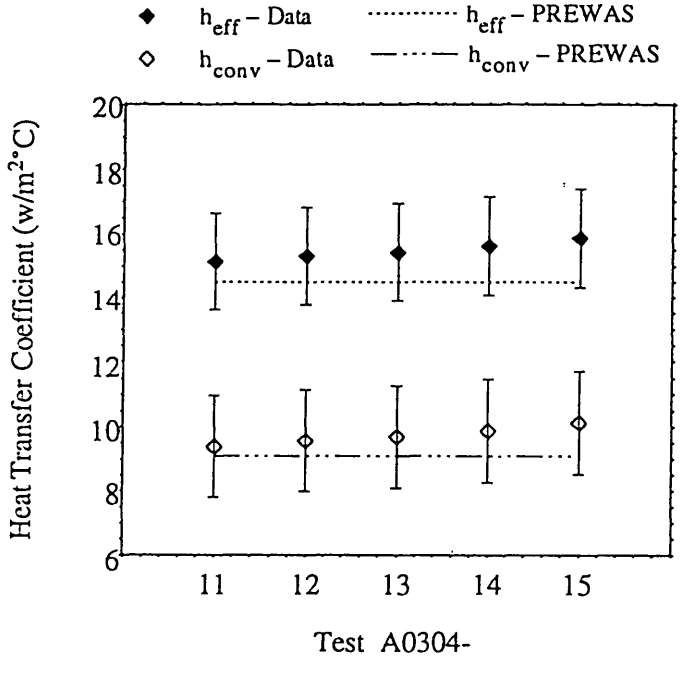

Figure B.2.b A0304 Test Results – Heat Transfer Coefficient

Table B.3.a Air-Only Tests Thermocouple Raw Data – A0429-11 to A0429-15

TC ID	Function	A0429-11 (°C)	A0429-12 (°C)	A0429-13 (°C)	A0429-14 (°C)	A0429-15 (°C)
TC1	T_{wo}	108.3	108.5	107.7	107.8	107.6
TC2	T_{wo}	108.8	108.9	108.4	108.4	108.3
TC3	T_{wo}	108.9	108.9	108.5	108.4	108.4
TC4	T_{wo}	108.9	109.0	108.6	108.5	108.5
TC5	T_{wo}	108.6	108.5	108.2	108.0	108.1
TC6	T_{wo}	108.6	108.6	108.2	108.1	108.1
TC7	T_{wo}	108.6	108.6	108.2	108.1	108.1
TC8	T_{wo}	108.7	108.8	108.4	108.3	108.3
TC9	T_{wo}	108.6	108.6	108.2	108.2	108.1
TC10	T_{wo}	108.6	108.7	108.2	108.1	108.1
TC11	T_{stm}	109.2	109.3	108.6	108.5	108.4
TC12	T_{stm}	109.3	109.4	108.9	108.9	108.8
TC13	T_{stm}	109.3	109.3	108.9	108.8	108.8
TC14	T_{stm}	109.4	109.4	109.0	108.9	108.9
TC15	T_{stm}	109.3	109.3	108.9	108.8	108.8
TC31	$T_{air,o}$	40.2	40.4	40.5	40.5	40.5
TC40	heat loss estimation	40.6	40.8	40.9	40.9	40.9
TC41	heat loss estimation	40.8	40.9	41.0	41.0	40.9
TC43	$T_{air,in}$	25.6	26.2	25.4	25.9	25.6
TC44	$T_{wi,PVC}$	29.1	29.5	29.6	29.6	29.6
TC45	$T_{wi,PVC}$	29.0	29.7	30.1	30.1	30.2
TC46	$T_{wi,gal}$	35.2	35.4	35.5	35.5	35.7
TC47	$T_{wi,gal}$	35.5	35.8	36.0	36.0	36.0

Notes: (1) see Figure 3.7 and Figure 3.8 for thermocouple (TC) location

(2) see Table 3.2 for T_i notation

Table B.3.b Air-Only Tests Raw Data – A0429-11 to A0429-15

TEST ID	P_{atm} (kPa)	ϕ_{in} (%)	$\overline{T}_{stm}$ (°C)	$\overline{T}_{wo}$ (°C)	$\overline{T}_{air,in}$ (°C)
A0429-11	102.5	32.0	109.3	108.7	25.6
A0429-12	102.5	32.0	109.3	108.7	26.2
A0429-13	102.5	32.0	108.9	108.3	25.4
A0429-14	102.5	32.0	108.8	108.2	25.9
A0429-15	102.5	32.0	108.7	108.2	25.6
TEST ID	$\overline{T}_{air,o}$ (°C)	$\overline{T}_{wi,PVC}$ (°C)	$\overline{T}_{wi,gal}$ (°C)	$\overline{V}_{air}$ (m/s)	$\dot{m}_{cond}$ (10^{-3}kg/s)
A0429-11	40.2	29.0	35.4	1.63	1.03
A0429-12	40.4	29.6	35.6	1.69	1.06
A0429-13	40.5	29.9	35.7	1.65	1.06
A0429-14	40.5	29.9	35.8	1.70	1.07
A0429-15	40.5	29.9	35.8	1.63	1.07

Table B.3.c Air-Only Test Results – A0429-11 to A0429-15

TEST ID	$\overline{T}_{stm}$ (°C)	$\dot{Q}_{cond}$ (kw)	$\dot{Q}_{air}$ (kw)	$\dot{Q}_{rad}$ (kw)	$\overline{q}''_{air}$ (kw/m^2)
A0429-11	109.3	2.29	2.07	0.80	0.94
A0429-12	109.3	2.37	2.15	0.80	0.97
A0429-13	108.9	2.38	2.13	0.79	0.97
A0429-14	108.8	2.38	2.17	0.79	0.98
A0429-15	108.7	2.39	2.09	0.78	0.95
TEST ID	$\overline{h}_{air,eff}$ (w/m^2°C)	$\overline{h}_{air,conv}$ (w/m^2°C)	Re ($\times 10^4$)	$\dot{m}_{air}$ (10^{-1}kg/s)	$\frac{\dot{Q}_{cond}}{\dot{Q}_{air}}$
A0429-11	12.33	7.57	2.14	1.35	1.11
A0429-12	12.83	8.08	2.22	1.40	1.11
A0429-13	12.80	8.07	2.16	1.37	1.12
A0429-14	13.09	8.35	2.23	1.41	1.10
A0429-15	12.60	7.87	2.14	1.35	1.14

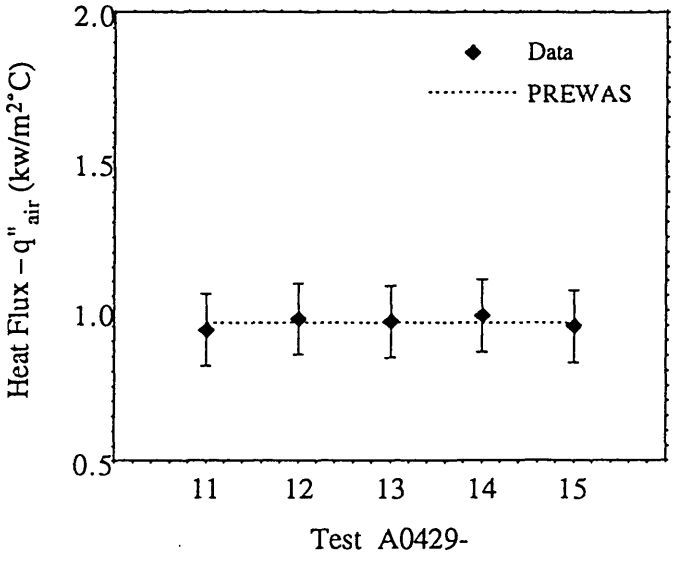

Figure B.3.a A0429-11 to 15 Test Results – Heat Flux

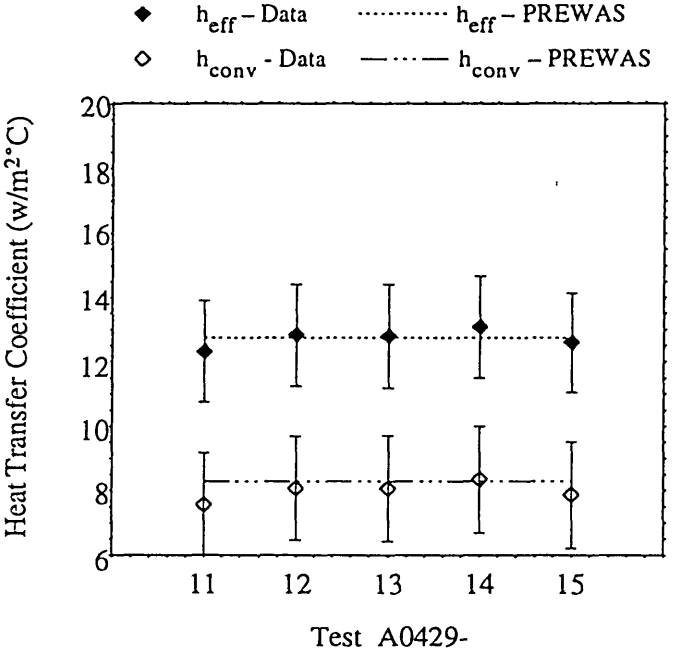

Figure B.3.b A0429-11 to 15 Test Results – Heat Transfer Coefficient

Table B.4.a Air-Only Tests Thermocouple Raw Data – A0429-21 to A0429-25

TC ID	Function	A0429-21 (°C)	A0429-22 (°C)	A0429-23 (°C)	A0429-24 (°C)	A0429-25 (°C)
TC1	T_{wo}	103.4	103.4	103.4	103.3	103.4
TC2	T_{wo}	103.9	103.9	103.8	103.7	103.9
TC3	T_{wo}	103.9	103.9	103.9	103.7	103.9
TC4	T_{wo}	104.0	104.0	103.9	103.8	104.0
TC5	T_{wo}	103.6	103.6	103.6	103.4	103.6
TC6	T_{wo}	103.6	103.6	103.6	103.4	103.7
TC7	T_{wo}	103.7	103.6	103.6	103.4	103.7
TC8	T_{wo}	103.8	103.8	103.7	103.6	103.8
TC9	T_{wo}	103.7	103.7	103.6	103.5	103.7
TC10	T_{wo}	103.7	103.7	103.5	103.5	103.7
TC11	T_{stm}	104.1	104.1	104.1	104.0	104.1
TC12	T_{stm}	104.3	104.3	104.3	104.1	104.3
TC13	T_{stm}	104.3	104.3	104.2	104.1	104.3
TC14	T_{stm}	104.4	104.4	104.3	104.2	104.4
TC15	T_{stm}	104.3	104.3	104.2	104.1	104.3
TC31	$T_{air,o}$	40.4	40.5	40.4	40.5	40.4
TC40	heat loss estimation	40.8	40.9	40.8	40.9	40.8
TC41	heat loss estimation	40.8	40.9	40.8	40.8	41.0
TC43	$T_{air,in}$	25.6	25.5	25.5	25.9	25.8
TC44	$T_{wi,PVC}$	29.9	30.0	29.9	30.0	29.9
TC45	$T_{wi,PVC}$	31.5	31.4	31.4	31.4	31.4
TC46	$T_{wi,gal}$	35.8	36.0	35.9	35.9	35.9
TC47	$T_{wi,gal}$	36.1	36.2	36.2	36.3	36.1

Notes: (1) see Figure 3.7 and Figure 3.8 for thermocouple (TC) location

(2) see Table 3.2 for T_i notation

Table B.4.b Air-Only Tests Raw Data – A0429-21 to A0429-25

TEST ID	P_{atm} (kPa)	ϕ_{in} (%)	$\overline{T}_{stm}$ (°C)	$\overline{T}_{wo}$ (°C)	$\overline{T}_{air,in}$ (°C)
A0429-21	102.5	35.0	104.3	103.7	25.6
A0429-22	102.5	35.0	104.3	103.7	25.5
A0429-23	102.5	35.0	104.2	103.7	25.5
A0429-24	102.5	35.0	104.1	103.5	25.9
A0429-25	102.5	35.0	104.3	103.7	25.8
TEST ID	$\overline{T}_{air,o}$ (°C)	$\overline{T}_{wi,PVC}$ (°C)	$\overline{T}_{wi,gal}$ (°C)	$\overline{V}_{air}$ (m/s)	$\dot{m}_{cond}$ (10^{-3}kg/s)
A0429-21	40.4	30.7	36.0	1.63	1.05
A0429-22	40.5	30.7	36.1	1.61	1.02
A0429-23	40.4	30.7	36.0	1.60	1.04
A0429-24	40.5	30.7	36.1	1.62	1.03
A0429-25	40.4	30.7	36.0	1.60	1.00

Table B.4.c Air-Only Test Results – A0429-21 to A0429-25

TEST ID	$\overline{T}_{stm}$ (°C)	$\dot{Q}_{cond}$ (kw)	$\dot{Q}_{air}$ (kw)	$\dot{Q}_{rad}$ (kw)	$\overline{q}''_{air}$ (kw/m^2)
A0429-21	104.3	2.34	2.02	0.72	0.92
A0429-22	104.3	2.29	2.03	0.72	0.92
A0429-23	104.2	2.34	2.22	0.72	0.91
A0429-24	104.1	2.32	1.99	0.72	0.90
A0429-25	104.3	2.25	1.97	0.72	0.89
TEST ID	$\overline{h}_{air,eff}$ (w/m^2°C)	$\overline{h}_{air,conv}$ (w/m^2°C)	Re ($\times 10^4$)	$\dot{m}_{air}$ (10^{-1}kg/s)	$\frac{\dot{Q}_{cond}}{\dot{Q}_{air}}$
A0429-21	12.98	8.36	2.13	1.35	1.16
A0429-22	13.01	8.39	2.11	1.33	1.13
A0429-23	12.87	8.25	2.10	1.32	1.17
A0429-24	12.85	8.22	2.12	1.34	1.16
A0429-25	12.62	8.00	2.10	1.32	1.14

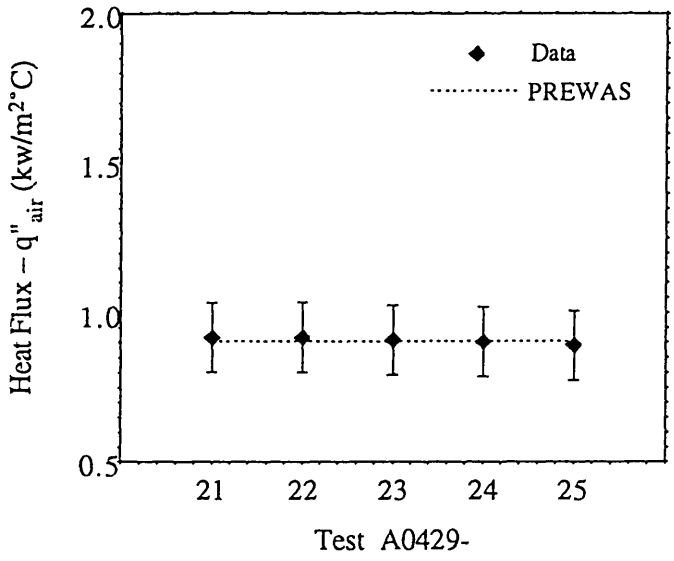

Figure B.4.a A0429-21 to 25 Test Results – Heat Flux

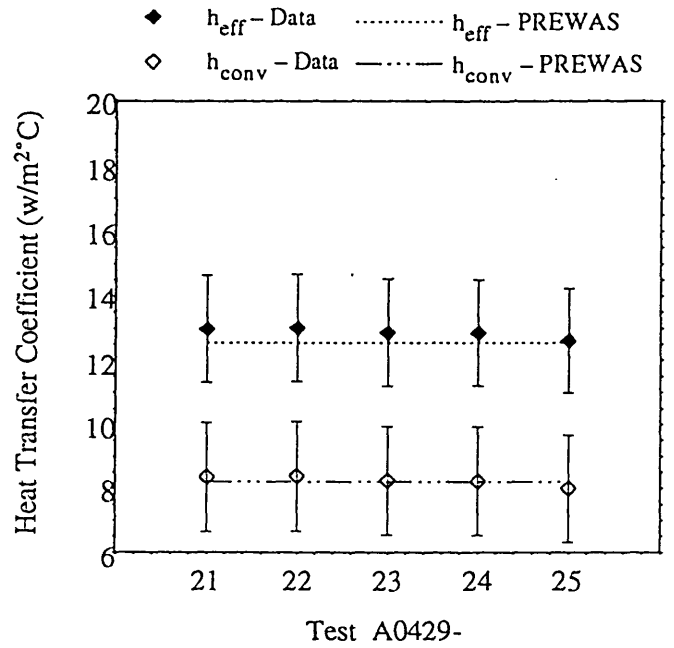

Figure B.4.b A0429-21 to 25 Test Results – Heat Transfer Coefficient

Table B.5.a Air-Only Tests Thermocouple Raw Data – A0430-11 to A0430-15

TC ID	Function	A0430-11 (°C)	A0430-12 (°C)	A0430-13 (°C)	A0430-14 (°C)	A0430-15 (°C)
TC1	T_{wo}	119.8	119.9	119.7	119.2	119.2
TC2	T_{wo}	120.2	120.3	120.1	119.6	119.5
TC3	T_{wo}	120.3	120.4	120.2	119.7	119.6
TC4	T_{wo}	120.3	120.4	120.3	119.8	119.7
TC5	T_{wo}	119.9	120.0	119.9	119.4	119.3
TC6	T_{wo}	119.9	120.0	119.8	119.4	119.3
TC7	T_{wo}	120.0	120.0	119.9	119.4	119.3
TC8	T_{wo}	120.2	120.2	120.1	119.6	119.5
TC9	T_{wo}	120.0	120.1	119.9	119.4	119.3
TC10	T_{wo}	119.9	120.1	120.0	119.5	119.4
TC11	T_{stm}	120.7	120.7	120.5	120.0	120.1
TC12	T_{stm}	120.8	120.9	120.7	120.2	120.2
TC13	T_{stm}	120.8	120.8	120.6	120.1	120.1
TC14	T_{stm}	120.9	120.9	120.7	120.3	120.3
TC15	T_{stm}	120.8	120.8	120.6	120.1	120.2
TC31	$T_{air,o}$	43.9	43.9	44.1	44.3	44.3
TC40	heat loss estimation	44.3	44.3	44.5	44.7	44.7
TC41	heat loss estimation	44.3	44.5	44.5	44.7	44.8
TC43	$T_{air,in}$	26.0	25.9	26.1	26.2	26.2
TC44	$T_{wi,PVC}$	31.1	31.1	31.2	31.2	31.3
TC45	$T_{wi,PVC}$	32.6	32.6	32.7	32.7	32.8
TC46	$T_{wi,gal}$	38.2	38.2	38.2	38.3	38.4
TC47	$T_{wi,gal}$	38.8	38.7	38.9	39.0	39.2

Notes: (1) see Figure 3.7 and Figure 3.8 for thermocouple (TC) location

(2) see Table 3.2 for T_i notation

Table B.5.b Air-Only Tests Raw Data – A0430-11 to A0430-15

TEST ID	P_{atm} (kPa)	ϕ_{in} (%)	$\overline{\overline{T}}_{stm}$ (°C)	$\overline{\overline{T}}_{wo}$ (°C)	$\overline{\overline{T}}_{air,in}$ (°C)
A0430-11	102.3	38.0	120.8	120.1	26.0
A0430-12	102.3	38.0	120.8	120.1	25.9
A0430-13	102.3	38.0	120.6	120.0	26.1
A0430-14	102.3	38.0	120.1	119.5	26.2
A0430-15	102.3	38.0	120.2	119.4	26.2
TEST ID	$\overline{\overline{T}}_{air,o}$ (°C)	$\overline{\overline{T}}_{wi,PVC}$ (°C)	$\overline{\overline{T}}_{wi,gal}$ (°C)	$\overline{V}_{air}$ (m/s)	$\dot{m}_{cond}$ (10^{-3}kg/s)
A0430-11	43.9	31.8	38.5	1.70	1.30
A0430-12	43.9	31.9	38.5	1.72	1.29
A0430-13	44.1	31.9	38.5	1.71	1.32
A0430-14	44.3	32.0	38.7	1.71	1.29
A0430-15	44.3	32.0	38.9	1.68	1.30

Table B.5.c Air-Only Test Results – A0430-11 to A0430-15

TEST ID	$\overline{\overline{T}}_{stm}$ (°C)	$\dot{Q}_{cond}$ (kw)	$\dot{Q}_{air}$ (kw)	$\dot{Q}_{rad}$ (kw)	$\overline{q}''_{air}$ (kw/m^2)
A0430-11	120.8	2.87	2.53	0.94	1.15
A0430-12	120.8	2.83	2.58	0.94	1.17
A0430-13	120.6	2.90	2.56	0.94	1.16
A0430-14	120.1	2.84	2.57	0.93	1.16
A0430-15	120.2	2.86	2.53	0.93	1.15
TEST ID	$\overline{h}_{air,eff}$ (w/m^2°C)	$\overline{h}_{air,conv}$ (w/m^2°C)	Re ($\times 10^4$)	$\dot{m}_{air}$ (10^{-1}kg/s)	$\frac{\dot{Q}_{cond}}{\dot{Q}_{air}}$
A0430-11	13.47	8.45	2.19	1.39	1.14
A0430-12	13.72	8.70	2.21	1.40	1.10
A0430-13	13.70	8.66	2.20	1.40	1.13
A0430-14	13.82	8.79	2.20	1.39	1.11
A0430-15	13.63	8.59	2.16	1.37	1.13

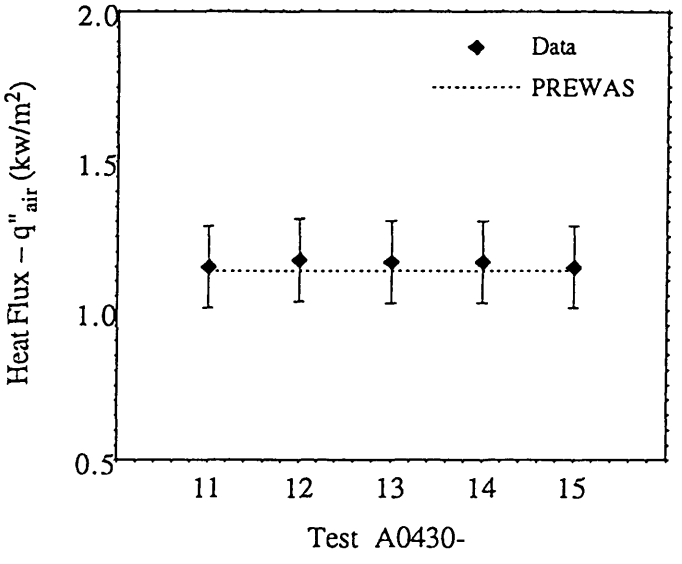

Figure B.5.a A0430 Test Results – Heat Flux

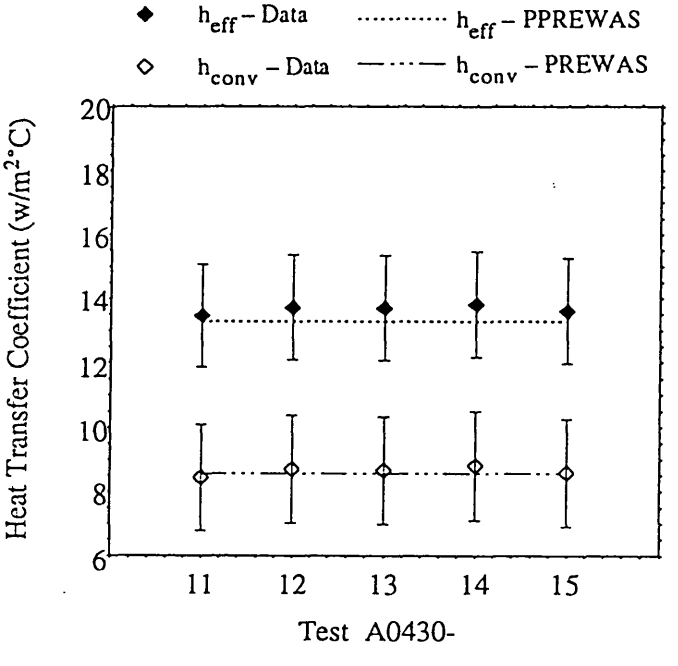

Figure B.5.b A0430 Test Results – Heat Transfer Coefficient

Table B.6.a Air-Only Tests Thermocouple Raw Data – A0502-11 to A0502-15

TC ID	Function	A0502-11 (°C)	A0502-12 (°C)	A0502-13 (°C)	A0502-14 (°C)	A0502-15 (°C)
TC1	T_{wo}	118.5	118.5	118.5	118.5	118.6
TC2	T_{wo}	119.3	119.3	119.3	119.4	119.4
TC3	T_{wo}	119.3	119.3	119.3	119.3	119.3
TC4	T_{wo}	119.6	119.5	119.5	119.6	119.6
TC5	T_{wo}	119.2	119.2	119.3	119.3	119.2
TC6	T_{wo}	119.5	119.4	119.5	119.5	119.5
TC7	T_{wo}	119.4	119.3	119.4	119.4	119.4
TC8	T_{wo}	119.5	119.5	119.5	119.6	119.5
TC9	T_{wo}	119.4	119.3	119.4	119.4	119.4
TC10	T_{wo}	119.4	119.4	119.4	119.5	119.4
TC11	T_{stm}	119.8	120.0	120.0	120.0	120.0
TC12	T_{stm}	120.1	120.0	120.1	120.1	120.1
TC13	T_{stm}	120.0	120.0	120.0	120.1	120.0
TC14	T_{stm}	120.2	120.1	120.2	120.2	120.2
TC15	T_{stm}	120.1	120.0	120.0	120.1	120.1
TC31	$T_{air,o}$	45.7	45.5	45.6	45.7	45.7
TC40	heat loss estimation	46.1	45.9	46.0	46.2	46.1
TC41	heat loss estimation	46.2	46.1	46.1	46.2	46.2
TC43	$T_{air,in}$	26.0	25.9	25.9	25.9	26.0
TC44	$T_{wi,PVC}$	32.2	32.0	32.0	32.1	32.1
TC45	$T_{wi,PVC}$	30.9	30.3	30.4	30.6	30.7
TC46	$T_{wi,gal}$	39.2	39.0	39.0	39.2	39.2
TC47	$T_{wi,gal}$	39.3	39.0	39.1	39.2	39.2

Notes: (1) see Figure 3.7 and Figure 3.8 for thermocouple (TC) location

(2) see Table 3.2 for T_i notation

(3) upper air windows were sealed in A0502-11 ~ A0502-15.

Table B.6.b Air-Only Tests Raw Data – A0502-11 to A0502-15

TEST ID	P_{atm} (kPa)	ϕ_{in} (%)	$\overline{T}_{stm}$ (°C)	$\overline{T}_{wo}$ (°C)	$\overline{T}_{air,in}$ (°C)
A0502-11	102.6	21.5	120.0	119.3	26.0
A0502-12	102.6	21.5	120.0	119.3	25.9
A0502-13	102.6	21.5	120.1	119.3	25.9
A0502-14	102.6	21.5	120.1	119.3	25.9
A0502-15	102.6	21.5	120.1	119.3	26.0
TEST ID	$\overline{T}_{air,o}$ (°C)	$\overline{T}_{wi,PVC}$ (°C)	$\overline{T}_{wi,gal}$ (°C)	$\overline{V}_{air}$ (m/s)	$\dot{m}_{cond}$ (10^{-3}kg/s)
A0502-11	45.7	31.5	39.2	1.63	1.29
A0502-12	45.5	31.1	39.0	1.60	1.28
A0502-13	45.6	31.2	39.0	1.60	1.29
A0502-14	45.7	31.3	39.2	1.59	1.28
A0502-15	45.7	31.4	39.2	1.63	1.31

Table B.6.c Air-Only Test Results – A0502-11 to A0502-15

TEST ID	$\overline{T}_{stm}$ (°C)	$\dot{Q}_{cond}$ (kw)	$\dot{Q}_{air}$ (kw)	$\dot{Q}_{rad}$ (kw)	$\overline{q}''_{air}$ (kw/m^2)
A0502-11	120.0	2.84	2.66	0.93	1.21
A0502-12	120.0	2.82	2.58	0.93	1.17
A0502-13	120.1	2.84	2.60	0.93	1.18
A0502-14	120.1	2.83	2.60	0.93	1.18
A0502-15	120.1	2.87	2.66	0.93	1.21
TEST ID	$\overline{h}_{air,eff}$ (w/m^2°C)	$\overline{h}_{air,conv}$ (w/m^2°C)	Re ($\times 10^4$)	$\dot{m}_{air}$ (10^{-1}kg/s)	$\frac{\dot{Q}_{cond}}{\dot{Q}_{air}}$
A0502-11	14.46	9.39	2.09	1.33	1.07
A0502-12	14.03	8.96	2.05	1.31	1.09
A0502-13	14.12	9.04	2.05	1.31	1.09
A0502-14	14.15	9.08	2.04	1.30	1.09
A0502-15	14.44	9.37	2.09	1.33	1.08

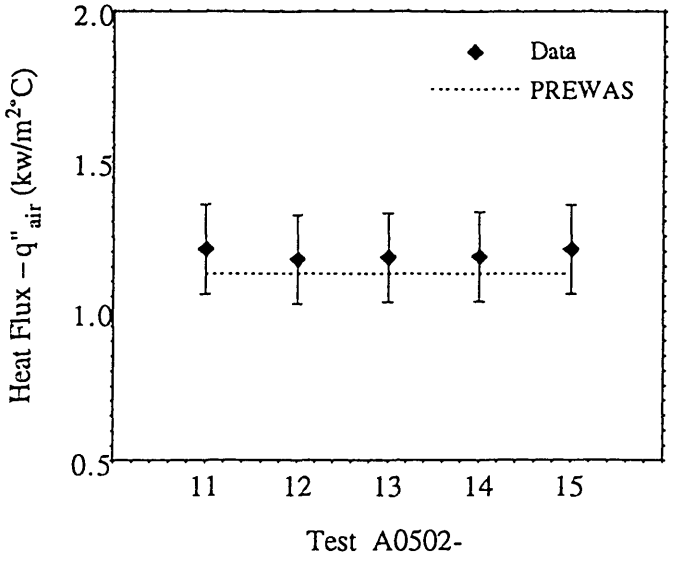

Figure B.6.a A0502 Test Results – Heat Flux

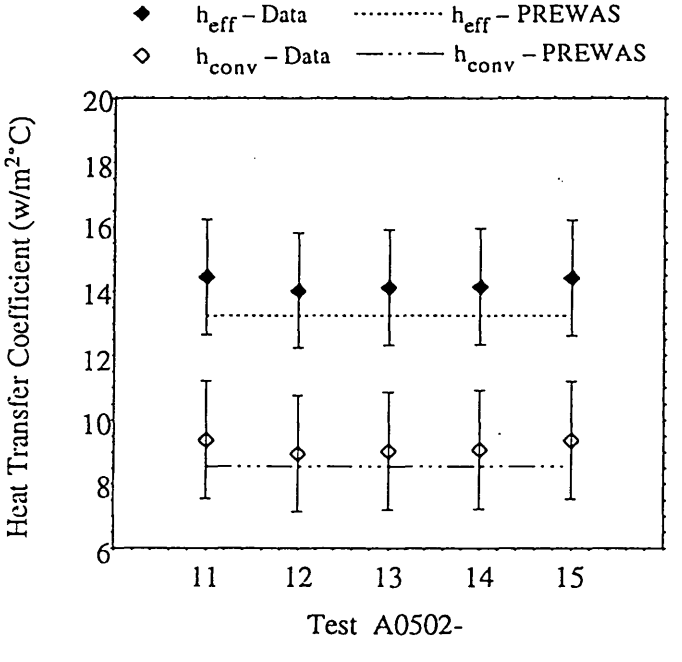

Figure B.6.b A0502 Test Results – Heat Transfer Coefficient

Table B.7.a Air-Only Tests Thermocouple Raw Data – A0503-11 to A0503-15

TC ID	Function	A0503-11 (°C)	A0503-12 (°C)	A0503-13 (°C)	A0503-14 (°C)	A0503-15 (°C)
TC1	T_{wo}	129.0	129.0	129.1	129.1	129.1
TC2	T_{wo}	129.5	129.5	129.5	129.6	129.6
TC3	T_{wo}	129.5	129.5	129.6	129.6	129.6
TC4	T_{wo}	129.6	129.6	129.6	129.6	129.7
TC5	T_{wo}	129.1	129.1	129.2	129.1	129.2
TC6	T_{wo}	129.1	129.1	129.2	129.2	129.3
TC7	T_{wo}	129.2	129.2	129.2	129.2	129.3
TC8	T_{wo}	129.4	129.4	129.5	129.5	129.5
TC9	T_{wo}	129.2	129.2	129.3	129.3	129.4
TC10	T_{wo}	129.3	129.2	129.3	129.4	129.5
TC11	T_{stm}	130.1	130.1	130.1	130.1	130.1
TC12	T_{stm}	130.1	130.1	130.2	130.2	130.2
TC13	T_{stm}	130.0	130.1	130.1	130.1	130.2
TC14	T_{stm}	130.2	130.2	130.3	130.3	130.3
TC15	T_{stm}	130.1	130.1	130.1	130.2	130.2
TC31	$T_{air,o}$	45.1	45.2	45.2	45.2	45.4
TC40	heat loss estimation	45.5	45.7	45.6	45.6	45.9
TC41	heat loss estimation	45.6	45.7	45.7	45.7	45.9
TC43	$T_{air,in}$	26.2	26.2	25.9	25.9	26.2
TC44	$T_{wi,PVC}$	32.2	32.1	32.1	32.1	32.2
TC45	$T_{wi,PVC}$	33.2	33.3	33.3	33.4	33.5
TC46	$T_{wi,gal}$	39.3	39.5	39.5	39.5	39.6
TC47	$T_{wi,gal}$	39.4	39.7	39.8	39.9	39.9

Notes: (1) see Figure 3.7 and Figure 3.8 for thermocouple (TC) location

(2) see Table 3.2 for T_i notation

Table B.7.b Air-Only Tests Raw Data – A0503-11 to A0503-15

TEST ID	P_{atm} (kPa)	ϕ_{in} (%)	$\overline{T}_{stm}$ (°C)	$\overline{T}_{wo}$ (°C)	$\overline{T}_{air,in}$ (°C)
A0503-11	102.8	22.0	130.1	129.3	26.2
A0503-12	102.8	22.0	130.1	129.3	26.2
A0503-13	102.8	22.0	130.2	129.4	25.9
A0503-14	102.8	22.0	130.2	129.4	25.9
A0503-15	102.8	22.0	130.2	129.4	26.2
TEST ID	$\overline{T}_{air,o}$ (°C)	$\overline{T}_{wi,PVC}$ (°C)	$\overline{T}_{wi,gal}$ (°C)	$\overline{V}_{air}$ (m/s)	$\dot{m}_{cond}$ (10^{-3}kg/s)
A0503-11	45.1	32.7	39.4	1.85	1.43
A0503-12	45.2	32.7	39.6	1.85	1.43
A0503-13	45.2	32.7	39.7	1.84	1.41
A0503-14	45.2	32.7	39.7	1.86	1.43
A0503-15	45.4	32.8	39.8	1.83	1.44

Table B.7.c Air-Only Test Results – A0503-11 to A0503-15

TEST ID	$\overline{T}_{stm}$ (°C)	$\dot{Q}_{cond}$ (kw)	$\dot{Q}_{air}$ (kw)	$\dot{Q}_{rad}$ (kw)	$\overline{q}''_{air}$ (kw/m²)
A0503-11	130.1	3.10	2.90	1.08	1.32
A0503-12	130.1	3.10	2.91	1.08	1.32
A0503-13	130.2	3.07	2.95	1.08	1.34
A0503-14	130.2	3.10	2.97	1.08	1.35
A0503-15	130.2	3.13	2.92	1.08	1.32
TEST ID	$\overline{h}_{air,eff}$ (w/m²°C)	$\overline{h}_{air,conv}$ (w/m²°C)	Re ($\times 10^4$)	$\dot{m}_{air}$ (10^{-1}kg/s)	$\frac{\dot{Q}_{cond}}{\dot{Q}_{air}}$
A0503-11	14.06	8.81	2.38	1.52	1.07
A0503-12	14.11	8.86	2.37	1.51	1.07
A0503-13	14.24	9.01	2.36	1.50	1.04
A0503-14	14.37	9.13	2.39	1.52	1.04
A0503-15	14.15	8.90	2.35	1.50	1.07

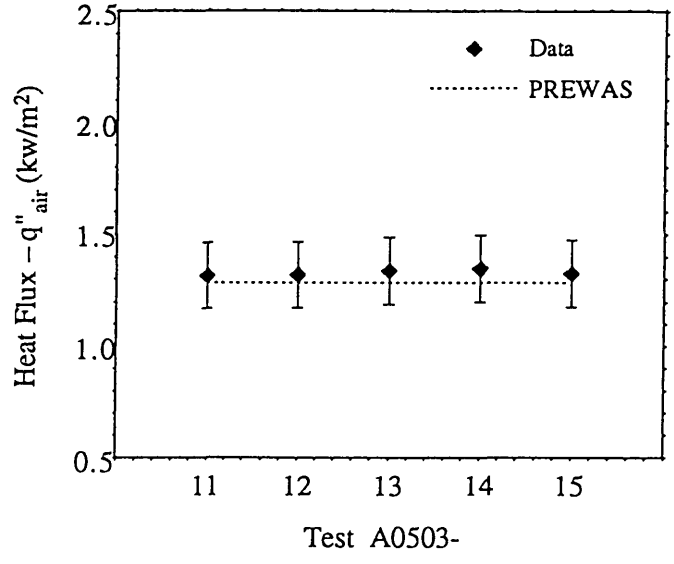

Figure B.7.a A0503-11 to 15 Test Results – Heat Flux

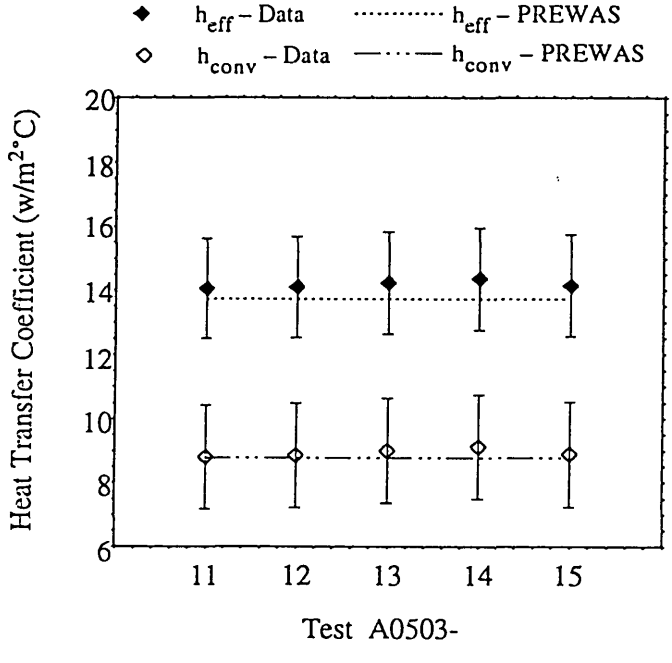

Figure B.7.b A0503-11 to 15 Test Results – Heat Transfer Coefficient

Table B.8.a Air-Only Tests Thermocouple Raw Data – A0503-21 to A0503-25

TC ID	Function	A0503-21 (°C)	A0503-22 (°C)	A0503-23 (°C)	A0503-24 (°C)	A0503-25 (°C)
TC1	T_{wo}	139.0	139.4	139.4	139.3	139.2
TC2	T_{wo}	139.5	139.9	139.9	139.9	139.8
TC3	T_{wo}	139.5	139.9	139.9	139.9	139.9
TC4	T_{wo}	139.6	140.0	140.0	140.0	139.9
TC5	T_{wo}	139.0	139.5	139.6	139.4	139.4
TC6	T_{wo}	139.1	139.5	139.5	139.5	139.4
TC7	T_{wo}	139.1	139.6	139.6	139.6	139.4
TC8	T_{wo}	139.4	139.8	139.9	139.8	139.7
TC9	T_{wo}	139.2	139.6	139.6	139.6	139.5
TC10	T_{wo}	139.3	139.7	139.8	139.6	139.6
TC11	T_{stm}	140.2	140.6	140.5	140.4	140.3
TC12	T_{stm}	140.2	140.6	140.6	140.6	140.5
TC13	T_{stm}	140.2	140.5	140.6	140.5	140.5
TC14	T_{stm}	140.3	140.7	140.7	140.7	140.6
TC15	T_{stm}	140.2	140.6	140.6	140.5	140.5
TC31	$T_{air,o}$	47.3	47.5	47.7	48.1	47.6
TC40	heat loss estimation	47.8	48.0	48.1	48.6	48.1
TC41	heat loss estimation	47.8	48.1	48.1	48.6	48.0
TC43	$T_{air,in}$	26.3	26.4	26.3	26.2	26.3
TC44	$T_{wi,PVC}$	32.9	33.0	33.0	33.2	33.2
TC45	$T_{wi,PVC}$	34.2	34.3	34.5	34.7	34.9
TC46	$T_{wi,gal}$	41.5	41.7	41.7	42.1	41.9
TC47	$T_{wi,gal}$	41.5	41.5	42.1	42.4	42.1

Notes: (1) see Figure 3.7 and Figure 3.8 for thermocouple (TC) location

(2) see Table 3.2 for T_i notation

Table B.8.b Air-Only Tests Raw Data – A0503-21 to A0503-25

TEST ID	P_{atm} (kPa)	ϕ_{in} (%)	$\overline{T}_{stm}$ (°C)	$\overline{T}_{wo}$ (°C)	$\overline{T}_{air,in}$ (°C)
A0503-21	102.8	22.5	140.2	139.3	26.3
A0503-22	102.8	22.5	140.6	139.7	26.4
A0503-23	102.8	22.5	140.6	139.7	26.3
A0503-24	102.8	22.5	140.5	139.7	26.2
A0503-25	102.8	22.5	140.5	139.6	26.3
TEST ID	$\overline{T}_{air,o}$ (°C)	$\overline{T}_{wi,PVC}$ (°C)	$\overline{T}_{wi,gal}$ (°C)	$\overline{V}_{air}$ (m/s)	$\dot{m}_{cond}$ (10^{-3}kg/s)
A0503-21	47.3	33.5	41.5	1.92	1.67
A0503-22	47.5	33.7	41.6	1.93	1.69
A0503-23	47.7	33.7	41.9	1.91	1.66
A0503-24	48.1	34.0	42.2	1.89	1.66
A0503-25	47.6	34.1	42.0	1.91	1.65

Table B.8.c Air-Only Test Results – A0503-21 to A0503-25

TEST ID	$\overline{T}_{stm}$ (°C)	$\dot{Q}_{cond}$ (kw)	$\dot{Q}_{air}$ (kw)	$\dot{Q}_{rad}$ (kw)	$\overline{q}''_{air}$ (kw/m²)
A0503-21	140.2	3.57	3.33	1.24	1.51
A0503-22	140.6	3.63	3.36	1.25	1.52
A0503-23	140.6	3.56	3.37	1.25	1.53
A0503-24	140.5	3.56	3.41	1.25	1.55
A0503-25	140.5	3.54	3.36	1.24	1.53
TEST ID	$\overline{h}_{air,eff}$ (w/m²°C)	$\overline{h}_{air,conv}$ (w/m²°C)	Re ($\times 10^4$)	$\dot{m}_{air}$ (10^{-1}kg/s)	$\frac{\dot{Q}_{cond}}{\dot{Q}_{air}}$
A0503-21	14.75	9.24	2.45	1.56	1.07
A0503-22	14.84	9.32	2.46	1.57	1.08
A0503-23	14.91	9.39	2.43	1.55	1.05
A0503-24	15.08	9.56	2.40	1.53	1.05
A0503-25	14.87	9.37	2.43	1.55	1.05

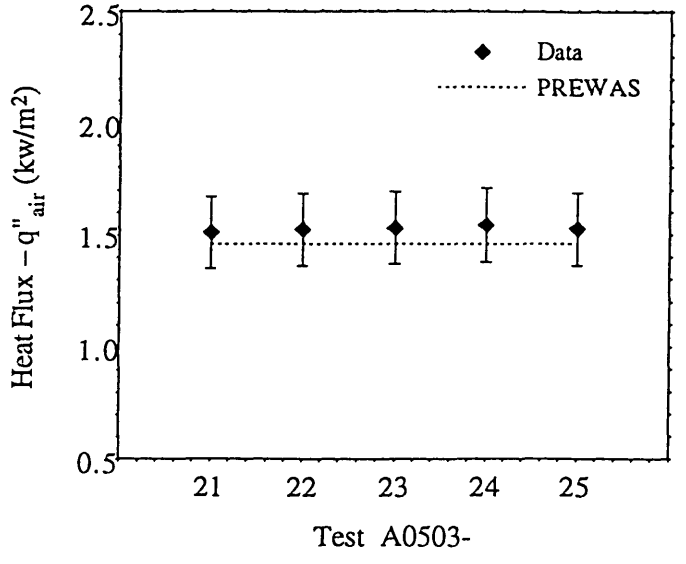

Figure B.8.a A0503-21 to 25 Test Results – Heat Flux

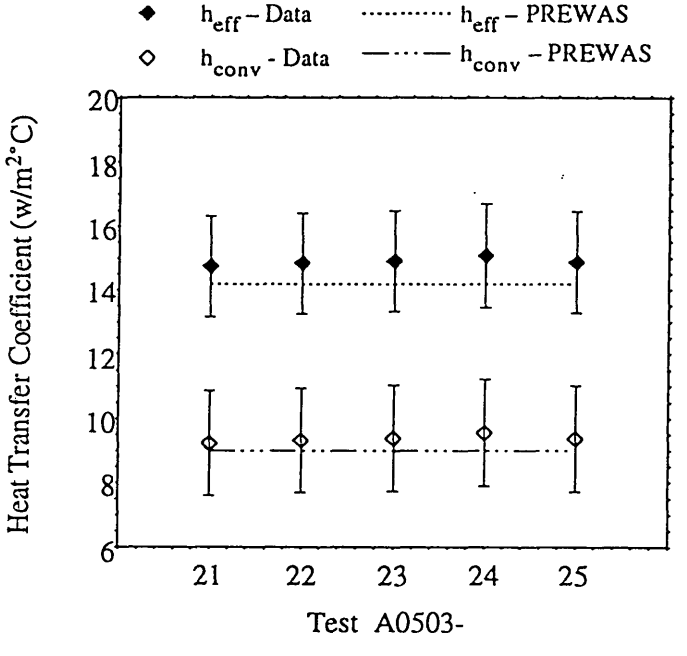

Figure B.8.b A0503-21 to 25 Test Results – Heat Transfer Coefficient

B.2 Summary of Water-Filled Tests

The results of the experiment for the water-filled tests are presented in this section. There are eight groups of test results, which were obtained between February 22, 1994 and April 30, 1994. Each test run documents the progress of the test with time for a given set of initial conditions and boundary conditions. Data are taken at various time intervals during each test. Two data sets taken at the adjacent time step are used to evaluate the heat transfer performance. The notation of the test identification number and the assigned file number for the analysis are described as follows.

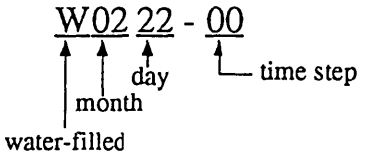

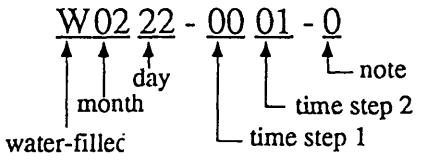

Note: 0 – evaluate the steam generation rate by humidity measurement

1 – evaluate the steam generation rate by water level measurement

The results of each water-filled test are also presented in three tables and two figures. The first two tables show the raw data of the test. The third table shows the results of the data analysis. The figures show the heat flux and the heat transfer coefficient, with their associated uncertainty as a function of time. The corresponding steam generation rates for data shown in the figures are evaluated by humidity measurement. Also included in these figures are the prediction of the heat flux and the heat transfer coefficient by PREWAS (see Appendix C for details). The estimated air to steam mass ratio in the water-filled tests are: 0.2 % for W0401, W0405,W0408, W0412, and W0430; 2 % for W0315; 3.5 % for W0304; and 4 % for W0222. The higher noncondensable concentrations for the high temperature tests (W0222, W0304, and W0315) come from the fact that the pool section heated wall outer surface temperatures are not uniformly distributed. The input form loss coefficient, emissivity, and conductivity of stainless steel are the same as in section B.1. The correlation constant for the nucleate boiling heat transfer coefficient (C_{sf}) in Equation C.16 is set to be 0.013 [C-2].

Table B.9.a Water-Filled Test Thermocouple Raw Data – W0222

TC ID	Function	W0222-00 (°C)	W0222-01 (°C)	W0222-02 (°C)	W0222-03 (°C)	W0222-04 (°C)	W0222-05 (°C)	W0222-06 (°C)	W0222-07 (°C)	W0222-08 (°C)
TC1	T_{wo}	-	90.0	101.9	107.0	107.6	107.6	107.5	107.5	107.4
TC2	T_{wo}	-	102.2	112.6	113.3	113.5	113.6	113.7	113.7	114.1
TC3	T_{wo}	-	142.5	145.2	145.2	144.5	145.0	144.8	144.9	145.1
TC4	T_{wo}	-	142.6	145.2	145.2	144.6	145.0	144.8	144.9	145.1
TC5	T_{wo}	-	140.5	143.1	143.1	142.3	142.9	142.6	142.8	143.1
TC6	T_{wo}	-	142.1	144.5	144.4	143.7	144.1	143.9	143.9	144.1
TC7	T_{wo}	-	142.0	144.4	144.3	143.5	144.0	143.8	144.0	144.1
TC8	T_{wo}	-	142.4	144.9	144.7	144.0	144.4	144.3	144.4	144.5
TC9	T_{wo}	-	142.2	144.6	144.4	143.5	144.0	143.9	144.0	144.1
TC10	T_{wo}	-	142.3	144.8	144.6	143.9	144.3	144.1	144.2	144.3
TC11	T_{stm}	-	143.3	145.9	145.7	145.0	145.4	145.2	145.4	145.5
TC12	T_{stm}	-	143.3	145.9	145.7	144.9	145.4	145.2	145.3	145.5
TC13	T_{stm}	-	143.3	145.9	145.7	144.9	145.3	145.2	145.3	145.4
TC14	T_{stm}	-	143.5	146.0	145.9	145.1	145.5	145.3	145.5	145.6
TC15	T_{stm}	-	143.3	145.9	145.7	144.9	145.5	145.4	145.3	145.5
TC16	T_{pi}	19.5	43.1	75.1	99.2	100.1	99.8	100.0	100.2	100.6
TC17	T_{pi}	27.4	59.7	90.8	100.5	100.6	100.6	100.6	100.6	100.6
TC21	T_{po}	15.1	16.3	19.4	20.9	29.0	45.0	72.2	94.6	98.9
TC22	T_{po}	19.2	19.4	20.0	21.2	29.2	45.2	71.5	93.3	98.7
TC31	$T_{mix,o}$	-	42.0	43.8	46.5	48.8	49.9	50.5	51.7	53.1
TC40	heat loss estimation	-	42.6	44.2	47.2	49.3	50.3	50.4	52.2	53.6
TC41	heat loss estimation	-	42.6	44.2	47.2	49.1	49.9	50.1	51.7	54.2
TC43	$T_{air,in}$	25.6	25.7	25.8	25.7	25.7	26.0	26.8	27.9	28.3
TC44	$T_{wi,PVC}$	-	30.4	30.8	31.8	36.1	37.5	37.3	38.6	41.2
TC45	$T_{wi,PVC}$	-	33.7	33.7	34.3	38.2	39.3	39.2	39.5	42.3
TC46	$T_{wi,gal}$	-	35.7	38.0	40.3	45.3	46.3	45.8	46.8	50.1
TC47	$T_{wi,gal}$	-	35.8	38.0	39.1	44.7	45.3	44.8	45.9	48.4

Notes: (1) see Figure 3.7 and Figure 3.8 for thermocouple (TC) location

(2) see Table 3.2 for T_i notation

Table B.9.b Water-Filled Test Raw Data – W0222

TEST ID	Time (min)	P_{atm} (kPa)	ϕ_{in} (%)	ϕ_o (%)	H_{pool} (m)	$\overline{T}_{stm}$ (°C)	$\overline{T}_{wo,pl}$ (°C)	$\overline{T}_{wo,mix}$ (°C)
W0222-00	0	102.0	29.5	-	1.524	-	-	-
W0222-01	3.45	102.0	29.5	9.5	1.524	143.3	96.1	142.1
W0222-02	8.27	102.0	29.5	14.5	1.524	145.9	107.3	144.6
W0222-03	11.72	102.0	29.5	52.5	1.524	145.7	110.2	144.5
W0222-04	21.53	102.0	29.5	82.6	1.495	145.0	110.5	143.8
W0222-05	38.05	102.1	30.0	77.0	1.449	145.4	110.6	144.2
W0222-06	68.20	102.1	31.0	70.5	1.368	145.2	110.6	144.0
W0222-07	102.45	102.3	31.0	86.3	1.283	145.4	110.6	144.1
W0222-08	129.32	102.3	31.0	81.0	1.192	145.5	110.7	144.3
TEST ID	$\overline{T}_{pi}$ (°C)	$\overline{T}_{po}$ (°C)	$\overline{T}_{air,in}$ (°C)	$\overline{T}_{mix,o}$ (°C)	$\overline{T}_{wi,PVC}$ (°C)	$\overline{T}_{wi,gal}$ (°C)	$\overline{V}_{mix}$ (m/s)	$\dot{m}_{cond}$ ($\times 10^{-3}$ kg/s)
W0222-00	23.5	17.2	25.6	-	-	-	-	-
W0222-01	51.4	17.9	25.7	42.0	32.0	35.7	1.94	29.26
W0222-02	83.0	19.7	25.8	43.8	32.3	38.0	2.00	22.80
W0222-03	99.8	21.1	25.7	46.5	33.1	39.7	2.44	23.09
W0222-04	100.4	29.1	25.7	48.8	37.1	45.0	2.46	22.04
W0222-05	100.2	45.1	26.0	49.9	38.4	45.8	2.59	21.77
W0222-06	100.3	71.8	26.8	50.5	38.3	45.3	2.50	20.28
W0222-07	100.4	94.0	27.9	51.7	39.0	46.3	2.46	17.54
W0222-08	100.6	98.9	28.3	53.1	41.8	49.2	2.64	17.54

Note that the humidities ϕ_{in}, ϕ_o are relative values at the corresponding local ambient temperature values. Hence it is possible for ϕ_{in} to exceed ϕ_o even though the actual mass per unit volume of water vapor is higher in the effluent. Also note that ϕ_o is much less than 100 %, so that there are no complications arising from condensation in the exit chimney.

Table B.9.c Water-Filled Test Results – W0222

TEST ID	$\dot{Q}_{cond}$ (kw)	$\dot{Q}_{pool}$ (kw)	$\dot{Q}_{mix}$ (kw)	$\dot{Q}_{rad}$ (kw)	$\bar{q}''_{pool}$ (kw/m^2)	$\bar{q}''_{mix}$ (kw/m^2)
W0222-0001-0	62.49	61.25	2.60	0.95	111.93	1.57
W0222-0102-0	48.59	52.77	2.70	0.96	96.42	1.63
W0222-0203-0	49.12	40.73	3.03	0.97	74.43	1.83
W0222-0304-0	46.91	31.75	3.13	0.96	58.56	1.88
W0222-0304-1	46.91	38.39	2.93	0.96	70.82	1.76
W0222-0405-0	46.34	40.00	3.20	0.95	75.64	1.91
W0222-0405-1	46.34	39.45	3.34	0.95	74.62	1.99
W0222-0506-0	43.17	37.08	3.35	0.96	72.15	1.98
W0222-0506-1	43.17	36.48	3.49	0.96	70.99	2.07
W0222-0607-0	37.34	34.38	3.09	0.98	72.24	1.79
W0222-0607-1	37.34	30.12	3.40	0.98	63.28	1.97
W0222-0708-0	37.34	31.78	3.08	0.99	71.53	1.75
W0222-0708-1	37.34	30.16	3.27	0.99	67.88	1.86
TEST ID	$\bar{h}_{pool}$ (kw/m^2°C)	$\bar{h}_{mix,eff}$ (w/m^2°C)	$\bar{h}_{mix,conv}$ (w/m^2°C)	Remix ($\times 10^4$)	$\dot{m}_{mix}$ (10^{-1}kg/s)	$\frac{\dot{Q}_{cond}}{\dot{Q}_{pool}+\dot{Q}_{mix}}$
W0222-0001-0	1.91	14.52	9.22	2.51	1.59	0.98
W0222-0102-0	2.79	14.99	9.65	2.54	1.61	0.88
W0222-0203-0	4.30	16.97	11.52	2.82	1.78	1.12
W0222-0304-0	5.89	18.08	12.55	3.07	1.93	1.34
W0222-0304-1	7.12	17.06	11.50	3.11	1.94	1.14
W0222-0405-0	7.36	18.70	13.16	3.14	1.96	1.07
W0222-0405-1	7.26	19.42	13.91	3.11	1.94	1.08
W0222-0506-0	6.78	19.46	13.90	3.15	1.97	1.07
W0222-0506-1	6.86	20.21	14.67	3.11	1.96	1.08
W0222-0607-0	7.04	17.84	12.19	3.05	1.91	1.00
W0222-0607-1	6.16	19.40	13.82	2.98	1.88	1.11
W0222-0708-0	7.02	17.68	11.99	3.12	1.95	1.07
W0222-0708-1	6.67	18.68	13.03	3.07	1.93	1.12

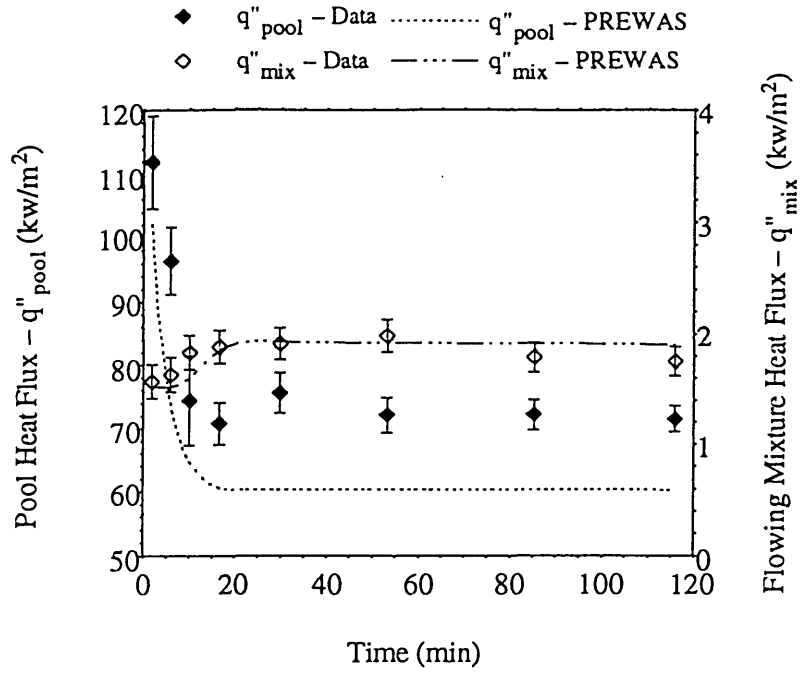

Figure B.9.a W0222 Test Results – Heat Flux

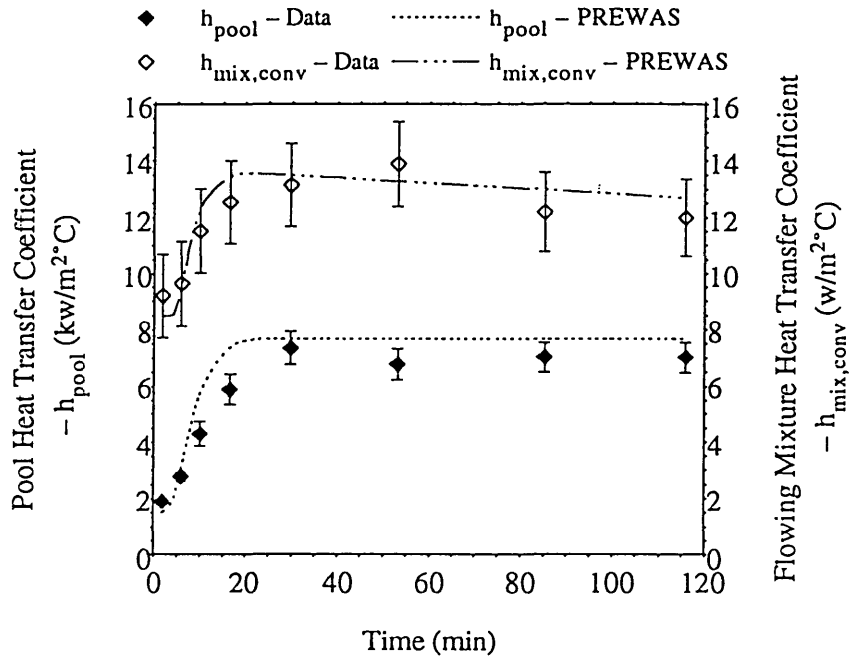

Figure B.9.b W0222 Test Results – Heat Transfer Coefficient

Table B.10.a Water-Filled Test Thermocouple Raw Data – W0304

TC ID	Function	W0304-00 (°C)	W0304-01 (°C)	W0304-02 (°C)	W0304-03 (°C)	W0304-04 (°C)	W0304-05 (°C)	W0304-06 (°C)	W0304-07 (°C)
TC1	T_{wo}	-	84.3	98.1	105.0	105.9	106.1	105.9	105.9
TC2	T_{wo}	-	98.0	108.6	109.8	110.5	110.5	110.6	110.7
TC3	T_{wo}	-	132.3	132.8	132.5	133.4	133.3	133.1	133.9
TC4	T_{wo}	-	132.3	132.8	132.4	133.4	133.3	133.1	133.9
TC5	T_{wo}	-	130.4	130.9	130.5	131.4	131.2	131.1	131.8
TC6	T_{wo}	-	131.9	132.3	131.7	132.6	132.5	132.3	133.2
TC7	T_{wo}	-	131.9	132.2	131.7	132.5	132.4	132.2	133.3
TC8	T_{wo}	-	132.2	132.6	132.1	132.9	132.8	132.6	133.5
TC9	T_{wo}	-	132.0	132.3	131.8	132.6	132.5	132.3	133.1
TC10	T_{wo}	-	132.1	132.5	132.0	132.8	132.7	132.5	133.4
TC11	T_{stm}	-	133.0	133.5	132.8	133.8	133.7	133.5	134.6
TC12	T_{stm}	-	133.0	133.4	132.8	133.8	133.8	133.6	134.6
TC13	T_{stm}	-	133.1	133.5	132.9	133.8	133.7	133.5	134.6
TC14	T_{stm}	-	133.3	133.7	133.1	134.0	133.9	133.6	134.8
TC15	T_{stm}	-	133.3	133.6	133.0	133.9	133.8	133.6	134.6
TC16	T_{pi}	6.7	40.5	69.2	97.7	99.9	99.7	99.8	99.8
TC17	T_{pi}	10.8	61.5	88.8	99.9	100.0	100.0	100.0	100.0
TC21	T_{po}	5.6	7.3	9.8	12.2	18.2	33.0	52.3	71.2
TC22	T_{po}	6.5	7.2	9.8	12.5	18.2	33.0	52.7	70.7
TC31	$T_{mix,o}$	-	40.8	41.2	43.1	45.3	45.7	46.0	45.8
TC40	heat loss estimation	-	41.3	41.7	43.9	45.7	46.2	46.5	46.5
TC41	heat loss estimation	-	41.3	41.6	44.2	45.7	46.2	46.5	46.7
TC43	$T_{air,in}$	24.0	24.3	24.3	24.3	24.4	24.4	24.4	25.0
TC44	$T_{wi,PVC}$	-	28.9	29.0	29.5	33.1	34.2	33.5	33.5
TC45	$T_{wi,PVC}$	-	31.2	31.2	31.6	34.3	35.4	35.3	34.7
TC46	$T_{wi,gal}$	-	35.5	36.1	36.9	41.3	42.0	41.9	41.2
TC47	$T_{wi,gal}$	-	35.7	36.3	37.0	40.8	41.1	41.0	40.5

Notes: (1) see Figure 3.7 and Figure 3.8 for thermocouple (TC) location

(2) see Table 3.2 for T_i notation

Table B.10.b Water-Filled Test Raw Data – W0304

TEST ID	Time (min)	P_{atm} (kPa)	ϕ_{in} (%)	ϕ_{o} (%)	H_{pool} (m)	$\overline{T}_{stm}$ (°C)	$\overline{T}_{wo,pl}$ (°C)	$\overline{T}_{wo,mix}$ (°C)
W0304-00	0	100.1	19.0	-	1.524	-	-	-
W0304-01	6.47	100.1	19.0	8.8	1.524	133.2	91.2	131.9
W0304-02	10.93	100.1	19.0	10.7	1.524	133.5	103.4	132.3
W0304-03	16.30	100.1	19.0	47.0	1.524	132.9	107.4	131.8
W0304-04	26.57	100.1	19.0	78.7	1.505	133.9	108.2	132.7
W0304-05	49.75	100.1	19.0	75.6	1.454	133.8	108.3	132.6
W0304-06	83.47	100.3	19.0	70.0	1.383	133.5	108.2	132.4
W0304-07	122.12	100.4	19.0	65.2	1.308	134.6	108.3	133.3
TEST ID	$\overline{T}_{pi}$ (°C)	$\overline{T}_{po}$ (°C)	$\overline{T}_{air,in}$ (°C)	$\overline{T}_{mix,o}$ (°C)	$\overline{T}_{wi,PVC}$ (°C)	$\overline{T}_{wi,gal}$ (°C)	$\overline{V}_{mix}$ (m/s)	$\dot{m}_{cond}$ ($\times 10^{-3}$ kg/s)
W0304-00	8.8	6.0	24.0	-	-	-	-	-
W0304-01	51.0	7.3	24.3	40.8	30.0	35.6	1.91	23.67
W0304-02	79.0	9.8	24.3	41.2	30.1	36.2	1.89	27.31
W0304-03	98.8	12.4	24.3	43.1	30.6	36.9	2.26	17.98
W0304-04	100.0	18.2	24.4	45.3	33.7	41.1	2.47	16.46
W0304-05	99.8	33.0	24.4	45.7	34.8	41.5	2.42	16.00
W0304-06	99.9	52.5	24.4	46.0	34.4	41.4	2.51	15.21
W0304-07	99.9	71.0	25.0	45.8	34.1	40.9	2.48	13.51

Table B.10.c Water-Filled Test Results – W0304

TEST ID	$\dot{Q}_{cond}$ (kw)	$\dot{Q}_{pool}$ (kw)	$\dot{Q}_{mix}$ (kw)	$\dot{Q}_{rad}$ (kw)	$\bar{q}''_{pool}$ (kw/m^2)	$\bar{q}''_{mix}$ (kw/m^2)
W0304-0001-0	51.89	49.98	2.15	0.83	91.33	1.30
W0304-0102-0	59.12	54.09	2.53	0.83	98.84	1.53
W0304-0203-0	38.92	33.88	2.66	0.83	61.92	1.61
W0304-0304-0	35.63	24.31	2.81	0.82	44.70	1.69
W0304-0304-1	35.63	25.67	2.81	0.82	47.21	1.70
W0304-0405-0	34.60	29.88	2.86	0.82	56.25	1.71
W0304-0405-1	34.60	29.10	2.97	0.82	54.78	1.78
W0304-0506-0	32.91	27.69	3.01	0.83	54.37	1.78
W0304-0506-1	32.91	26.98	3.11	0.83	52.97	1.84
W0304-0607-0	29.22	24.47	3.09	0.85	50.65	1.79
W0304-0607-1	29.22	23.25	3.22	0.85	48.12	1.87
TEST ID	$\bar{h}_{pool}$ (kw/m^2°C)	$\bar{h}_{mix,eff}$ (w/m^2°C)	$\bar{h}_{mix,conv}$ (w/m^2°C)	Remix ($\times 10^4$)	$\dot{m}_{mix}$ (10^{-1}kg/s)	$\frac{\dot{Q}_{cond}}{\dot{Q}_{pool}+\dot{Q}_{mix}}$
W0304-0001-0	1.49	12.86	7.91	2.48	1.56	1.00
W0304-0102-0	3.06	15.38	10.33	2.43	1.54	1.04
W0304-0203-0	3.75	16.44	11.33	2.63	1.66	1.07
W0304-0304-0	5.37	17.78	12.58	2.96	1.85	1.31
W0304-0304-1	5.68	17.80	12.61	2.96	1.85	1.25
W0304-0405-0	6.75	18.20	12.99	3.04	1.90	1.06
W0304-0405-1	6.58	18.82	13.63	3.02	1.89	1.08
W0304-0506-0	6.46	18.90	13.69	3.06	1.91	1.07
W0304-0506-1	6.30	19.48	14.29	3.04	1.90	1.09
W0304-0607-0	6.04	19.07	13.84	3.10	1.94	1.06
W0304-0607-1	5.74	19.79	14.58	3.08	1.93	1.10

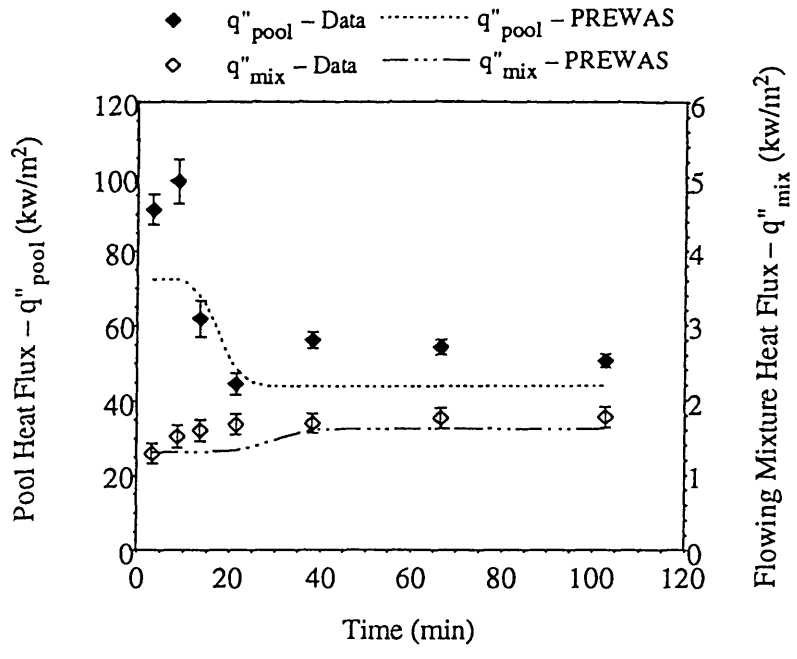

Figure B.10.a W0304 Test Results – Heat Flux

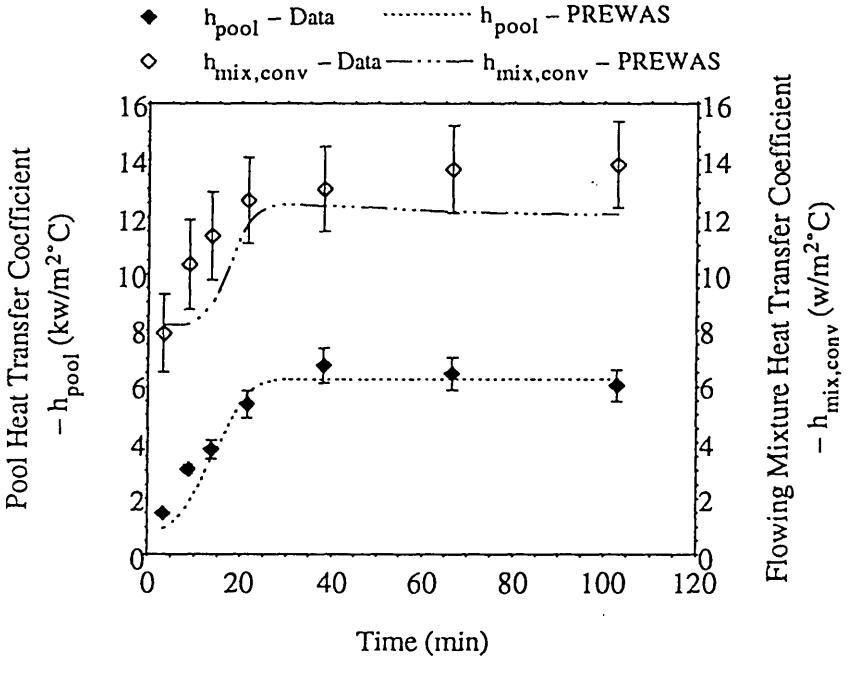

Figure B.10.a W0304 Test Results – Heat Transfer Coefficient

Table B.11.a Water-Filled Test Thermocouple Raw Data – W0315

TC ID	Function	W0315-00 (°C)	W0315-01 (°C)	W0315-02 (°C)	W0315-03 (°C)	W0315-04 (°C)	W0315-05 (°C)	W0315-06 (°C)	W0315-07 (°C)	W0315-08 (°C)	W0315-09 (°C)
TC1	T_{wo}	-	78.8	89.7	97.4	103.6	105.0	105.1	105.2	105.1	105.1
TC2	T_{wo}	-	88.3	98.5	104.7	107.4	107.5	107.5	107.6	107.4	107.5
TC3	T_{wo}	-	115.7	117.6	119.0	120.4	120.2	120.5	121.1	120.7	121.3
TC4	T_{wo}	-	115.8	117.6	119.0	120.4	120.2	120.4	121.1	120.7	121.2
TC5	T_{wo}	-	114.3	116.1	117.6	118.9	118.4	118.7	119.3	119.1	119.4
TC6	T_{wo}	-	115.4	117.3	118.5	119.9	119.6	119.9	120.5	120.0	120.6
TC7	T_{wo}	-	115.4	117.3	118.6	120.0	119.7	119.9	120.5	120.1	120.7
TC8	T_{wo}	-	115.6	117.5	118.8	120.2	119.9	120.1	120.7	120.3	120.9
TC9	T_{wo}	-	115.6	117.5	118.7	120.1	119.7	119.9	120.5	120.2	120.7
TC10	T_{wo}	-	115.6	117.6	118.9	120.2	119.8	120.0	120.6	120.2	120.7
TC11	T_{stm}	-	116.2	118.1	119.5	120.8	120.5	120.8	121.4	121.0	121.5
TC12	T_{stm}	-	116.2	118.2	119.5	120.8	120.5	120.8	121.4	121.0	121.6
TC13	T_{stm}	-	116.2	118.1	119.5	120.8	120.5	120.8	121.4	121.0	121.5
TC14	T_{stm}	-	116.4	118.3	119.7	121.0	120.6	120.9	121.6	121.2	121.7
TC15	T_{stm}	-	116.2	118.1	119.5	120.8	120.5	120.8	121.4	121.1	121.6
TC16	T_{pi}	14.9	34.0	57.4	74.3	94.2	99.8	100.1	100.1	100.1	100.1
TC17	T_{pi}	24.3	50.3	74.5	88.8	99.2	100.0	100.1	100.1	100.1	100.1
TC21	T_{po}	6.9	7.7	9.4	12.3	14.3	17.0	28.6	40.1	49.0	57.4
TC22	T_{po}	7.8	8.1	9.8	11.7	14.6	17.0	28.9	40.2	49.4	57.8
TC31	$T_{mix,o}$	-	39.1	40.2	40.5	41.1	42.4	43.7	44.2	44.6	44.8
TC40	heat loss estimation	-	39.6	40.7	41.0	41.5	42.9	44.1	44.7	45.1	45.1
TC41	heat loss estimation	-	39.4	40.6	41.1	41.6	43.0	44.2	44.6	45.4	45.0
TC43	$T_{air,in}$	23.7	23.6	23.9	23.8	24.2	24.2	24.2	25.4	25.7	25.5
TC44	$T_{wi,PVC}$	-	28.2	28.4	28.5	28.7	30.1	32.1	32.7	33.0	32.5
TC45	$T_{wi,PVC}$	-	31.4	31.4	31.4	31.5	32.0	33.5	33.9	34.1	34.5
TC46	$T_{wi,gal}$	-	34.5	35.2	35.5	35.8	37.2	38.9	39.5	40.0	40.1
TC47	$T_{wi,gal}$	-	35.2	36.0	36.3	36.6	37.7	39.1	39.5	39.8	40.1

Notes: (1) see Figure 3.7 and Figure 3.8 for thermocouple (TC) location

(2) see Table 3.2 for T_i notation

Table B.11.b Water-Filled Test Raw Data – W0315

TEST ID	Time (min)	P_{atm} (kPa)	ϕ_{in} (%)	ϕ_o (%)	H_{pool} (m)	$\overline{T}_{stm}$ (°C)	$\overline{T}_{wo,pl}$ (°C)	$\overline{T}_{wo,mix}$ (°C)
W0315-00	0	100.6	24.5	-	1.524	-	-	-
W0315-01	4.18	100.6	24.5	12.2	1.524	116.3	83.6	115.4
W0315-02	9.37	100.6	24.5	13.6	1.524	118.2	94.1	117.3
W0315-03	14.22	100.6	24.5	15.7	1.524	119.5	101.1	118.6
W0315-04	20.90	100.6	24.5	22.7	1.524	120.9	105.5	120.0
W0315-05	27.20	100.6	24.5	61.4	1.519	120.5	106.3	119.7
W0315-06	58.00	100.6	24.5	64.8	1.480	120.8	106.3	119.9
W0315-07	90.25	100.6	24.5	64.8	1.437	121.4	106.4	120.5
W0315-08	120.02	100.6	24.5	62.1	1.399	121.1	106.3	120.2
W0315-09	150.60	100.6	24.5	59.3	1.359	121.6	106.3	120.7
TEST ID	$\overline{T}_{pi}$ (°C)	$\overline{T}_{po}$ (°C)	$\overline{T}_{air,in}$ (°C)	$\overline{T}_{mix,o}$ (°C)	$\overline{T}_{wi,PVC}$ (°C)	$\overline{T}_{wi,gal}$ (°C)	$\overline{V}_{mix}$ (m/s)	$\dot{m}_{cond}$ ($\times 10^{-3}$ kg/s)
W0315-00	19.6	7.3	23.7	-	-	-	-	-
W0315-01	42.1	7.9	23.6	39.1	29.8	34.9	1.29	17.59
W0315-02	65.9	9.6	23.9	40.2	29.9	35.6	1.37	16.37
W0315-03	81.6	12.0	23.8	40.5	30.0	35.9	1.34	14.95
W0315-04	96.7	14.5	24.2	41.1	30.1	36.2	1.42	11.65
W0315-05	99.9	17.0	24.2	42.4	31.0	37.4	1.83	10.53
W0315-06	100.1	28.7	24.2	43.7	32.8	39.0	1.91	9.98
W0315-07	100.1	40.2	25.4	44.2	33.3	39.5	1.98	9.68
W0315-08	100.1	49.2	25.7	44.6	33.5	39.9	1.96	9.22
W0315-09	100.1	57.6	25.5	44.8	33.5	40.1	1.94	8.93

Table B.11.c Water-Filled Test Results – W0315

TEST ID	$\dot{Q}_{cond}$ (kw)	$\dot{Q}_{pool}$ (kw)	$\dot{Q}_{mix}$ (kw)	$\dot{Q}_{rad}$ (kw)	$\bar{q}''_{pool}$ (kw/m^2)	$\bar{q}''_{mix}$ (kw/m^2)
W0315-0001-0	38.92	41.08	1.66	0.64	75.06	1.00
W0315-0102-0	36.18	38.14	1.75	0.65	69.70	1.06
W0315-0203-0	32.97	27.58	1.86	0.67	50.39	1.12
W0315-0304-0	25.65	24.73	1.92	0.68	45.19	1.16
W0315-0405-0	23.17	14.51	1.91	0.69	26.55	1.15
W0315-0405-1	23.17	15.49	1.93	0.69	28.35	1.16
W0315-0506-0	21.97	16.44	2.14	0.68	30.53	1.29
W0315-0506-1	21.97	17.27	2.18	0.68	32.07	1.31
W0315-0607-0	21.29	17.07	2.23	0.69	32.59	1.33
W0315-0607-1	21.29	16.99	2.31	0.69	32.44	1.38
W0315-0708-0	20.27	16.17	2.20	0.69	31.76	1.31
W0315-0708-1	20.27	15.55	2.33	0.69	30.54	1.38
W0315-0809-0	19.63	15.08	2.25	0.70	30.47	1.32
W0315-0809-1	19.63	15.10	2.33	0.70	30.50	1.37

TEST ID	$\bar{h}_{pool}$ (kw/m^2°C)	$\bar{h}_{mix,eff}$ (w/m^2°C)	$\bar{h}_{mix,conv}$ (w/m^2°C)	Re$_{mix}$ ($\times 10^4$)	$\dot{m}_{mix}$ (10^{-1}kg/s)	$\frac{\dot{Q}_{cond}}{\dot{Q}_{pool} + \dot{Q}_{mix}}$
W0315-0001-0	1.42	11.90	7.28	1.67	1.05	0.91
W0315-0102-0	2.00	12.50	7.85	1.72	1.08	0.91
W0315-0203-0	2.11	13.05	8.35	1.75	1.10	1.12
W0315-0304-0	3.20	13.36	8.62	1.78	1.12	0.96
W0315-0405-0	3.95	13.52	8.66	2.07	1.30	1.41
W0315-0405-1	4.22	13.63	8.78	2.07	1.30	1.33
W0315-0506-0	4.84	15.40	10.51	2.37	1.48	1.18
W0315-0506-1	5.08	15.61	10.73	2.36	1.48	1.13
W0315-0607-0	5.19	15.95	11.03	2.45	1.54	1.10
W0315-0607-1	5.17	16.48	11.57	2.44	1.53	1.10
W0315-0708-0	5.08	15.85	10.90	2.48	1.55	1.10
W0315-0708-1	4.88	16.56	11.64	2.45	1.54	1.13
W0315-0809-0	4.88	15.96	11.00	2.45	1.54	1.13
W0315-0809-1	4.89	16.46	11.52	2.43	1.53	1.13

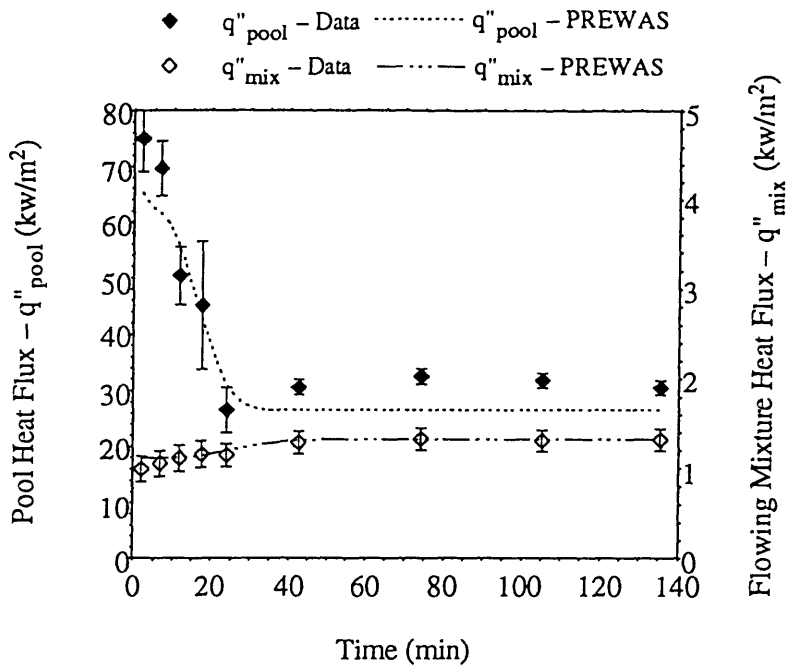

Figure B.11.a W0315 Test Results – Heat Flux

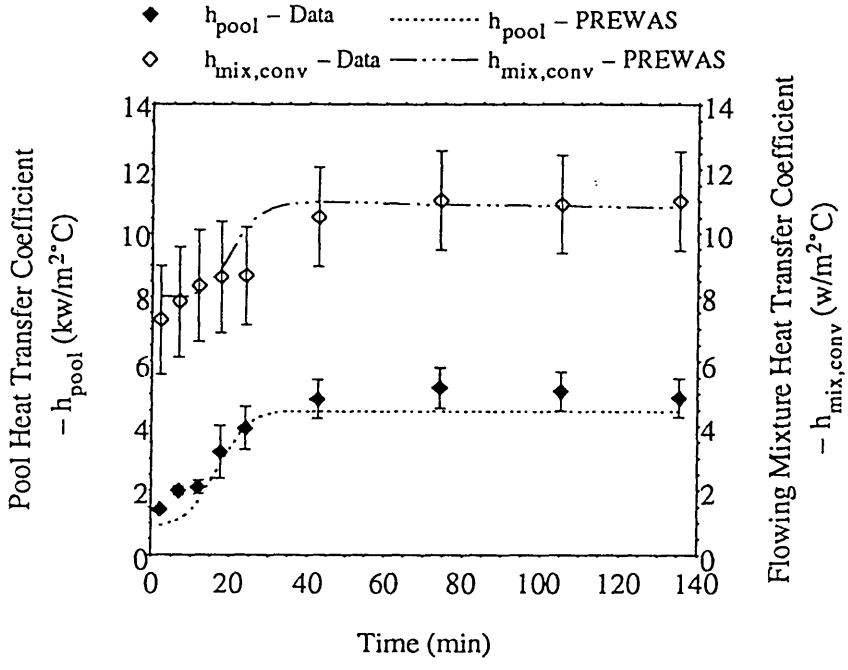

Figure B.11.b W0315 Test Results – Heat Transfer Coefficient

Table B.12.a Water-Filled Test Thermocouple Raw Data – W0401

TC ID	Function	W0401-00 (°C)	W0401-01 (°C)	W0401-02 (°C)	W0401-03 (°C)	W0401-04 (°C)	W0401-05 (°C)	W0401-06 (°C)	W0401-07 (°C)	W0401-08 (°C)	W0401-09 (°C)
TC1	T_{wo}	-	79.4	92.6	100.3	104.5	104.6	104.6	104.7	104.8	104.7
TC2	T_{wo}	-	87.4	98.6	103.1	104.4	104.4	104.3	104.4	104.4	104.3
TC3	T_{wo}	-	107.8	108.8	108.6	108.5	108.7	108.4	108.9	108.9	108.8
TC4	T_{wo}	-	107.8	108.8	108.6	108.5	108.6	108.4	108.9	108.8	108.7
TC5	T_{wo}	-	106.5	107.5	107.3	107.1	107.3	107.1	107.4	107.6	107.4
TC6	T_{wo}	-	107.5	108.4	108.2	108.0	108.2	107.9	108.4	108.3	108.3
TC7	T_{wo}	-	107.5	108.5	108.3	108.0	108.2	108.0	108.4	108.4	108.3
TC8	T_{wo}	-	107.7	108.7	108.4	108.2	108.4	108.2	108.6	108.6	108.5
TC9	T_{wo}	-	107.5	108.6	108.3	108.1	108.2	108.0	108.4	108.5	108.3
TC10	T_{wo}	-	107.6	108.6	108.3	108.1	108.3	108.0	108.5	108.5	108.4
TC11	T_{stm}	-	108.3	109.3	109.0	108.8	109.0	108.7	109.2	109.2	109.1
TC12	T_{stm}	-	108.6	109.3	109.0	108.9	109.0	108.7	109.2	109.2	109.1
TC13	T_{stm}	-	108.3	109.3	109.0	108.8	109.0	108.7	109.2	109.1	109.1
TC14	T_{stm}	-	108.4	109.4	109.1	109.0	109.1	108.9	109.3	109.3	109.2
TC15	T_{stm}	-	108.2	109.3	109.0	108.9	109.0	108.8	109.2	109.2	109.1
TC16	T_{pi}	8.8	41.4	70.9	89.7	100.0	100.3	100.4	100.4	100.4	100.4
TC17	T_{pi}	12.4	66.7	83.9	95.3	100.3	100.5	100.5	100.5	100.5	100.7
TC21	T_{po}	7.2	8.6	11.2	14.6	19.6	24.1	29.3	35.5	41.8	48.6
TC22	T_{po}	7.9	9.0	11.7	14.8	20.1	24.6	29.8	35.9	42.1	48.9
TC31	$T_{mix,o}$	-	37.7	38.4	38.6	39.1	39.5	39.8	39.9	40.5	40.6
TC40	heat loss estimation	-	38.1	38.8	39.0	39.5	39.8	40.1	40.2	40.8	41.0
TC41	heat loss estimation	-	38.1	38.8	39.0	39.4	39.8	40.1	40.1	40.9	41.0
TC43	$T_{air,in}$	25.4	25.4	25.4	25.3	25.0	25.3	25.4	25.6	25.9	26.0
TC44	$T_{wi,PVC}$	-	28.7	28.8	28.9	29.0	29.3	29.6	29.7	29.9	30.3
TC45	$T_{wi,PVC}$	-	29.2	29.3	29.5	29.7	30.0	30.3	30.7	31.0	31.5
TC46	$T_{wi,gal}$	-	33.6	34.1	34.3	34.7	35.2	35.5	35.5	36.0	36.4
TC47	$T_{wi,gal}$	-	33.7	34.1	34.3	34.6	35.0	35.4	35.6	35.9	36.4

Notes: (1) see Figure 3.7 and Figure 3.8 for thermocouple (TC) location

(2) see Table 3.2 for T_i notation

Table B.12.b Water-Filled Test Raw Data – W0401

TEST ID	Time (min)	P_{atm} (kPa)	ϕ_{in} (%)	ϕ_{o} (%)	H_{pool} (m)	$\overline{T}_{stm}$ (°C)	$\overline{T}_{wo,pl}$ (°C)	$\overline{T}_{wo,mix}$ (°C)
W0401-00	0	102.4	20.0	-	1.524	-	-	-
W0401-01	9.50	102.4	20.0	19.3	1.524	108.4	83.4	107.5
W0401-02	18.50	102.4	20.0	20.2	1.524	109.3	95.6	108.5
W0401-03	29.12	102.4	20.0	21.3	1.524	109.0	101.7	108.2
W0401-04	48.58	102.4	20.0	24.5	1.519	108.9	104.5	108.1
W0401-05	66.80	102.4	20.0	25.6	1.513	109.0	104.5	108.2
W0401-06	90.87	102.4	20.0	25.8	1.503	108.8	104.4	108.0
W0401-07	120.28	102.4	20.0	25.5	1.494	109.2	104.6	108.4
W0401-08	148.23	102.4	20.0	26.5	1.481	109.2	104.6	108.4
W0401-09	181.10	102.4	20.0	26.7	1.468	109.1	104.5	108.4
TEST ID	$\overline{T}_{pi}$ (°C)	$\overline{T}_{po}$ (°C)	$\overline{T}_{air,in}$ (°C)	$\overline{T}_{mix,o}$ (°C)	$\overline{T}_{wi,PVC}$ (°C)	$\overline{T}_{wi,gal}$ (°C)	$\overline{V}_{mix}$ (m/s)	$\dot{m}_{cond}$ ($\times 10^{-3}$ kg/s)
W0401-00	10.6	7.6	25.4	-	-	-	-	-
W0401-01	48.5	8.8	25.4	37.7	28.9	33.6	1.73	15.83
W0401-02	77.4	11.4	25.4	38.4	29.1	34.1	1.67	10.87
W0401-03	92.5	14.7	25.3	38.6	29.2	34.3	1.68	8.05
W0401-04	100.2	19.9	25.0	39.1	29.4	34.7	1.81	4.92
W0401-05	100.4	24.4	25.3	39.5	29.7	35.1	1.84	4.53
W0401-06	100.4	29.5	25.4	39.8	30.0	35.4	1.85	4.27
W0401-07	100.4	35.7	25.6	39.9	30.2	35.6	1.93	4.55
W0401-08	100.5	41.9	25.9	40.5	30.4	36.0	1.89	4.60
W0401-09	100.5	48.8	26.0	40.6	30.9	36.4	1.96	4.64

Table B.12.c Water-Filled Test Results – W0401

TEST ID	$\dot{Q}_{cond}$ (kw)	$\dot{Q}_{pool}$ (kw)	$\dot{Q}_{mix}$ (kw)	$\dot{Q}_{rad}$ (kw)	$\bar{q}''_{pool}$ (kw/m^2)	$\bar{q}''_{mix}$ (kw/m^2)
W0401-0001-0	35.36	30.85	1.55	0.57	56.37	0.93
W0401-0102-0	24.28	27.61	1.82	0.57	50.45	1.10
W0401-0203-0	17.98	15.25	1.85	0.57	27.87	1.12
W0401-0304-0	10.99	7.28	1.80	0.57	13.32	1.08
W0401-0304-1	10.99	7.28	1.87	0.57	13.32	1.13
W0401-0405-0	10.11	7.35	1.79	0.57	13.49	1.08
W0401-0405-1	10.11	7.12	1.87	0.57	13.08	1.13
W0401-0506-0	9.53	7.19	1.88	0.57	13.28	1.13
W0401-0506-1	9.53	6.97	1.96	0.57	12.87	1.18
W0401-0607-0	10.16	7.12	1.95	0.57	13.24	1.17
W0401-0607-1	10.16	6.23	2.07	0.57	11.59	1.24
W0401-0708-0	10.26	7.42	1.96	0.57	13.89	1.17
W0401-0708-1	10.26	7.50	2.03	0.57	14.04	1.21
W0401-0809-0	10.36	7.54	2.02	0.57	14.25	1.21
W0401-0809-1	10.36	6.70	2.14	0.57	12.64	1.28

TEST ID	$\bar{h}_{pool}$ (kw/m^2°C)	$\bar{h}_{mix,eff}$ (w/m^2°C)	$\bar{h}_{mix,conv}$ (w/m^2°C)	Remix ($\times 10^4$)	$\dot{m}_{mix}$ (10^{-1}kg/s)	$\frac{\dot{Q}_{cond}}{\dot{Q}_{pool}+\dot{Q}_{mix}}$
W0401-0001-0	1.05	12.16	7.71	2.30	1.45	1.09
W0401-0102-0	1.90	14.36	9.85	2.25	1.41	0.83
W0401-0203-0	2.03	14.60	10.7	2.21	1.39	1.05
W0401-0304-0	1.98	14.37	9.80	2.30	1.45	1.21
W0401-0304-1	1.98	14.87	10.32	2.28	1.44	1.20
W0401-0405-0	3.22	14.42	9.84	2.29	1.44	1.11
W0401-0405-1	3.12	14.99	10.42	2.27	1.44	1.12
W0401-0506-0	3.29	15.18	10.59	2.40	1.51	1.05
W0401-0506-1	3.18	15.78	11.20	2.38	1.50	1.07
W0401-0607-0	3.26	15.71	11.12	2.47	1.56	1.12
W0401-0607-1	2.85	16.58	12.01	2.45	1.55	1.22
W0401-0708-0	3.39	15.77	11.16	2.47	1.56	1.09
W0401-0708-1	3.43	16.27	11.68	2.46	1.55	1.08
W0401-0809-0	3.56	16.33	11.71	2.53	1.60	1.08
W0401-0809-1	3.16	17.20	12.61	2.51	1.59	1.17

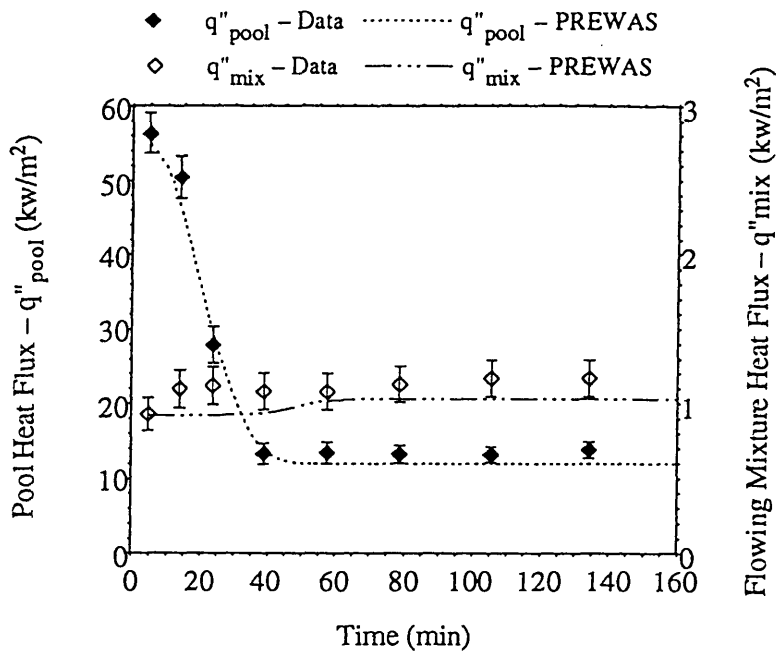

Figure B.12.a W0401 Test Results – Heat Flux

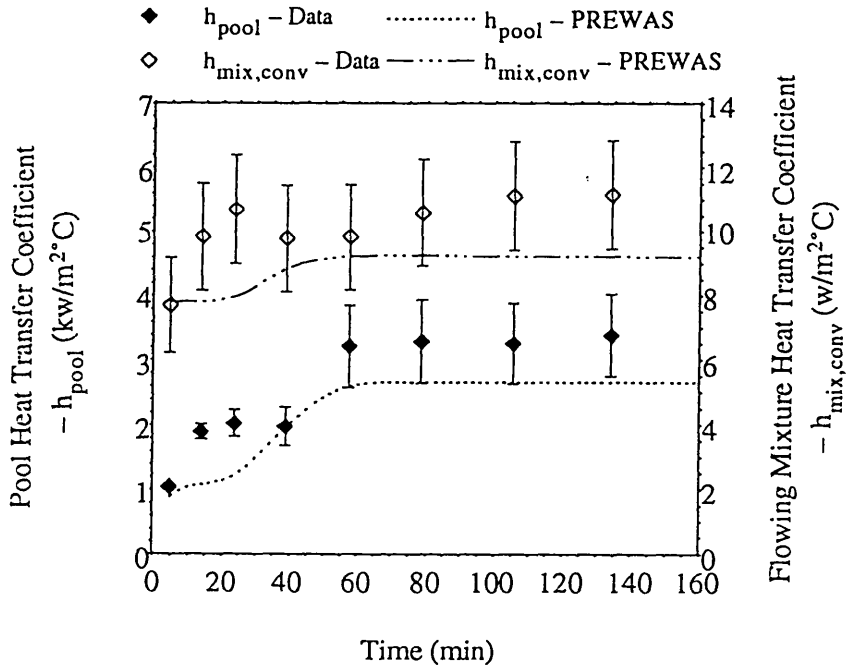

Figure B.12.b W0401 Test Results – Heat Transfer Coefficient

Table B.13.a Water-Filled Test Thermocouple Raw Data – W0405

TC ID	Function	W0405-00 (°C)	W0405-01 (°C)	W0405-02 (°C)	W0405-03 (°C)	W0405-04 (°C)	W0405-05 (°C)	W0405-06 (°C)	W0405-07 (°C)	W0405-08 (°C)
TC1	T_{wo}	-	75.6	92.5	100.1	102.0	102.7	102.7	103.0	102.7
TC2	T_{wo}	-	82.8	97.5	101.3	102.2	102.6	102.5	102.7	102.6
TC3	T_{wo}	-	104.1	104.5	104.3	103.8	104.3	104.0	104.2	104.1
TC4	T_{wo}	-	104.1	104.5	104.2	103.7	104.2	103.9	104.2	104.1
TC5	T_{wo}	-	102.7	103.3	102.8	102.5	103.1	102.6	103.0	102.8
TC6	T_{wo}	-	103.7	104.1	103.8	103.4	103.8	103.5	103.7	103.7
TC7	T_{wo}	-	103.8	104.2	103.8	103.5	104.0	103.6	103.9	103.8
TC8	T_{wo}	-	104.0	104.3	104.0	103.6	104.1	103.8	104.1	104.0
TC9	T_{wo}	-	103.8	104.2	103.8	103.5	104.0	103.7	104.0	103.9
TC10	T_{wo}	-	103.9	104.2	103.9	103.5	104.0	103.7	104.0	103.9
TC11	T_{stm}	-	104.8	105.0	104.7	104.1	104.6	104.3	104.6	104.5
TC12	T_{stm}	-	105.1	105.0	104.7	104.1	104.6	104.3	104.6	104.5
TC13	T_{stm}	-	104.5	104.9	104.6	104.1	104.6	104.3	104.6	104.5
TC14	T_{stm}	--	104.9	105.1	104.8	104.2	104.7	104.4	104.7	104.6
TC15	T_{stm}	-	104.6	105.0	104.7	104.1	104.6	104.3	104.6	104.5
TC16	T_{pi}	10.7	37.0	76.0	93.2	97.9	98.4	98.9	99.1	98.6
TC17	T_{pi}	14.8	50.6	86.6	95.6	98.3	98.8	99.2	99.4	99.0
TC21	T_{po}	7.8	8.9	13.3	17.1	21.4	25.9	30.5	34.5	37.5
TC22	T_{po}	8.6	9.2	13.4	17.4	21.8	26.4	30.9	34.9	37.9
TC31	$T_{mix,o}$	-	37.4	37.6	37.4	38.6	39.0	38.8	39.0	39.2
TC40	heat loss estimation	-	37.8	37.9	37.7	39.0	39.4	39.2	39.3	39.6
TC41	heat loss estimation	-	37.7	37.8	37.5	38.9	39.4	39.1	39.3	39.6
TC43	$T_{air,in}$	25.2	25.5	25.5	25.2	25.4	25.5	25.4	25.6	25.7
TC44	$T_{wi,PVC}$	-	28.6	28.7	28.8	28.9	28.9	29.0	29.3	29.2
TC45	$T_{wi,PVC}$	-	30.2	30.1	30.0	30.1	30.3	30.6	30.8	30.9
TC46	$T_{wi,gal}$	-	33.4	33.6	33.6	34.1	34.5	34.6	35.0	35.0
TC47	$T_{wi,gal}$	-	33.8	33.6	33.5	34.4	35.0	35.0	35.3	35.4

Notes: (1) see Figure 3.7 and Figure 3.8 for thermocouple (TC) location

(2) see Table 3.2 for T_i notation

Table B.13.b Water-Filled Test Raw Data – W0405

TEST ID	Time (min)	P_{atm} (kPa)	ϕ_{in} (%)	ϕ_o (%)	H_{pool} (m)	$\overline{T}_{stm}$ (°C)	$\overline{T}_{wo,pl}$ (°C)	$\overline{T}_{wo,mix}$ (°C)
W0405-00	0	102.1	23.5	-	1.524	-	-	-
W0405-01	7.05	102.1	23.5	12.5	1.524	104.8	79.2	103.8
W0405-02	21.48	102.1	23.5	14.7	1.524	105.0	95.0	104.2
W0405-03	37.15	102.1	23.5	16.3	1.524	104.7	100.7	103.8
W0405-04	52.90	102.1	23.5	19.7	1.524	104.1	102.1	103.4
W0405-05	73.05	102.1	23.5	20.5	1.521	104.7	102.7	103.9
W0405-06	97.63	102.1	23.5	20.5	1.518	104.3	102.6	103.6
W0405-07	120.00	102.1	23.5	20.2	1.514	104.6	102.8	103.9
W0405-08	150.35	102.1	23.5	19.8	1.510	104.5	102.6	103.8
TEST ID	$\overline{T}_{pi}$ (°C)	$\overline{T}_{po}$ (°C)	$\overline{T}_{air,in}$ (°C)	$\overline{T}_{mix,o}$ (°C)	$\overline{T}_{wi,PVC}$ (°C)	$\overline{T}_{wi,gal}$ (°C)	$\overline{V}_{mix}$ (m/s)	$\dot{m}_{cond}$ ($\times 10^{-3}$ kg/s)
W0405-00	12.8	8.2	25.2	-	-	-	-	-
W0405-01	43.8	9.1	25.5	37.4	29.4	33.6	1.53	18.42
W0405-02	81.3	13.3	25.5	37.6	29.4	33.6	1.62	9.87
W0405-03	94.4	17.3	25.2	37.4	29.4	33.6	1.62	5.59
W0405-04	98.1	21.6	25.4	38.6	29.5	34.2	1.57	4.14
W0405-05	98.6	26.1	25.5	39.0	29.6	34.7	1.57	3.46
W0405-06	99.1	30.7	25.4	38.8	29.8	34.8	1.53	3.12
W0405-07	99.2	34.7	25.6	39.0	30.1	35.2	1.52	2.87
W0405-08	98.8	37.6	25.7	39.3	30.1	35.2	1.57	2.48

Table B.13.c Water-Filled Test Results – W0405

TEST ID	$\dot{Q}_{cond}$ (kw)	$\dot{Q}_{pool}$ (kw)	$\dot{Q}_{mix}$ (kw)	$\dot{Q}_{rad}$ (kw)	$\bar{q}''_{pool}$ (kw/m^2)	$\bar{q}''_{mix}$ (kw/m^2)
W0405-0001-0	41.33	33.74	1.55	0.53	61.65	0.94
W0405-0102-0	22.15	23.38	1.54	0.53	42.73	0.93
W0405-0203-0	12.53	10.11	1.55	0.53	18.48	0.94
W0405-0304-0	9.29	6.36	1.56	0.53	11.62	0.94
W0405-0405-0	7.76	5.07	1.60	0.53	9.28	0.97
W0405-0405-1	7.76	5.27	1.66	0.53	9.64	1.00
W0405-0506-0	7.00	4.43	1.59	0.53	8.12	0.96
W0405-0506-1	7.00	4.34	1.67	0.53	7.95	1.00
W0405-0607-0	6.44	4.20	1.56	0.53	7.72	0.94
W0405-0607-1	6.44	4.26	1.63	0.52	7.82	0.98
W0405-0708-0	5.57	2.82	1.60	0.53	5.20	0.96
W0405-0708-1	5.57	3.02	1.66	0.53	5.56	1.00

TEST ID	$\bar{h}_{pool}$ (kw/m^2°C)	$\bar{h}_{mix,eff}$ (w/m^2°C)	$\bar{h}_{mix,conv}$ (w/m^2°C)	Remix ($\times 10^4$)	$\dot{m}_{mix}$ (10^{-1}kg/s)	$\frac{\dot{Q}_{cond}}{\dot{Q}_{pool}+\dot{Q}_{mix}}$
W0405-0001-0	1.21	12.96	8.56	2.03	1.28	1.17
W0405-0102-0	1.74	12.87	8.44	2.08	1.31	0.89
W0405-0203-0	1.85	12.97	8.54	2.13	1.35	1.07
W0405-0304-0	1.89	13.21	8.76	2.10	1.32	1.17
W0405-0405-0	2.34	13.61	9.14	2.06	1.30	1.16
W0405-0405-1	2.44	14.06	9.61	2.04	1.29	1.12
W0405-0506-0	2.04	13.53	9.06	2.03	1.28	1.16
W0405-0506-1	2.00	14.09	9.64	2.02	1.28	1.17
W0405-0607-0	2.21	13.30	8.84	2.00	1.26	1.12
W0405-0607-1	2.23	13.80	9.36	1.99	1.26	1.09
W0405-0708-0	1.47	13.57	9.10	2.03	1.28	1.26
W0405-0708-1	1.58	14.03	9.58	2.02	1.28	1.19

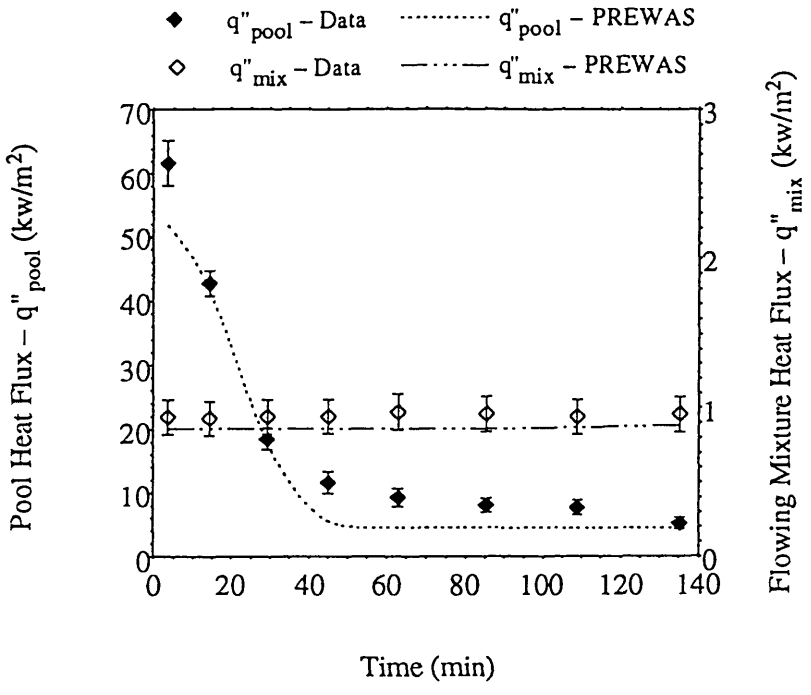

Figure B.13.a W0405 Test Results – Heat Flux

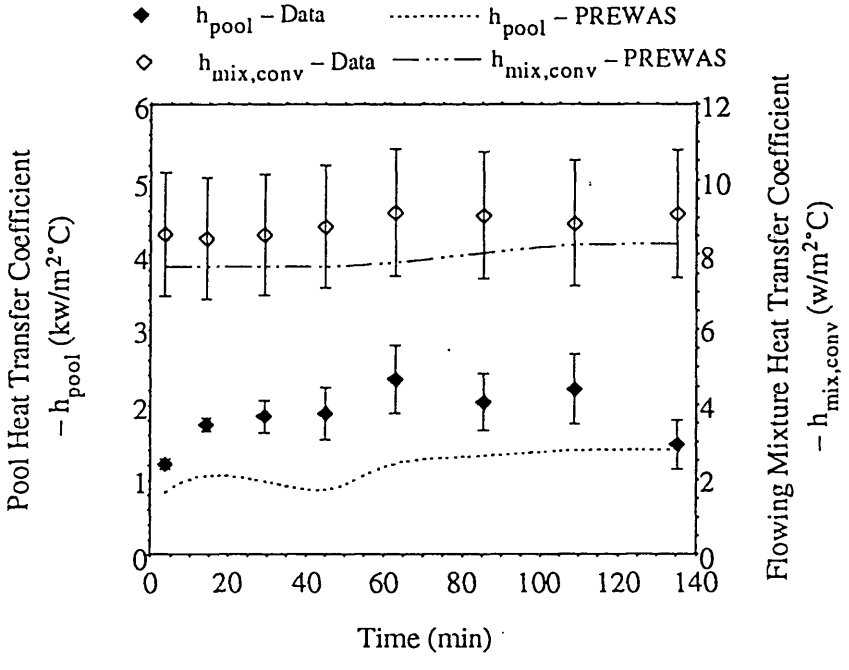

Figure B.13.b W0405 Test Results – Heat Transfer Coefficient

Table B.14.a Water-Filled Test Thermocouple Raw Data – W0408

TC ID	Function	W0408-00 (°C)	W0408-01 (°C)	W0408-02 (°C)	W0408-03 (°C)	W0408-04 (°C)	W0408-05 (°C)	W0408-06 (°C)	W0408-07 (°C)	W0408-08 (°C)	W0408-09 (°C)
TC1	T_{wo}	-	79.2	91.6	98.7	102.9	104.4	104.5	104.7	104.6	104.7
TC2	T_{wo}	-	86.5	97.4	102.1	104.0	104.3	104.2	104.2	104.1	104.2
TC3	T_{wo}	-	107.5	108.2	108.4	108.5	108.2	108.0	108.0	107.8	107.9
TC4	T_{wo}	-	107.6	108.3	108.4	108.4	108.2	107.9	108.0	107.7	107.9
TC5	T_{wo}	-	106.4	106.9	107.1	107.1	106.8	106.6	106.6	106.3	106.4
TC6	T_{wo}	-	107.3	107.7	108.0	108.1	107.7	107.5	107.5	107.3	107.3
TC7	T_{wo}	-	107.3	107.9	108.1	108.2	107.8	107.6	107.7	107.4	107.5
TC8	T_{wo}	-	107.5	108.1	108.3	108.3	108.0	107.7	107.8	107.5	107.6
TC9	T_{wo}	-	107.4	108.0	108.1	108.2	107.8	107.7	107.7	107.4	107.5
TC10	T_{wo}	-	107.5	108.0	108.2	108.2	107.9	107.6	107.7	107.4	107.5
TC11	T_{stm}	-	108.3	108.7	108.9	108.8	108.5	108.1	108.3	108.1	108.2
TC12	T_{stm}	-	108.2	108.8	108.9	108.8	108.6	108.3	108.4	108.1	108.2
TC13	T_{stm}	-	108.0	108.7	108.9	108.8	108.5	108.3	108.3	108.1	108.2
TC14	T_{stm}	-	108.2	108.8	109.0	109.0	108.7	108.4	108.5	108.2	108.3
TC15	T_{stm}	-	108.1	108.7	108.9	108.9	108.6	108.3	108.4	108.1	108.2
TC16	T_{pi}	9.9	41.7	68.9	85.3	95.5	100.1	100.2	100.4	100.5	100.6
TC17	T_{pi}	12.9	54.6	81.3	92.9	98.0	100.5	100.5	100.7	100.7	100.7
TC21	T_{po}	8.9	10.4	13.1	15.2	17.8	21.0	25.4	30.3	34.2	38.5
TC22	T_{po}	9.7	10.6	13.2	15.7	18.1	21.4	25.9	30.7	34.6	38.9
TC31	$T_{mix,o}$	-	38.0	38.6	38.9	39.1	39.7	40.1	40.7	40.3	40.3
TC40	heat loss estimation	-	38.5	39.0	39.2	39.5	40.1	40.5	41.0	40.7	40.6
TC41	heat loss estimation	-	38.4	38.9	39.2	39.5	40.0	40.4	41.1	40.7	40.6
TC43	$T_{air,in}$	25.7	26.1	26.0	25.8	25.7	25.9	25.9	26.2	26.0	26.2
TC44	$T_{wi,PVC}$	-	29.0	29.3	29.4	29.5	29.8	30.2	30.4	30.5	30.5
TC45	$T_{wi,PVC}$	-	30.8	30.8	30.8	30.7	30.8	31.1	31.4	31.5	31.5
TC46	$T_{wi,gal}$	-	34.0	34.6	34.7	34.9	35.5	35.9	36.4	36.3	36.2
TC47	$T_{wi,gal}$	-	34.1	34.8	34.8	35.0	35.5	36.0	36.7	36.2	36.1

Notes: (1) see Figure 3.7 and Figure 3.8 for thermocouple (TC) location

(2) see Table 3.2 for T_i notation

Table B.14.b Water-Filled Test Raw Data – W0408

TEST ID	Time (min)	P_{atm} (kPa)	ϕ_{in} (%)	ϕ_o (%)	H_{pool} (m)	$\overline{T}_{stm}$ (°C)	$\overline{T}_{wo,pl}$ (°C)	$\overline{T}_{wo,mix}$ (°C)
W0408-00	0	103.1	16.0	-	1.524	-	-	-
W0408-01	7.70	103.1	16.0	8.7	1.524	108.2	82.8	107.3
W0408-02	16.60	103.1	16.0	10.5	1.524	108.7	94.5	107.9
W0408-03	25.37	103.1	16.0	12.4	1.524	108.9	100.4	108.1
W0408-04	34.23	103.1	16.0	15.1	1.524	108.9	103.4	108.1
W0408-05	50.75	103.1	16.0	21.8	1.519	108.6	104.4	107.8
W0408-06	86.35	103.1	16.0	22.0	1.510	108.3	104.3	107.6
W0408-07	122.72	103.1	16.0	25.0	1.499	108.4	104.5	107.6
W0408-08	150.13	103.1	16.0	24.0	1.491	108.1	104.4	107.3
W0408-09	180.05	103.1	16.0	24.9	1.481	108.2	104.4	107.5
TEST ID	$\overline{T}_{pi}$ (°C)	$\overline{T}_{po}$ (°C)	$\overline{T}_{air,in}$ (°C)	$\overline{T}_{mix,o}$ (°C)	$\overline{T}_{wi,PVC}$ (°C)	$\overline{T}_{wi,gal}$ (°C)	$\overline{V}_{mix}$ (m/s)	$\dot{m}_{cond}$ ($\times 10^{-3}$ kg/s)
W0408-00	11.4	9.3	25.7	-	-	-	-	-
W0408-01	48.1	10.5	26.1	38.0	29.9	34.0	1.44	17.14
W0408-02	75.1	13.1	26.0	38.6	30.0	34.7	1.53	10.77
W0408-03	89.1	15.5	25.8	38.9	30.1	34.8	1.54	8.04
W0408-04	96.7	18.0	25.7	39.1	30.1	35.0	1.53	5.64
W0408-05	100.3	21.2	25.9	39.7	30.3	35.5	1.55	2.42
W0408-06	100.4	25.7	25.9	40.1	30.6	35.9	1.61	2.38
W0408-07	100.5	30.5	26.2	40.7	30.9	36.5	1.60	2.86
W0408-08	100.6	34.4	26.0	40.3	31.0	36.3	1.63	3.99
W0408-09	100.6	38.7	26.2	40.3	31.0	36.1	1.64	3.44

Table B.14.c Water-Filled Test Results – W0408

TEST ID	$\dot{Q}_{cond}$ (kw)	$\dot{Q}_{pool}$ (kw)	$\dot{Q}_{mix}$ (kw)	$\dot{Q}_{rad}$ (kw)	$\bar{q}''_{pool}$ (kw/m^2)	$\bar{q}''_{mix}$ (kw/m^2)
W0408-0001-0	38.32	36.73	1.48	0.56	67.13	0.90
W0408-0102-0	24.06	26.42	1.50	0.56	48.27	0.91
W0408-0203-0	17.96	15.79	1.60	0.57	28.85	0.96
W0408-0304-0	12.59	10.89	1.63	0.57	19.90	0.98
W0408-0405-0	5.41	4.77	1.63	0.56	8.74	0.98
W0408-0405-1	5.41	4.77	1.62	0.56	8.74	0.98
W0408-0506-0	5.32	4.05	1.70	0.56	7.46	1.03
W0408-0506-1	5.32	4.41	1.73	0.56	8.11	1.04
W0408-0607-0	6.39	4.43	1.69	0.56	8.20	1.02
W0408-0607-1	6.39	4.81	1.72	0.56	8.90	1.04
W0408-0708-0	8.27	4.76	1.70	0.56	8.86	1.02
W0408-0708-1	8.27	4.83	1.75	0.56	9.00	1.05
W0408-0809-0	7.68	4.78	1.74	0.56	8.95	1.04
W0408-0809-1	7.68	5.04	1.78	0.56	9.45	1.07

TEST ID	$\bar{h}_{pool}$ (kw/m^2°C)	$\bar{h}_{mix,eff}$ (w/m^2°C)	$\bar{h}_{mix,conv}$ (w/m^2°C)	Remix ($\times 10^4$)	$\dot{m}_{mix}$ (10^{-1}kg/s)	$\frac{\dot{Q}_{cond}}{\dot{Q}_{pool} + \dot{Q}_{mix}}$
W0408-0001-0	1.27	11.88	7.38	1.93	1.22	1.00
W0408-0102-0	1.79	12.07	7.55	1.97	1.25	0.86
W0408-0203-0	1.88	12.78	8.25	2.04	1.29	1.03
W0408-0304-0	2.21	13.03	8.48	2.03	1.29	1.01
W0408-0405-0	1.63	13.14	8.59	2.04	1.29	0.84
W0408-0405-1	1.63	13.10	8.54	2.04	1.29	0.85
W0408-0506-0	1.86	13.85	9.28	2.08	1.32	0.92
W0408-0506-1	2.02	14.07	9.52	2.08	1.31	0.87
W0408-0607-0	2.07	13.80	9.24	2.11	1.33	1.04
W0408-0607-1	2.25	14.03	9.48	2.11	1.33	0.98
W0408-0708-0	2.29	13.84	9.28	2.13	1.34	1.28
W0408-0708-1	2.33	14.19	9.64	2.12	1.34	1.26
W0408-0809-0	2.36	14.23	9.66	2.15	1.36	1.18
W0408-0809-1	2.49	14.51	9.95	2.15	1.36	1.13

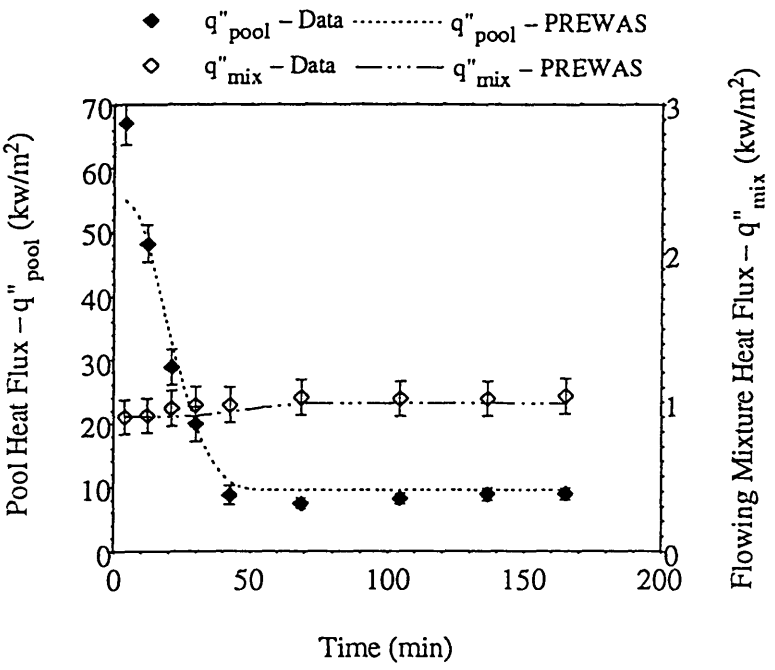

Figure B.14.a W0408 Test Results – Heat Flux

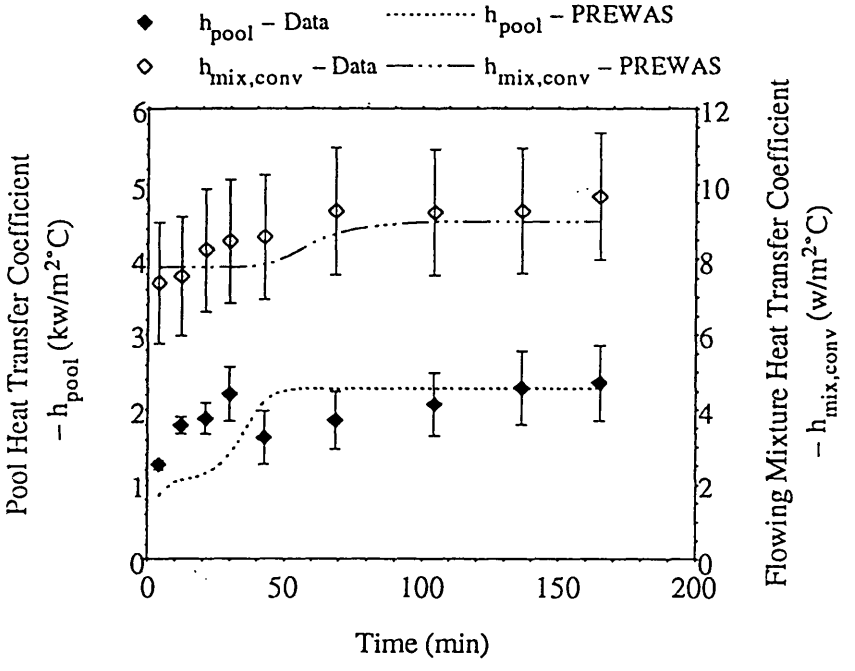

Figure B.14.b W0408 Test Results – Heat Transfer Coefficient

Table B.15.a Water-Filled Test Thermocouple Raw Data – W0412

TC ID	Function	W0412-00 (°C)	W0412-01 (°C)	W0412-02 (°C)	W0412-03 (°C)	W0412-04 (°C)	W0412-05 (°C)	W0412-06 (°C)	W0412-07 (°C)	W0412-08 (°C)
TC1	T_{wo}	-	79.9	92.3	100.0	105.1	105.3	105.1	104.8	104.8
TC2	T_{wo}	-	87.9	99.7	104.7	105.6	105.8	105.6	105.5	105.6
TC3	T_{wo}	-	112.5	113.4	113.2	113.3	113.6	113.1	113.1	113.3
TC4	T_{wo}	-	112.5	113.4	113.2	113.3	113.5	113.0	113.0	113.2
TC5	T_{wo}	-	110.9	111.8	111.6	111.6	112.1	111.4	111.4	111.7
TC6	T_{wo}	-	111.9	112.9	112.6	112.7	112.9	112.4	112.4	112.6
TC7	T_{wo}	-	112.0	113.0	112.8	112.8	113.1	112.5	112.6	112.8
TC8	T_{wo}	-	112.3	113.2	113.0	113.0	113.3	112.8	112.8	112.9
TC9	T_{wo}	-	112.2	113.1	112.9	112.8	113.1	112.6	112.6	112.8
TC10	T_{wo}	-	112.2	113.1	112.9	112.9	113.1	112.6	112.6	112.8
TC11	T_{stm}	-	113.0	113.9	113.7	113.6	113.9	113.4	113.4	113.6
TC12	T_{stm}	-	113.4	114.0	113.8	113.7	113.9	113.4	113.4	113.6
TC13	T_{stm}	-	112.9	113.8	113.6	113.6	113.9	113.4	113.4	113.6
TC14	T_{stm}	-	113.1	114.0	113.8	113.8	114.0	113.5	113.5	113.7
TC15	T_{stm}	-	113.0	114.0	113.8	113.7	113.9	113.4	113.4	113.6
TC16	T_{pi}	10.5	39.4	67.0	85.0	100.2	100.6	100.7	100.7	100.7
TC17	T_{pi}	14.3	53.2	81.2	94.5	100.6	100.7	100.6	100.6	100.7
TC21	T_{po}	9.4	10.6	13.6	16.2	19.1	29.1	38.1	43.5	49.9
TC22	T_{po}	10.0	10.9	13.6	16.2	19.5	29.1	38.1	43.6	50.1
TC31	$T_{mix,o}$	-	38.2	38.6	38.3	39.4	40.8	40.8	41.4	41.1
TC40	heat loss estimation	-	38.5	38.9	38.6	39.7	41.2	41.2	41.8	41.5
TC41	heat loss estimation	-	38.5	38.9	38.6	39.7	41.2	41.1	42.0	41.5
TC43	$T_{air,in}$	24.6	24.8	24.7	24.6	24.6	24.9	25.2	24.8	24.9
TC44	$T_{wi,PVC}$	-	28.2	28.3	28.2	28.3	29.1	29.4	29.6	29.7
TC45	$T_{wi,PVC}$	-	29.9	30.0	30.1	30.2	30.8	31.4	31.8	32.0
TC46	$T_{wi,gal}$	-	33.4	33.9	33.8	34.5	35.9	36.0	36.5	36.4
TC47	$T_{wi,gal}$	-	33.9	34.6	34.4	34.9	36.0	36.1	36.7	36.7

Notes: (1) see Figure 3.7 and Figure 3.8 for thermocouple (TC) location

(2) see Table 3.2 for T_i notation

Table B.15.b Water-Filled Test Raw Data – W0412

TEST ID	Time (min)	P_{atm} (kPa)	ϕ_{in} (%)	ϕ_o (%)	H_{pool} (m)	$\overline{T}_{stm}$ (°C)	$\overline{T}_{wo,pl}$ (°C)	$\overline{T}_{wo,mix}$ (°C)
W0412-00	0	103.2	23.5	-	1.524	-	-	-
W0412-01	6.63	103.2	23.5	12.8	1.524	113.1	83.9	112.1
W0412-02	14.38	103.2	23.5	14.5	1.524	114.0	96.0	113.0
W0412-03	21.63	103.2	23.5	16.1	1.524	113.7	102.4	112.8
W0412-04	32.15	103.2	23.5	31.4	1.521	113.7	105.4	112.8
W0412-05	61.72	103.2	23.5	45.4	1.502	114.0	105.6	113.1
W0412-06	97.95	103.2	23.5	42.9	1.476	113.4	105.3	112.5
W0412-07	120.73	103.2	23.5	43.4	1.461	113.4	105.2	112.6
W0412-08	150.75	103.2	23.5	43.0	1.438	113.6	105.2	112.8
TEST ID	$\overline{T}_{pi}$ (°C)	$\overline{T}_{po}$ (°C)	$\overline{T}_{air,in}$ (°C)	$\overline{T}_{mix,o}$ (°C)	$\overline{T}_{wi,PVC}$ (°C)	$\overline{T}_{wi,gal}$ (°C)	$\overline{V}_{mix}$ (m/s)	$\dot{m}_{cond}$ ($\times 10^{-3}$ kg/s)
W0412-00	12.4	9.7	24.6	-	-	-	-	-
W0412-01	46.3	10.8	24.8	38.2	29.1	33.6	1.60	16.94
W0412-02	74.1	13.63	24.7	38.6	29.2	34.3	1.71	13.14
W0412-03	89.7	16.2	24.6	38.3	29.1	34.1	1.82	10.05
W0412-04	100.4	19.3	24.6	39.4	29.2	34.7	1.77	7.94
W0412-05	100.7	29.1	24.9	40.8	30.0	35.9	1.80	6.44
W0412-06	100.6	38.1	25.2	40.8	30.4	36.1	1.85	5.70
W0412-07	100.7	43.5	24.8	41.4	30.7	36.6	1.85	6.13
W0412-08	100.7	50.0	24.9	41.1	30.8	36.6	1.89	5.93

Table B.15.c Water-Filled Test Results – W0412

TEST ID	$\dot{Q}_{cond}$ (kw)	$\dot{Q}_{pool}$ (kw)	$\dot{Q}_{mix}$ (kw)	$\dot{Q}_{rad}$ (kw)	$\bar{q}''_{pool}$ (kw/m^2)	$\bar{q}''_{mix}$ (kw/m^2)
W0412-0001-0	37.63	39.40	1.89	0.61	71.99	1.14
W0412-0102-0	29.18	31.69	1.90	0.62	57.90	1.15
W0412-0203-0	22.30	21.22	1.95	0.62	38.78	1.18
W0412-0304-0	17.63	12.50	1.95	0.62	22.86	1.18
W0412-0304-1	17.63	13.15	1.99	0.62	24.06	1.20
W0412-0405-0	14.29	9.69	1.83	0.62	17.85	1.10
W0412-0405-1	14.29	11.06	1.84	0.62	20.38	1.11
W0412-0506-0	12.65	9.35	1.86	0.62	17.49	1.11
W0412-0506-1	12.65	10.04	1.91	0.62	18.76	1.14
W0412-0607-0	13.61	9.47	2.06	0.62	17.95	1.23
W0412-0607-1	13.61	9.77	2.12	0.62	18.53	1.27
W0412-0708-0	13.17	9.17	2.13	0.62	17.62	1.27
W0412-0708-1	13.17	9.68	2.18	0.62	18.59	1.30
TEST ID	$\bar{h}_{pool}$ (kw/m^2°C)	$\bar{h}_{mix,eff}$ (w/m^2°C)	$\bar{h}_{mix,conv}$ (w/m^2°C)	Re$_{mix}$ ($\times 10^4$)	$\dot{m}_{mix}$ (10^{-1}kg/s)	$\frac{\dot{Q}_{cond}}{\dot{Q}_{pool}+\dot{Q}_{mix}}$
W0412-0001-0	1.32	14.16	9.57	2.21	1.39	0.91
W0412-0102-0	1.94	14.20	9.60	2.24	1.41	0.87
W0412-0203-0	2.24	14.52	9.90	2.35	1.48	0.96
W0412-0304-0	3.32	14.61	9.97	2.38	1.50	1.22
W0412-0304-1	3.49	14.88	10.25	2.38	1.50	1.16
W0412-0405-0	3.63	13.86	9.18	2.36	1.49	1.24
W0412-0405-1	4.14	13.89	9.22	2.36	1.49	1.11
W0412-0506-0	3.66	14.16	9.46	2.41	1.51	1.13
W0412-0506-1	3.93	14.46	9.78	2.40	1.51	1.06
W0412-0607-0	3.90	15.77	11.05	2.43	1.53	1.18
W0412-0607-1	4.02	16.20	11.50	2.41	1.52	1.15
W0412-0708-0	3.91	16.22	11.50	2.45	1.54	1.17
W0412-0708-1	4.13	16.57	11.87	2.44	1.54	1.11

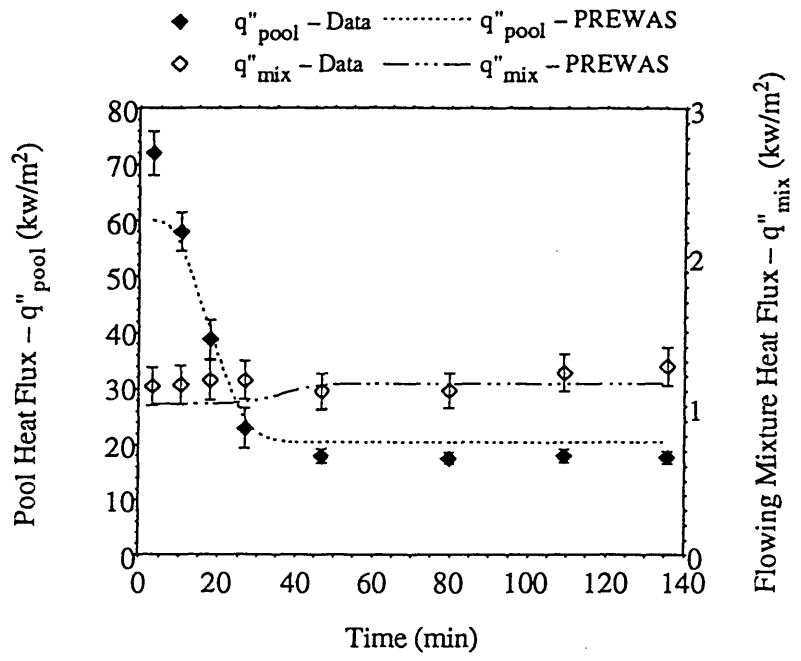

Figure B.15.a W0412 Test Results – Heat Flux

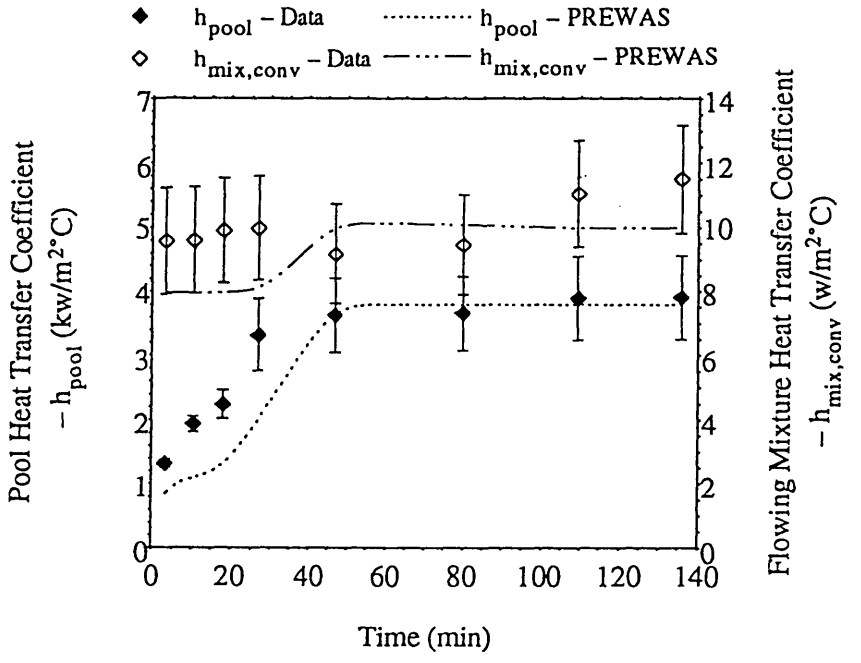

Figure B.15.b W0412 Test Results – Heat Transfer Coefficient

Table B.16.a Water-Filled Test Thermocouple Raw Data – W0430

TC ID	Function	W0430-00 (°C)	W0430-01 (°C)	W0430-02 (°C)	W0430-03 (°C)	W0430-04 (°C)	W0430-05 (°C)	W0430-06 (°C)	W0430-07 (°C)	W0430-08 (°C)
TC1	T_{wo}	-	86.8	96.2	99.9	104.5	104.8	104.6	104.6	104.5
TC2	T_{wo}	-	93.7	101.1	103.3	104.6	104.5	104.5	104.4	104.4
TC3	T_{wo}	-	109.6	109.6	109.1	110.3	109.9	109.8	109.8	109.9
TC4	T_{wo}	-	109.6	109.6	109.1	110.1	109.8	109.7	109.7	109.9
TC5	T_{wo}	-	108.2	108.3	107.7	108.8	108.4	108.4	108.4	108.4
TC6	T_{wo}	-	109.2	109.2	108.7	109.7	109.3	109.1	109.2	109.3
TC7	T_{wo}	-	109.3	109.3	108.8	109.9	109.5	109.4	109.4	109.5
TC8	T_{wo}	-	109.4	109.4	108.9	110.0	109.6	109.5	109.5	109.6
TC9	T_{wo}	-	109.3	109.3	108.8	109.8	109.5	109.4	109.4	109.4
TC10	T_{wo}	-	109.3	109.4	108.8	109.9	109.5	109.4	109.4	109.5
TC11	T_{stm}	-	110.0	110.1	109.5	110.6	110.3	110.1	110.1	110.2
TC12	T_{stm}	-	110.2	110.1	109.6	110.6	110.3	110.1	110.1	110.2
TC13	T_{stm}	-	110.0	110.1	109.5	110.5	110.2	110.1	110.1	110.2
TC14	T_{stm}	-	110.1	110.2	109.7	110.7	110.4	110.2	110.2	110.3
TC15	T_{stm}	-	110.2	110.1	109.6	110.6	110.3	110.1	110.1	110.2
TC16	T_{pi}	15.0	54.4	76.9	87.4	100.0	100.3	100.3	100.4	100.4
TC17	T_{pi}	26.0	68.9	89.1	95.3	100.3	100.4	100.4	100.4	100.5
TC21	T_{po}	13.6	15.7	18.1	20.5	24.9	29.9	34.5	40.4	45.5
TC22	T_{po}	14.3	16.0	18.6	20.6	25.0	30.2	34.9	40.6	45.8
TC31	$T_{mix,o}$	-	39.0	39.3	39.4	40.3	40.6	41.2	41.3	41.4
TC40	heat loss estimation	-	39.4	39.7	39.8	40.7	41.0	41.5	41.7	41.7
TC41	heat loss estimation	-	39.3	39.7	39.8	40.8	40.9	41.5	41.6	41.6
TC43	$T_{air,in}$	25.7	26.0	26.0	26.1	26.1	26.2	26.2	26.3	26.4
TC44	$T_{wi,PVC}$	-	29.6	29.7	29.8	30.1	30.5	30.8	31.0	31.1
TC45	$T_{wi,PVC}$	-	31.7	31.5	31.4	31.3	31.4	31.6	31.7	31.9
TC46	$T_{wi,gal}$	-	34.8	35.0	35.2	35.8	36.5	37.0	37.0	37.2
TC47	$T_{wi,gal}$	-	34.9	34.9	35.0	35.6	36.2	36.7	36.7	37.0

Notes: (1) see Figure 3.7 and Figure 3.8 for thermocouple (TC) location

(2) see Table 3.2 for T_i notation

Table B.16.b Water-Filled Test Raw Data – W0430

TEST ID	Time (min)	P_{atm} (kPa)	ϕ_{in} (%)	ϕ_o (%)	H_{pool} (m)	$\overline{T}_{sm}$ (°C)	$\overline{T}_{wo,pl}$ (°C)	$\overline{T}_{wo,mix}$ (°C)
W0430-00	0	102.3	40.0	-	1.524	-	-	-
W0430-01	9.97	102.3	40.0	20.7	1.524	110.1	90.2	109.2
W0430-02	19.30	102.3	40.0	22.3	1.524	110.1	98.7	109.3
W0430-03	25.70	102.3	40.0	23.9	1.524	109.6	101.6	108.7
W0430-04	40.75	102.3	40.0	36.4	1.519	110.6	104.5	109.8
W0430-05	61.33	102.3	40.0	40.5	1.511	110.3	104.6	109.5
W0430-06	88.00	102.3	40.0	39.8	1.499	110.1	104.6	109.3
W0430-07	117.52	102.3	40.0	40.1	1.486	110.1	104.5	109.4
W0430-08	150.10	102.3	40.0	40.2	1.470	110.2	104.5	109.4
TEST ID	$\overline{T}_{pi}$ (°C)	$\overline{T}_{po}$ (°C)	$\overline{T}_{air,in}$ (°C)	$\overline{T}_{mix,o}$ (°C)	$\overline{T}_{wi,PVC}$ (°C)	$\overline{T}_{wi,gal}$ (°C)	$\overline{V}_{mix}$ (m/s)	$\dot{m}_{cond}$ ($\times 10^{-3}$ kg/s)
W0430-00	20.5	13.9	25.7	-	-	-	-	-
W0430-01	61.7	15.9	26.0	39.0	30.6	34.9	1.64	15.15
W0430-02	83.0	18.4	26.0	39.3	30.6	35.0	1.64	9.36
W0430-03	91.3	20.5	25.7	39.4	30.6	35.1	1.66	7.84
W0430-04	100.1	25.0	26.1	40.3	30.7	35.7	1.74	5.90
W0430-05	100.3	30.0	26.2	40.6	31.0	36.3	1.84	5.03
W0430-06	100.4	34.7	26.2	41.2	31.2	36.9	1.79	4.23
W0430-07	100.4	40.5	26.3	41.3	31.4	36.9	1.80	4.35
W0430-08	100.4	45.7	26.4	41.4	31.5	37.1	1.78	4.23

Table B.16.c Water-Filled Test Results – W0430

TEST ID	$\dot{Q}_{cond}$ (kw)	$\dot{Q}_{pool}$ (kw)	$\dot{Q}_{mix}$ (kw)	$\dot{Q}_{rad}$ (kw)	$\bar{q}''_{pool}$ (kw/m^2)	$\bar{q}''_{mix}$ (kw/m^2)
W0430-0001-0	33.78	32.79	1.72	0.58	59.92	1.04
W0430-0102-0	20.87	20.61	1.69	0.58	37.66	1.02
W0430-0203-0	17.49	14.94	1.67	0.57	27.30	1.01
W0430-0304-0	13.16	9.96	1.69	0.58	18.23	1.02
W0430-0304-1	13.16	10.93	1.77	0.58	18.87	1.07
W0430-0405-0	11.21	7.37	1.76	0.58	13.53	1.06
W0430-0405-1	11.21	7.42	1.90	0.58	13.64	1.15
W0430-0506-0	9.43	6.60	1.82	0.58	12.19	1.10
W0430-0506-1	9.43	6.98	1.95	0.57	12.90	1.17
W0430-0607-0	9.70	6.97	1.85	0.58	13.00	1.11
W0430-0607-1	9.70	6.89	2.00	0.58	12.87	1.20
W0430-0708-0	9.42	6.32	1.84	0.58	11.91	1.10
W0430-0708-1	9.42	6.68	1.96	0.58	12.59	1.17
TEST ID	$\bar{h}_{pool}$ (kw/m^2°C)	$\bar{h}_{mix,eff}$ (w/m^2°C)	$\bar{h}_{mix,conv}$ (w/m^2°C)	Re$_{mix}$ ($\times 10^4$)	$\dot{m}_{mix}$ (10^{-1}kg/s)	$\frac{\dot{Q}_{cond}}{\dot{Q}_{pool}+\dot{Q}_{mix}}$
W0430-0001-0	1.22	13.57	9.02	2.16	1.36	0.98
W0430-0102-0	1.70	13.36	8.79	2.16	1.36	0.94
W0430-0203-0	2.11	13.33	8.75	2.16	1.37	1.05
W0430-0304-0	3.11	13.55	8.94	2.22	1.40	1.13
W0430-0304-1	3.42	14.14	9.55	2.20	1.39	1.03
W0430-0405-0	3.11	14.18	9.53	2.33	1.47	1.23
W0430-0405-1	3.14	15.17	10.56	2.30	1.46	1.20
W0430-0506-0	2.87	14.74	10.09	2.35	1.48	1.12
W0430-0506-1	3.03	15.62	11.01	2.33	1.47	1.06
W0430-0607-0	3.12	14.99	10.33	2.33	1.47	1.10
W0430-0607-1	3.09	16.03	11.41	2.30	1.46	1.10
W0430-0708-0	2.90	14.85	10.18	2.32	1.46	1.15
W0430-0708-1	3.07	15.73	11.10	2.30	1.45	1.09

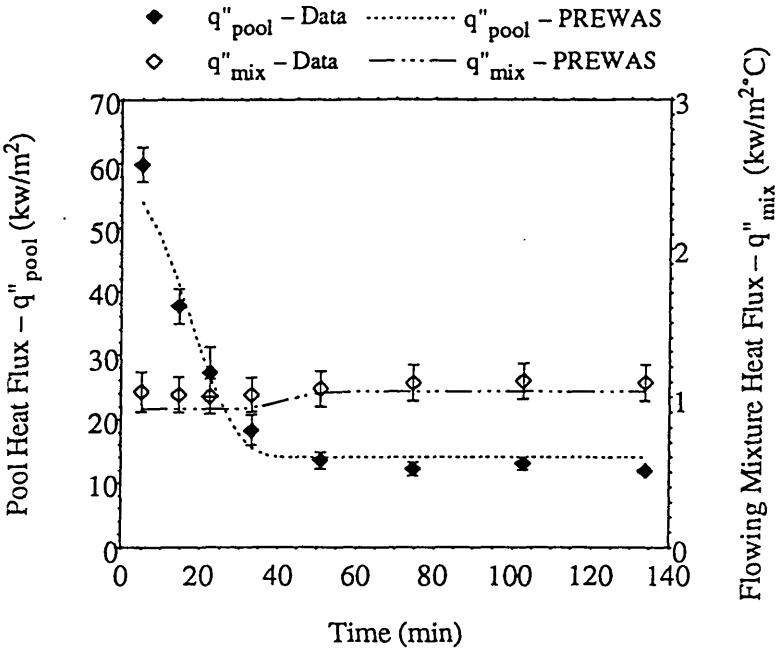

Figure B.16.a W0430 Test Results – Heat Flux

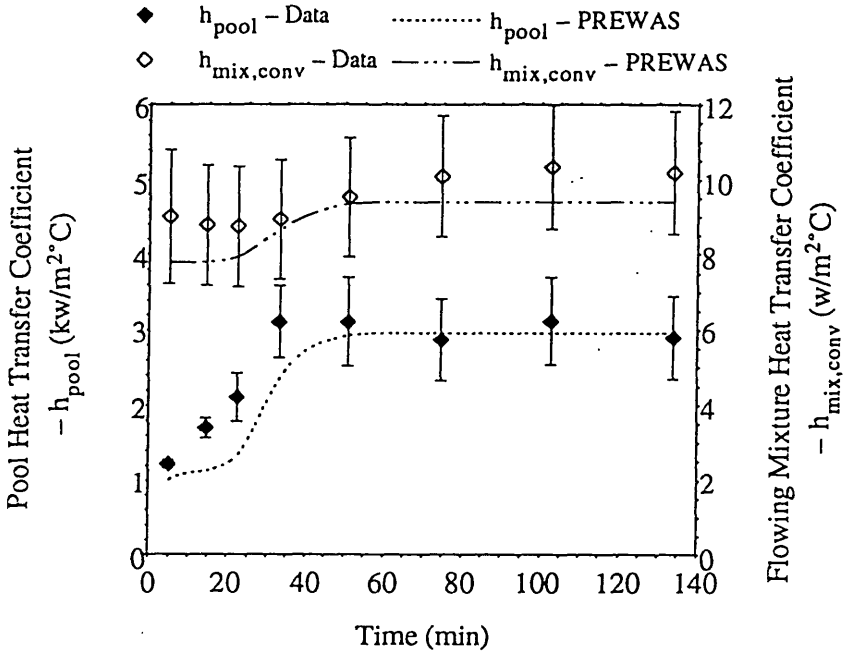

Figure B.16.b W0430 Test Results – Heat Transfer Coefficient

APPENDIX C

COMPUTER PROGRAM FOR THE PREDICTION OF THE PREFILLED WATER-AIR ANNULUS PASSIVE CONTAINMENT COOLING SYSTEM HEAT TRANSFER PERFORMANCE

C.1 Introduction

In the prefilled water-air annulus passive containment cooling system, it is assumed that core decay heat is removed by evaporation of water in the prefilled water pool and natural air convection. A schematic diagram of the system is shown in Figure C.1. Heat transfer to the water-filled section and the air-filled section are coupled together through the steam generation rate in the water pool. The steam flow is considered to be uniformly mixed at the beginning of the air section with incoming air flow from an air window. In the air section, momentum balance equations are employed to evaluate air mass flow rate, but energy balance equations are applied to the steam-air mixture flow to evaluate the heat transfer rate. In the water-filled section, continuity equations and energy balance equations are applied to evaluate the heat transfer rate and the steam generation rate. The following sections present a brief description of the model. The assumptions employed in the computer program are summarized as follows.

- uniform mixing of steam and air inside containment and in the air section of the annulus
- core decay heat as given by ORNL-6554 [F-1]
- inner and outer pool are only connected at the bottom window, and the outer surface of the duct wall is perfectly insulated
- the air flow is considered one dimensional, fully developed and turbulent
- the air is a non-participating medium with respect to radiation
- acceleration pressure drop is neglected
- air is a perfect gas

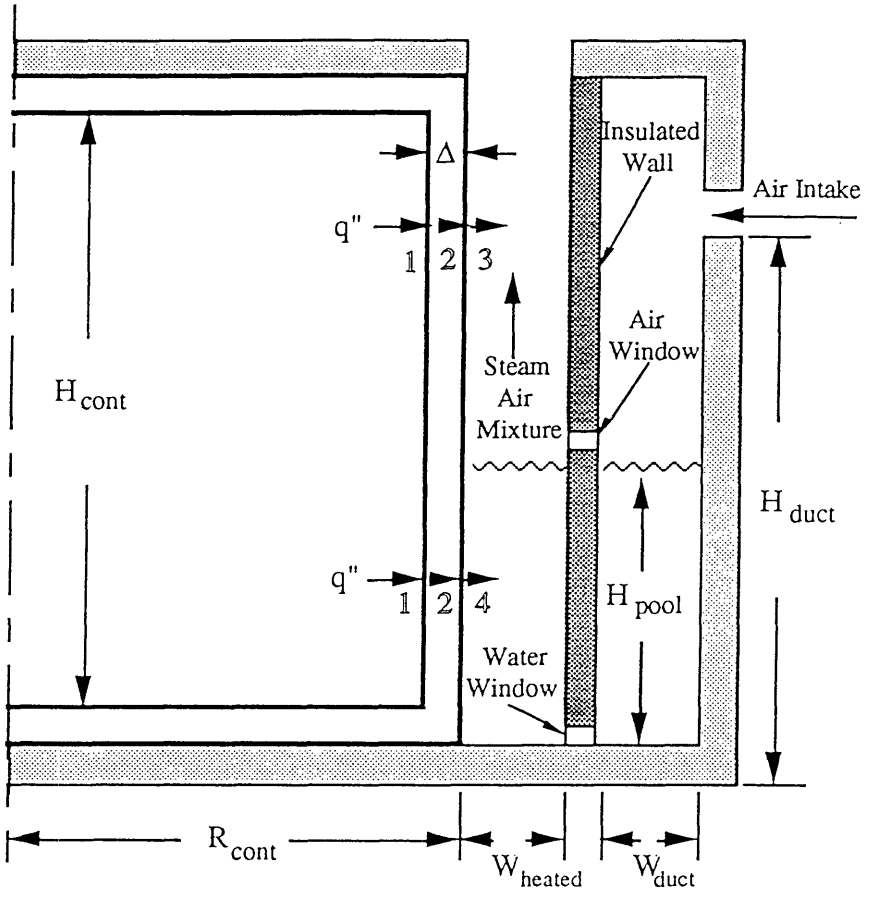

1: Condensation Heat Transfer
2: Conduction Heat Transfer
3: Natural Convection and Radiative Heat Transfer
4: Nucleate Boiling or Free Convection Heat Transfer

Figure C.1 Heat Transfer Model of Prefilled Water-Air Annulus Passive Containment Cooling System

C.2 Heat Transfer in Water-Filled Section

As shown in Figure C.2, the inner annulus water pool (heated region) is divided into N nodes with equal length. Node N+1 represents the outer annulus water pool (unheated region). The inner and outer pool can only communicate at the bottom window, therefore, there is no convection between the inner and outer pool. The total heat transfer rate to pool water is the summation of the heat transfer rate to each heated node, that is,

$$\dot{Q}_{pool} = \sum_{j=1}^{N} \dot{Q}_{pool,j} . \tag{C.1}$$

Heat transfer mechanisms in each node can be free convection, subcooled nucleate boiling, or saturated pool boiling, depending on the degree of wall superheat and pool temperature. Bergles and Rohsenow's nucleation correlation [T-2] is adopted as a criterion for boiling inception.

$$q_i'' = 15.6 P^{1.156} (T_{wo} - T_{sat})_i^{2.3/P^{0.0234}} \tag{C.2}$$

where P is in psi; T_{wo} and T_{sat} are in °F; $(T_{wo}-T_{sat})_i$ is required wall superheat for boiling incipience; and q" is in BTU/hr-ft². An alternative boiling inception criterion provided in the code is the Frost and Dzakowic correlation [F-5]:

$$q_i'' = \frac{k_f h_{fg}}{8 T_{sat} \nu_{fg} \sigma} \left[\frac{(T_w - T_{sat})_i^2}{Pr_f} \right]. \tag{C.3}$$

It is assumed that subcooled nucleate boiling will occur if the wall superheat is equal to or greater than the required wall superheat for boiling incipience. Moreover, if the pool temperature reaches saturation temperature, saturated pool boiling is assumed. Continuity equations and energy balance equations are applied in each node to evaluate the heat transfer rate. The governing equations employed in free convection and nucleate boiling heat transfer at each node are described as follows.

(1) Free Convection Heat Transfer

$$\dot{Q}_{pool,j} = [\pi D_{cont} H_{pool} U_{FC} (T_{cont} - T_{pool})]_j \tag{C.4}$$

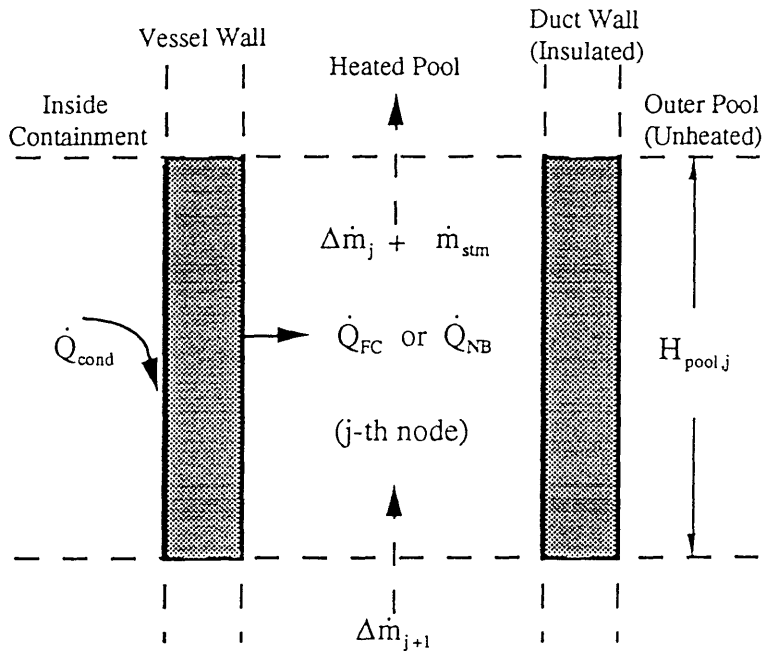

Figure C.2 Pool Section Nodal Heat Balance

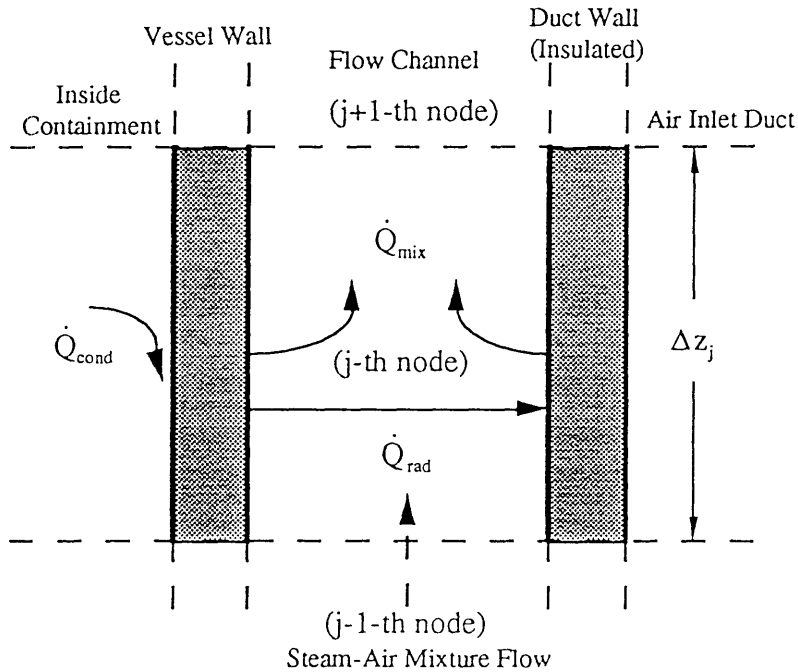

Figure C.3 Air Section Nodal Heat Balance

where U_{FC} is the total thermal conductance between in-containment condensation heat transfer and free convection heat transfer in the water pool. Uchida's condensation heat transfer correlation * [U-1, G-3] and Hitachi's free convection heat transfer correlation [K-3] are employed in this program.

$$U_{FC} = \left(\frac{1}{h_{cond}} + \frac{\Delta}{k_w} + \frac{1}{h_{FC}}\right)^{-1} \tag{C.5}$$

$$h_{cond} = 450 \cdot \left(\frac{m_{air,cont}}{m_{stm,cont}}\right)^{-0.8} \tag{C.6}$$

$$h_{FC} = Nu \frac{k_f}{L} \tag{C.7}$$

$$Nu = 0.13\ Ra^{1/3} \tag{C.8}$$

After heat is added to the pool, the pool temperature at each node will increase according to the following equation:

$$T_{pool,j}(t_2) = T_{pool,j}(t_1) + \left(\frac{\dot{Q}_{pool}\Delta t}{m_{pool} C_{pf}}\right)_j . \tag{C.9}$$

If the pool temperature reaches the corresponding saturation temperature, water will boil and the void-free pool height will decrease due to evaporation of water. The new pool height of each node, $H_{pool,j}(t_2)$, can be evaluated by an energy balance equation.

$$H_{pool,j}(t_2) = H_{pool,j}(t_1) - H_{pool,j}(t_1)\frac{A_{pi}}{A_{pi} + A_{po}}\left[\frac{C_{pf}(T_{pool} - T_{sat})}{h_{fg}}\right]_j \tag{C.10}$$

* Note: The Tagami-Uchida (T-U) correlation, which best represents condensation heat transfer over the whole containment transient reverts to the Uchida-only result for times after the occurrence of peak pressure. Since our interest is in the post-peak pressure period, and the simpler Uchida-only correlation is conservative relative to the T-U correlation, it was used in this thesis.

The steam generation rate due to water evaporation can be evaluated by:

$$\dot{m}_{stm,j} = (\frac{\dot{Q}_{pool}}{h_{fg}})_j, \tag{C.11}$$

or

$$\dot{m}_{stm,j} = [\frac{H_{pool,j}(t_1) - H_{pool,j}(t_2)}{\Delta t}](A_{pi} + A_{po})\rho_f, \tag{C.12}$$

and

$$\dot{m}_{stm} = \sum_{j=1}^{N} \dot{m}_{stm,j}. \tag{C.13}$$

(2) Nucleate Boiling Heat Transfer

$$\dot{Q}_{pool,j} = [\pi D_{cont} H_{pool} U_{NB} (T_{cont} - T_{sat})]_j \tag{C.14}$$

where, U_{NB} is the total thermal conductance between in-containment condensation heat transfer and nucleate pool boiling heat transfer in a water pool. Rohsenow's nucleate pool boiling heat transfer correlation [R-1] is employed in the program.

$$U_{NB} = (\frac{1}{h_{cond}} + \frac{\Delta}{k_w} + \frac{1}{h_{NB}})^{-1} \tag{C.15}$$

$$h_{NB} = (\frac{C_{pf}\Delta T_{sat}}{C_{sf} h_{fg} Pr_f})^{\frac{1}{0.33}} \cdot \frac{\mu_f h_{fg}}{\Delta T_{sat}[\frac{\sigma}{g(\rho_f - \rho_g)}]^{0.5}}, \tag{C.16}$$

where C_{sf} is the correlation constant, which depends on both the surface and the fluid. The water-filled test results of our experiment shows that C_{sf} equals 0.013 for the stainless steel and water as the heated surface and the fluid, respectively.

In case of subcooled boiling, there is no net vapor generation and the heat addition is used to raise the pool temperature. Equation C.9 can again be used to evaluate the new pool temperature. In saturated pool boiling situation, the pool temperature will still equal the corresponding saturation temperature, but the pool height will decrease due to boiling.

$$H_{pool,j}(t_2) = H_{pool,j}(t_1) - \frac{\dot{Q}_{pool,j}\Delta t}{(A_{pi} + A_{po})\rho_f h_{fg}} \qquad (C.17)$$

The steam generation rate can be evaluated in the same way as in free convection heat transfer, Equations C.11 to C.13.

Since the outer annulus water pool is assumed unheated and it can communicate with the inner pool through the bottom window, water consumption due to boiling at each node will be partially supplied by its neighboring node. The temperature of each node should, then, be reevaluated as the mixed temperature at time t_2, $T_{pool,j}(t_2)$ by applying the energy balance equation.

$$(m_{pool,j} - \dot{m}_{stm,j}\Delta t - \Delta m_{pool,j})C_{pf,j}[T_{pool,j}(t_2) - T_{pool,j}(t_1)]$$

$$= \Delta m_{pool,j+1}C_{pf,j+1}[T_{pool,j+1}(t_1) - T_{pool,j}(t_2)] \qquad (C.18)$$

Therefore,

$$T_{pool,j}(t_2) = \frac{T_{pool,j}(t_1) + T_{pool,j+1}(t_1)\dfrac{\Delta m_{pool,j+1}C_{pf,j+1}}{(m_{pool,j} - \dot{m}_{stm,j}\Delta t - \Delta m_{pool,j})C_{pf,j}}}{1 + \dfrac{\Delta m_{pool,j+1}C_{pf,j+1}}{(m_{pool,j} - \dot{m}_{stm,j}\Delta t - \Delta m_{pool,j})C_{pf,j}}}. \qquad (C.19)$$

where, $\dot{m}_{stm,j}$ is the steam generation rate at the j-th node. It can be evaluated from Equations C.11 or C.12. $\Delta m_{pool,j}$ is the amount of water supplied from the j-th node to the (j-1)-th node. $\Delta m_{pool,j+1}$ is the amount of water supplied from the (j+1)-th node to the j-th node. $\Delta m_{pool,j}$ and $\Delta m_{pool,j+1}$ can be evaluated by assuming the inner and outer pools will be at the same height after water boil-off.

C.3 Heat Transfer Above Water Pool Section

As shown in Figure C.3, the heated air flow channel is divided into NI nodes of equal length. The total heat transfer rate to the air flow channel is equal to the summation of heat transfer rate to each node, that is,

$$\dot{Q}_{mix} = \sum_{j=1}^{NI} \dot{Q}_{mix,j} \cdot \tag{C.20}$$

The heat transfer rate through the containment steel wall is equal to the power removed by the steam-air mixture, since it is assumed the outside surface of the duct wall is insulated.

$$\dot{Q}_{mix,j} = \dot{m}_{mix} C_{p,mix,j} (T_{mix,j} - T_{mix,j-1}) \tag{C.21}$$

$$= S_{cont,j} U_{mix} (T_{cont} - T_{wo,j}) \tag{C.22}$$

where, U_{mix} is the thermal conductance between in-containment condensation heat transfer and steel wall conduction heat transfer,

$$U_{mix} = (\frac{1}{h_{cond}} + \frac{\Delta}{k_w})^{-1}, \tag{C.23}$$

and T_{mix} is the steam-air mixture temperature. The inlet mixture temperature of the first node (j = 1) can be evaluated by the energy balance equation:

$$\dot{m}_{air} C_{p,air} (T_{mix} - T_{air}) = \dot{m}_{stm} C_{p,stm} (T_{stm} - T_{mix}). \tag{C.24}$$

Therefore,

$$T_{mix} = \frac{T_{air} \dot{m}_{air} C_{p,air} + T_{stm} \dot{m}_{stm} C_{p,stm}}{\dot{m}_{air} C_{p,air} + \dot{m}_{stm} C_{p,stm}}. \tag{C.25}$$

The heat balance for the j-th node can also be written to reflect that the mixture is heated by convection from both bounding walls. The governing equation is

$$\dot{Q}_{mix,j} = [h_{mix,cont} S_{cont} (T_{wo} - T_{mix}) + h_{mix,duct} S_{duct} (T_{duct} - T_{mix})]_j. \tag{C.26}$$

The power radiated from the containment wall to the duct wall must also be in equilibrium with the power convected to the mixture from the duct wall.

$$[h_{mix,duct} S_{duct} (T_{duct} - T_{mix})]_j = [C_1 S_{cont} (T_{wo}^4 - T_{duct}^4)]_j \tag{C.27}$$

where

$$C_1 = \sigma[\frac{1}{\varepsilon_{cont}} + \frac{D_{cont}}{D_{duct}}(\frac{1}{\varepsilon_{duct}} - 1)]^{-1} \quad (C.28)$$

Equations C.20 to C.28 are complemented by closure equations for heat transfer coefficients, $h_{mix,cont,j}$ and $h_{mix,duct,j}$, and by an equation for mixture mass flow rate, $\dot{m}_{mix}$. The heat transfer coefficient adopted is the ANL (Argonne National Laboratory) heat transfer correlation [H-1].

$$h_{mix} = 0.0229 Re^{0.8} Pr^{0.4} \frac{k_{mix}}{D} (\frac{T_{wo}}{T_{mix}})^{-0.4} [1 + (\frac{L}{W})^{-0.36}] \quad (C.29)$$

In addition, Gang Fu's mixed convection heat transfer correlation [F-3] can also be selected in the program.

$$h_{mix} = \frac{0.021 Re^{0.8} Pr^{0.4}}{1 + (\frac{5500}{Re})^3} \frac{k_{mix}}{D_h} (\frac{T_{wo}}{T_{mix}})^{-0.5} \quad (C.30)$$

However, the air-only test results show ANL's heat transfer correlation can well predict the experimental results.

The mixture flow rate is the summation of steam flow rate, derived in the previous section, and buoyancy induced air flow rate.

$$\dot{m}_{mix} = \dot{m}_{stm} + \dot{m}_{air} \quad (C.31)$$

The air flow rate is derived from a momentum balance equation under the assumption of incompressible, one-dimensional fully-developed turbulent flow. The governing equations are:

$$\dot{m}_{air} = (\frac{\Delta P_b}{C_2 + C_3})^{0.5}, \quad (C.32)$$

where the thermal buoyancy is evaluated as

$$\Delta P_b = g\sum_{i=1}^{N1}\rho_i\Delta z_i - g\sum_{i=1}^{N2}\rho_i\Delta z_i - g\sum_{j=1}^{NI}\rho_i\Delta z_j . \quad (C.33)$$

C_2 and C_3 represent the pressure drop due to form and friction losses in the heated channel and unheated channel, respectively.

$$C_2 = \sum_{j=1}^{NI}(K_{c,j} + K_{f,j})\frac{1}{\rho_j A_{mix,j}^2} \quad (C.34)$$

$$C_3 = \sum_{i=1}^{N1+N2}(K_{c,i} + K_{f,i})\frac{1}{\rho_i A_{mix,i}^2} \quad (C.35)$$

N1 and N2 represent number of nodes in the duct region and chimney region, if applicable, respectively. K_f and K_c are friction and form loss coefficients, respectively. Idelchik's formulas are employed in the program [I-1],

$$K_{f,j} = [0.11(\frac{\delta}{D_h} + \frac{68}{Re})^{0.25}\frac{\Delta z}{D_h}]_j, \quad (C.36)$$

$$K_{f,i} = [0.11(\frac{\delta}{D_e} + \frac{68}{Re})^{0.25}\frac{\Delta z}{D_e}]_i . \quad (C.37)$$

C.4 Evaluation of Containment Atmospheric Temperature

It is assumed that steam and air contained inside the containment are uniformly mixed. The containment atmosphere temperature can be evaluated by applying an energy balance equation.

$$T_{cont}(t_2) = T_{cont}(t_1) + \frac{[(1 - SF)\dot{Q}_{decay} - \dot{Q}_{removal}]\Delta t}{(m_{stm}C_{v,stm} + m_{air}C_{v,air})_{cont}} \quad (C.38)$$

where, $\dot{Q}_{removal}$ is the total power removed by the water pool and air channel.

$$\dot{Q}_{removal} = \dot{Q}_{pool} + \dot{Q}_{mix} \quad (C.39)$$

$\dot{Q}_{decay}$ is the decay power. Mass of air inside containment ($m_{air,cont}$) is evaluated using the perfect gas law; and mass of steam inside containment ($m_{stm,cont}$) is evaluated from saturated steam tables. SF is the heat storage factor of the containment structure at a given time following decay heat dumping initiation.

For the closure of the equations listed above for solution, a set of formulas for material properties are needed. The dynamic viscosity, thermal conductivity, and specific heat at constant pressure for air at a given temperature are calculated from Irvine's polynomial equations [I-3]. The saturation pressure of steam at a given temperature is also calculated from Irvine's polynomial equations. The thermodynamic properties for the steam and liquid water at a given temperature are calculated by interpolation in Keenan's steam tables [K-4]. To obtain the thermodynamic properties of the steam-air mixture, simplified mixing laws are applied [S-1]:

$$k_{mix} = \frac{y_{air} k_{air} M_{air}^{1/3} + y_{stm} k_{stm} M_{stm}^{1/3}}{y_{air} M_{air}^{1/3} + y_{stm} M_{stm}^{1/3}}, \tag{C.40}$$

$$\mu_{mix} = \frac{y_{air} \mu_{air} M_{air}^{1/2} + y_{stm} \mu_{stm} M_{stm}^{1/2}}{y_{air} M_{air}^{1/2} + y_{stm} M_{stm}^{1/2}}, \tag{C.41}$$

$$C_{p,mix} = y_{air} C_{p,air} + y_{stm} C_{p,stm}, \tag{C.42}$$

where, y_{air} and y_{stm} are the mole fractions of air and steam in the mixture, respectively. They are evaluated by Dalton's partial pressure law.

C.5 Computer Program - PREWAS

A computer program - PREWAS, written in FORTRAN 77 has been developed, based on the equations given above, to evaluate the heat transfer performance of the prefilled water-air annulus passive containment cooling system. The achievement of the computation is through the calculation of a set of iteration loops. Figure C.4 shows a simplified flow diagram for the computation. Table C.1 provides the input and output data description for a constant in-containment temperature and air-cooled-only sample case.

Table C.1 Input and Output Data Description
(Constant In-Containment Temperature and Air-Cooled-Only Sample Case)

Input Data			
Card No	Symbol	Description	Sample Data
1	ITITLE	title	–
2	TCONT	containment temperature	4.10650D+02
	EPS	iteration error (%)	2.00000D+00
	EKR	containment wall conductivity	4.00000D+01
	HPOOL	pool height	0.00000D+00
	ELT	containment height	6.00000D+01
	ELD	duct height	6.00000D+01
3	DELR	containment inner diameter	5.99100D+01
	DELD	duct wall inner diameter	6.05000D+01
	DTR	containment outer diameter	6.00000D+01
	DTD	duct wall outer diameter	6.05900D+01
	DG	gap width of outer pool	2.50000D–01
4	E1	containment wall surface emissivity	7.00000D–01
	E2	duct wall surface emissivity	7.00000D–01
	SIGM	Stefan-Boltzman constant	5.66900D–08
5	N1	total number of nodes in air section	2
	IR	node number of heated region (air section)	2
	NR	number of axial nodes in heated region (air section)	20
	NP(1-N1)	number of parallel air flow path of individual nodes, NP(1)	1
		NP(2)	1
	N1	number of time step	2
	NDT	time step	30
	NN	number of nodes in water section	0
6	D1(1-N1)	hydraulic diameter of individual nodes (air section), D1(1)	5.00000D–01
		D1(2)	5.00000D–01
7	A1(1-N1)	flow area of individual nodes (air section), A1(1)	4.78000D+01
		A1(2)	4.75000D+01

Note: All in SI units except as noted.

Table C.1 Input and Output Data Description (Continued)

Input Data			
Card No	Symbol	Description	Sample Data
9	EK1(1-N1)	form loss coefficient of individual nodes, EK1(1)	1.50000D+01
		EK1(2)	1.50000D+01
10	DEL(1-N1)	wall roughness of individual nodes, DEL(1)	4.60000D-04
		DEL(2)	4.60000D-04
11	DZ1(1-N1)	elevation difference of individual nodes (air section), DZ1(1)	6.00000D+01
		DZ1(2)	6.00000D+01
12	T(1-N1)	inlet temperature of individual nodes (air section), T(1)	2.99360D+02
		T(2)	3.00000D+02
13	TPOOL(1-NN)	initial pool temperature of individual nodes, TPOOL(1)	0.00000D+02
		TPOOL(2)	0.00000D+02
	TPOOL(NN+1)	outer pool temperature, TPOOL(3)	0.00000D+02
14	PIN	atmospheric pressure	1.02330D+05
	RH	inlet air relative humidity	4.00000D-01
15	AIR	in-containment air mass	1.16000D+05
	VCONT	containment free volume	1.00000D+05
16	QRATED	reactor rated thermal power	4.00000D+09
	S	heat storage factor	0.00000D+00
	STM	heat storage time	0.00000D+00
	CSF	Rohsenow nucleate boiling correlation constant	1.30000D-02
Output Data			
Group No	Symbol	Description	Sample Data
1	Time	time (min)	5.0000D-01
	Twall(1-NN)	heated wall outer surface temperature (pool section)	0.0000D+00
	Tpool(1-NN)	pool temperature of individual nodes	0.0000D+00

Note: All in SI units except as noted.

Table C.1 Input and Output Data Description (Continued)

Output Data			
Group No	Symbol	Description	Sample Data
2	Time	time (min)	5.0000D–01
	Hpool	pool height	0.0000D+00
	Tcont	containment temperature	4.1065D+00
	Pair	partial pressure of air (MPa)	1.3673D–01
	Psteam	partial pressure of steam (MPa)	3.3546D–01
	Pcont	containment pressure (MPa)	4.7220D–01
3	Time	time (min)	5.0000D–01
	Qpool	heat transfer rate to pool	0.0000D+00
	Qair	heat transfer to air	8.3990D+06
	Qtotal	total heat transfer rate	8.3990D+06
	Qdecay	decay power fraction (per 1MWth)	3.3426D–02
4	Time	time (min)	5.0000D–01
	hmix,e	effective heat transfer coefficient to steam-air mixture	1.0334D+01
	hmix,c	convective heat transfer coefficient to steam-air mixture	6.9769D+01
	hpool	averaged heat transfer coefficient to pool	0.0000D+00
	hcond	condensation heat transfer coefficient	6.4087D+02
5	Time	time (min)	5.0000D01
	Tmix,out	flowing mixture exit temperature	3.7423D+02
	Twall,air	heated wall outer surface temperature (air section)	4.0866D+02
	Mmix	flowing mixture mass flowrate	1.1079D+02
	Mair	air mass flowrate	1.0986D+02
	RE	flowing mixture Reynolds number	5.3924D+04
6	Time	time (min)	5.0000D–01
	q"pl	heat flux to pool section	0.0000D+00
	q"air	heat flux to air section	7.4263D+02

Note: All in SI units except as noted.

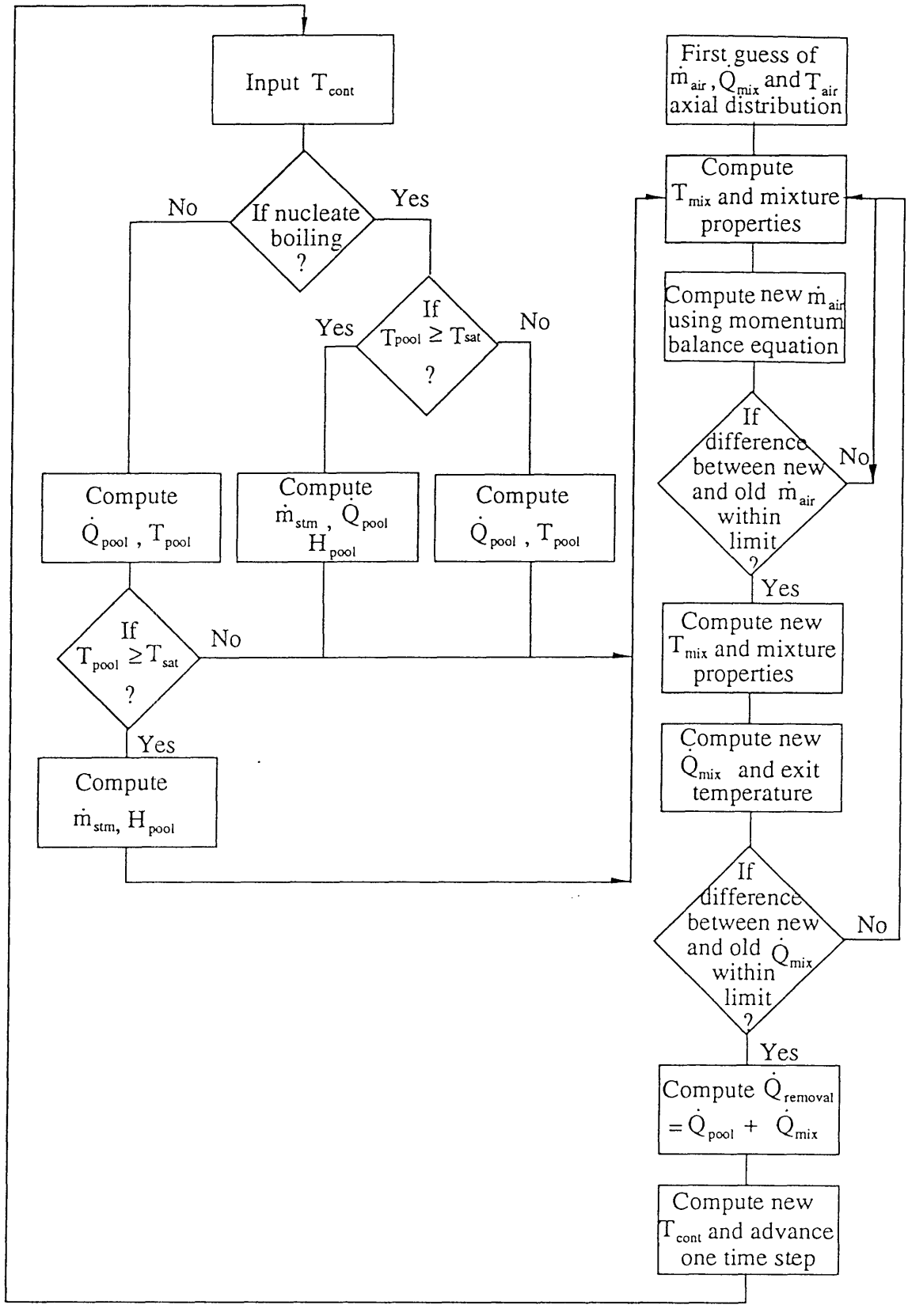

Figure C.4 Simplified Flow Diagram for Evaluation of Heat Transfer Performance

```
$DEBUG
C      MODEL OF PREFILLED WATER-AIR ANNULUS PCCS (TCONT=CONSTANT)
C
       IMPLICIT REAL*8(A-H,O-Z)
       CHARACTER*24 INDAT,OUTPT
       CHARACTER*72 ITITLE
       COMMON/PRE/D1(10),A1(10),DEL(10),DP(10),EK1(10),DZ1(10),
      /TR(100),QR(100),DPR(100),T2P(100),T3P(100),TWA(100),
      /QC(100),QRD(100),TMIXO(100),HMIXE(100),EMAA(100),EMMT(100),
      /REY(100),HCPL(100),HCD(100),SM(100),HMIXC(100),
      /T(10),ROMX(10),P(10),EL1(10),NP(10),QPI(100),QAI(100),
      /HPL(100),TWL(100,50),TPL(100,50),TCT(100),QTL(100),QDY(100),
      /TIME(100),PAR(100),PSTM(100),PCT(100),QHF(100),QPHF(100),
      /TPOOL(50),HP(50),QP(50),PP(50),TSAT(50),TWALL(50),DT(50),
      /ROFS(50),ROF(50),CPFS(50),CPF(50),HP3(50),HP31(50),INB(50)
       DATA PI/3.14159D0/, G/9.81D0/, R/2.8704D2/, RS/4.62D2/
       WRITE(*,1000)
 1000 FORMAT(' ENTER INPUT FILE NAME-------')
       READ(*,1010) INDAT
 1010 FORMAT(A16)
       OPEN(5,FILE=INDAT,STATUS='OLD',ERR=8888)
       WRITE(*,1020)
 1020 FORMAT(' ENTER OUTPUT FILE NAME-------')
       READ(*,1010) OUTPT
       OPEN(6,FILE=OUTPT,STATUS='NEW',ERR=9999)
       READ(5,201) ITITLE
  201 FORMAT(A72)
       WRITE(6,201) ITITLE
  200 FORMAT(6D12.5)
C-----------------------------------------------------------------------
C  TCONT - TEMP. OF CTMT ATM.          TPOOL(1-NN) - TEMP. OF HEATED POOL
C  EPS -ITERATION ERROR                TPOOL(NN+1) - TEMP. OF OUTER POOL
C  DTD - O.D. OF RISER WALL            CSF - CORRELATION CONSTANT
C  DTR - OUTER DIAM. OF CTMT           ELT - CTMT HEIGHT
C  DELR - ID OF CTMT                   DELD - ID OF RISER ANNULI WALL
C  HPOOL - WATER LEVEL HEIGHT          DG - GAP WIDTH OF DUCT
C  STEAM - IN-CTMT STEAM MASS          AIR - IN-CTMT AIR MASS
C  VCONT - FREE CTMT VOLUME            ELD - DUCT HEIGHT
C  EKR - CONDUCTIVITY OF CTMT VESSEL   T(N1) - INITIAL AIR SECT TEMP
C  S - HEAT STORAGE FACTOR             QRATED - RATED POWER
C  STM - STORAGE TIME
C  NN - NO. OF NODES IN WATER POOL     NI - NO OF TIME STEP
C  N1-TOTAL NUMBER OF AXIAL NODES WITH DIFFERENT FLOW AREA
C  NR-TOTAL NUMBER OF AXIAL NODES IN HEATED LENGTH
C  E1,E2,SIG- EMISSIVITIES OF HOT AND COLD WALLS, BOLTZMAN CONST.
C  IR -NUMBER OF HEATED NODE           NDT - TIME STEP
C  D1,A1,EL1,EK1 - HYDR.DIAM.,FLOW AREA, LENGTH, FORM LOSSES OF NODES
C  DEL,DZ1- WALL ROUGHNESS, HEIGHT OF INDIVIDUAL NODES
C  PIN - ATMOSPHERIC PRESSURE          RH - RELATIVE HUMIDITY
C  ALL IN SI UNITS
C-----------------------------------------------------------------------
       READ(5,200) TCONT,EPS,EKR,HPOOL,ELT,ELD
       WRITE(6,202) TCONT,EPS,EKR,HPOOL,ELT,ELD
  202 FORMAT(//'  TCONT,        EPS,          EKR,          HPOOL,        EL
     /T,          Hduct'/6(1X,1PD12.5))
       READ(5,200) DELR,DELD,DTR,DTD,DG
       WRITE(6,203) DELR,DELD,DTR,DTD,DG
  203 FORMAT('  DELR,         DELD,         DTR,          DTD,        DG'/
```

```
     /6(1X,1PD12.5))
      READ(5,200) E1,E2,SIGM
      WRITE(6,212) E1,E2,SIGM
  212 FORMAT('  E1,           E2,           SIG'/3(1X,1PD12.5))
      READ(5,205) N1,IR,NR,(NP(I),I=1,N1),NI,NDT,NN
  205 FORMAT(14I5)
      WRITE(6,206) N1,IR,NR,(NP(I),I=1,N1),NI,NDT,NN
  206 FORMAT('  N1,IR,NR,NP(1-N1),NI,NDT,NN'14I5)
      IF(IR.EQ.1) GOTO 666
      READ(5,200) (D1(I),I=1,N1)
      WRITE(6,211) (D1(I),I=1,N1)
  211 FORMAT('  D1(1-N1)    ',5(1X,1PD12.5))
      READ(5,200) (A1(I),I=1,N1)
      READ(5,200) (EL1(I),I=1,N1)
      READ(5,200) (EK1(I),I=1,N1)
  222 FORMAT('  EK1(1-N1)   ',5(1X,1PD12.5))
      WRITE(6,221) (A1(I),I=1,N1)
  221 FORMAT('  A1(1-N1)    ',5(1X,1PD12.5),2X)
      WRITE(6,230) (EL1(I),I=1,N1)
  230 FORMAT('  EL1(1-N1)   ',5(1X,1PD12.5))
      WRITE(6,222) (EK1(I),I=1,N1)
      READ(5,200) (DEL(I),I=1,N1)
      WRITE(6,231) (DEL(I),I=1,N1)
  231 FORMAT('  DEL(1-N1)   ',5(1X,1PD12.5))
      READ(5,200) (DZ1(I),I=1,N1)
      READ(5,200) (T(I),I=1,N1)
      WRITE(6,232) (DZ1(I),I=1,N1)
  232 FORMAT('  DZ1(1-N1)   ',5(1X,1PD12.5))
      WRITE(6,233) (T(I),I=1,N1)
  233 FORMAT('  T(1-N1)     ',5(1X,1PD12.5))
      READ(5,200) (TPOOL(I),I=1,NN+1)
      WRITE(6,234) (TPOOL(I),I=1,NN+1)
  234 FORMAT('  TPOOL(1-NN+1)'/6(1X,1PD12.5))
      READ(5,200) PIN,RH
      WRITE(6,235) PIN,RH
  235 FORMAT('  Patm,         RH',5(1X,1PD12.5))
      READ(5,200) AIR,VCONT
      WRITE(6,236) AIR,VCONT
  236 FORMAT('  Mair,        Vcont'/6(1X,1PD12.5))
      READ(5,200) QRATED,S,STM,CSF
      WRITE (6,237) QRATED,S,STM,CSF
  237 FORMAT('  Qrated,      S,           STM,         CSF'/6(1X,1PD12.5
      /))
C
      TI=1.D-10
      JK=1
      PCONT0=0.
      PCONT1=0.
      HPL(1)=HPOOL
      TMIXO(1)=T(N1)
      DO 2 JA=1,NN
      TPL(1,JA)=TPOOL(JA)
      TWL(1,JA)=TPL(1,JA)
    2 HP(JA)=HPOOL/NN
      DO 99 JC=1,NI
C HEAT TRANSFER IN WATER SECTION, QPP
C CONDENSATION HEAT TRANSFER, UCHIDA CORRELATION
      CALL PSAT(PSTEAM,TCONT)
```

```
      CALL SATWP(X1,PSTEAM,X2,X3,X4,X5,X6,X7,ROV)
      STEAM=VCONT*ROV
      IF(AIR.NE.0.) HCOND=450*(AIR/STEAM)**(-0.8)
      DK=(2.*EKR)/(DTR-DELR)
      IF(HCOND.GT.0.) U2=1./(1./DK+1./HCOND)
      IF(HCOND.EQ.0.) U2=DK
      IF(HPOOL.EQ.0.) GOTO 8
      DO 3 JB=1,NN
      IF(HP(JB).GT.0.) GOTO 4
      QP(JB)=0.
      TPOOL(JB)=0.
      SM(JB)=0.
      TWALL(JB)=0.
      GOTO 3
    4 HPO=0.
      AW1=PI*(DELD**2-DTR**2)/4.
      AW2=PI*((DTD+2.*DG)**2-DTD**2)/4.
      DO 5 JI=1,JB-1
    5 HPO=HPO+HP(JI)
      HPI=HPO+.5*HP(JB)
      CALL SUBWP(TPOOL(JB),DVFS,CPFS(JB),EKWS,ROFS(JB),BETA)
      PP(JB)=PIN+G*ROFS(JB)*HPI
C     PP(JB)=PIN
      CALL SATWP(TSAT(JB),PP(JB),DVF,CPF(JB),EKW,HFG,SURT,ROF(JB),ROG)
      SAPL=PI*DTR*HP(JB)
C FREE CONVECTIVE HEAT TRANSFER, HITACHI CORRELATION
      IF((TCONT-TPOOL(JB)).GT.0.) GOTO 70
      QP(JB)=0.
      GOTO 3
   70 C21=0.13*(G*BETA*CPFS(JB)/DVFS*(ROFS(JB)*EKWS)**2)**(1./3.)
      QPPP=1.D6
      DO 36 I=1,30
      DT(JB)=(QPPP/(C21*SAPL))**(3./4.)
      HFC=C21*DT(JB)**(1./3.)
      UFC=1./(1./U2+1./HFC)
      QP(JB)=SAPL*UFC*(TCONT-TPOOL(JB))
      IF(DABS(QPPP-QP(JB))/QPPP*100..LE.EPS)  GOTO 38
      QPPP=QP(JB)
   36 CONTINUE
      WRITE(6,37)
   37 FORMAT(' QPPFC DOES NOT CONVERGE')
      GOTO 89
C CHECK IF BOILING INCIPIENT
   38 TWALL(JB)=TPOOL(JB)+DT(JB)
      IF((TWALL(JB)-TSAT(JB)).LE.0.) GOTO 35
      DTS0=TWALL(JB)-TSAT(JB)
C BERGLES-ROHSENOW NUCLEATION CORRELATION
      DTSI=(QP(JB)/(SAPL*3.155)/(15.6*(PP(JB)*1.4505*1.D-4)**1.156))**((
     /PP(JB)*1.4505)**.0234/2.3)
C FROST-DZAKOWIC POOL NUCLEATION CORREATION
C     DTSI=(QP(JB)/SAPL*8.*TSAT(JB)*SURT*DVF*CPF(JB)*(1./ROG-1./ROF(JB))
C    //HFG/EKW**2)**.5
      IF(DTS0.GE.DTSI) INB(JB)=1
      IF(INB(JB).EQ.1) GOTO 40
   35 WATER=ROFS(JB)*HP(JB)*AW1
      TPOOL(JB)=TPOOL(JB)+(QP(JB)*NDT)/(CPFS(JB)*WATER)
      TWALL(JB)=TPOOL(JB)+DT(JB)
      IF(TPOOL(JB).LT.TSAT(JB))  GOTO 3
```

```
C CALC. MIXING TEMP.& NEW POOL HEIGHT DUE TO WATER FLASHING
   43 HP11=HP(JB)*(1.-CPF(JB)*(TPOOL(JB)-TSAT(JB))/HFG)
      HP21=HP(JB)*(1.-AW1*CPF(JB)*(TPOOL(JB)-TSAT(JB))/HFG/(AW1+AW2))
      SM(JB)=(HP(JB)-HP21)*(AW1+AW2)*ROFS(JB)/NDT
      IF(JB.GT.1) GOTO 76
      HP31(JB)=HP21-HP11
      HP41=HP11
      GOTO 77
   76 HP31(JB)=HP21-HP11+HP31(JB-1)
      HP41=HP11-HP31(JB-1)
   77 IF(HP41.LE.0.) GOTO 74
      IF(JB.EQ.NN) CALL SUBWP(TPOOL(JB+1),DX,CPFS(JB+1),EX,ROFS(JB+1),X)
      TJB2=HP31(JB)*ROFS(JB+1)*CPFS(JB+1)/(HP41*ROFS(JB)*CPFS(JB))
      TPOOL(JB)=(TSAT(JB)+TPOOL(JB+1)*TJB2)/(1.+TJB2)
      GOTO 75
   74 TPOOL(JB)=TPOOL(JB+1)
   75 HP(JB)=HP21
      IF(HP(JB).LT.0.001) HP(JB)=0.
      IF(HP(JB).EQ.0.) TPOOL(JB)=0.
      IF(TPOOL(JB).GT.TSAT(JB)) TPOOL(JB)=TSAT(JB)
C     WRITE(6,39) QP(JB),HFC,UFC,TPOOL(JB),HP(JB)
C  39 FORMAT(' QP(JB),HFC,UFC,TPOOL(JB),HP(JB)'/7(1X,1PD11.4))
      GOTO 3
   40 IF(TPOOL(JB).LT.TSAT(JB)) GOTO 41
      HP(JB)=HP(JB)*(1.-AW1*CPF(JB)*(TPOOL(JB)-TSAT(JB))/HFG/(AW1+AW2))
      TPOOL(JB)=TSAT(JB)
C NUCLEATE POOL BOILING, ROHSENOW CORRELATION
   41 PRF=DVF*CPF(JB)/EKW
      C11=(CPF(JB)/(CSF*HFG*PRF))**(1./.33)
      C12=DVF*HFG/(SURT/(G*(ROF(JB)-ROG)))**.5
      C1=C11*C12
      DO 30  I=1,50
      DT(JB)=(QPPP/(C1*SAPL))**.33
      UHB=1./(1./U2+1./(C1*DT(JB)**(.67/.33)))
      QP(JB)=SAPL*UHB*(TCONT-TSAT(JB))
      IF(DABS(QPPP-QP(JB))/QPPP*100..LE.EPS)  GOTO 33
      QPPP=QP(JB)
   30 CONTINUE
      WRITE(6,32)
   32 FORMAT(' QP(NB) DOES NOT CONVERGE')
      GOTO 89
   33 IF(TPOOL(JB).GE.TSAT(JB)) GOTO 42
      CALL SUBWP(TPOOL(JB),X1,CPFS(JB),X2,ROFS(JB),X3)
      WATER=ROFS(JB)*HP(JB)*AW1
      TPOOL(JB)=TPOOL(JB)+(QP(JB)*NDT)/(CPFS(JB)*WATER)
      IF(TPOOL(JB).GT.TSAT(JB)) GOTO 43
      TWALL(JB)=TSAT(JB)+DT(JB)
      GOTO 3
C CALC. MIXING TEMP.& NEW POOL HEIGHT DUE TO SATURATED POOL BOILING
   42 HP1=HP(JB)-QP(JB)*NDT/(ROF(JB)*HFG*AW1)
      HP2=HP(JB)-QP(JB)*NDT/(ROF(JB)*HFG*(AW1+AW2))
      IF(JB.GT.1) GOTO 78
      HP3(JB)=HP2-HP1
      HP4=HP1
      GOTO 79
   78 HP3(JB)=HP2-HP1+HP3(JB-1)
      HP4=HP1-HP3(JB-1)
   79 IF(HP4.LE.0.) GOTO 72
```

```
      IF(JB.EQ.NN) CALL SUBWP(TPOOL(JB+1),DX,CPF(JB+1),EX,ROF(JB+1),X)
      TJB1=HP3(JB)*ROF(JB+1)*CPF(JB+1)/(HP4*ROF(JB)*CPF(JB))
      TPOOL(JB)=(TPOOL(JB)+TPOOL(JB+1)*TJB1)/(1.+TJB1)
      GOTO 73
   72 TPOOL(JB)=TPOOL(JB+1)
   73 HP(JB)=HP2
      SM(JB)=QP(JB)/HFG
      TWALL(JB)=TPOOL(JB)+DT(JB)
      IF(HP(JB).LE.0.001) HP(JB)=0.
      IF(HP(JB).EQ.0.) TPOOL(JB)=0.
C     WRITE(6,34) QP(JB),HNB,UNB,HP(JB)
C  34 FORMAT(' QP(JB),HNB,UNB,HP(JB)'/6(1X,1PD12.5))
    3 CONTINUE
      HPOOL=0.
      SMT=0.
      TSM0=0.
      QPP=0.
      SMTCP=0.
      DO 7 JD=1,NN
      HPOOL=HPOOL+HP(JD)
      CALL CPVSTM(CPVS,XCV,TSAT(JD))
      TSM0=TSM0+SM(JD)*TSAT(JD)*CPVS
      SMTCP=SMTCP+SM(JD)*CPVS
      SMT=SMT+SM(JD)
    7 QPP=QPP+QP(JD)
C CALC. AVERAGED POOL HEAT TRANSFER COEFF., HCPA
      ATWL=0.
      ATPL=0.
      DO 9 IH=1,NN
      ATWL=ATWL+HP(IH)*TWALL(IH)
    9 ATPL=ATPL+HP(IH)*TPOOL(IH)
      IF((ATWL-ATPL).EQ.0.) GOTO 8
      HCPA=QPP/(PI*DTR*(ATWL-ATPL))
    8 IF(SMTCP.GT.0.) TSM=TSM0/SMTCP
      IF(SMTCP.EQ.0) TSM=T(1)
C
C HEAT TRANSFER ABOVE WATER SECTION (RADIATIVE INCLUDED), QQ
      IF((ELT-HPOOL).GT.0.) GOTO 80
      QQ=0.
      GOTO 88
   80 S2=PI*DTR*(ELT-HPOOL)/NR
      S3=PI*DELD*(ELT-HPOOL)/NR
      CR=SIGM/(1./E1+DTR/DELD*(1./E2-1))
      IF(N1.GE.IR+1) GOTO 81
      DZ1(IR-1)=ELT-HPOOL
      GOTO 83
   81 DO 82 I=IR+1,N1
   82 DZ1(IR-1)=ELT+DZ1(I)-HPOOL
   83 DZ1(IR)=ELT-HPOOL
      EL1(IR-1)=ELD-HPOOL
      EL1(IR)=ELT-HPOOL
C FIRST GUESS OF FLOW RATE
      VAIR=1.
      EM=NP(IR)*A1(IR)*VAIR
C ITERATION ON THE CIRCULATED AND CONDUCTED HEAT
C GUESS OF OUTLET TEMPERATURE TO2 AND TEMPERATURE DISTRIBUTION
      TO2=TCONT
C CALC. VAPOR CONTENT IN INLET MOIST AIR, EMV
```

```
      CALL PSAT(PSV,T(1))
      IF(RH.GT.0.) GOTO 23
      EMA=EM
      EMV=0.
      GOTO 24
   23 EMV=EM/(1.+((PIN-RH*PSV)*RS)/(RH*PSV*R))
      EMA=EM-EMV
C CALC. AIR-STEAM MIXTURE TEMP.
   24 CALL CPVSTM(CPVI,CVX,T(IR-1))
      CALL CPVAIR(CPA,CX,T(IR-1))
      CALL CPVSTM(CPSTM,CVS,TSM)
      T(IR)=((EMV*CPVI+EMA*CPA)*T(IR-1)+TSM*SMT*CPSTM)/(EMV*CPVI+EMA*CPA
     /+SMT*CPSTM)
      EMT=EM+SMT
      XAIR=EMA/EMT
      CALL ASMP((TO2+T(IR))*.5,XAIR,CONM,DVM,CPM)
      QQ=CPM*EMT*(TO2-T(IR))
      NR1=NR+1
      TR(1)=T(IR)
      DO 22 I=2,NR1
   22 TR(I)=T(IR)+(TO2-T(IR))/NR*(I-1)
      DO 20 KK1=1,30
      DO 21 I=1,N1
   21 DP(I)=0.D0
C ITERATION FOR MOIST AIR FLOW RATE (MOMENTUM BALANCE), EM
      DO 50 KK=1,20
      DO 60 I=IR,N1
   60 T(I)=TO2
      CT=0.D0
      HH1=0.D0
      DPPH1=0.D0
      DPPH2=0.D0
      DO 100 I=1,N1
      IF(I.NE.IR) GOTO 103
C  AXIAL NODES FOR HEAT TRANSFER IN HEATED LENGTH
      HHR=0.
      DO 90 JRS=2,NR1
      TT=(TR(JRS)+TR(JRS-1))*0.5
      CALL ASMP(TT,XAIR,X1,DVM,X2)
      CALL FRICTN(EM,D1(I),A1(I),DVM,DEL(I),FF,NP(I))
      PRS=PIN-HH1-HHR-DPR(JRS)*0.5
C CALC. MOIST AIR DENSITY
C DALTON'S PARTIAL PRESSURE LAW
      CALL PSAT(PS1,TT)
      RHO=(SMT+EMV)*RS*PRS/(PS1*((SMT+EMV)*RS+EMA*R))
      IF(RHO.LE.1.) PS1=PS1*RHO
      ROSR=PS1/(RS*TT)
      ROAR=(PRS-PS1)/(R*TT)
      ROMIX=ROAR+ROSR
      CT1=(FF*EL1(I)/(NR*D1(I)))/(2.*ROMIX*(NP(I)*A1(I))**2)
      DPR(JRS)=CT1*EM*EM
      HHR=HHR+DPR(JRS)
      DPPH2=DPPH2+DZ1(I)/NR*ROMIX
C  EVALUATE DPHH1 IN CASE THERE IS NO VERTICAL DUCT OPPOSITE TO RISER
      IF(DZ1(IR-1).LE.0.) DPPH1=DPPH1+DZ1(I)/NR*ROMX(IR-1)
   90 CT=CT+CT1
      ROMX(IR)=ROMIX
C  K-LOSSES INCLUDED FOR AIR AT AVERAGE TEMPERATURE
```

```
      ROM=(ROMIX+ROMX(IR-1))*.5
      CT2=EK1(I)/(2.*ROM*(NP(I)*A1(I))**2)
      CT=CT+CT2
      HHR=HHR+CT2*EM*EM
      HH1=HH1+HHR
      DP(IR)=HHR
      GOTO 102
  103 TT=T(I)
      IF(I.LE.(IR-1)) XAIR=EMA/EM
      CALL ASMP(TT,XAIR,X1,DVM,X2)
      CALL FRICTN(EM,D1(I),A1(I),DVM,DEL(I),FF,NP(I))
      P(I)=PIN-HH1-DP(I)*.5
C CALC. MOIST AIR DENSITY
C DALTON'S PARTIAL PRESSURE LAW
      CALL PSAT(PS2,T(I))
      IF(I.GT.IR) GOTO 105
      IF(RH.LE.1.) PS2=PS2*RH
      GOTO 106
  105 RHOO=(SMT+EMV)*RS*P(I)/(PS2*((SMT+EMV)*RS+EMA*R))
      IF(RHOO.LE.1.) PS2=RHOO*PS2
  106 ROA1=(P(I)-PS2)/(R*T(I))
      ROS1=PS2/(RS*T(I))
      ROMX(I)=ROA1+ROS1
      CT1=(EK1(I)+FF*EL1(I)/D1(I))/(2.*ROMX(I)*(NP(I)*A1(I))**2)
      DP(I)=CT1*EM*EM
      HH1=HH1+DP(I)
      CT=CT+CT1
  102 IF(I.EQ.IR) GOTO 100
      IF(I.GT.IR) GOTO 104
      DPPH1=DPPH1+DZ1(I)*ROMX(I)
      GOTO 100
  104 DPPH2=DPPH2+DZ1(I)*ROMX(I)
  100 CONTINUE
      DPP=G*(DPPH1-DPPH2)
      HH1=DPP/CT
      SIG=DSIGN(1.D0,HH1)
      HH1=DABS(HH1)
      EMN=DSQRT(HH1)
      IF(DABS(EMN-EM)/EM*100..LT.EPS) GOTO 51
      EM=EMN
      IF(RH.GT.0.) GOTO 53
      EMA=EM
      GOTO 54
   53 EMV=EM/(1.+((PIN-RH*PSV)*RS)/(RH*PSV*R))
      EMA=EM-EMV
   54 EMT=SMT+EM
      XAIR=EMA/EMT
   50 CONTINUE
      WRITE(6,111) EM
  111 FORMAT(' EM DOES NOT CONVERGE',1X,1PD12.5)
      QQ=0.
      GOTO 88
   51 EM=EMN
      IF(RH.GT.0.) GOTO 55
      EMA=EM
      GOTO 56
   55 EMV=EM/(1.+((PIN-RH*PSV)*RS)/(RH*PSV*R))
      EMA=EM-EMV
```

```
   56 EMT=SMT+EM
      XAIR=EMA/EMT
      IF(SIG.GE.0.) GOTO 52
      WRITE(6,3333)
 3333 FORMAT(' EM IS LESS THAN ZERO')
      QQ=0.
      GOTO 88
C  ITERATION ON EXIT MIXTURE TEMPERATURE (ENERGY BALANCE), TO2
   52 IPQ=0
      T(IR)=((EMV*CPVI+EMA*CPA)*T(IR-1)+TSM*SMT*CPSTM)/(EMV*CPVI+EMA*CPA
     /+SMT*CPSTM)
      T2P(IR)=TCONT
      T3P(IR)=TCONT
      DO 110 KK2=1,20
      TR(1)=T(IR)
      IPR=0
      QS=0.
      QSC=0.
      QSCR=0.
      DO 120 I=2,NR1
      TT=(TR(I)+TR(I-1))*0.5
      CALL HCMIX(D1(IR),A1(IR),TT,CPM,HM2,HM3,EMT,RE,NP(IR),T2P(IR),T3P(
     /IR),XAIR,EL1(IR),.5*(DELD-DTR))
C SOLUTION FOR NODE OUTLET AIR TEMPERATURE
      HH1=EMT*CPM/(S2*U2)
      HH=EMT*CPM*(1.+HM2/U2)+HM2*S2
      THH=(EMT*CPM*TR(I-1)+HM2*S2*TCONT+HM2/U2*EMT*CPM*TR(I-1))/HH
      CK1=CR*S2/HH
      CK2=EMT*CPM/(S3*HM3)
      CK3=HM2*S2/(HM3*S3)
      TRN=(TCONT+TR(I-1))*0.5
C ITERATION THROUGH METODA TECEN
      DO 121 IT=1,30
C Y(Ti) = F(Ti)
      T2=TCONT-HH1*(TRN-TR(I-1))
      T3=(EMT*CPM*(TRN-TR(I-1))-HM2*S2*(T2-TRN))/(HM3*S3)+TRN
      FI=TRN-(THH+CK1*((T2*T2)**2-(T3*T3)**2))
C  DERIVATIVE F'(Ti)
      FP=1-CK1*(4.*T2*T2*T2*(-HH1)-4.*T3*T3*T3*(CK2-CK3*(-HH1-1.)+1.))
      TI1=TRN-FI/FP
      IF(DABS((TRN-TI1)/TRN)*100..LE.0.01*EPS) GOTO 125
      DTC=TI1-TRN
      TRN=TI1
  121 CONTINUE
      WRITE(3,126) DTC,TRN,T2,T3
  126 FORMAT(' DOES NOT CONVERGE DT,T,T2,T3',4(1X,1PD11.4))
  125 TRN=TI1
      IF(DABS(TRN-TR(I))/TRN*100..GT.EPS) IPR=1
      TR(I)=TRN
      T2P(I)=T2
      T3P(I)=T3
      QR(I-1)=EMT*CPM*(TRN-TR(I-1))
      QC(I-1)=HM2*(T2P(I)-TR(I))*S2
      QRD(I-1)=HM3*S3*(T3P(I)-TR(I))
      QS=QS+QR(I-1)
      QSC=QSC+QC(I-1)
      QSCR=QSCR+QRD(I-1)+QC(I-1)
  120 CONTINUE
```

```
      TO2OLD=TO2
      IF(IPR.EQ.0) GOTO 112
  110 CONTINUE
      WRITE(6,111) TO2
  112 TO2=TR(NR1)
      QQN=QS
      IF(DABS(QQN-QSCR)/QQN*100..GT.5*EPS) IPQ=1
      IF(DABS(QQN-QQ)/QQN*100..GT.EPS) IPQ=1
      IF(DABS((TO2-TO2OLD)/TO2)*100..GT.EPS) IPQ=1
      IF(IPQ.EQ.0) GOTO 88
      QQ=QQN
   20 CONTINUE
      WRITE(6,111) QQ
      STOP
   88 QTTL=QPP+QQ
      TWAR=TCONT-QQ/(NR*S2*U2)
      HCMIXE=QQ/(S2*NR*(TWAR-.5*(TO2+TR(1))))
      HCMIXC=QSC/(S2*NR*(TWAR-.5*(TO2+TR(1))))
      CALL DECAY(TI,DPF,DPFI)
      QDECAY=QRATED*DPF
      RPF=QTTL/QRATED
      PAIR=AIR*R*TCONT/VCONT
C FIND PEAK PRESSURE
      PCONT=PSTEAM+PAIR
      PCONT2=PCONT1
      PCONT1=PCONT0
      PCONT0=PCONT
      IF(PCONT0.LT.PCONT1.AND.PCONT1.GT.PCONT2) GOTO 580
C OUTPUT FORMAT
      IF(JC.GE.1.AND.JC.LE.11) GOTO 580
      IF(JC.GT.11.AND.JC.LE.110) GOTO 581
      IF(JC.GT.110.AND.JC.LE.1100) GOTO 582
      IF(JC.GT.1100.AND.JC.LE.11000) GOTO 583
      IF(JC.GT.11000) GOTO 584
  581 IF(MOD(JC-1,10).EQ.0) GOTO 580
  582 IF(MOD(JC-1,100).EQ.0) GOTO 580
  583 IF(MOD(JC-1,1000).EQ.0) GOTO 580
  584 IF(MOD(JC-1,10000).EQ.0) GOTO 580
      GOTO 98
  580 HPL(JK+1)=HPOOL
      DO 585 JM=1,NN
      TWL(JK+1,JM)=TWALL(JM)
  585 TPL(JK+1,JM)=TPOOL(JM)
      TCT(JK)=TCONT
      TMIXO(JK+1)=TO2
      TWA(JK)=TWAR
      HMIXE(JK)=HCMIXE
      HMIXC(JK)=HCMIXC
      EMAA(JK+1)=EMA
      EMMT(JK+1)=EMT
      REY(JK+1)=RE
      HCPL(JK)=HCPA
      HCD(JK)=HCOND
      QTL(JK+1)=QTTL
      QDY(JK)=DPF
      QPI(JK+1)=QPP
      QAI(JK+1)=QQ
      PAR(JK)=PAIR*1.D-6
```

```
      PSTM(JK)=PSTEAM*1.D-6
      PCT(JK)=PCONT*1.D-6
      IF((ELT-HPOOL).LE.0.) QHF(JK+1)=0.
      IF((ELT-HPOOL).GT.0.) QHF(JK+1)=QQ/(PI*DTR*(ELT-HPOOL))
      IF(HPOOL.EQ.0.) QPHF(JK+1)=0.
      IF(HPOOL.GT.0.) QPHF(JK+1)=QPP/(PI*DTR*HPOOL)
      TIME(JK)=TI/60.
      IF(TIME(JK).LT.1.D-3) TIME(JK)=0.
      JK=JK+1
C INTEGRAL DECAY POWER WITHIN TIME STEP NDT
   98 TI1=TI
      TI2=TI+NDT
      CALL DECAY(TI1,DPF1,DPFI1)
      CALL DECAY(TI2,DPF2,DPFI2)
      ENERGD=QRATED*(DPFI2-DPFI1)*8.64D+04
C HEAT ABSORPTION IN-CTMT STRUCTURES WITHIN STM (SEC)
      IF(TI.GT.STM) S=0.
      CALL CPVAIR(X1,CVA,TCONT)
      IF(PSTEAM.GT.3.9776D6)  GOTO 89
      CALL CPVSTM(X1,CVS,TCONT)
      ENERGR=NDT*QTTL
      TCONT=TCONT+((1.-S)*ENERGD-ENERGR)/(STEAM*CVS+AIR*CVA)
   99 TI=JC*NDT
   89 WRITE(6,557)
  557 FORMAT(///'   Time(min),   Twall(1-NN), Tpool(1-NN)' )
      DO 570 I=1,JK-1
  570 WRITE(6,561) (TIME(I),TWL(I,J),TPL(I,J),J=1,NN)
  561 FORMAT(3(1X,1PD12.4))
  558 FORMAT(6(1X,1PD12.4))
      WRITE(6,559)
  559 FORMAT(/'   Time(min),   Hpool(m),    Tcont(K),    Pair(MPa),   Ps
     /team(MPa), Pcont(MPa)')
      DO 571 I=1,JK-1
  571 WRITE(6,558) TIME(I),HPL(I),TCT(I),PAR(I),PSTM(I),PCT(I)
      WRITE(6,560)
  560 FORMAT(/'   Time(min),   Qpool(w),    Qair(w),     Qtotal,      Qd
     /ecay')
      DO 572 I=1,JK-1
  572 WRITE(6,558) TIME(I),QPI(I),QAI(I),QTL(I),QDY(I)
      WRITE(6,562)
  562 FORMAT(/'   Time(min),   hmix,e,      hmix,c,      hpool,       hc
     /ond')
      DO 573 I=1,JK-1
  573 WRITE(6,558) TIME(I),HMIXE(I),HMIXC(I),HCPL(I),HCD(I)
      WRITE(6,563)
  563 FORMAT(/'   Time(min),   Tmix,out,    Twall,air,   Mmix,        Ma
     /ir,        RE')
      DO 574 I=1,JK-1
  574 WRITE(6,558) TIME(I),TMIXO(I),TWA(I),EMMT(I),EMAA(I),REY(I)
      WRITE(6,564)
  564 FORMAT(/'   Time(min),   q"pl,        q"air')
      DO 575 I=1,JK-1
  575 WRITE(6,558) TIME(I),QPHF(I),QHF(I)
      GOTO 777
  666 WRITE(6,665) IR
  665 FORMAT(' IR CANNOT BE EQ TO 1',I5)
      GOTO 777
 8888 WRITE(6,8000)
```

```
 8000 FORMAT(' NO FILE BY THAT NAME')
      GOTO 777
 9999 WRITE(6,9000)
 9000 FORMAT(' THIS FILE ALREADY EXISTS')
  777 STOP
      END
C
      SUBROUTINE FRICTN(EM,D,A,EMI,DEL,F,N)
      IMPLICIT REAL*8(A-H,O-Z)
      RE=EM*D/(N*A*EMI)
      F=0.11*(DEL/D+68./RE)**0.25
      RETURN
      END
C
C HEAT TRANSFER COEFF. CALCULATION
      SUBROUTINE HCMIX(D,A,T,CP,HC2,HC3,EMT,RE,N,TWA2,TWA3,XA,EL,G)
      IMPLICIT REAL*8(A-H,O-Z)
      CALL ASMP(T,XA,ELAM,EMI,CP)
      RE=EMT*D/(EMI*A*N)
      PR=EMI*CP/ELAM
C ANL CORRELATION
      ENU2=.0229*RE**.8*PR**.4*(TWA2/T)**(-.4)*(1.+(EL/G)**(-.36))
      ENU3=.0229*RE**.8*PR**.4*(TWA3/T)**(-.4)*(1.+(EL/G)**(-.36))
C GANG FU CORRELATION (REVISED BY PAVEL)
C     ENU2=.021*RE**.8*PR**.4*(TWA2/T)**(-.5)/(1.+(5500./RE)**3)
C     ENU3=.021*RE**.8*PR**.4*(TWA3/T)**(-.5)/(1.+(5500./RE)**3)
      HC2=ENU2*ELAM/D
      HC3=ENU3*ELAM/D
C     WRITE(6,1) T,EMI,ELAM,RE,PR,HC
C    1 FORMAT(' ***T,EMI,ELAM,RE,PR,HC',6(1X,1PD11.4))
      RETURN
      END
C
C DYNAMIC VISCOSITY OF AIR  EMI(KG/M-S), T(K)
C IRVINE T.F. STEAM AND GAS TABLES WITH COMP. EQS., NY., 1984
      SUBROUTINE VISAIR(EMI,T)
      IMPLICIT REAL*8(A-H,O-Z)
      DIMENSION B1(5),B2(5)
      DATA B1/-9.8601D-1, 9.080125D-2, -1.17635575D-4, 1.2349703D-7,
     /        -5.7971299D-11/
      DATA B2/4.8856745, 5.43232D-2, -2.4261775D-5, 7.9306D-9,
     /        -1.10398D-12/
      IF(T.LT.250.OR.T.GT.1050) GOTO 3
      EMI=0.
      IF(T.GE.600.) GOTO 2
      DO 10 I=1,5
   10 EMI=EMI+B1(I)*T**(I-1)
      EMI=EMI*1.D-6
      RETURN
    2 DO 20 I=1,5
   20 EMI=EMI+B2(I)*T**(I-1)
      EMI=EMI*1.D-6
      RETURN
    3 WRITE(6,100) T
  100 FORMAT(' **ERROR IN VISAIR T(K)=',1PD11.4)
      STOP 333
      END
C
```

```
C DYNAMIC VISCOSITY OF STEAM  EMI(KG/M-S), T(K)
      SUBROUTINE VISSTM(EMI,T)
      IMPLICIT REAL*8(A-H,O-Z)
      DIMENSION TM(26),DV(26)
      DATA TM/1.D-2,1.D1, 2.D1, 3.D1, 4.D1, 5.D1, 6.D1, 7.D1, 8.D1,
     /        9.D1,1.D2,1.1D2,1.2D2,1.3D2,1.4D2,1.5D2,1.6D2,1.7D2,
     /        1.8D2,1.9D2,2.D2,2.1D2,2.2D2,2.3D2,2.4D2,2.5D2/
      DATA DV/8.105D-6,8.504D-6,8.903D-6,9.305D-6,9.701D-6,1.010D-5,
     /        1.050D-5,1.089D-5,1.129D-5,1.167D-5,1.206D-5,1.245D-5,
     /        1.283D-5,1.320D-5,1.357D-5,1.394D-5,1.430D-5,1.466D-5,
     /        1.502D-5,1.537D-5,1.572D-5,1.607D-5,1.642D-5,1.678D-5,
     /        1.714D-5,1.751D-5/
      TT=T-273.15
      DO 1 I=2,26
      IF(TM(I-1).LE.TT.AND.TM(I).GE.TT) GOTO 2
    1 CONTINUE
      WRITE(6,100) T
  100 FORMAT(' **ERROR IN VISSTM T(K)', 1PD11.4)
      STOP
    2 T1=TM(I-1)
      T2=TM(I)
      EMI1=DV(I-1)
      EMI2=DV(I)
      EMI=EMI1+(EMI2-EMI1)/(T2-T1)*(TT-T1)
      RETURN
      END
C
C THERMAL CONDUCTIVITY OF AIR  CON(W/M-K), T(K)
C IRVINE T.F. STEAM AND GAS TABLES WITH COMP. EQS., NY., 1984
      SUBROUTINE CONAIR(CON,T)
      IMPLICIT REAL*8(A-H,O-Z)
      DIMENSION B(6)
      DATA B/-2.276501D-3, 1.2598485D-4, -1.4815235D-7, 1.73550646D-10,
     /       -1.066657D-13, 2.47663035D-17/
      IF(T.LT.250.OR.T.GT.1050) GOTO 3
      CON=0.
      DO 10 I=1,6
   10 CON=CON+B(I)*T**(I-1)
      RETURN
    3 WRITE(6,100) T
  100 FORMAT(' **ERROR IN CONAIR T(K)=',1PD11.4)
      STOP 333
      END
C
C THERMAL CONDUCTIVITY OF STEAM  CON(W/M-K), T(K)
      SUBROUTINE CONSTM(CON,T)
      IMPLICIT REAL*8(A-H,O-Z)
      DIMENSION TM(26),CK(26)
      DATA TM/1.D-2,1.D1, 2.D1, 3.D1, 4.D1, 5.D1, 6.D1, 7.D1, 8.D1,
     /        9.D1,1.D2,1.1D2,1.2D2,1.3D2,1.4D2,1.5D2,1.6D2,1.7D2,
     /        1.8D2,1.9D2,2.D2,2.1D2,2.2D2,2.3D2,2.4D2,2.5D2/
      DATA CK/1.76D-2,1.82D-2,1.88D-2,1.95D-2,2.02D-2,2.09D-2,
     /        2.16D-2,2.24D-2,2.32D-2,2.40D-2,2.49D-2,2.58D-2,
     /        2.67D-2,2.78D-2,2.89D-2,3.00D-2,3.13D-2,3.26D-2,
     /        3.41D-2,3.57D-2,3.74D-2,3.94D-2,4.15D-2,4.39D-2,
     /        4.65D-2,4.95D-2/
      TT=T-273.15
      DO 1 I=2,26
```

```
      IF(TM(I-1).LE.TT.AND.TM(I).GE.TT) GOTO 2
    1 CONTINUE
      WRITE(6,100) T
  100 FORMAT(' **ERROR IN CONSTM T(K)', 1PD11.4)
      STOP
    2 T1=TM(I-1)
      T2=TM(I)
      CON1=CK(I-1)
      CON2=CK(I)
      CON=CON1+(CON2-CON1)/(T2-T1)*(TT-T1)
      RETURN
      END
C
C SPECIF.HEAT AT CONST.PRESSURE OF AIR  CP(J/KG-K), T(K)
C SPECIF.HEAT AT CONST.VOLUME OF AIR  CV(J/KG-K), T(K)
C IRVINE T.F. STEAM AND GAS TABLES WITH COMP. EQS., NY., 1984
      SUBROUTINE CPVAIR(CP,CV,T)
      IMPLICIT REAL*8(A-H,O-Z)
      DIMENSION B(5)
      DATA B/0.103409D1, -0.2848870D-3,  0.7816818D-6, -0.4970786D-9,
     /       0.1077024D-12/,            R/287.04/
      IF(T.LT.250.OR.T.GT.2000) GOTO 3
      CP=0.
      DO 10 I=1,5
   10 CP=CP+B(I)*T**(I-1)
      CP=CP*1000.
      CV=CP-R
      RETURN
    3 WRITE(6,100) T
  100 FORMAT(' **ERROR IN CPAIR T(K)=',1PD11.4)
      STOP 333
      END
C
C SPECIFIC HEAT OF STEAM  CP(J/KG-K), T(K)
      SUBROUTINE CPVSTM(CP,CV,T)
      IMPLICIT REAL*8(A-H,O-Z)
      DIMENSION TM(26),CG(26)
      DATA TM/1.D-2,1.D1, 2.D1, 3.D1, 4.D1, 5.D1, 6.D1, 7.D1, 8.D1,
     /        9.D1,1.D2,1.1D2,1.2D2,1.3D2,1.4D2,1.5D2,1.6D2,1.7D2,
     /        1.8D2,1.9D2,2.D2,2.1D2,2.2D2,2.3D2,2.4D2,2.5D2/
      DATA CG/1.863D+3,1.870D+3,1.880D+3,1.890D+3,1.900D+3,1.912D+3,
     /        1.924D+3,1.946D+3,1.970D+3,1.999D+3,2.034D+3,
     /        2.076D+3,2.125D+3,2.180D+3,2.245D+3,2.320D+3,
     /        2.406D+3,2.504D+3,2.615D+3,2.741D+3,2.883D+3,
     /        3.043D+3,3.223D+3,3.426D+3,3.656D+3,3.918D+3/
      DATA R/462/
      TT=T-273.15
      DO 1 I=2,26
      IF(TM(I-1).LE.TT.AND.TM(I).GE.TT) GOTO 2
    1 CONTINUE
      WRITE(6,100) T
  100 FORMAT(' **ERROR IN CPVSTM T(K)', 1PD11.4)
      STOP
    2 T1=TM(I-1)
      T2=TM(I)
      CP1=CG(I-1)
      CP2=CG(I)
      CP=CP1+(CP2-CP1)/(T2-T1)*(TT-T1)
```

```
      CV=CP-R
      RETURN
      END
C
C AIR-STAEAM MIXTURE PROPERTIES
      SUBROUTINE ASMP(T,XA,CON,DV,CP)
      IMPLICIT REAL*8(A-H,O-Z)
      AIRM=2.897D-2
      STMM=1.8D-2
      CALL VISAIR(DVA,T)
      CALL VISSTM(DVS,T)
      CALL CONAIR(CONA,T)
      CALL CONSTM(CONS,T)
      CALL CPVAIR(CPA,CVA,T)
      CALL CPVSTM(CPS,CVS,T)
      YAIR=XA/AIRM/(XA/AIRM+(1.-XA)/STMM)
      YSTM=(1.-XA)/STMM/(XA/AIRM+(1.-XA)/STMM)
      CON1=YAIR*CONA*AIRM**(1./3.)+YSTM*CONS*STMM**(1./3.)
      CON2=YAIR*AIRM**(1./3.)+YSTM*STMM**(1./3.)
      CON=CON1/CON2
      DV1=YAIR*DVA*AIRM**.5+YSTM*DVS*STMM**.5
      DV2=YAIR*AIRM**.5+YSTM*STMM**.5
      DV=DV1/DV2
      CP=YAIR*CPA+YSTM*CPS
      RETURN
      END
C
C SATURATION PRESSURE OF STEAM  P(Pa)
C IRVINE T.F. STEAM AND GAS TABLES WITH COMP. EQS., NY, 1984
      SUBROUTINE PSAT(P,T)
      IMPLICIT REAL*8(A-H,O-Z)
      IF(T.LT.273.15.OR.T.GT.600.) GOTO 3
      P=EXP(-3892.7/(T-42.6776)+9.48654)
      P=P*1.D6
      RETURN
    3 WRITE(6,100) T
  100 FORMAT('**ERROR IN PSAT T(K)',1PD11.4)
      STOP 333
      END
C
      SUBROUTINE DECAY(TAU,POWER,ENERG)
      IMPLICIT REAL*8(A-H,O-Z)
      DIMENSION TM(36),DEP(36),DEPI(36)
C DECAY POWER DATA
      DATA TM/1.D-10,6.D1,3.D2,6.D2,1.2D3,2.4D3,3.6D3,1.44D4,2.88D4,
     /     4.32D4, 8.64D4,1.728D5,2.592D5,3.456D5,4.32D5,5.184D5,
     /     6.048D5,6.912D5,7.776D5,8.64D5,9.504D5,1.0368D6,
     /     1.1232D6,1.2096D6,1.8144D6,2.4192D6,3.024D6,3.6288D6,
     /     4.2336D6,4.8384D6,5.4432D6,6.048D6,6.6528D6,
     /     7.2576D6,1.5779D7,3.1558D7/
      DATA DEP/5.775D-02,3.295D-02,2.399D-02,2.084D-02,1.765D-02,
     /         1.441D-02,1.265D-02,8.347D-03,6.948D-03,6.233D-03,
     /         5.110D-03,4.110D-03,3.562D-03,3.190D-03,2.909D-03,
     /         2.689D-03,2.510D-03,2.363D-03,2.238D-03,2.132D-03,
     /         2.040D-03,1.959D-03,1.888D-03,1.824D-03,1.506D-03,
     /         1.305D-03,1.161D-03,1.050D-03,9.631D-04,8.921D-04,
     /         8.326D-04,7.816D-04,7.370D-04,6.977D-04,3.861D-04,
     /         2.007D-04/
```

```
      DATA DEPI/1.D-10,3.150D-5,1.106D-4,1.884D-4,3.221D-04,5.447D-04,
     /          7.326D-04,2.045D-03,3.319D-03,4.418D-03,7.253D-03,
     /          1.186D-02,1.570D-02,1.908D-02,2.212D-02,2.492D-02,
     /          2.752D-02,2.996D-02,3.226D-02,3.445D-02,3.653D-02,
     /          3.853D-02,4.045D-02,4.231D-02,5.396D-02,6.380D-02,
     /          7.244D-02,8.017D-02,8.722D-02,9.371D-02,9.975D-02,
     /          1.054D-01,1.107D-01,1.157D-01,1.692D-01,2.228D-01/
C
      DO 1 I=2,36
      IF(TM(I-1).LE.TAU.AND.TM(I).GE.TAU) GOTO 2
    1 CONTINUE
      WRITE(6,100) TAU
  100 FORMAT((' DECAY**TIME  IS OUTSIDE RANGE '),1PE12.5,'S')
      STOP
    2 TAUL=DLOG10(TAU)
      D1=DLOG10(DEP(I-1))
      D2=DLOG10(DEP(I))
      T1=DLOG10(TM(I-1))
      T2=DLOG10(TM(I))
      POWEL=D1+(D2-D1)/(T2-T1)*(TAUL-T1)
      POWER=10**(POWEL)
      C1=DLOG10(DEPI(I-1))
      C2=DLOG10(DEPI(I))
      ENERGL=C1+(C2-C1)/(T2-T1)*(TAUL-T1)
      ENERG=10**(ENERGL)
      RETURN
      END
C
C SATURATION WATER PROPERTIES INTERPOLATION
C J. H. KEENAN, STEAM TABLE, 1978
      SUBROUTINE SATWP(T,P,U,CPF,WK,HD,SIG,ROL,ROV)
      IMPLICIT REAL*8(A-H,O-Z)
      DIMENSION TM(26),PR(26),UF(26),CF(26),CK(26),ED(26),
     /          ST(26),VL(26),VV(26)
      DATA TM/1.D-2,1.D1, 2.D1, 3.D1, 4.D1, 5.D1, 6.D1, 7.D1, 8.D1,
     /        9.D1,1.D2,1.1D2,1.2D2,1.3D2,1.4D2,1.5D2,1.6D2,1.7D2,
     /        1.8D2,1.9D2,2.D2,2.1D2,2.2D2,2.3D2,2.4D2,2.5D2/
      DATA PR/6.113D+2, 1.2276D+3,2.3390D+3,4.2460D+3,7.3784D+3,
     /        1.2349D+4,1.9940D+4,3.1190D+4,4.7390D+4,7.0140D+4,
     /        1.01350D+5,1.4327D+5,1.9853D+5,2.7010D+5,3.6130D+5,
     /        4.7580D+5,6.1780D+5,7.9170D+5,1.0021D+6,1.2544D+6,
     /        1.5538D+6,1.9062D+6,2.3180D+6,2.7950D+6,3.3440D+6,
     /        3.9730D+6/
      DATA VL/1.0002D-3,1.0004D-3,1.0018D-3,1.0043D-3,1.0078D-3,
     /        1.0121D-3,1.0172D-3,1.0228D-3,1.0291D-3,1.0360D-3,
     /        1.0435D-3,1.0516D-3,1.0603D-3,1.0697D-3,1.0797D-3,
     /        1.0905D-3,1.1020D-3,1.1143D-3,1.1274D-3,1.1414D-3,
     /        1.1565D-3,1.1726D-3,1.1900D-3,1.2088D-3,1.2291D-3,
     /        1.2512D-3/
      DATA VV/2.06136D+2,1.06379D+2,5.7791D+1,3.2894D+1,1.9526D+1,
     /        1.2032D+1, 7.6710D+0, 5.0420D+0,3.4070D+0,2.3610D+0,
     /        1.6729D+0, 1.2102D+0, 8.9190D-1,6.6850D-1,5.0890D-1,
     /        3.9280D-1, 3.0710D-1, 2.4280D-1,1.9405D-1,1.5654D-1,
     /        1.2736D-1, 1.04410D-1,8.6190D-2,7.1580D-2,5.9760D-2,
     /        5.0130D-2/
      DATA ED/2.5013D+6,2.4777D+6,2.4541D+6,2.4305D+6,2.4067D+6,
     /        2.3827D+6,2.3585D+6,2.3338D+6,2.3088D+6,2.2832D+6,
     /        2.2570D+6,2.2302D+6,2.2026D+6,2.1742D+6,2.1447D+6,
```

```
     /        2.1143D+6,2.0826D+6,2.0495D+6,2.0150D+6,1.9788D+6,
     /        1.9407D+6,1.9007D+6,1.8585D+6,1.8138D+6,1.7665D+6,
     /        1.7162D+6/
      DATA UF/1.786D-3,1.304D-3,1.002D-3,7.983D-4,6.539D-4,5.478D-4,
     /        4.673D-4,4.048D-4,3.554D-4,3.156D-4,2.831D-4,
     /        2.548D-4,2.310D-4,2.109D-4,1.941D-4,1.798D-4,
     /        1.677D-4,1.574D-4,1.485D-4,1.407D-4,1.339D-4,
     /        1.279D-4,1.224D-4,1.175D-4,1.129D-4,1.087D-4/
      DATA CF/4.218D+3,4.194D+3,4.182D+3,4.179D+3,4.179D+3,4.181D+3,
     /        4.185D+3,4.191D+3,4.198D+3,4.207D+3,4.218D+3,
     /        4.230D+3,4.244D+3,4.262D+3,4.282D+3,4.306D+3,
     /        4.334D+3,4.366D+3,4.403D+3,4.446D+3,4.494D+3,
     /        4.550D+3,4.613D+3,4.685D+3,4.769D+3,4.866D+3/
      DATA CK/5.69D-1,5.87D-1,6.03D-1,6.18D-1,6.31D-1,6.43D-1,6.53D-1,
     /        6.62D-1,6.70D-1,6.76D-1,6.81D-1,6.84D-1,6.87D-1,6.88D-1,
     /        6.88D-1,6.87D-1,6.84D-1,6.81D-1,6.77D-1,6.71D-1,6.64D-1,
     /        6.57D-1,6.48D-1,6.39D-1,6.28D-1,6.16D-1/
      DATA ST/7.56D-2, 7.424D-2,7.278D-2,7.123D-2,6.961D-2,6.793D-2,
     /        6.619D-2,6.440D-2,6.257D-2,6.069D-2,5.878D-2,5.683D-2,
     /        5.485D-2,5.283D-2,5.079D-2,4.870D-2,4.659D-2,4.444D-2,
     /        4.226D-2,4.005D-2,3.781D-2,3.553D-2,3.323D-2,3.090D-2,
     /        2.856D-2,2.619D-2/
C
      DO 1 I=2,26
      IF(PR(I-1).LE.P.AND.PR(I).GE.P) GOTO 2
    1 CONTINUE
      WRITE(6,100) P
  100 FORMAT(' SATWP PRESSURE IS OUTSIDE RANGE', 1PD11.4)
      STOP
    2 P1=PR(I-1)
      P2=PR(I)
      T1=TM(I-1)
      T2=TM(I)
      P3=(P-P1)/(P2-P1)
      T3=T1+(T2-T1)*P3
      T=T3+273.15
      U1=UF(I-1)
      U2=UF(I)
      U=U1+(U2-U1)*P3
      CPF1=CF(I-1)
      CPF2=CF(I)
      CPF=CPF1+(CPF2-CPF1)*P3
      WK1=CK(I-1)
      WK2=CK(I)
      WK=WK1+(WK2-WK1)*P3
      HD1=ED(I-1)
      HD2=ED(I)
      HD=HD1+(HD2-HD1)*P3
      SIG1=ST(I-1)
      SIG2=ST(I)
      SIG=SIG1+(SIG2-SIG1)*P3
      ROL1=VL(I-1)
      ROL2=VL(I)
      ROL3=ROL1+(ROL2-ROL1)*P3
      ROL=1./ROL3
      ROV1=VV(I-1)
      ROV2=VV(I)
      ROV3=ROV1+(ROV2-ROV1)*P3
```

```
      ROV=1./ROV3
      RETURN
      END
C
C SUBCOOL WATER PROPERTIES INTERPOLATION
      SUBROUTINE SUBWP(T,DV,CP,EK,RF,B)
      IMPLICIT REAL*8(A-H,O-Z)
      DIMENSION TM(26),UF(26),CF(26),CK(26),VL(26)
      DATA TM/1.D-2,1.D1, 2.D1, 3.D1, 4.D1, 5.D1, 6.D1, 7.D1, 8.D1,
     /        9.D1,1.D2,1.1D2,1.2D2,1.3D2,1.4D2,1.5D2,1.6D2,1.7D2,
     /        1.8D2,1.9D2,2.D2,2.1D2,2.2D2,2.3D2,2.4D2,2.5D2/
      DATA VL/1.0002D-3,1.0004D-3,1.0018D-3,1.0043D-3,1.0078D-3,
     /        1.0121D-3,1.0172D-3,1.0228D-3,1.0291D-3,1.0360D-3,
     /        1.0435D-3,1.0516D-3,1.0603D-3,1.0697D-3,1.0797D-3,
     /        1.0905D-3,1.1020D-3,1.1143D-3,1.1274D-3,1.1414D-3,
     /        1.1565D-3,1.1726D-3,1.1900D-3,1.2088D-3,1.2291D-3,
     /        1.2512D-3/
      DATA UF/1.786D-3,1.304D-3,1.002D-3,7.983D-4,6.539D-4,5.478D-4,
     /        4.673D-4,4.048D-4,3.554D-4,3.156D-4,2.831D-4,
     /        2.548D-4,2.310D-4,2.109D-4,1.941D-4,1.798D-4,
     /        1.677D-4,1.574D-4,1.485D-4,1.407D-4,1.339D-4,
     /        1.279D-4,1.224D-4,1.175D-4,1.129D-4,1.087D-4/
      DATA CF/4.218D+3,4.194D+3,4.182D+3,4.179D+3,4.179D+3,4.181D+3,
     /        4.185D+3,4.191D+3,4.198D+3,4.207D+3,4.218D+3,
     /        4.230D+3,4.244D+3,4.262D+3,4.282D+3,4.306D+3,
     /        4.334D+3,4.366D+3,4.403D+3,4.446D+3,4.494D+3,
     /        4.550D+3,4.613D+3,4.685D+3,4.769D+3,4.866D+3/
      DATA CK/5.69D-1,5.87D-1,6.03D-1,6.18D-1,6.31D-1,6.43D-1,6.53D-1,
     /        6.62D-1,6.70D-1,6.76D-1,6.81D-1,6.84D-1,6.87D-1,6.88D-1,
     /        6.88D-1,6.87D-1,6.84D-1,6.81D-1,6.77D-1,6.71D-1,6.64D-1,
     /        6.57D-1,6.48D-1,6.39D-1,6.28D-1,6.16D-1/
C
      TT=T-273.15
      DO 1 I=2,26
      IF(TM(I-1).LE.TT.AND.TM(I).GE.TT) GOTO 2
    1 CONTINUE
      WRITE(6,100) T
  100 FORMAT(' SUBWP TEMPERATURE IS OUTSIDE RANGE', 1PD11.4)
      STOP
    2 T1=TM(I-1)
      T2=TM(I)
      RF1=VL(I-1)
      RF2=VL(I)
      RF3=RF1+(RF2-RF1)/(T2-T1)*(TT-T1)
      RF=1./RF3
      B=-1.*(1./RF2-1./RF1)/((T2-T1)*(1./RF1+1./RF2)/2.)
      DV1=UF(I-1)
      DV2=UF(I)
      DV=DV1+(DV2-DV1)/(T2-T1)*(TT-T1)
      CP1=CF(I-1)
      CP2=CF(I)
      CP=CP1+(CP2-CP1)/(T2-T1)*(TT-T1)
      EK1=CK(I-1)
      EK2=CK(I)
      EK=EK1+(EK2-EK1)/(T2-T1)*(TT-T1)
      RETURN
      END
```

APPENDIX D

FORM LOSS COEFFICIENT CALCULATION

Form loss coefficients at each flow transition section of the test apparatus are presented in this appendix. There are five locations which involve flow area change and/or flow direction change as discussed in the following sequence.

(1) Entrance Form Loss Coefficient

The inlet air flow geometry from ambient to the duct between the inner and outer annulus is analogous to Idelchik's handbook of hydraulic resistance [I-1], diagram 3-2: entrance from an infinite space with zero ambient air flowrate into a tube mounted flush into a wall. For a 90 degree turn in flowing angle, the form loss coefficient K_c is 0.5.

(2) Air Window Form Loss Coefficient

The flow geometry through the air windows can be approximated by the configuration in Idelchik's handbook diagram 6-28: symmetric turn through 180° in one plane with fairing as shown in Figure D.1. The form loss coefficient is a function of h/a (see Figure D.1). To evaluate the form loss coefficient through the air windows, the corresponding h/a of the apparatus is calculated by equating the ratio of the gap (or window) to outlet flow area of Figure D.1 and that of the apparatus.

$$\frac{A_{gap}}{A_o} = \frac{\pi a h}{\frac{\pi}{4}a^2} = 4\frac{h}{a}, \tag{D.1}$$

where

A_{gap}: flow area of the bottom gap,

A_o: flow area of the outlet flow.

$$\frac{A_{window}}{A_{annulus}} = \frac{3L^2}{\frac{\pi}{4}(D_{PVC}^2 - D_{ss}^2)}, \tag{D.2}$$

where

A_{window}: total flow area of air windows,

$A_{annulus}$: flow area between inner annulus wall and heated vessel,

L: length of air window = 6.5 inches,

D_{ss}: outer diameter of heated vessel = 4.5 inches,

D_{PVC}: inner diameter of PVC pipe = 12.4 inches.

Equating D.1 and D.2, a/h of the apparatus is 0.302, therefore, K_c is 3.7.

(3) Form Loss Coefficient for Flow Transition at Flange

There is a flange atop the heated vessel to facilitate installation and handling of this tall heavy component. Figure D.2 shows the dimensions at the heated vessel flange. For a thick flange ($l/D_h > 0.015$), the form loss coefficient can be expressed as [Idelchik, diagram 4-12]:

$$K_c = 0.05(1-\frac{A_0}{A_1}) + (1-\frac{A_0}{A_2})^2 + \tau\sqrt{1-\frac{A_0}{A_1}}(1-\frac{A_0}{A_2}) + K_f\frac{l}{D_h}, \qquad (D.3)$$

where

l: thickness of the flange = 1.375 inches,

D_h: equivalent hydraulic diameter at flange section = 3 inches,

A_0: flow area at flange section = 49.5 in^2,

A_1: flow area upstream of the flange = 97.2 in^2,

A_2: flow area downstream of the flange = 113.1 in^2,

τ: function of l/D_h, τ = 1.025, for l/D_h = 0.458,

K_f: friction coefficient ≈ 0.04, (wall roughness = $4\cdot10^{-3}$ in, Re = $5\cdot10^4$).

Hence

$K_c = 0.8$.

(4) Chimney Bend Form Loss Coefficient

There are two bends, 9° each, downstream of the location of the velocity meter for the chimney and flow exit alignment. Referring to diagram 6-4 and 6-5 of Idelchik's handbook, K_c is approximately 0.1 each for these two bends.

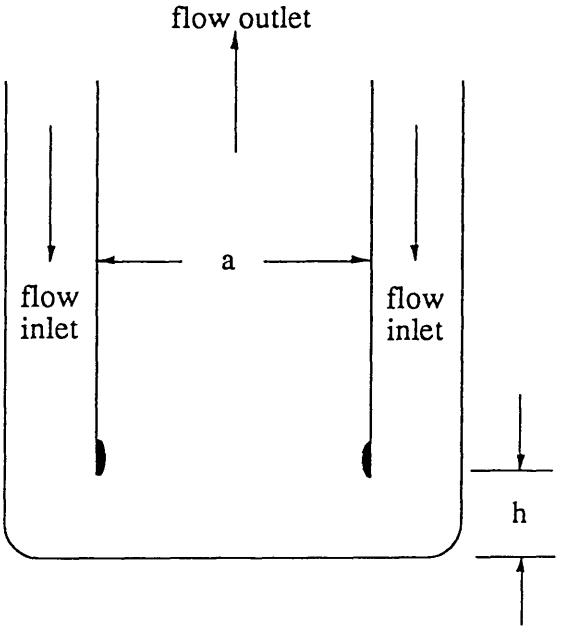

Figure D.1 Air Window Flow Geometry in Terms of Handbook Configuration

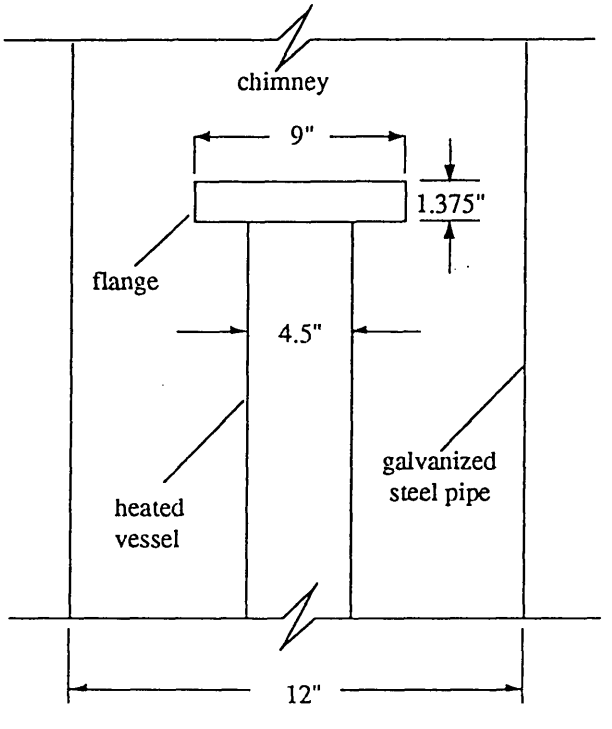

Figure D.2 Dimensions of Heated Vessel Flange

(5) Chimney Exit Form Loss Coefficient

The outlet of the chimney is connected to a 3 feet by 3 feet chimney cap, provided by Norman Associates Inc., type RLX - aluminum louvered penthouse. The manufacturer's data shows that the pressure drop across the chimney cap is 0.031 inches of water at the velocity of 395 feet per minute [Table II of the manufacturer's instruction manual]. The form loss coefficient can be calculated by:

$$K_c = \frac{\Delta P}{\frac{1}{2}\rho V^2}, \tag{D.4}$$

to yield

$$K_c \approx 3.2.$$

The form loss coefficient estimated by Idelchik's handbook, diagram 11-17, is 3.5 (4 louvers, 45° angle, width to height ratio: 1.5).

The above values are provided as input to the PREWAS code, which also considers the frictional losses in the various segments of system ductwork.

As discussed in Section 4.3.2, the heat transfer performance of the test apparatus is insensitive to the inlet form loss coefficients, which include the entrance form loss coefficient and the air window form loss coefficient.. Meanwhile, the heat transfer performance is moderately sensitive to the outlet form loss coefficients, which include form loss coefficients for flow transition at the flange, chimney bend, and chimney exit. As shown in Figures 4.10 and 4.11, 20 % uncertainty in the outlet form loss coefficient will introduce 5 % error in the prediction of the parameter of interest. Moreover, the total form loss is higher than the friction loss.